UNIVERSIDAD NACIONAL AUTÓNOMA DE MÉXICO

Maestría y Doctorado en Ciencias Bioquímicas

PAPEL DE LA ONCOPROTEÍNA E1B 55K EN LA REPLICACIÓN Y EXPRESIÓN
DEL GENOMA DE ADENOVIRUS

TESIS

QUE PARA OPTAR POR EL GRADO DE:

Doctor en Ciencias

PRESENTA:
M. en C. PALOMA ROSSANA HIDALGO OCAMPO

DIRECTOR DE TESIS:
DR. RAMÓN A. GONZALEZ GARCÍA-CONDE
CIDC, IICBA, UAEM

MIEMBROS DEL COMITÉ TUTOR:
DR. SUSANA LÓPEZ CHARRETÓN
IBT, UNAM
DR. ANA LORENA GUTIÉRREZ ESCOLANO
CINVESTAV

Cuernavaca, Morelos. Enero, 2018

UNIVERSIDAD NACIONAL AUTÓNOMA DE MÉXICO

Graduate Program in Biochemical Sciences

ROLE OF THE E1B 55K ONCOPROTEIN ON ADENOVIRUS GENOME
REPLICATION AND EXPRESSION

A THESIS

PRESENTED IN CANDIDACY FOR THE DEGREE
OF:

Doctor of Philosophy in Biochemical Sciences

BY:
M. Sc. PALOMA ROSSANA HIDALGO OCAMPO

Advisory committee:
DR. RAMÓN A. GONZALEZ GARCÍA-CONDE
CIDC, IICBA, UAEM

DR. SUSANA LÓPEZ CHARRETÓN
IBT, UNAM
DR. ANA LORENA GUTIÉRREZ ESCOLANO
CINVESTAV

Cuernavaca, Morelos. January, 2018

2

3

ABSTRACT

Adenovirus gene-products re-shape the cellular environment and induce formation of viral Replication Compartments (RC), where anti-viral defenses are counteracted, while promoting efficient genome replication and expression. The E1B-55kDa (E1B) oncoprotein is a multifunctional regulator of the viral replication cycle, and the accumulated evidence indicates the protein impacts various activities that are associated with RC, such as mRNA metabolism and DNA replication, as well as inhibition of cellular antiviral responses. However, the molecular mechanisms that implicate E1B to subserve an efficient viral replication cycle are unknown, at least in part because of the lack of quantitative information about formation, morphology and activities associated to RC.

To determine the role of E1B on specific steps of the viral replication cycle, we obtained quantitative data for viral early and late genes at multiple time-points post-infection in normal human cells, and quantitatively analyzed the viral gene expression program. We performed quantitative and high-resolution assays; quantitative RT-PCR; next generation sequencing; mass spectrometry analyses; super-resolution microscopy; sub-cellular and sub-nuclear fractionation, to study early and late gene expression in adenovirus-infected cells. Because of the importance of RC in viral gene expression, we studied RC-associated activities, composition and morphology. Our results show for the first time that E1B is necessary to stabilize early and late mRNA and that E1B significantly impacts viral gene transcription and can act as an enhancer or repressor for different viral promoters. We have also found that E1B is necessary for efficient viral DNA replication, as well as splicing of viral mRNA. Additionally, we found that E1B regulates the anti-viral response by promoting the localization of proteins in RC that could otherwise block viral replication. Surprisingly, we found that in the absence of E1B, the size and number of RC are decreased, and that E1B influences the protein and RNA composition of these virus-induced nuclear structures. Thus, E1B is a crucial viral factor for efficient formation of viral RC, viral genome replication and biogenesis of viral mRNA by promoting their stabilization, synthesis and splicing.

4

Abbreviations

Ab	Antibody
ActD	Actinomycin D
Ad	Adenovirus (es)
Ad WT	H5pg4100 (Adenovirus wild type)
APS	Ammonium persulfate
ATM	Ataxia telangiectasia mutated
ATP	Adenine triphosphate
ATR	ATM and Rad related
ATRIP	ATR Interacting Protein
BLM	Bloom helicase
bp	Base pairs
BRCA1	Breast cancer 1
CAR	Coxsackie virus and adenovirus receptor
CB	Cajal Bodies
CBP	CREB-binding protein
CC	Correlation coefficient
cDNA	Complementary DNA
CP	Creatine phosphate
CREB	cAMP response element-binding
CYT	Cytoplasmic fraction
DAPI	4', 6-Diamidino-2-Fenilindol
DBP	viral ssDNA-binding protein
DEPC	Diethilpyrocarbonate
DLS	Dynamic light scattering
DMEM	Dulbecco's Modified Eagle's medium
DNA	Deoxyribonucleic acid
dNTP	Deoxy-nucleotide triphosphate
DFC	Dense fibrillar component
ds	Double-stranded
DTT	Dithiotreitol
E	Adenoviral early genes
E1B$^-$	H5pm4149 (E1B-null mutant virus)
E1B PM	H5pm4227 (E1B mutant virus with substitutions S490, 491D/T495D)
EMCCD	Electron multiplying charge-coupled device
ER	Endoplasmic reticulum
Ery	Erythromycin
FC	Fibrillar centers

FFU	Foci forming units
GC	Granular component
HAT	Histone-acetyl transferase
HDAC	Histone-deacetylase
HEPES	4-(2-hydroxiethil)-1-piperazinaetanosulfonic acid
HFF	Human foreskin fibroblasts
hpi	hours post-infection
IFN	Interferon
IG	Interchromatin granules
INB	Intra-nucleolar body
IRF	Interferon regulator factor
ITR	Inverted terminal repeats
K/kDa	Kilo Dalton
L	Adenoviral late genes
mAb	Monoclonal antibody
MK	Mock
ML	Major Late
MOI	Multiplicity of infection
MRN	Mre11-Rad50-Nbs1
NCLDV	Nucleocytoplasmic large DNA viruses
ND10	Nuclear domains 10
NES	Nuclear export signal
NLS	Nuclear localization signal
NPC	Nuclear pore complex
Npl	Nucleoplasm
NTC	Non-template control
NTP	Nucleotide triphosphate
NUC	Nuclear fraction
ORF	Open reading frame
P	Promoter
pAb	Polyclonal antibody
PAGE	Polyacrylamide gel electrophoresis
PBS	Phosphate buffer saline
PCAF	P300/CBP-associated factor
PCR	Polymerase chain reaction
PKR	Protein kinase R
PML	Promyelocytic leukemia protein
pol	Viral DNA polymerase
pRB	Retinoblastome protein
PRZ	Peripheral replicative zone

RC	Replication Compartments
RNA	Ribonucleic acid
RNApol	RNA polymerase
RNP	Ribonucleoprotein complex
RPA32	Replication protein A
RT	Reverse Transcriptase
S	Svedberg
SDS	Sodium dodecyl-sulphate
SR	Super-resolution microscopy
ss	Single-stranded
STAT1	Signal transducer and activator of transcription 1
SUMO	Small ubiquitin-like modifier
SWI/SNF	SWItch/Sucrose Non Fermentable
TBP	TATA-binding protein
TCEP	Tris (2-carboxyethyl) phosphine
TEMED	Tetramethylethylenediamine
TIA-1	T1 cell-restricted intracellular antigen
TIRF	Total internal reflection fluorescence
TopBP1	Topoisomerase (DNA) II Binding Protein 1
TP	Terminal protein
TPL	Tripartite leader
TU	Transcription unit
Usp7	Ubiquitin Specific Peptidase 7
UTR	Untranslated region
VA RNA	Virus-associated RNA
v/v	Volume per volume
w/v	Weight per volume

TABLE OF CONTENTS

9

INDEX OF FIGURES

10

11

INDEX OF TABLES

1 INTRODUCTION

1.1 Adenoviruses in the context of clinical, applied and basic sciences.

Adenoviruses (Ad) were first isolated from human adenoid tissues in 1953 [1]. These viruses are ubiquitous infectious agents implicated in diseases such as acute respiratory infections, keratoconjunctivitis and gastroenteritis [2], and more recently, the serotypes 36 and 37 have been proposed to be etiological factors of obesity, since they have been associated with the altered differentiation and proliferation of pre-adipocytes [3]. Additionally, it has been demonstrated that human Ad type 12 (Ad12) can induce tumors in laboratory rodents; in 1962, Trentin and coworkers discovered for the first time the oncogenic properties of a human virus by inoculating Ad12 in newly-born hamsters, inducing malignant tumors [4].

Their ability to infect multiple cellular types, including post-mitotic cells, the relative ease with which their genome can be manipulated and the possibility to generate high viral titers, have made Ad one of the most commonly used systems for the design and development of candidate vectors for gene therapy and more recently, combined anti-cancer therapies [5].

Adenoviruses induce alterations in the host-cell gene expression program. Although Ad-infection does not have a major impact on cellular transcription, it does inhibit cellular DNA replication, most of the cellular mRNA are not exported to the cytoplasm, cellular protein synthesis is blocked and the cell cycle is reprogrammed [6-10]. Thus, adenoviruses have been used as a model system to understand eukaryotic cellular processes, such as transcription, post-transcriptional processing, nuclear organization, cell cycle control and cell death [11, 12].

1.2 General aspects of adenoviruses

1.2.1 Taxonomy

Adenoviruses belong to the *Adenoviridae* family, which comprises more than 130 different types divided in five genera [2]. The *Mastadenovirus* and *Aviadenovirus* include the types that infect mammals and fowl, respectively. The *Atadenovirus* and *Siadenovirus*, include viruses that can infect a wider spectrum of animals; the *Atadenovirus* were named for the high content of A+T in their genomes and infect mainly reptiles, fowl and ruminants; the *Siadenovirus* were named because of a gene that encodes a sialidase and encompass viruses that can infect birds and frogs. The fifth genus, *Icthadenovirus*, include viruses that infect fish [13]. Human adenoviruses belong to the genus *Mastadenovirus* and are further classified into subgroups (A-G) using several characteristics such as DNA sequence homology, hemagglutination properties, and oncogenicity in immunosuppressed experimental

13

animals [14]. There are around 63 adenovirus types, with HAd2 and HAd5 being the prototypes, as they have been most extensively studied and most commonly used in gene therapy due to their non-oncogenic properties [15].

1.2.2 Structure

Adenoviruses form non-enveloped particles characterized by an icosahedral capsid and a linear double-stranded DNA genome (dsDNA) of close to 36 kb. The adenovirus type 5 (Ad5) capsid has a diameter of close to 90 nm and is composed by eleven structural proteins (Fig. 1). The protein II, commonly known as hexon, is organized in 240 trimers forming the most abundant structure of the capsid. The protein III constitutes a structure named penton base, which is associated to protein IV, which forms the fiber spikes that protrude from the surface of each one of the twelve vertices of the icosahedral particle. Associated to the inner surface of the capsid are the proteins IX, IIIa, VI and VIII. The underlying core is formed by proteins V, VII, Mu and TP. These proteins, except for TP, have a high content of Arginine residues that interact with the negative charges of the viral genome. The viral DNA is organized surrounding protein VII, which is the most abundant protein of the viral core [2]. The protein TP is bound to the 5' ends of the viral DNA. Additionally, approximately ten copies of the viral protease L3-23K are located inside the viral particles, which are essential for the infectious cycle; the protease is required for maturation of the viral progeny by cleaving the precursors (p) pIIIa, pVI, pVIII, pVII, pMu and pTP; the viral protease also promotes the disassembly and release of the viral particle from the endosome during entry into the infected-cell [16].

Major Capsid Proteins	Minor Capsid Proteins	Core Proteins
Hexon	Protein VI	Terminal Protein
Penton Base	Protein IIIa	Protein Mu
	Protein VIII	Protein VII
Fiber	Protein IX	Protein V
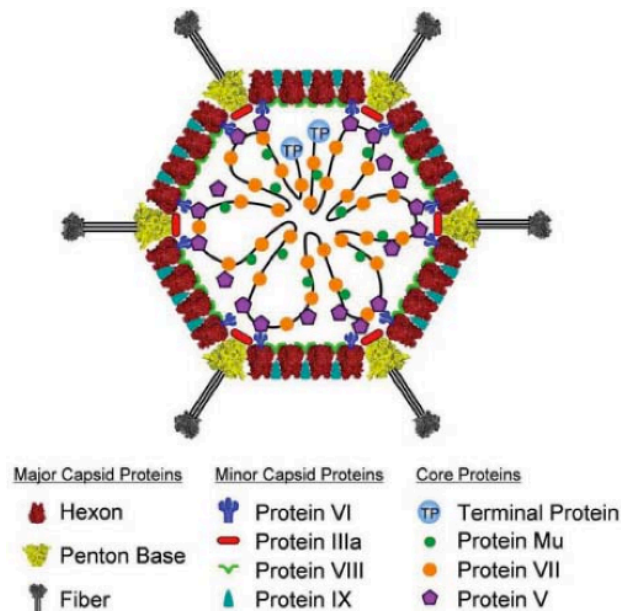
Figure 1.   **Diagram of the structure of Ad.** The cartoon shows the eleven structural proteins of the virion [17].

1.2.3 Viral genome organization

The viral genome is a dsDNA molecule, of close to 36 kb. The 5' ends of the genome are covalently bound to the terminal protein (TP). This protein is necessary for the viral genome to be localized to the nuclear matrix and also works as a primer during the initiation of replication of the viral DNA. The terminal sequences of the genome are inverted-terminal repeats (ITR), where the origins of replication are localized [2].

The viral genome is organized in four groups of transcription units (TU) that are chronologically regulated (Fig. 2). The early TU are E1A, E1B, E2, E3 and E4, while IVa2 and IX are early-delayed TU. Expression of the latter depends on viral DNA replication, as it does for the late TU, which is named Major Late (MLTU) [2]. These TU are all transcribed by the cellular RNA polymerase II (RNAPII). In addition, two viral TU, VA I and II, are transcribed by the cellular RNAPIII, which produce two small transcripts named virus-associated RNA (VA RNA I and II) [2]. However, classification of early and late is not the most accurate description for these viral genes, as some continue to be expressed during the late phase and the viral promoter that controls the expression of all late genes, the Major Late Promoter (MLP), is active during the early phase of infection [11, 18, 19].

By convention, the adenovirus genome is represented beginning with the E1A TU on the left side. The E1A, E1B, IX, ML, VA RNA and E3 TU are encoded on the strand that is read from left to right, while the E4, E2 and IVa2 TU are encoded on the complementary strand and are read from right to left [2].
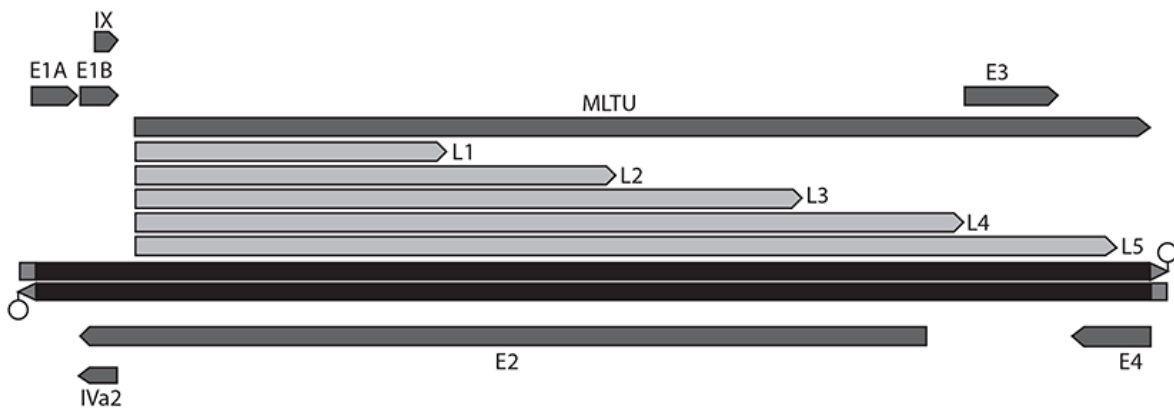
Figure 2. **Diagram of the adenovirus genome.** Representation of the adenovirus dsDNA (black bars) with the E2B-TP protein attached to the 5' ends (white circles). The gray squares represent the 3' ends. The dark gray arrows represent the viral early (E1-E4), intermediate early (IX and IVa2) and the Major Late (ML) transcription units (TU). Light grey arrows indicate the L1-L5 viral late mRNA families, which are defined by different poly (A) sites.

Most of the viral mRNA, except IX are processed by splicing [2]. The main transcript of the MLTU is a pre-mRNA processed by selection of a different polyadenylation site for each mRNA family (L1-L5, Fig. 2). Additionally, each mRNA is produced by alternative splicing site selection, generating a minimum of

15

20 different mRNA (Fig. 3). Moreover, all viral late mRNA share a common 5' sequence of 201 bases named tripartite leader (TPL) formed by the junction of three exons named leader 1, 2 and 3 [2].
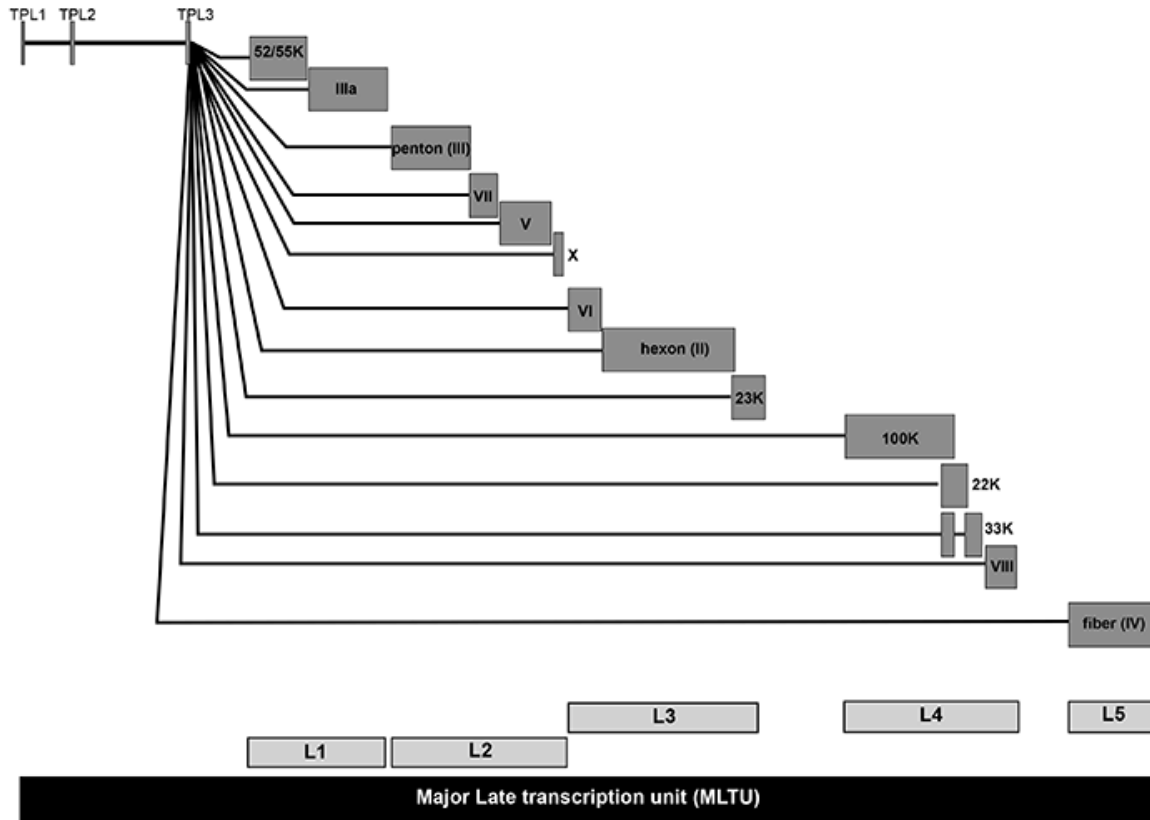
Figure 3. **Diagram of the adenovirus Major Late transcription unit.** The viral late families are represented in the light gray boxes named L1-L5. The mRNA produced from each family by alternative splicing are represented by lines (introns) and dark gray boxes (exons). TPL1-3 indicates the tripartite leader, a sequence formed by the three exons that constitute the 5' end of all viral late mRNA.

The proteins encoded in E1A are named according to the sedimentation coefficient of their corresponding mRNA (e. g. 12S and 13S), and are transcriptional activators and regulators of cell cycle control mechanisms. E1A proteins interact with pRB proteins inducing the release of the cellular factor E2F, which results in the expression of cellular genes necessary to enter the S phase of the cell cycle. E1A proteins also regulate the infected-cell by regulating transcription factors that control the cell cycle and chromatin remodeling factors such as the histone acetyltransferases (HAT) CBP/p300 and PCAF, the SWI/SNF family member p400, and the histone deacetylase complex HDAC. One of the consequences of this modulation is the stabilization and accumulation of the tumor suppressor, p53, but also the inactivation of the transcription activation domain of p53, which abolish the normal biological function of p53 [20, 21]. Hence, E1A products control antiviral

responses, activate transcription of cellular and viral genes and induce the infected-cell to enter S-phase, to establish an optimal environment for viral DNA replication.

The E1B and E3 proteins are named according to their molecular mass, e. g. E1B 55K and E3 14.5K. These proteins are involved in modulation of a wide variety of antiviral responses that inhibit apoptosis, or prevent premature recognition and elimination of the infected cell by the immune system of the host organism [2, 22].

The E2 products participate directly in viral DNA replication and are named according to their function: the viral DNA polymerase (pol), the pre-terminal protein (pTP) that works as a primer, and the ssDNA-binding protein (DBP) [23]. The E2 TU can be transcribed from two alternative promoters, the early and late promoters (E2E and E2L). Two major classes of transcripts, E2A and E2B, are produced by selection of two different polyadenylation signals [24-26]. The DBP protein is encoded in E2A, while the viral pol and the pTP proteins are produced from E2B [25-28].

The E4 proteins are designated depending on the open reading frame (ORF) of the corresponding mRNA produced by alternative splicing; unlike all other adenoviral genes, the E4 TU is the only one that encodes proteins with varied and unrelated activities, such as transcription and translation regulation, splicing, selective export of viral mRNA, modulation of viral DNA replication and apoptosis [2].

The IVa2 protein participates in the encapsidation of the viral genome and also activates transcription of viral late promoters [29], as does the IX product, pIX, which is a structural protein that stabilizes interactions between hexon protomers [30], and works as a transcriptional regulator of cellular and viral TATA box-containing promoters [31].

The proteins encoded in the MLTU are named by the roman numerals, II to VIII, and, as described above are structural proteins or proteins required for the assembly of new viral particles and for the expression of viral late genes [2]. The late genes from the MLTU are under the regulation of two viral promoters, the L4 and the ML promoters. During the transition to the late phase of infection, when viral DNA molecules begin to accumulate as a consequence of DNA replication, transcription of the early delayed TU IX and IVa2 begins [32, 33]. At this time, the L4P, localized inside the gene for L4-100K, is activated, which directs the expression of L4-22K and 33K [34]. IVa2, IX and these two L4 proteins then induce the expression of the ML promoter [31, 35, 36]. However, the major late promoter is also active at a low level early during infection, producing exclusively the L1 mRNA 52/55K.

1.2.4 Regulation of viral promoters

E1A is the first TU to be transcribed, just after the viral DNA enters the nucleus [37]. The large E1A protein activates transcription of the E1A TU and stimulates

17

transcription from the E1B, E2 early, E3, and E4 TU 10- (in the case of E1B) to about 100-fold (in the case of E2E, E3, and E4) [38]. This transcriptional activity is enhanced by the interaction of the large E1A protein with MED32, MED14 and MED26, as well as the catalytic component of the elongation complex, CDK9, which results in the assembly of preinitiation complexes on promoters and stimulation of transcription elongation [39]. E1A also interacts with the acetyl transferases p300/CBP and PCAF, promoting transcriptional activation [40, 41]. Following E1A expression, E1B, E4, E3, E2 and ML (L1, as described before) TU are expressed. Then the intermediate early genes, IVa2 and IX are expressed. After the onset of viral DNA replication, transcription is switched from an early to a late phase, when the MLTU is highly and completely expressed, but also early genes continue to be transcribed. Table 1 shows the known transcription factors that enhance or repress each viral promoter.

Table 1.   Viral and cellular factors that regulate viral promoters

Promoter	Enhancers	Repressors	References
E1A	cAMP, pIX, E1A	E1A, E1B-19K	[31, 42-45].
E1B	E1A, E1B-19K, Sp1, TFIID		[44, 46]
E4	E1A, pIX, cAMP, E4F, ATF2, E1B-19K	DBP, E4Orf4	[31, 43, 47, 48]
E3	E1A, TNF-α, NFκB, NF-1, AP-1, ATF, E1B-19K		[44, 49, 50]
E2E	E1A, PML-II, E2F, E4Orf6/7, ATF, TBP, DBP, E1B-19K		[44, 51-55]
E2L	YB1 and CTCF	E1A	[56, 57]
IVa2	E1A, TFIID, TBP, MLTF	IVa2-RF	[53, 58-60]
pIX	E1A, E1B-19K, E4, Sp1, TFIID, L4-22K		[33]
L4	E1A, p53, E4Orf3, IVa2	L4-33K, TFII-I	[34, 61, 62]
ML	E1A, pIX, DBP, IVa2, USP, TFIID, USF1, CP-1, CTCF, MLTF, MAZ, Sp1, TBP, L4-22K, L4-33K	L4-22K+Sp1 on R1	[31, 51, 56, 59, 63-67]

1.3 Viral replication cycle

The adenovirus replication cycle, as for other DNA viruses that replicate in the nucleus of the infected-cell, is divided by convention into an early and a late phase, separated by the onset of viral DNA replication.

The early phase commences with the interaction of the fiber protein with the host cell through the receptor CAR (Coxsackie B and Adenovirus Receptor) [17]. CAR is a component of tight junctions of epithelial cells. After this interaction, the penton base interacts with integrins $\alpha_v\beta_3$ with a lower affinity than that of CAR-fiber [17]. This event induces the disassembly of the fibers from the virion and subsequent endocytosis mediated by clathrins. Inside the endosome, partial disassembly of the capsid continues due to the low pH that activates the viral protease associated to the virion, releasing the penton, IIIa and hexon proteins. It is believed that protein VI facilitates lysis of the endosome, which releases the viral core to the cytoplasm. The core then is bound to dyneins to be transported through microtubules and directed to the nuclear pore complex (NPC) [17]. The viral DNA is then imported into the nucleus through the NPC, and viral early expression begins [68, 69]. During this phase, the optimal intracellular conditions necessary for efficient replication and expression of the viral genome are established: i) induction of the host cell to enter the S phase of the cell cycle in order to provide the precursor dNTP required for viral DNA synthesis, NTP and RNA processing proteins required for viral transcription, and to activate pathways required for protein synthesis [2]; ii) inhibition of the immune response, apoptosis and other antiviral mechanisms that may otherwise block viral replication; iii) and expression of E2 genes responsible for viral DNA replication [70-72].

As described before, viral DNA replication represents the switch to the late phase. Viral DNA replication proceeds through an asymmetric strand displacement mechanism. As mentioned before, the viral genome ends contain ITR that function as DNA replication origins. The ITR enable displaced single strands, stabilized by DBP polymerization, of viral DNA to circularize by base pairing. The resulting panhandles function as origins for replication of the displaced strand. The TP proteins bound to the 5' ends of the DNA function as primers for the viral pol to synthesize new DNA molecules [2]. Additionally, the cellular transcription factors NFI and Oct-1 participate in viral DNA replication. This two cellular proteins bind to sequences inside the ITR, inducing the viral DNA molecule to bend 82°, therefore facilitating displacement of the DNA strands and progression of viral DNA replication [2].

With the accumulation of viral DNA molecules, expression of IX and IVa2 begins, and activation of the MLP increases [34]. The L4P is activated, resulting in the production of 22K and 33K proteins. These proteins are required to increase MLP activity and to produce the rest of the late transcripts from the L2, L3, L4 and L5 families [34]. The L4 22K protein promotes transcription and processing of viral late

19

mRNA and the L4 33K protein is a splicing factor [35]. Most of the proteins encoded by viral late mRNA are structural proteins needed for the assembly of viral progeny [73, 74]. Viral late mRNA are subject to a selective expression program. Synthesis of cellular mRNA continues during the infection, but their export to cytoplasm is inhibited, while viral mRNA are efficiently accumulated in the cytoplasm [75]. It is believed that this selective export is mediated by the interactions of two viral early proteins, E4Orf6 and E1B 55K (E1B). Assays with mutant viruses that block interaction between these two proteins have shown a decrease in cytoplasmic accumulation of viral late mRNA while cellular mRNA export is not blocked [76, 77] (see further description in E1B 55K section below). Viral late mRNA are exported through the cellular Nxf1/Tap-Nxt1/p15 machinery [78]. In addition to selective export mechanisms, viral late mRNA translation is also selectively regulated. This process involves the viral protein L4 100K and the VA RNA I [79-82]. Cellular protein synthesis is inhibited by dephosphorylation of the translation factor eIF4E, inhibiting cap-dependent translation [9]. Moreover, the L4-100K protein together with the un-translated region (UTR) of the TPL from viral late mRNA, which is complementary to the 3' end of the 18S rRNA, induce a mechanism called "ribosome shunting" which allows the 40S ribosomal subunit to be directed to the start codon [83, 84] to efficiently and selectively produce viral proteins. With accumulation of viral proteins required for the assembly and formation of viral capsids, viral progeny is produced. This results in production of up to 10^5 viral particles per cell, along with an excess of structural proteins and viral DNA that are not assembled into virions.
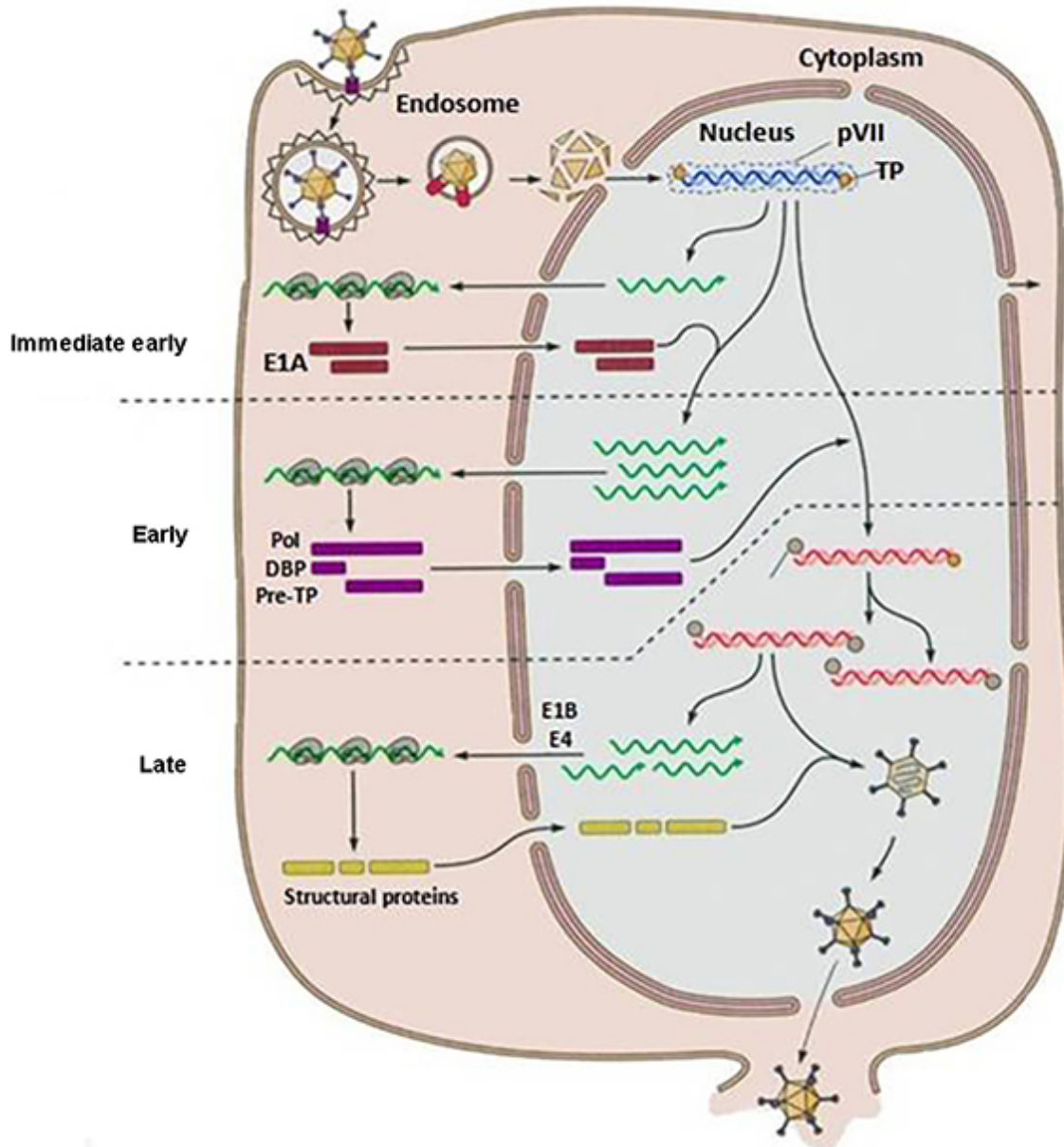
Figure 4. **Schematic representation of the adenovirus replication cycle.** Just after the viral genome is imported into the nucleus, E1A genes are transcribed. E1A products induce activation of viral genes. During the early phase of infection, proteins necessary for viral DNA replication are produced. The onset of viral DNA replication delineates the transition to the late phase. The viral DNA molecules can be used to transcribed late genes that encode the viral structural proteins and to be encapsidated, resulting in viral progeny production that is released by cell lysis (Modified from [85]).

1.4   Compartmentalized viral gene expression.

Regulation of viral gene expression is not just temporal, but requires different viral proteins that participate in each step of gene expression, from mRNA synthesis and processing, mRNA stabilization, transport and translation, as well as specific nuclear environments [29, 79, 86-92]. A strategy that seems to be common for all

21

viruses involves formation of specialized cellular microenvironments where cellular and viral macromolecules are recruited. These have been termed virus factories, viroplasms, replication centers or compartments (RC). RC are the sites where viral genome replication and expression occur, and in some cases these virus-induced structures are associated or juxtaposed with sites of virion assembly. Through this strategy viruses not only promote progression of a productive replication cycle but also concomitantly co-opt cellular factors and counteract a variety of anti-viral responses [93-95].

Early adenoviral gene expression is associated to early replicative sites, which contain ssDNA, dsDNA, and viral spliced and un-spliced mRNA [11, 96-98]. After the onset of viral DNA replication, specialized viral inclusions containing early viral E2A single stranded DNA binding protein, DBP, are formed. These viral inclusions are termed Replication Centers or Compartments (RC), which are nuclear microenvironments where the viral genome replicates and viral late gene expression takes place [92]. Moreover, these compartments also constitute a regulation hub for essential activities that promote efficient viral replication [95, 99, 100].

1.4.1 Viral Replication Compartments or Centers (RC)

For DNA viruses that replicate in the nucleus, formation of RC does not seem to require membranous structures, as it does for viruses that replicate in the cytoplasm [101-103]. Rather nuclear RC are formed in association or adjacent to defined nuclear domains, such as the PML NB (nuclear domains implicated in DNA replication and transcription regulation, epigenetic silencing, DNA repair, cell senescence, apoptosis, and regulation of the interferon-induced antiviral response), (reviewed in [104]), the nucleolus or other nuclear domains [105, 106]. While less information is available for the RC of DNA viruses that replicate in the nucleus compared to cytoplasmic RNA viruses, it is known that these nuclear compartments are vital for virus replication, and that they contain DNA and RNA polymerases, transcriptional and post-transcriptional processing factors, and RNA export factors. Like other DNA viruses that replicate in the nucleus, upon infection of the cell, adenovirus DNA is delivered into the cell nucleus, where it localizes to PML NB by an uncharacterized mechanism [107]. Assembly of nuclear replication compartments is accompanied by extensive reorganization of nuclear components that are major constituents of nuclear domains, such as PML NB, interchromatin granules (IG), paraspeckles, Cajal bodies (CB) and nucleoli (reviewed in [95, 107-112].). In addition, as for cytoplasmic viruses, nuclear RC also impact cellular anti-viral mechanisms [113-124]. Table 2 includes some examples of cellular antiviral proteins recruited to RC.

22

Table 2. Cellular proteins with antiviral activity, recruited to viral RC

Activity	Example	Reference
DNA Damage Response	FANCD2	[125]
	PCNA	[126]
	USP7	[127]
	SPOC1	[128]
	ATM	[115]
	ATR	[115]
	Mre11	[114]
	Nbs1	[114]
	Rad50	[114]
	RPA32	[115]
	ATRIP	[115]
	TopBP1	[115]
	SLX4	[129]
	ERCC6L	[129]
Innate immune response	SP100	[130]
	NDP55	[130]
	IRF3	[131]
	STAT1	[116]
	PKR	[132]
Tumor suppressor	p53	[117]
	BRCA1	[119]
	PML	[118]

Since proteins that promote efficient viral replication as well as factors that participate in the antiviral response are co-opted and concentrated there, replication compartments may represent a control hub for virus-cell interactions that promotes efficient viral replication and simultaneously protects viral macromolecules from cellular anti-viral activities. Nevertheless, because of the complexity of the nuclear milieu, RC assembled in the infected cell nucleus have not been isolated and thus, they have only been studied within the complexity of the infected cell-nucleus.

Adenoviral RC and nucleoli seem to have similar functional organization. Neither of these sub-nuclear structures is membrane enclosed, they both consist of proteins and nucleic acids, and their size ranges between 0.5 and 5 µm in diameter. Furthermore, both structures appear to have subcompartments or regions that are morphologically and functionally distinguishable [92, 96, 133, 134]. The ultrastructural analysis of nucleoli has revealed three subcompartments that

include the fibrillar centers (FC) surrounded by the dense fibrillar components (DFC), both embedded in the granular component (GC). Transcription of rRNA genes has been suggested to take place at the interface of FC and DFC, while ribosome assembly takes place in the granular component [134, 135]. Beside these main regions, an additional subcompartment, referred to as intranucleolar body (INB) has been reported, in which proteins involved in DNA repair, RNA metabolism, nuclear export, protein turnover and the posttranslational modifiers SUMO1 and SUMO2/3 are localized [136]. In comparison, fluorescence and electron microscopy of adenovirus RC suggest that they are also functionally compartmentalized: dsDNA that is not actively replicated nor transcribed is localized in the center of RC; separately, ssDNA is associated with DBP, surrounded by the peripheral replicative zone (PRZ), where spatially separated sites of active replication and transcription are organized. Active transcription leads to the accumulation of clusters of IG surrounding RC [96, 133, 137, 138] (more details described below). Interestingly, SUMO1 and SUMO2/3 paralogues associate with RC displaying distinct localization, where SUMO2/3 exhibits a pattern similar to DBP while SUMO1 localizes to the periphery of DBP foci [124], a pattern that is comparable with their distribution in PML NB [139].

Adenovirus RC have been studied by fluorescence and electron microscopy in infected cells [92, 133, 138, 140-146]. These studies have provided valuable information about their morphological organization, such as the localization of viral and cellular factors that participate in viral DNA synthesis and gene expression, suggesting a spatial separation of replication and transcription regions [133]:

- E4Orf3 nuclear-tracks: Early in infection, adenovirus type 5 (Ad5) E4 open reading frame 3 (ORF3) induces the redisruption of nuclear domain 10 (ND10) bodies by redistributing the PML protein into 'fibrous-like' tracks.

- ssDNA accumulation sites (DBP-accumulation sites) and Viral genome storage: The onset of viral DNA replication occurs simultaneously with formation of fibrillar regions that contain ssDNA and dsDNA. Later, these types of DNA are separated in contiguous structures. Viral ssDNA accumulates in compact fibrillar masses together with the E2A DBP protein, with intermittent viral replicative activity [96, 97]. Moreover, dsDNA that is not involved in transcription, nor replication, accumulates at the center of RC (viral genome storage). Traces of ssDNA and DBP can be found near the viral genome storage, while abundant viral particles can be localized near ssDNA and dsDNA sites [92, 133, 147].

- pIX bodies: pIX is a viral structural protein but also a transcriptional factor. This early delayed protein participates in the virus-induced nuclear reorganization after the onset of viral DNA replication, resulting in formation of defined nuclear structures, which can be visualized as dispersed nuclear

globules by immunofluorescence staining or as clear amorphous spherical inclusions by electron microscopy [148]. [118]. The exact activity of these viral structures is unknown, but IFN-inducible proteins such as PML and Sp100, as well as the cellular kinases PKR and CK2α are sequestered at these sites, which correlates with efficient viral proliferation [118, 132].

- Protein crystals: These inclusions are formed at late steps of the virus life cycle and represent the heteromeric capsid protein formed by penton base and fiber subunits [149]. Additionally, CK2β, as well as traces of PKR and PML can be localized to these compartments [118, 132, 149, 150].

- Peripheral replicative zone (PRZ): This region forms a fribrillo-granular network, as visualized by electron microscopy. The PRZ contains dsDNA and little DBP, as compared to ssDNA accumulation sites, where both transcription and replication of viral DNA occur [92].

- Compact rings and Interchromatin granule clusters (IG): Compact rings are nuclear sites induced by the viral VA1 RNA. These sites also contain viral RNA without poly(A) tails and the viral protein IVa2, and are localized adjacent to IG. IG are arranged at the periphery of the PRZ, where snRNP and other splicing factors, rRNA, viral pre-mRNA and mRNA with poly(A) tails are accumulated [11, 147].
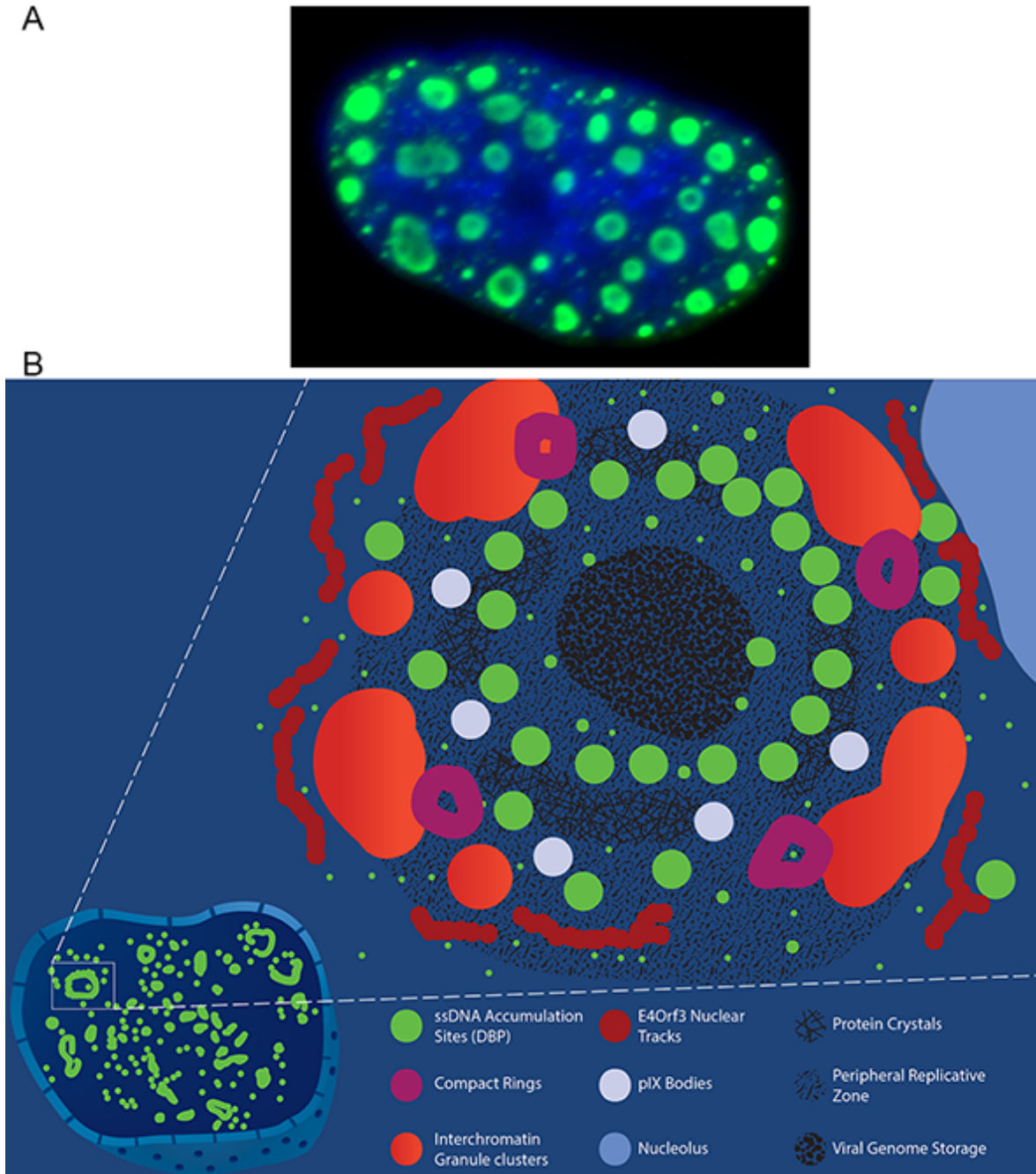
Figure 5. Schematic representation of adenovirus Replication Compartments. A. Fluorescence micrograph of an Ad-infected cell showing in green the DBP rings and in blue, DNA (DAPI). B. Representation of the compartmentalized organization of Ad RC in the infected cell nucleus.

1.4.2 The E1B-55K (E1B) protein

The viral early gene product, E1B-55K (E1B) is a multifunctional phosphoprotein that promotes efficient progression of the viral replication cycle. E1B undergoes posttranslational modification by SUMOylation at lysine 104 and phosphorylation at the C-terminal region, on Serines 490, 491 and Threonine 495 that regulate the

protein's activities [151, 152]. This protein is implicated in the degradation of cellular anti-viral factors [153]; efficient viral genome replication and transcription [76, 117, 154-158]; regulation of intranuclear steps that lead to efficient export of viral late mRNA during the late phase of infection [77, 87, 156, 158, 159]; transcriptional repression of genes implicated in anti-viral responses [160]; and regulation of protein synthesis [161, 162]. It has been suggested that E1B could have a role in viral mRNA metabolism, prior to transcription; in the absence of E1B, low steady-state levels of viral late mRNA were measured without observing defects in transcription rates. These studies have also shown reductions of up to 50% in cytoplasmic mRNA accumulation that correlates with a reduction in viral late protein synthesis in the absence of E1B [87, 154, 158, 163]. Babiss and co-workers concluded that the major effect of E1B on mRNA metabolism was in the accumulation of these transcripts, probably stabilizing them or promoting their export to cytoplasm. They found that in cells infected with an E1B-null mutant virus, viral late gene transcription began normally but total viral late mRNA exhibited a 10-fold decrease [87]. In contrast to these results, other groups reported direct defects in late gene transcription rates when E1B was absent [76, 154, 156-158]. The accumulated evidence described above suggests that E1B might exert control at some or various steps of the viral gene expression program. Nevertheless, the molecular mechanism(s) by which E1B subserves an efficient viral replication cycle is not known, but its activities have been correlated with regulation of the anti-viral response in the infected cell, and the reorganization and relocalization of nuclear components to RC.

1.4.3 Impact of E1B on RC

During the viral replication cycle, E1B can be localized in the cytoplasm or in the nucleus depending on the cells used and the presence of other viral proteins [164-167]. In transformed cell lines E1B can be localized to juxtanuclear cytoplasmic bodies similar to aggresomes [168]. In the nucleus, the protein associates with the viral early protein E4Orf3 and localizes to PML-nuclear bodies [169] or with the nuclear matrix, independent from its association with E4Orf3 [170]. Additionally, E1B associates with RC [167, 171-173]. The presence of E1B in RC seems to be necessary for efficient replication and expression of the viral genome and concomitantly to recruit cellular proteins that are inhibited during infection [57, 117, 124, 157, 174]. In HeLa cells infected with Ad WT, the cellular transcription factor YB1 is relocalized from the cytoplasm to the nucleus. YB1 facilitates DNA replication by binding to the E2-late (E2L) promoter and activating the expression of the E2 genes. Nuclear YB1 colocalized with a major viral component of RC, the early protein E2A-DBP (DBP) and with E1B. Nevertheless, when the cells were infected with the E1B null-mutant virus, Ad338, DBP displayed a diffuse nuclear pattern and YB1 remained in the cytoplasm. These results suggest that targeting of

YB1 by E1B to RC favors viral DNA replication at late times of infection, when the E2L promoter is active [57]. Our group has also reported that E1B, in association with E4Orf6, binds p53 and relocalizes this tumor suppressor to RC. Moreover, in normal human cells (HFF) infected with either an E1B-null mutant virus (Hr6) or a virus that expresses an E1B unable to bind p53, viral DNA replication is inefficient [77, 117]. These observations suggest that the reorganization of the cell nucleus that results in formation of RC and later promotes efficient genome replication and expression, may underlie the mechanism(s) by which E1B regulates cellular activities and promotes efficient progression of the viral replication cycle.

Several studies point to an impact of E1B on RC-associated activities, such as mRNA metabolism and DNA replication. Some reports have shown reductions of up to 50% in cytoplasmic mRNA accumulation that correlates with a reduction in viral late protein synthesis in cells infected with mutant viruses null for production of E1B [87, 154, 158, 163]. In addition, it has been reported that in the absence of E1B, late gene transcription is reduced [76, 154, 156-158]. E1B has also been shown to impact viral late mRNA partitioning in different compartments of the infected cell nucleus. In the absence of this viral early protein, viral late mRNA do not accumulate efficiently in a soluble nuclear compartment after their dissociation from the nuclear matrix, and previous to their association with the nuclear membrane (Leppard and Shenk, 1989). Although the role of E1B was not defined, in a similar study employing Ad2 WT, it was reported that movement of cellular transcripts from a matrix fraction to a salt-extractable fraction is inhibited, whereas viral mRNA were efficiently recovered within this soluble fraction [175]. Since DNA replication, transcription and mRNA splicing are processes associated with the nuclear matrix [176-180], these observations suggest that E1B promotes the intranuclear movement of viral mRNA from RC to the nuclear envelope, while simultaneously limiting cellular mRNA movement. According to these observations, Ornelles and Shenk proposed a model in which the association between E1B and E4Orf6, results in the relocalization to RC of a cellular factor(s) required for the intranuclear movement of cellular mRNA. This relocalization of the cellular factor could facilitate the efficient movement of viral late mRNA from their site of synthesis/processing (RC) while blocking cellular mRNA transport to the nuclear membrane (Ornelles and Shenk, 1991).

E1B interacts with a nuclear RNA-binding protein that belongs to the hnRNP U family, named E1B-AP5 [181]. Previous works have shown that high levels of E1B-AP5 promote the export of viral late transcripts and shutoff of cellular mRNA export [181]. Furthermore, E1B-AP5 localizes to viral RC [113] and it has been demonstrated that E1B-AP5 binds to Nxf1/Tap, the cellular nuclear receptor responsible for the export of viral late mRNA [78, 182]. These results are in agreement with the suggestion that E1B facilitates cytoplasmic accumulation of viral transcripts by binding to a host factor that may promote viral mRNA transport

28

to the nuclear membrane [156, 157, 167, 181] (Ornelles and Shenk, 1991; Leppard, 1993). However, the molecular mechanism by which the E1B/E1B-AP5 complex facilitates the selective mRNA export mechanism established during the late phase of Ad infection remains to be elucidated.

YB1 is a multifunctional cellular protein involved in a number of cellular processes including proliferation, differentiation, and stress response. YB1 is a DNA- and RNA-binding protein involved in DNA replication and repair, transcription, splicing and mRNA translation [183]. This cellular protein has been reported to be a component of cytoplasmic messenger ribonucleoprotein (RNP) complexes [184, 185]. Its nuclear localization is induced by expression of oncogenes [186-188] in response to cellular stress and during DNA damage [189, 190]. As mentioned before, E1B interacts with YB1 and this interaction induces YB1 nuclear translocation to viral RC [57]. YB1 activates transcription of the E2 late promoter, thus inducing the expression of viral proteins directly implicated in viral DNA replication [57]. In addition, YB1 over-expression results in an increase in the 13S isoform of E1A, suggesting it can influence splicing of E1A mRNA [191]. Moreover, YB1 promotes efficient replication of E1A deleted (Ad312) and E1A-mutant (Ad520) adenoviruses that do not express the large 289 amino acid long E1A protein [192]. These data suggest YB1 impacts viral DNA replication and might participate together with E1B in facilitating activities associated with RC.

E1B can interact and regulate p53 activities [193]. An early function of E1B in normal cells is to relocalize p53 [117] to RC. Human adenoviruses have evolved mechanisms to regulate p53 function and stability to permit efficient viral replication. These include degradation of p53 [194] but also co-opting p53 to promote viral DNA replication and transcription. Viral mutants in which the E1B-p53 interaction is impaired [195], result in the inhibition of viral DNA replication [77, 165, 196] in normal human cells (HFF). However, this is not the case for every cell type or virus mutant [117, 154, 155] [87, 158]. Recently, it was reported that p53 is a transcriptional activator of the novel viral promoter of the L4 genes 22K and 33K genes, which are required for complete activation of the viral late genes [34, 35, 62]. Nevertheless, the mechanism by which p53 subserves viral DNA replication and expression is unknown. The tumor suppressor p53 interact with both YB1 and E1B-AP5 [197, 198]. Moreover, under cellular stress, p53 induces YB1 nuclear translocation, linking p53 DNA-damage response to YB1. Additionally, it has been reported that YB1 inhibits p53-induced cell death and activation of transcription [190]. These evidences suggest that during Ad-infection, a cross-talk between E1B, YB1, p53 and E1B-AP5 might be implicated in the efficient progression of the viral replication cycle. Taken together, the data described in this section suggest that E1B promotes efficient viral genome replication and expression, most likely through an indirect mechanism that depends on the proteins that interact with E1B and localization in viral RC.

29

2   HYPOTHESIS

The E1B 55K protein promotes efficient viral genome replication and biogenesis of viral late mRNA in adenovirus replication compartments.

3   GENERAL AND SPECIFIC AIMS

To determine the role of E1B 55K (E1B) on adenovirus genome replication and expression, this work aimed to:

- Study the effect of E1B on the efficient establishment and progression of the viral gene expression program.
- Evaluate the effect of E1B on RC-associated activities.
- Analyze the effect of E1B on RC morphology, organization and composition.

4   MATERIALS AND METHODS

Cells and viruses. Primary human foreskin fibroblasts (HFF) were maintained in monolayer cultures in Dulbecco's modified Eagle's medium (DMEM) supplemented with 10% (vol/vol) fetal calf serum (Gibco-Invitrogen Corp.) for no more than 14 passages. H1299 cells were maintained in monolayer cultures in DMEM supplemented with 10% (vol/vol) bovine serum (Biowest). HFF were infected with Ad5 at 30 PFU/cell, as described previously [77] and H1299 cells were infected with 10 PFU/cell. The viruses used in this work were as follows: H5pg4100, which is phenotypically indistinguishable from Ad wild-type (Ad WT) in cell culture, but contains a deletion within the E3 region [199, 200]. H5pm4227, which contains the substitutions of S490D, S491D, T495D in the E1B 55K protein, and directs the production of an E1B protein that mimics a constitutively phosphorylated state (E1B PM) at the C-terminus of the protein [201]. H5pm4149, which is null for expression of E1B (E1B⁻) as it contains four premature stop-codons at the 5'-end of E1B 55K-CDS, thus abrogating the synthesis of the protein [202]. All viruses were propagated in monolayers of HEK-293 cells, and were titered as fluorescent forming units (FFU) as described previously [200].

Antibodies. The primary antibodies used for western blotting and immunofluorescence assays were as follow: antibody (Ab) specific for Ad5 DBP included mouse monoclonal Ab (mAb) B6-8 [203], anti-E1B mouse mAb 2a6 [204], anti-CTCF rabbit polyclonal Ab (pAb) (Millipore), anti-SUMO2/3 rabbit mAb (18H8, Cell Signaling Technology), anti-YB1 rabbit mAb (EP2706Y, Millipore), anti-Tap rabbit mAb (EPR8009, Abcam), anti-BRCA1 mouse mAb (Novus Biological) and anti-Nucleolin mouse mAb (Invitrogen). The secondary antibody used for WB was an anti-mouse horseradish peroxidase (HRP) conjugated antibody (Jackson ImmunoResearch) and for immunofluorescence analyses, Alexa Fluor 488, 568 and 405 antibodies (all from ThermoScientific).

Primers design. The CLC Sequence Viewer (CLC Bio), Primer Plex (Premier Biosoft) and Primer-Blast (NCBI) programs were used to design primers specific for the viral and cellular nucleic acid sequences of interest. All primers allowed the amplification of a unique product of the expected size. The primers are shown in Table 3.

Table 3.   Primers used for RT-PCR

Gene	Primer sequence	Amplicon (bp)
E1A	Sense: TTGAACCACCTACCCTTCACG Antisense: CCTCCTCGTTGGGATCTTCG	69
E1B	Sense: TAGCGGTACGGTTTTCCTGG Antisense: CCGAACCCTTACATCGGTCC	106
E2A-DBP	Sense: AGCAGATCAAGGCTTTTATGCAGG Antisense: GGCGAACGGAGTCAACTTTGG	149
E2B-pol	Sense: AGTTCTACATGCTAGGCTCTTACC Antisense: CGCAGTAGTCCAGGGTTTCC	156
E4Orf6/7	Sense: CGCACTCCGTACAGTAGGGATCG Antisense: GGAGAAGTCCACGCGTTGTGC	132
IVa2	Sense: AGGGCGTCTCCAAGTTCTTCC Antisense: TGTTCCCAGCCATATCCCTCC	126
ML	Sense: GCCTCCGAACGGTACTCCGCC Antisense: CGCCACGGTGCTCAGCCTACC	121
L1-52/55K	Sense: CAGTCGCAAGATGCATCCGG Antisense: GATGTCGCCCCTCCTGACG	126
L1-pIIIa	Sense: AGTCGCAAGATGATGCAAGACG Antisense: CAGTCGTCCGTGGAGTTAAGG	89
L4-22K and 33K	Sense: CAGTCGCAAGATGGCACCCA Antisense: CTCTCCCAGTCTTCCATCATGTCC	132
L5	Sense: GTCACAGTCGCAAGATGAAGCG Antisense: GGTAACTAGAGGTTCGGATAGGCG	139
ß-Actin	Sense: CTTCCTTCCTGGGCATGGAGTCC Antisense: GCAATGCCAGGGTACATGGTGG	139

DNA purification. Sub-nuclear fractions from two independent experiments were treated with 1 mg/ml of proteinase K and 1:200 of Tween20 (both from Promega). This preparation was incubated 1 h at 55°C. Proteinase K inactivation was performed for 10 min at 95°C. The reactions were centrifuged for 2 min, 14,000 rpm at room temperature and the supernatant was collected. The DNA was precipitated with 1/10 volume of 3M sodium acetate and one volume of isopropanol overnight at 4°C. The samples were centrifuged at 14,000 rpm for 10 min at room temperature. The pellet was washed with 70% ethanol and centrifuged for 5 min, 14,000 rpm at 4°C. The DNA was resuspended in 10 mM Tris-HCl pH 7.4, quantified using Nano Drop and stored at 4°C.

RNA purification. RNA was purified from total cell-lysates or from RC fractions from at least two independent experiments using Trizol according to the manufacturer's instructions (Invitrogen). The RNA pellet was resuspended in DEPC (diethilpyrocarbonate)-treated water, quantified using Nano Drop. Purified RNA was checked for absence of DNA contamination by RT[-] reactions and stored at -70°C.

32

cDNA synthesis. To analyze RNA, 100 ng of RNA obtained from each sub-nuclear fraction from two independent experiments were reverse-transcribed using Revert-Aid Reverse Transcriptase according to manufacturer's instructions (Thermo Scientific) in 20 µl of reaction volume.

End-point PCR. Amplification of viral DNA or cDNA from sub-nuclear and sub-cellular fractions obtained from two independent experiments was carried out by PCR using Taq DNA polymerase as recommended by the manufacturer (Thermo Scientific) in 25 µl of reaction volume. For RT-PCR assays, RT⁻ reactions were prepared to confirm the absence of DNA contamination. After PCR amplification, 10 µl of the reaction were loaded in 2% agarose gels, subjected to electrophoresis and visualized using ethidium bromide staining.

Quantitative PCR or RT-PCR. Viral DNA or cDNA were quantified in total cell lysates using the Power SYBR Green PCR Master Mix kit according to the manufacturer's instructions (Applied Biosystems). ß-actin was used as endogenous control. All primers were validated and had amplification efficiency close to 100% as calculated by the linear regression obtained from standard curve assays. The primers allowed the amplification of a unique product of the expected size, as determined by melt-curve analyses. The StepOne system (Applied Biosystems) was used for thermocycling; RT⁻ and NTC controls were prepared for each experiment. The samples were analyzed by the ΔΔCt comparative method using triplicate samples from two independent experiments. ß-actin was used as normalizer. The primers used to quantify different mRNA are shown in Table 2.

Densitometry analysis. The DNA and RNA gel electrophoresis images as well as WB films were analyzed by densitometry using ImageJ [205]. Graph Prism was used to plot the data and for statistical analysis by the t-test.

Statistical Analysis. For gene expression measurements, it is important that the data express proportional changes (biologically relevant changes) rather than additive changes [206] (Section 5.1). For this reason, the fold-change values were log transformed (logarithm base=10) as a first approach of our statistical analysis process. The approach was divided in three sections: a) expression kinetics of Ad WT genes (5.1.1), b) analysis of the effect of E1B on viral gene expression kinetics (5.1.2), c) Linear regression analysis of accumulation of each mRNA as a function of E1A mRNA accumulation, for Ad WT, E1B⁻ and E1B PM viruses. The statistical studies were divided into early times (4-16 hpi) and late times (20-36 hpi) of the viral replication cycle. The results are shown as boxplots, curves for the mean gene expression values, heatmaps and hierarchical cluster analysis. All comparisons between two distribution functions were validated through a Kolmogorov-Smirnov hypothesis test [207]. The selection of this non-parametric hypothesis test was based on the following characteristics of the data presented: i) the fold-change distribution function of each gene does not follow a Gaussian distribution (therefore a Shapiro test to study the distribution function was

33

employed [208], ii) existence of heteroscedasticity (i. e., the existence of variability in the variance of the fold-change distribution functions between genes), which was validated through a Levene's test [209]. Several "Simple Linear Regression" models [210] were adjusted considering E1A as independent variable and each of the other mRNA as dependent variables at the early and late times postinfection (see Supplementary Information for details). All statistical tests were performed using R, version 3.4.2 (2017-09-28) Copyright (C) 2017, The R Foundation for Statistical Computing Platform: x86_64-pc-linux-gnu (64-bit).

mRNA stability assays. HFF cells were seeded on 6-well plates at a density of 2.5×10^4 cells/cm^2 and infected with Ad WT, E1B$^-$ or E1B PM mutants. At 24 hpi, cells were treated with 1 µM Triptolide (Sigma) in 500 µl DMEM for 1 h to inhibit transcription. Cells were collected using 500 µl of Trizol (Invitrogen) at 0, 2, 4, 6, 8 and 12 hpt (hours post-treatment), which correspond to 24, 26, 28, 30, 32 and 36 hpi (hours post-infection), respectively. cDNA synthesis was prepared using 1/10 of the total RNA and quantitative RT-PCR assays were performed as described above to measure E1A and L5 mRNA. The values were plotted against time post-treatment with triptolide using GraphPad Prism.

Plasmids and transient transfections. The Ad E1B proteins examined in this study were expressed from their respective complementary DNAs under the control of the cytomegalovirus immediate early promoter derived from the pcDNA3 vector (Invitrogen) to produce Ad WT E1B 55K [211], or E1B 3XPD (S490/491D, T495D) (pE1BPM). Promoter constructs were based on the pGL3-basic vector (Promega). For transient transfection, subconfluent cells were treated with a transfection mixture of DNA and 25-kDa linear polyethylenimine as described recently [212].

Luciferase reporter assays. For dual luciferase assays, subconfluent H1299 cells were transfected prior to preparation of total cell extracts (48 h) [213], or transfected and infected (for the times indicated in Figure 5) with the E1B$^-$ virus as shown. Promoter activity was assayed with lysed extracts in an automated luminometer (*Berthold Technologies*). All samples were normalized for transfection efficiency by measuring Renilla-luciferase activity from the co-transfected plasmid pTK-RL (Promega). All experiments shown were performed in triplicate and data are presented as mean values with the corresponding standard deviation using GraphPad Prism.

Preparation of sub-cellular and sub-nuclear fractions from infected HFF cells [214]. To isolate cytoplasmic and nuclear fractions, Ad5-infected HFF cells were fractionated essentially according to a procedure designed to isolate nucleoli described previously [215] and recently adapted [216], with the following modifications [214]: All procedures were carried out on ice, except as indicated. HFF cells were grown in monolayer cultures to 90% confluence. Ad5-infected or mock-infected cells were harvested at the indicated times post-infection and were

34

washed with ice-cold PBS (137 mM NaCl, 2.7 mM KCl, 10 mM Na_2HPO_4 and 1.8 mM KH_2PO_4). To disrupt the cellular membrane 1×10^7 cells were resuspended in ice-cold hypotonic buffer (10 mM HEPES pH 7.9, 10 mM KCl, 1.5 mM $MgCl_2$, 0.5 mM DTT, 20 µg/ml phenylmethylsulfonyl fluoride (PMSF), 10 µg/ml aprotinin, 10 µg/ml pepstatin A and 10µg/ml leupeptin). After extensive swelling, cell membranes were lysed by 80 strokes with a dounce homogenizer, constantly monitored by phase contrast microscopy to ensure complete cell membrane lysis while avoiding damage to nuclei. The cell homogenate was centrifuged at 300 × g, 4ºC for 5 min and the supernatant containing the cytoplasmic fraction (CYT) was stored at -20ºC. To remove cellular debris from nuclei, the pellet was resuspended in solution 1 (S1) (0.25 M sucrose, 10 mM $MgCl_2$, 20 µg/ml PMSF, 10 µg/ml aprotinin, 10 µg/ml pepstatin A and 10µg/ml leupeptin) and was layered over an equal volume of solution 2 (S2) (0.35 M sucrose, 0.5 mM $MgCl_2$, 20 µg/ml PMSF, 10 µg/ml aprotinin, 10 µg/ml pepstatin A and 10µg/ml leupeptin), and were centrifuged at 1,400 × g, 4ºC for 5 min. The supernantant contained cellular debris and the pellet containing isolated nuclei (NUC) was resuspended in S2 and stored at -20ºC. To isolate subnuclear fractions enriched with adenovirus RC (RC fractions), nuclei were sonicated with a Branson 1510 ultrasonic bath, using two 5 min pulses, until all nuclei were lysed as observed by phase contrast microscopy. The sonicated nuclei were then layered over an equal volume of solution 3 (S3) (0.88 M sucrose and 0.5 mM $MgCl_2$) and centrifuged at 3,000 × g, 4ºC for 10 min. The supernantant containing the nucleoplasmic fraction (Npl) and the pellet containing the RC fractions or nucleolar fraction (Nlo, in mock-infected cells) were stored at -70ºC. This procedure has been performed several times and has proven to be highly reproducible. Data from at least two independent experiments are shown in all procedures.

Phase-contrast microscopy, immunofluorescence microscopy and super-resolution analysis. Phase-contrast microscopy with a 40x or 60x objective, as indicated, was used to monitor preparations of sub-nuclear fractions. For immunofluorescence, HFF cells grown on coverslips to approximately 90% confluence were mock-infected or infected with Ad5. Cells were processed for immunofluorescence as described previously [77]. After application of specific primary antibodies, cells were incubated with secondary antibodies. The coverslips were mounted on glass slides in PBS/10% glycerol and samples were examined using a Zeiss Axiovert 200M inverted microscope, with a 63x/1.4 numerical aperture oil-immersion objective lens, with an Axiocam MRM and Axiovision 3.1 software (Carl Zeiss, Inc.). Additionally, the cells were examined using an Olympus IX-81 inverted microscope, with a100x/1.49 numerical aperture oil-immersion objective lens with an extra 1.6x intermediate magnification lens, with an electron-multiplying charge couple device (EMCCD) camera (iXon 897, Model No: DU-897E-CS0-#BV; Andor).

For super-resolution microscopy, cells were mounted on coverslips and treated as described above. In the case of RC and nucleolar fractions they were spotted onto silane-coated slides (Sigma) as described before [214] and incubated with primary antibodies against DBP (1:50,000) and nucleolin (1:1,500) for 2 h at room temperature. After successive washes with PBS-Tween 0.02% (PBS-T), secondary antibodies coupled to Alexa Fluor 568 or Alexa Fluor 488 (1:1,500 each) were added. Samples were washed with PBS-T and mounted in PBS-10% glycerol and stored at -20ºC. All super-resolution imaging measurements were performed on an Olympus IX-81 inverted microscope configured for total internal reflection fluorescence (TIRF) excitation (Olympus, cellTIRF™ Illuminator). The critical angle was set-up such that the evanescence field had a penetration depth of ~200 nm (Xcellence software v1.2, Olympus soft imaging solution GMBH). The samples were continuously illuminated using excitation sources depending on the fluorophore used. Blue (Alexa Fluor 488)- and yellow (Alexa Fluor 568)- absorbing dyes were either excited with a 488 nm or a 561 nm diode-pumped solid-state laser. Beam selection and modulation of laser intensities were controlled via Xcellence software v.1.2. A full multiband laser cube set was used to discriminate the selected light sources (LF 405/488/561/635 A-OMF, Bright Line; Semrock). Fluorescence was collected using an Olympus UApo N 100x/1.49 numerical aperture oil-immersion objective lens with an extra 1.6x intermediate magnification lens. All movies were recorded onto a 65×65 pixel region of an EMCCD camera (iXon 897, Model No: DU-897E-CS0-#BV; Andor) at 100 nm per pixel. Sub-diffraction images were derived from the Bayesian analysis of the stochastic Blinking and Bleaching of Alexa Fluor dyes [217]. For each super-resolution reconstruction, 300 images were acquired at 37 Hz with an exposure time of 23 ms, at full laser power. The maximum laser power coming out of the optical fiber, measured at the back focal plane of the objective lens, for the 488 nm and the 561 nm laser lines were 23.1 mW and 19.1 mW, respectively. Each of the image sequences was fed into the 3B microscopy analysis plugin of image J [218], considering a pixel size of 100 nm and a full width half maximum of the point spread function of 270 nm (for Alexa Fluor 488) and 290 nm (for Alexa Flour 568), both measured experimentally with 0.17 µm fluorescent beads (PS-Speck™ Microscope Point Source Kit, Molecular Probes, Inc.). All other parameters were set up as the default values. The Three B analysis was run over 200 iterations, as recommended [217, 218], and the final super-resolution reconstructions were created at a pixel size of 10 nm. The spatial resolution observed in our imaging set up by Three B analysis was to approximately 50 nm [219].

Western blot analyses. To analyze the steady-state concentrations of E1B and DBP, RC fractions and Npl were obtained from MK-infected or Ad-infected HFF cells at 16, 24 and 36 hpi. For immunoblotting, gels were transferred onto polyvinylidene difluoride PVDF membranes (Millipore), and incubated as described

previously [76]. Briefly, membranes were blocked for 2 h at room temperature with 3% nonfat milk and incubated overnight at 4ºC with primary antibodies (B6-8, 1:500; 2a6, 1:50). After successive washes with PBS/0.1% Tween20, the membranes were incubated with secondary antibody coupled to HRP for 2 h at room temperature. Membranes were developed by enhanced chemiluminescence as recommended by the manufacturer (Pierce, Thermo Fisher Scientific) and bands were visualized on X-ray films (Kodak).

DNA Replication assay in isolated RC. RC fractions-associated DNA polymerase activity was assayed in duplicate samples from two independent experiments, incubating RC fractions for 30 min at 30ºC in a solution containing 200 mM ammonium sulfate, 40 mM Tris-HCl pH 7.9, 5 mM MgCl$_2$, 3 mM dithiothreitol (DTT), 50 µM of each deoxyribonucleoside triphosphate (dNTP) and 1 mM ATP (modified from [220]). After this time, DNA was purified as described in the DNA Purification section, and DNA synthesis was determined by amplifying a region of the adenoviral genome within the TPL sequence by PCR and for cellular DNA 18S rRNA and U1 snRNA primers were used. The products were amplified for 25 cycles to avoid signal saturation. The amplified PCR products were separated in agarose gels and bands were quantified by densitometry. 100 ng/ml of Actinomycin D (ActD) were used to inhibit DNA replication. Replication assays were carried out using duplicate samples obtained from two independent experiments and data were analyzed by the t-test.

Transcription assay in isolated RC. RC transcriptional activity was assayed in duplicate from two independent experiments, incubating RC fractions for 10 min at 37ºC in a solution containing 200 mM ammonium sulfate, 80 mM Tris-HCl pH 7.9, 2 mM MnCl$_2$, 0.05 mM DTT and 1 mM of each ribonucleoside triphosphate (NTP) (modified from [221]). After this time, RNA was isolated using Trizol reagent as described above, checked for the absence of DNA contamination and RNA synthesis was determined by RT-PCR using viral primers within the TPL sequence and cellular primers for actin mRNA and 18S rRNA. The products were amplified for 20 cycles to avoid signal saturation. 25 µg/ml of Actinomycin D (ActD) were used to inhibit transcription. Transcription assays were carried out using duplicate samples from two independent experiments and analyzed by the t-test.

Splicing assay in isolated RC. Splicing activity associated to RC fractions was assayed in duplicate from two independent experiments, incubating the fractions for 90 min at 30ºC in a reaction containing 1 mM ATP, 20 mM creatine phosphate (CP), 3.2 mM MgCl$_2$, 0.25 U/µl of RiboLock (ThermoScientific), 1 mM DTT, 72.5 mM KCl and 12 mM Hepes-KOH pH 7.9 (modified from [222]). After this time, RNA was isolated, checked for the absence of DNA contamination and pre-mRNA splicing was determined by RT-PCR using primers that hybridized on splice junctions within the TPL (for viral mRNA) and within the actin mRNA (for cellular mRNA). The products were amplified for 25 cycles to avoid signal saturation. 500

37

μM erythromycin (Ery) was used to inhibit splicing, as previously reported [223]. Splicing assays were carried out using duplicate samples from two independent experiments and analyzed by the t-test.

DLS. Dynamic light scattering of Ad WT, E1B⁻, E1B PM and MK RC particles was carried out in a Malvern Zetasizer Nano SP instrument at 4ºC. The S2 viscosity coefficient at 4ºC calculated using a Rheometer was 1.88 Ns/m². The refractive index calculated for S2 was 1.3504. Three measurements were performed for each sample, with 12 reads of 10 s per each measurement. The values of correlation coefficient (CC) per time (μs), intensity per size (d:nm) and volume per size were plotted. The hydrodynamic diameter was calculated by the Stokes-Einstein equation:

$$d(H) = \frac{kT}{3\pi\eta D}$$

where:
d(H) = hydrodynamic diameter
D = translational diffusion coefficient
k = Boltzmann's constant
T = absolute temperature
η = viscosity

Ellipse adjustment for the automatic detection of viral RC. An automatic, deterministic, non iterative, algorithm we recently developed to simultaneously detect multiple viral RC by adjusting ellipses was used to compare the area of RC in Ad WT, E1B⁻ or E1B PM-infected cells. Details about the algorithm as well as validation procedures are described in [224].

RNA extraction and cDNA library preparation for RNA next generation sequencing. Total RNA from RC fractions isolated at 36 hpi from Ad-infected HFF cells was extracted as described above. The quality of the total RNA was checked with Bioanalyzer using the RNA nano Chip from Agilent Technologies. The sequencing libraries were generated with the ScriptSeq v2 RNA Seq Kit from Epicenter. The quality check of libraries (size and quality) was visualized on a BioAnalyzer High Sensitivity DNA Chip (High Sensitivity DNA Kit from Agilent Technologies). The cDNA libraries were sequenced on the Illumina HiSeq 2500 system.

Computational analysis for RNA sequencing. In order to map the splice sites for Ad5, the H5pg4100 genome (Ad WT virus that lacks a portion of E3, including the z-leader [200]), was aligned to the Ad2 genome annotated sequences (NCBI AC_000007.1). FASTQ files were aligned to the human genome, and these sequences were removed for this analysis from the FASTQ file. Using strand specific FASTQ files, the reads were aligned using Bowtie2 aligner [225] to exon-exon junctions between leaders 2-i, i-3 and 2-3, as well as the exon-exon junctions

38

for fiber mRNA (x, y and fiber). The quantification of reads aligned to the exon-exon junction was done using the tool Multicov, within the Bedtools package, considering at least 10 nucleotides of overlap in the exon-exon junctions.

ESI-QTOF analysis of RC. RC fractions from HFF cells infected with the Ad WT, E1B$^-$ or E1B PM mutant viruses were analyzed by mass spectrometry. RC were centrifuged at 14,000 rpm for 30 min at 4 ºC. The RC pellet was washed with buffer Tris-HCl 10 mM, pH 7.4/ 0.5 mM MgCl$_2$ and centrifuged at 14,000 rpm for 30 min at 4 ºC. The pellet was resuspended in 500 µl 9 M urea/50 mM NH$_4$CO$_3$ and stored at -80 ºC. The samples were shipped in dry ice to Birmingham University, UK to be analyzed by an ESI-QTOF mass spectrometer. The samples were trypsin digested, HPLC purified and analyzed by ESI-QTOF ("Electronspray ionization quadrupole time-of-flight"). The peptide identification was made using Mascot and ProteinScape 3.0.

MS Analysis of Isobaric Tagged Samples. RC pellets were resuspended in lysis buffer (0.1M ammonium bicarbonate, 2.5%(w/v) sodium deoxycolate, 10mM pH neutral TCEP (tris(2-carboxyethyl)phosphine), 40mM choloroacetamide (CAM) and protein concentration was measured by BCA protein assay. Chloroacetamide was quenched with 40mM cysteine and 100 mg of proteins were diluted 1:2.5 in water containing 2 mg of MS-grade trypsin for overnight digestion at 37 ºC. Ethyl acetate was added at a 1:1 ratio and mixed for extraction of detergents. The aqueous phase was collected for C18 Stage-Tip clean-up (3M Analytical Biotechnologies) by adjusting the peptides to 0.5% trifluoroacetic acid (TFA) to bind them to the column, washing with 0.5% TFA, and eluting in 70% ACN/0.1% TFA in water. TMT labeling of each sample was performed using the TMT sixplex label set (40 mg TMT in 50mM HEPES buffer, pH 8.0) for 1hr. TMT was quenched with hydroxylamine, and peptides were subject to 2-dimensional off-line fractionation by sequential StageTip as described next. TMT-labeled peptides were acidified to a final trifluoracatic acid (TFA) concentration of 0.5% (v/v) and bound to a StageTip containing C18 discs on top and Cation Exchange-SR (SCX) (3M Analytical Biotechnologies) discs on the bottom for fractionation by cation exchange chromatography. Samples were washed with 0.5% TFA and eluted from the C18 discs to the SCX discs with 80% acetonitrile (ACN) /0.5% formic acid (FA). Peptides were eluted in four fractions (A to D) with the solutions shown in the table below. The eluted peptides were concentrated in a Savant SpeedVac to remove the ACN and were bound to a StageTip containing SDB-RPS discs (3M Analytical Biotechnologies). The column-bound peptides were washed with 0.2% TFA, and eluted in four fraction (1 to 4) with the solutions shown in the table below. Since the fractionation was not fully orthogonal, the following fractions were pooled as they contained less peptides than the rest: A3 with A4, C1 with C2, and D1 with D2. Samples were concentrated to remove ACN and diluted into 1% FA / 2% ACN for MS analysis. Samples were analyzed by nLC-MS in a Dionex Ultimate nRSLC

39

coupled to an LTQ-Orbitrap Velos (Thermo Fischer). Peptides were separated in a 150 min reverse-phase gradient. The mass spectrometer was operated in data-dependent acquisition with dynamic exclusion enabled (repeat count = 1; exclusion duration = 45 s). Full scan range set to 400-1700 m/z with a resolution of 30,000 at m/z = 400 in the Orbitrap. HCD fragmentation was performed for the top 10 most intense precursors with minimal signal of 1E4 in the IT. Isolation window set to 1.2 Th, normalized collision energy of 40, and activation time of 0.1ms. Target values for FT full-scan MS and IT MS2 were 1E6 and 5E4, respectively. The composition of elution Buffers for Peptide-Based Fractionation were as shown in Table 4.

Table 4.   Elution Buffers for Peptide-Based Fractionation

Fraction	Buffer composition
A	0.05M ammonium formate, 20% acetonitrile
B	0.05M ammonium acetate, 20% acetonitrile
C	0.05M ammonium bicarbonate, 20% acetonitrile
D	0.1% ammonium hydroxide, 20% acetonitrile
1	0.15M ammonium formate, 50% acetonitrile, 0.5% formic acid
2	0.2M ammonium formate, 60% acetonitrile, 0.5% formic acid
3	0.2M ammonium formate, 60% acetonitrile, 0.5% acetic acid
4	5% ammonium hydroxide, 80% acetonitrile

Protein Identification and Quantification. The peptide identification and quantification of the TMT dataset was performed in Maxquant version 1.5.2.8, (Cox and Mann, 2008). To identify peptides, spectra were searched against the human subset of the UniProt protein sequence database, appended with adenovirus type 5 sequences and common sample contaminants. PSM and protein identification probabilities were set to an FDR of 1%, using reverse decoy sequences. For label-free quantification, protein iBAQ values were extracted for downstream analysis in R v3.2. PSMs were included if they met the following criteria: isolation specificity > 0.85, < 4 missing TMT reporter ion values, unique peptide, and a PEP < 0.05. TMT reporter ions were normalized to the sum of all channels, and protein-level relative quantification was obtained as the median from all PSMs assigned to a protein. Proteins with 2 or less peptides or a coefficient of variation > 50% for TMT channels were excluded.

5   RESULTS

5.1   E1B is necessary for establishment and progression of viral gene expression *(manuscript in preparation)*.

Most of the studies of adenovirus gene expression have been performed in established human cell lines, which have several limitations, such as impaired cell cycle regulation, an abnormal genotype and alterations in growth and metabolism. Moreover, the viral replication cycle lasts approximately only 24 h, where the early phase comprises the first 6-8 h of infection [226]. A time course analysis of cellular gene expression during the infection of normal human cells has been reported [227], but the expression kinetics of viral genes at various times post-infection that span the entire viral replication cycle are limited and, as mentioned before, have been performed in transformed cells [18, 58, 158, 228, 229]. Additionally, most of these experiments were not quantitative and relied on densitometry techniques. Such is the case of northern blots, dot blots, pulse-chase and run-on assays using radioactive labels which were used to determine the level and temporal expression of viral genes [18, 58, 158, 228, 229]. These studies need to be complemented with temporal studies of mRNA expression in cells with an unaltered cell cycle. In adenovirus-infected normal human cells, such as the human fibroblasts used in this study, the viral replication cycle, from adsorption to initial viral progeny production lasts 36 h. However, cell lysis is observed until 48 hpi. The initial accumulation of viral DNA can be detected from 20-24 hpi [77]. These cells allow the study of cellular changes due solely to the viral infection, and provide a larger window of time to analyze viral gene expression since entry into the late phase and cell lysis are delayed, compared to cell-lines [77]. Moreover, novel, more sensitive and quantitative techniques, such as, quantitative RT-PCR should allow for a more accurate measurement of mRNA levels.

5.1.1   Measurement and analysis of adenovirus early and late gene expression at multiple time-points during the viral replication cycle in Ad-infected HFF cells.

To determine the kinetics of viral gene expression, viral early and late mRNA species that comprise most viral transcription units were measured by qRT-PCR, at early (4, 6, 8, 12 and 16 hpi) and late (20, 24, 28 and 36 hpi) times post-infection (Fig. 6). The data were obtained from two biological experiments measured in triplicate using RNA extracted from total lysates of Ad WT, E1B$^-$ or E1B PM-infected HFF cells. The mean values where plotted vs. time post-infection (Fig. 6 A and C) and box-plots from these measurements were included for statistical description of the data distribution (Fig. 6 B and D). The statistical difference for

each gene between 2 continuous time-points was validated using a Kolmogorov-Smirnov test (non-parametric test that quantifies a distance between two empirical distribution functions) [207, 230]. The results related to the Kolmogorov-Smirnov statistical test are presented in Figure S1 in Supplementary Information.

Our data provide, for the first time, the overall kinetics of early and late gene expression throughout an entire viral replication cycle (from 4 hpi to 36 hpi). As expected, the results confirmed previously established information, as the E1A mRNA were the first viral transcripts to be synthesized, followed by synthesis of E4, E2A and E1B, and latter, IVa2 and E2B mRNA (Fig. 6A and B). Moreover, the expected increase in viral late mRNA levels after initiation of viral DNA synthesis was also observed. However, our data also provide details and new insights into the time, chronological order and level of expression of the early and late genes: For example, the E2A-DBP mRNA showed a close to 200-fold increase from 8 to 16 hpi, while E4Orf6/7 reached a maximum that was much lower and decreased after 12 hpi, suggesting that the high levels of E2A expression, which should correlate with production of the E2A-DBP protein, a known repressor of E4 [51], result in down regulation of the E4 promoter. In addition, the high levels of expression of E1A, E2A-DBP and IVa2 correlated with the initial expression of the MLTU. Since the products of these genes are known to act as transcriptional activators of the Major Late promoter (MLP) [51, 58], these results confirm that this experimental approach can be used to correlate the pattern and level of expression of early genes that are known to regulate early or late promoters on the level of expression of their target genes, and therefore to study the regulation of the viral gene expression program.

Two novel and potentially significant observations on the chronological order of gene expression could be drawn from the data: i) The unexpected increase in IVa2 levels before the onset of viral DNA replication (Fig. 6A, B and E). It has been reported that in HeLa cells an unidentified cellular repressor inhibits IVa2, but the repressor is titered by the accumulation of IVa2 and by newly synthesized viral DNA molecules during the transition to the late phase [74]. Our data indicate that in normal human cells (HFF) the regulation of IVa2 expression by DNA synthesis-dependent titration does not occur. ii) The L4-22K and 33K, L5 and L1-pIIIa, were all synthesized, albeit at lower levels, before the onset of viral DNA replication, at around 16 hpi (Fig. 1B and D). As described above, previous reports, using transformed cell lines have shown that the only late mRNA produced during the early phase is that of L1-52/55K [19]. Production of the L4-22K and 33K mRNA could result in more efficient progression of the replication cycle to the late phase, as these proteins participate in activation of MLP and regulation of mRNA splicing [35].

The transition to the late phase, between 16 and 20 hpi, was clearly evidenced by an initial 8-fold increase compared to the input DNA at 4 hpi (Fig. 6 E). As E2

mRNA levels increase, each viral genome being transcribed can in principle be replicated; however, whether ongoing transcription of viral genes is modulated or otherwise affected by DNA replication has not been addressed. Interestingly, at 20 hpi a decrease in the levels of all transcripts was measured (Fig. 6 A-D), with the most prominent changes (10-fold) measured for E2A-DBP, E2B-pol, IVa2 and L1-pIIIa mRNA. In human primary lung fibroblasts infected with adenovirus, the period from 12 to 24 hpi, prior to viral DNA replication in those cells, is linked to an increase in expression of cellular genes involved in cell cycle regulation, necessary to induce the infected cell to enter S-phase and therefore, facilitate viral DNA replication [227]. These results suggest that during the transition to the late phase of infection, down-regulation of viral mRNA accumulation is required, possibly due to a preferential use of the transcription machinery on cellular genes that are necessary to induce the cell to enter the S-phase. An alternative explanation, not necessarily mutually exclusive, is that down-regulation of all viral mRNA synthesis is required to allow for efficient DNA replication.

The data obtained provide the most complete analysis of the program of expression of the adenoviral genome and the results show that these data can be used to make specific predictions that can be tested with experiments for detailed analysis of the role of each viral gene product on regulation of gene expression at the level of mRNA.
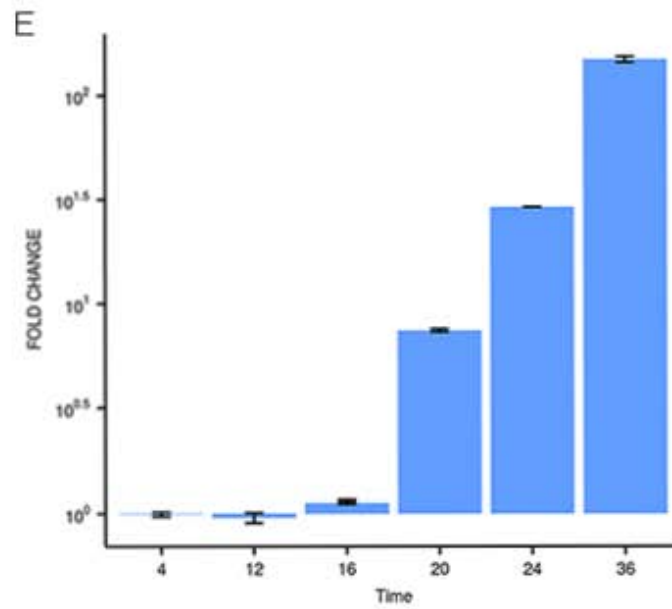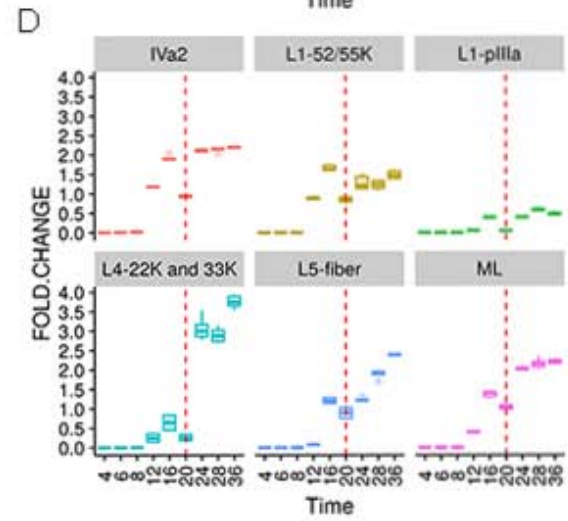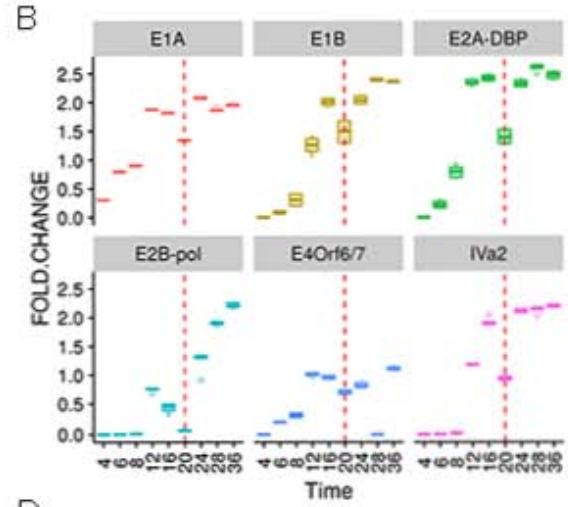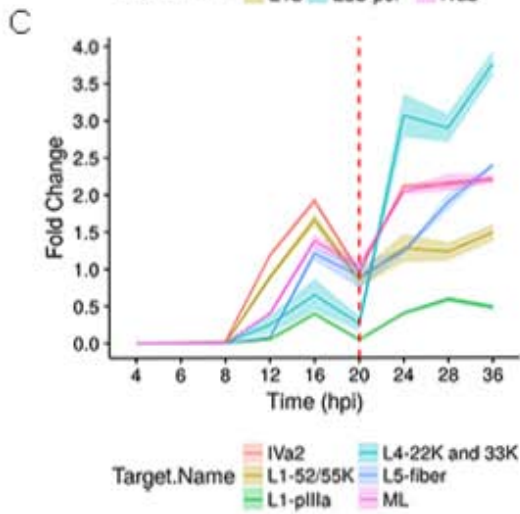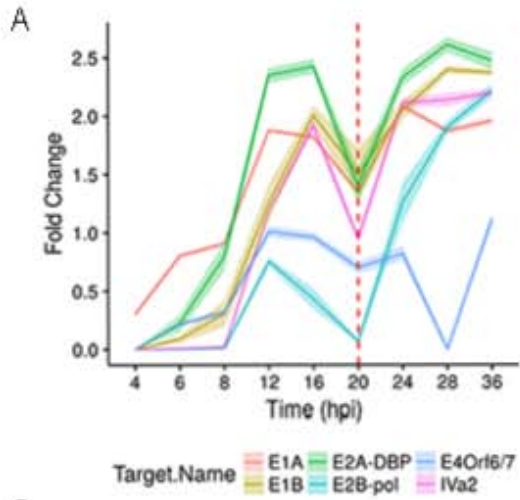
Figure 6. **Steady-state levels of viral early and late mRNA at different times post-infection.** Total RNA from HFF cells infected with Ad WT adenovirus was measured by quantitative RT-PCR to determine the steady-state levels of the indicated viral mRNAs at different times post-infection. A and B. Semilogarithmic plots of the mean fold-change (A) or box-plot (B) of viral early mRNA at various time-points. C and D. Semilogarithmic plots of the mean fold-change (A) or box-plot (D) of viral late mRNA at the indicated time-points. E. Semilogarithmic plot of the mean fold-change of the steady-state levels of viral DNA extracted from total lysates of Ad WT-infected HFF at the indicated times post-infection. The mean values are the result from two biological replicates, with internal triplicates.

Taking into account the slope between the mean values of two continuous time points, a hierarchical cluster analysis was developed to analyze which genes have a similar accumulation pattern in each phase of the viral replication cycle (Fig. 7). The hierarchical clustering maps are presented as dendrograms on the heatmaps, at early (Fig. 7A) and late (Fig. 7B) times post-infection. The dendrograms indicate the following conglomerates: At early times of infection (Fig. 7A) the genes were grouped in two clusters. E1A was grouped with E2 (pol and DBP) and E4Orf6/7, while E1B and IVa2 grouped with late mRNA. In contrast, at late times, the mRNA formed two clusters (Fig. 7B); one occupied exclusively by L4-22K and 33K mRNA, and the other further grouped in two clusters, where one was occupied by E4Orf6/7 and all the other mRNA occupied the second cluster. The latter was further grouped in two clusters, where IVa2 clustered with the E2 mRNA, E1B with L5 and L1-pIIIa and E1A with L1-52/55K. These conglomerates are in agreement with previous reports that have established the program of gene expression changes between the early and late phases, as described in the introduction. However, they also provide novel insight into the complex networks that regulate viral early and late genes throughout the replication cycle. For example, while the data confirm that a loop exists for regulation of E2 (pol and DBP) expression that implicates E1A and E4Orf6/7 [53], the data also indicate that a novel regulatory loop is established between E1B and IVa2 in the regulation of the viral late mRNA. For the late phase the conglomerates confirm that accumulation of L4-22K and 33K determine the full activation of expression of viral late genes, which may be influenced by IVa2 in the DNA-replication dependent transition to the late phase (E2), and a cross-talk between E1A and E1B for the transition in the production of the early L1-52/55K to the late L1-pIIIa mRNA and the full activation from the MLP that results in the production of the L5 mRNA. Taken together, the results suggest these data can be used to make specific predictions on the role early genes play on regulation of viral genome expression. One such prediction is that E1B may participate in the regulation of expression of both early and late viral genes

45
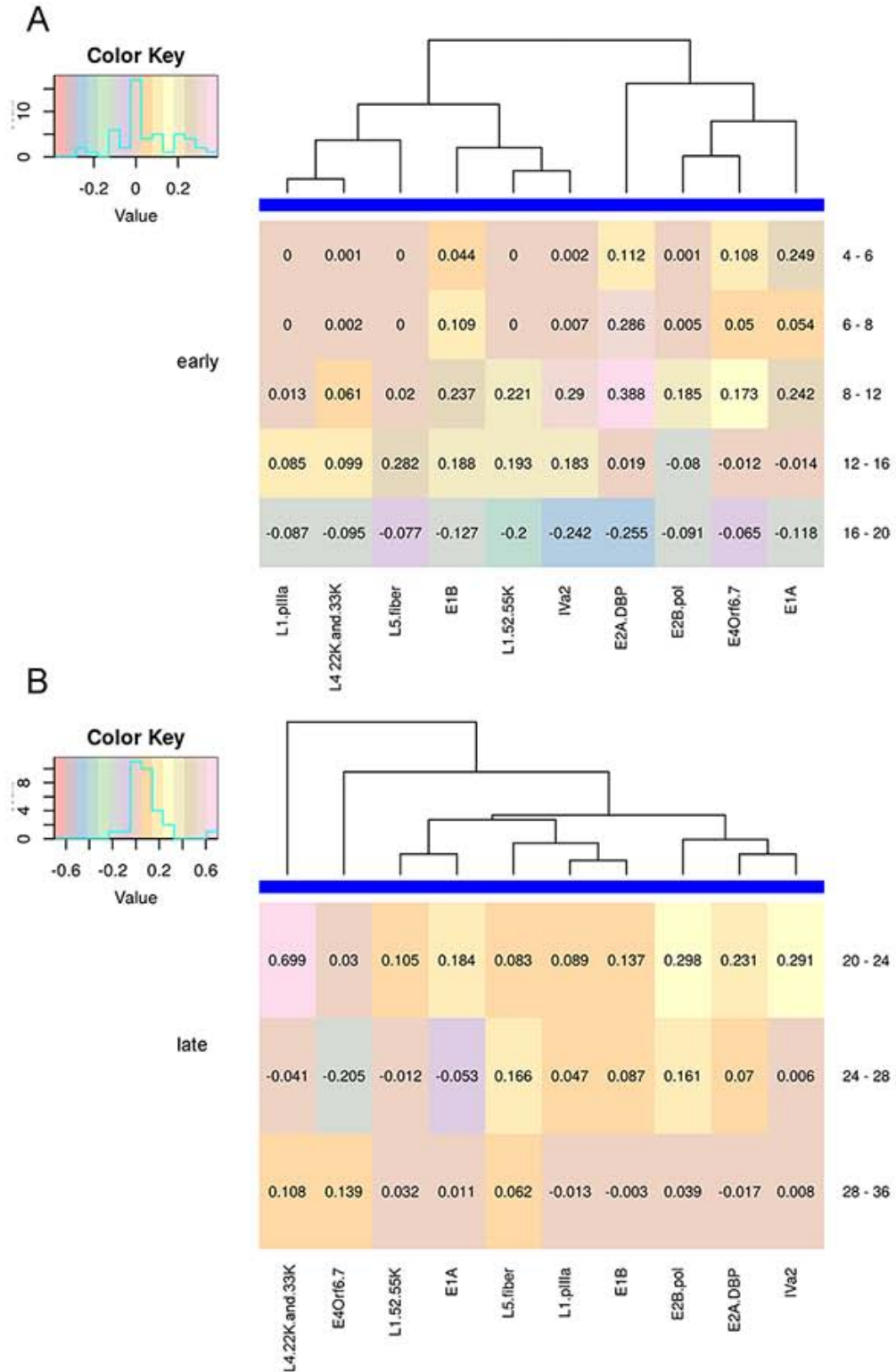
Figure 7. **Hierarchically clustered heatmap of Ad WT mRNA.** The heatmaps are presented as dendrograms at early (A) and late (B) times post-infection for all viral mRNA measured by qRT-PCR from Ad WT-infected HFF cells.

5.1.2 E1B 55K regulates expression of viral early and late genes

To analyze if E1B impacts the accumulation kinetics of different viral mRNA, we used the same experimental approach as above. Viral early and late mRNA were measured at multiple time-points during the viral replication cycle in HFF cells infected either with Ad WT or with the E1B⁻ or E1B PM mutant viruses described above (Fig. 8). Interestingly, the results showed that IVa2 mRNA accumulated earlier in E1B PM-infected cells than in Ad WT-infected cells, while in the absence of E1B, IVa2 mRNA was delayed and reached lower levels. The same observation was made for the down-regulation of IVa2 observed at the transition from the early to late phase. These results suggest that phosphorylation of E1B promotes efficient expression of IVa2, which correlates with anticipated synthesis of viral DNA (Fig. 8B) and efficient expression of viral late genes. Furthermore, even in the absence of E1B, IVa2 expression began before viral DNA replication, indicating that E1B is not necessary for synthesis of this intermediate viral mRNA.

Unexpectedly, during the late phase, a 2-fold increase in E1A mRNA was observed when E1B was absent, while the phenotypes observed for E1B PM were similar to those of Ad WT, suggesting a potential role of E1B as an E1A-repressor during this phase. In addition, the results showed that phosphorylation of E1B resulted in a decrease in the accumulation of E1A, E4Orf6/7, L1-52/55K and E2A-DBP at early times, and of E2A-DBP mRNA at late times, suggesting that in the constitutively phosphorylated state, E1B may work as a repressor also for these genes.

A significant finding was that most of the viral mRNA levels were reduced at 16 hpi, in cells infected with the E1B PM mutant virus (Fig. 8A and Fig. S2a in Supplementary Information), in contrast to the observed decrease at 20 hpi during infection with Ad WT. Since for E1B PM, viral DNA synthesis initiates at 16 hpi (Fig. 8B), these results indicate that phosphorylation of E1B correlated with the anticipated synthesis of viral DNA and transition to the late phase. In contrast, decreased mRNA levels, concomitant with the onset of viral DNA replication, were not observed in the absence of E1B, suggesting that E1B is necessary for the temporal regulation of different viral genes at different times of the viral replication cycle and for the control of viral gene expression during the transition between the early and late phases of infection. Figure S3a-b and Figure S4a-g (Supplementary Information) show the boxplots for each virus at different times post-infection.
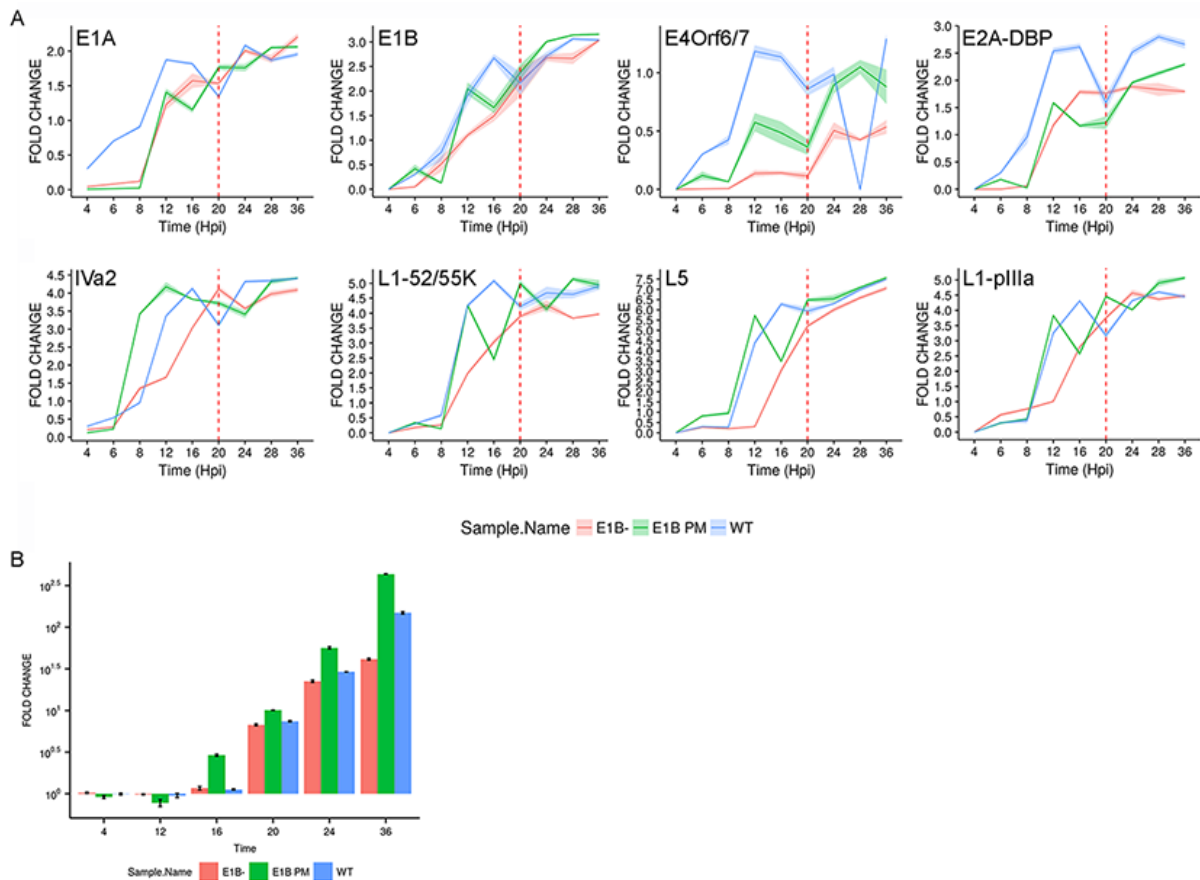
Figure 8. **Kinetics of viral early and late mRNA through different times of the replication cycle.** A. Total RNA from HFF infected with Ad WT, E1B⁻ or E1B PM viruses was used to quantify the indicated viral transcripts at different times post-infection. B. Semilogarithmic plot of the accumulation of viral DNA in Ad WT, E1B⁻ or E1B PM-infected HFF at different times of the replication cycle. The mean values are the result from two biological replicates, with internal triplicates.

The measurements were validated by hypothesis tests. For each gene Kolmogorov-Smirnov test were applied to compare the empirical distribution functions of two samples. Ad WT was compared with each of the mutant viruses (Ad WT~E1B⁻ and Ad WT~E1B PM) for all the viral mRNA in the early and late phases. When Ad WT was compared to E1B⁻, significant differences were found for all viral mRNA in the early phase, while in the late phase only the comparison for L5-fiber and L1pIIIa mRNA were not significant. This indicated that there is not enough data for these two transcripts to ensure that the distributions of WT and E1B⁻ are different (at least for a confidence level = 0.05, see Materials and Methods). The comparison between Ad WT and E1B PM showed less statistical significance between the mRNA. In the early phase, there was no sufficient evidence for significant differences in L4-22K and 33K mRNA, L1-pIIIa and L1-5255K, and this was also the same case for L4-22K and 33K mRNA, IVa2, E4Orf6/7 and E1A during the late phase. The information relative to the p-values

for each of the hypothesis tests performed is available in Fig. S5 (Supplementary Information).

5.1.3 Phosphorylation of E1B 55K promotes viral mRNA stability

The experiments described in the previous two sections allowed measurement of mRNA steady-state levels, which can be influenced by both transcription rates or mRNA stability. In order to determine if E1B can affect viral mRNA stability, we measured viral early and late mRNA half-lives (Fig. 9). Triptolide is an irreversible inhibitor of the TFIIH subunit XPB and induces proteasome-degradation of RNA-pol II. Therefore, we used triptolide in infected cells to measure the stability of E1A (Fig. 9A) and L5 (Fig. 9B) mRNA (representatives of an early and a late mRNA) during the late phase of infection. In Ad WT-infected cells, E1A mRNA displayed a half-life close to 3 h. When E1B was absent, E1A mRNA half-life decreased to less than 2 h, while in E1B PM-infected cells the stability increased almost 2 h compared to Ad WT (Fig. 9A). In the case of L5, in Ad WT-infected cells, the mRNA half-life was 2 h, and a mild decrease in stability was observed in the absence of E1B (half-life=1.5 h), while the stability increased in E1B PM (half-life=2.5 h). The levels of L5 mRNA in the E1B^{-} virus showed a steep drop to almost undetectable levels by the first 4 h of triptolide treatment, while in Ad WT and E1B PM infected cells, even 12 h after RNAPII inhibition, L5 mRNA were still detected (Fig. 9B). These results show that E1B impacts mRNA stability, with a greater effect on the half-life of early mRNA (E1A) than on late mRNA (L5).
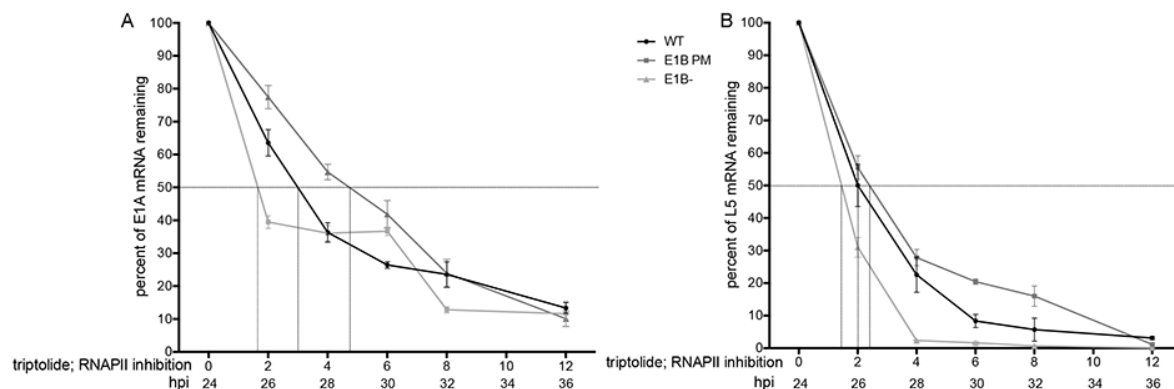
Figure 9. **Stability of E1A and L5 mRNA after treatment of HFF with triptolide at late times of infection.** HFF cells were infected with Ad WT, E1B^{-} or E1B PM viruses. At 24 hpi, cells were treated with the RNA pol II inhibitor, triptolide, and RNA was extracted at the indicated times post-treatment. The relative quantities of mRNA specific for E1A or L5 were measured by qRT-PCR and plotted against time. The mean values are the result from two biological replicates, with internal triplicates.

49

5.1.4 E1B 55K has repressive and/or enhancing roles on different viral promoters

As described in the introduction, the adenoviral gene expression program depends on the orderly regulation of a variety of promoters. The E1A promoter is constitutively active and participates in the activation of all viral promoters, in combination with the viral and cellular transcription factors described in Table 1. To determine if E1B may activate viral promoters, reporter assays using luciferase gene expression directed by several viral promoters were performed (Fig. 10). The effect of E1B on the activation of viral promoters was measured without the presence of other viral molecules (in transfection assays) or in the context of viral infection (in transfection + infection with the E1B⁻ mutant virus). The assays where performed at 8 hpi (early time) and at 24 hpi (late time) in the easily transfectable cell line H1299. A clear effect of E1B on various promoters was obtained.

The E1B in a constitutively phosphorylated state (E1B PM) resulted in lower levels of expression from E1A, pIX and E4 promoters at the early time of infection, as well as pIX and ML promoters at the late time (Fig. 10). The repression of both of these promoters was induced in the absence of other viral molecules, in Ad WT E1B transfected-cells. In contrast, the phosphorylated form of E1B resulted in the activation of its own promoter and the E2 late promoter (E2L), both in the absence of other viral molecules or during the early and late times of infection. E1B was also able to induce activation of E2 early (E2E) promoter, but only in the context of infection. E1B PM resulted in the activation of the E3 promoter in the absence of other viral molecules, while in the context of the late phase of infection E1B PM correlated with the activation of E3 and E4 promoters. Taken together, the results from these and the mRNA half-life experiments show that E1B can impact viral mRNA synthesis and stability, and that this viral early protein may act as a differential transcriptional repressor or enhancer on viral early and late promoters.

E1A promoter

E1B promoter

E2E promoter

E2L promoter

E3 promoter

E4 promoter

pIX promoter

ML promoter

Prom	+	+	+	+	+	+	+	+	+
pE1B WT	-	+	-	-	+	-	-	+	-
pE1B PM	-	-	+	-	-	+	-	-	+
H5pm4149	-	-	-	+	+	+	+	+	+

8 hpi   24 hpi

51

Figure 10. **Dual luciferase assays to evaluate viral promoter activation.** H1299 cells were transfected with the specified promoters cloned in the pGL3-Basic vector and co-transfected with Ad WT or E1B PM expressing plasmids, analyzed for luciferase activity at 48 hours post-transfection (hp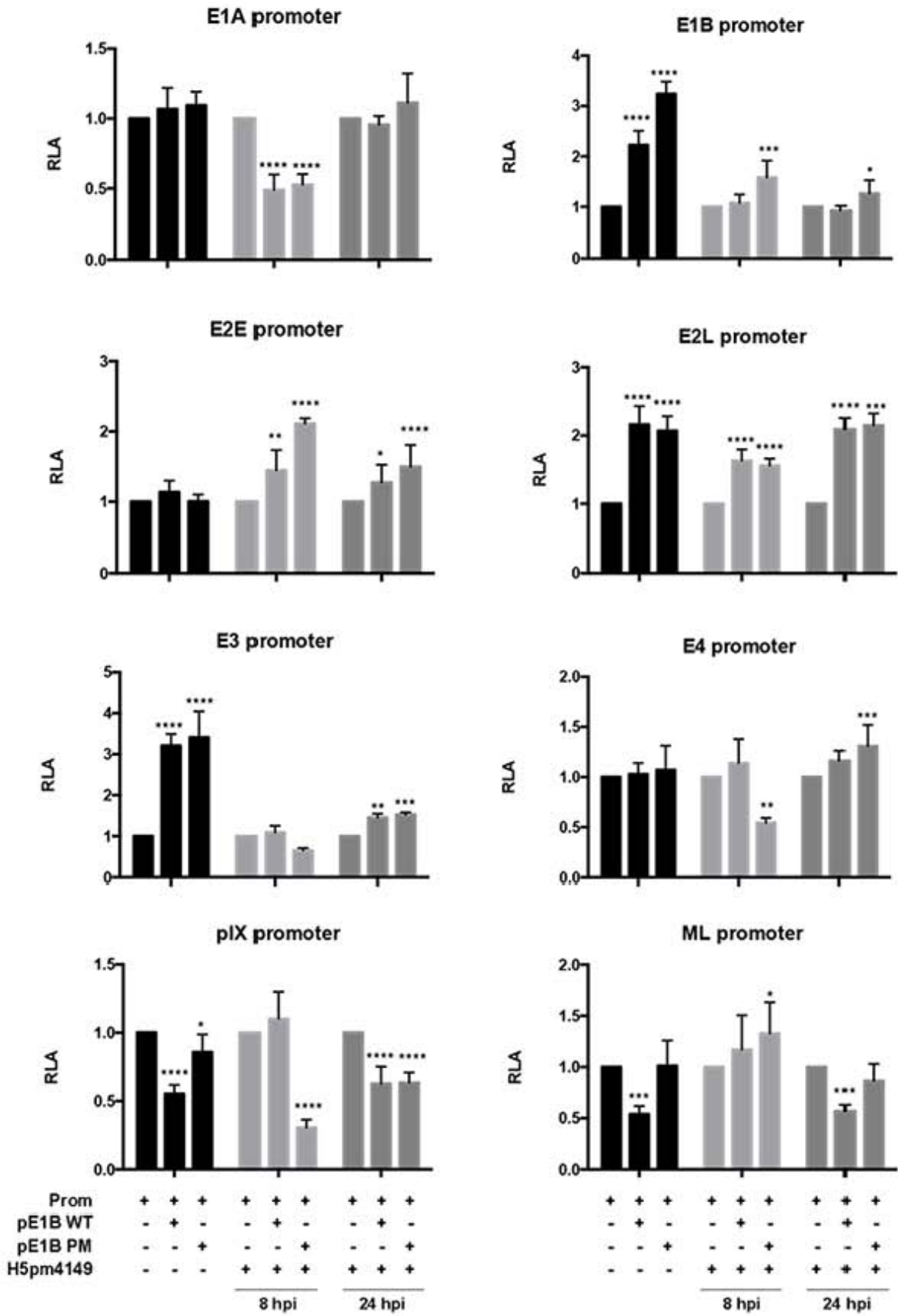t). In addition, these conditions were analyzed in the context of infection at 8 and 24 hpi. The firefly luciferase signal was normalized against Renilla luciferase signal to yield the relative luciferase activity (RLA). The H5pm4149 virus is null for expression of E1B, as described above and in materials and methods. The mean values are the result from three biological replicates, with internal triplicates.

5.1.5 E1B 55K can either repress or enhance viral gene expression at different time-points of the viral replication cycle.

To further examine the effect of E1B and the effect of the protein's phosphorylation on viral gene expression, a linear regression analysis was made to compare the expression of each gene measured by qRT-PCR dependent on the expression of E1A (Fig. 11, see Materials and Methods section and Supplementary Information text), as a general transcriptional activator of all adenoviral genes, for Ad WT, E1B⁻ and E1B PM.

The analysis was divided into early and late times of infection. A total of 66 linear regression models were adjusted (see Materials and Methods). Specific information and validation details about each model are presented in the Supplementary Information (Figures S9-S19 and Table S1). To analyze the data the slopes of the linear regressions were compared for each gene. Good linear regression adjustments were obtained in 60 of the 66 models, showing they are useful to predict the expression of viral genes in early and late times of infection, depending on E1A expression levels. In correlation with the results from the viral promoter assays (Fig. 10), it was found that accumulation of E1A, as well as L1-pIIIa mRNA increased in the absence of the E1B protein, confirming that E1B can repress both the E1A and ML promoters. Moreover, this analysis also confirmed that E1B enhances expression of IVa2 and that phosphorylation of E1B results in higher levels of IVa2 expression (Fig. 11E), as shown in the experiments in section 5.1.1.

Interestingly, higher than 30% reductions in accumulation levels were observed during the early phase for E4Orf6/7, E2B-pol, IVa2, L1-52/55K, L1-pIIIa, L4-22K, L4-33K and L5, while during the late phase only E2B-pol, E2A-DBP, L4-22K and L4-33K varied to similar extents in the absence of E1B. These data further indicate that E1B exhibits distinguishable effects on different viral late mRNA at different times post-infection. For example, while phosphorylation of E1B correlated with increased L1-pIIIa levels during the early phase, Ad WT E1B resulted in down-regulation of L1-pIIIa in the late phase. In contrast, L5 mRNA accumulation depends on E1B, regardless of the time of infection.
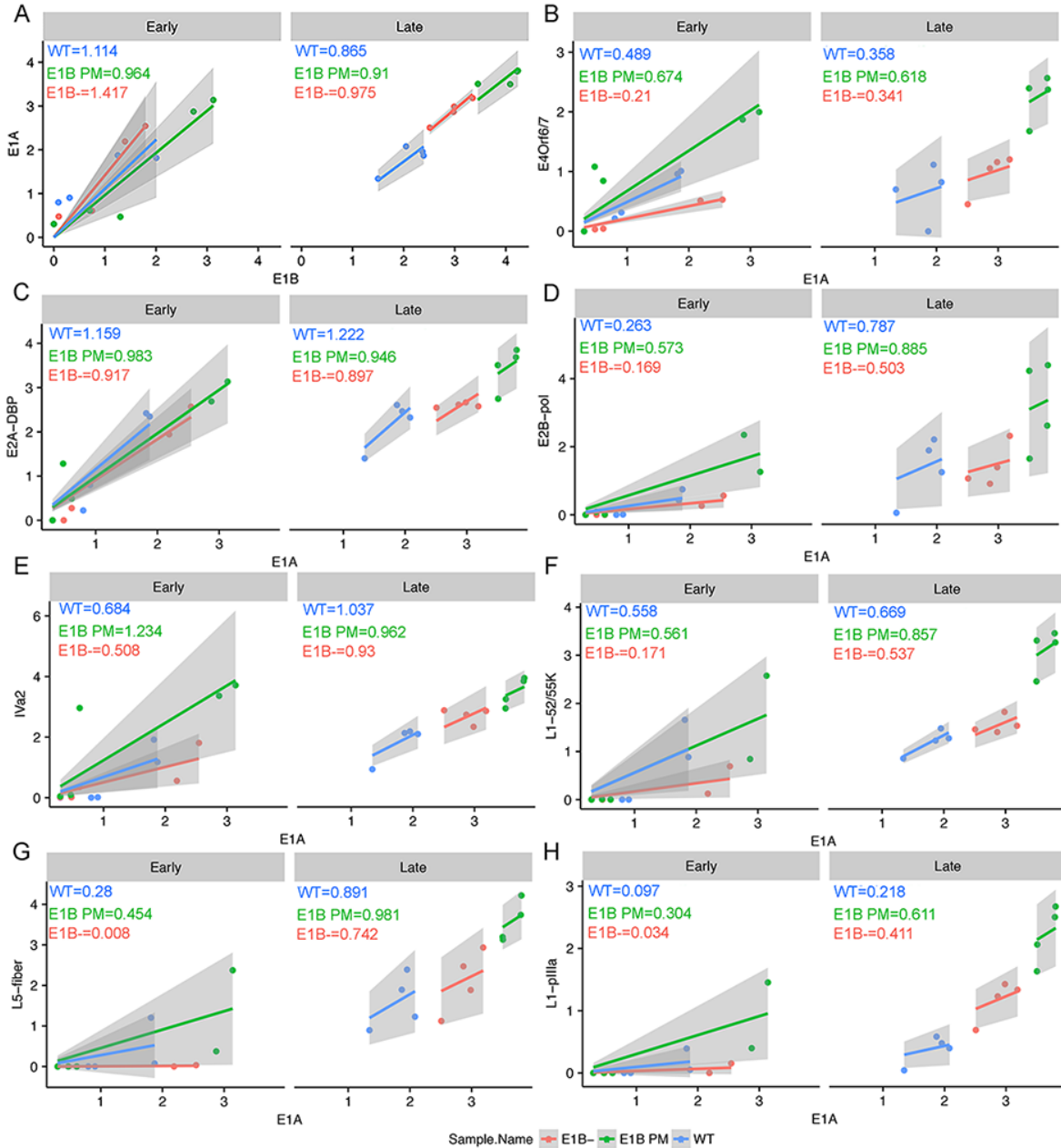
Figure 11.   Linear regression analysis of the expression of viral mRNA. Viral early and late mRNA accumulation was compared dependent on the level of the E1A mRNA, except for E1A mRNA, which was compared dependent on the accumulation of E1B mRNA. The analysis was divided in early (4, 6, 8, 12 and 16 hpi) and late (20, 24, 28 and 36 hpi) times. The gray shade represents a pointwise 95% confidence interval on the fitted values. The values in the top left corner are the slopes of the linear regression model for each case. The rest of the linear regressions are shown in Fig. S6-S8 in the Supplementary Information.

53

Taken together, the results included in section 5.1 show that E1B can repress or enhance expression of viral genes, and that these activities depend on the time post-infection, and on the modification of the protein by phosphorylation.

A summary of the results from sections 5.1.4, 5.1.5 in combination with proteins known to regulate viral promoters (described in Table 1) is shown in Table 5.

Promoter	E1B regulation on viral promoter*		mRNA	E1B regulation on mRNA levels (Compared to WT)*				Enhancers	Repressors	References
	Early	Late		Early		Late				
				E1B PM	E1B⁻	E1B PM	E1B⁻			
E1A	-	n. c.	E1A 13S	n. c.	+	n. c.	n. c.	cAMP, pIX, E1A	E1A, E1B-19K	[31, 42-45].
E1B	+	+	E1B-55K	+	n. c.	n. c.	n. c.	E1A, E1B-19K, Sp1, TFIID		[44, 46]
E4	-	+	E4Orf6/7	+	--	++	n. c.	E1A, pIX, cAMP, E4F, ATF2, E1B-19K	DBP, E4Orf4	[31, 43, 47, 48]
E3	-	+		n. d.		n. d.		E1A, TNF-α, NFκB, NF-1, AP-1, ATF, E1B-19K		[44, 49, 50]
E2E	+	+	E2A-DBP	-	-	-	-	E1A, PML-II, E2F, E4Orf6/7, ATF, TBP, DBP, E1B-19K		[44, 51-55]
E2L	+	+	E2B-pol	+++	-	n. c.	-	YB1 and CTCF	E1A	[56, 57]
IVa2	n. d.	n. d.	IVa2	++	-	n. c.	n. c.	E1A, TFIID, TBP, MLTF	IVa2-RF	[53, 58-60]
pIX	-	-		n. d.		n. d.		E1A, E1B-19K, E4, SP-1, TFIID, L4-22K		[33]

L4	n. d.	n. d.	22K and 33K	+++	--	-	--	E1A, p53, E4Orf3, IVa2	L4-33K, TFII-I	[34, 61, 62]
ML	+	-	L1-52/55K	n. c.	--	+	-	E1A, pIX, DBP, IVa2, USP, TFIID, USF1, CP-1, CTCF, MLTF, MAZ, Sp1, TBP, L4-22K, L4-33K	L4-22K+Sp1 on R1	[31, 51, 56, 59, 63-67]
			L1-pIIIa	+++	--	+++	--			
			L5-fiber	++	---	n. c.	-			

∗ in this study; n. c. (no change); n. d. (not-determined);

Promoters: + (enhancement); - (repression)

mRNA levels: + (20-40% enhancement); ++ (>40%, ≤2-fold enhancement); +++ (>2-fold enhancement)

- (20-40% repression); -- (>40%, ≤2-fold repression); --- (>2-fold repression)

MEASUREMENT AND ANALYSIS OF ADENOVIRUS EARLY AND LATE GENE
EXPRESSION AT MULTIPLE TIME POINTS DURING THE VIRAL REPLICATION
CYCLE IN HFF-INFECTED CELLS
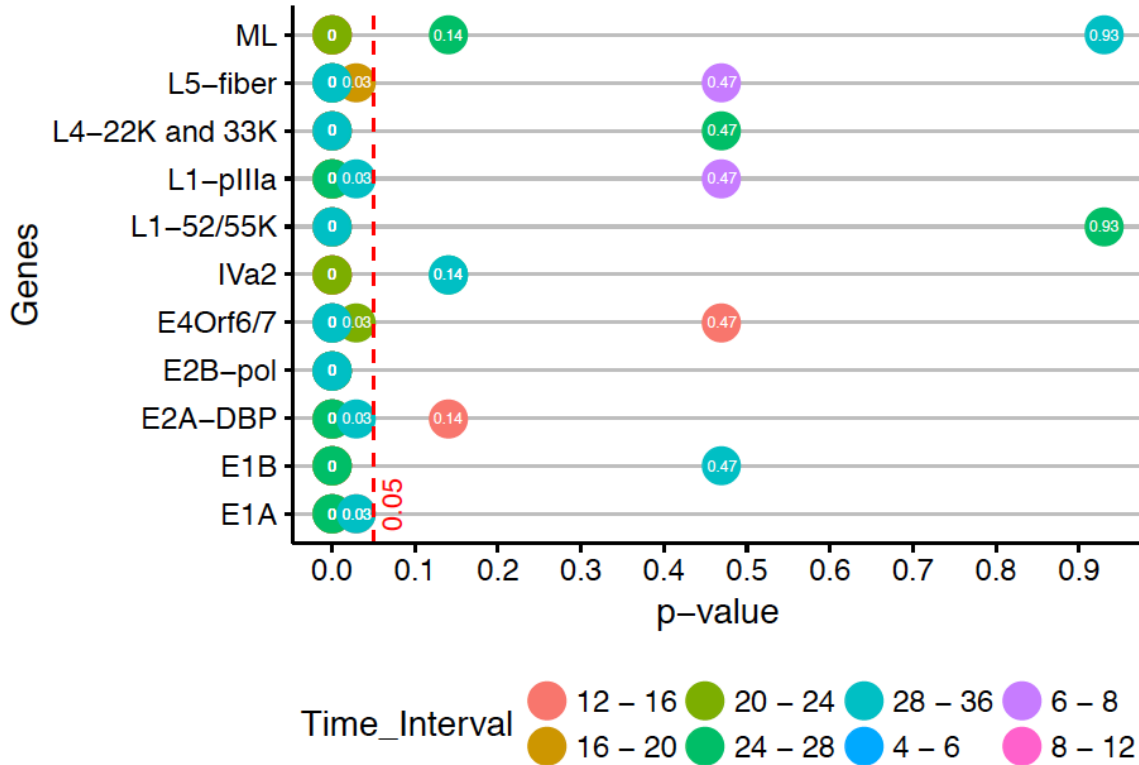

Figure S1. P-value of the Kolmogorov-Smirnov test. The hypothesis test evaluates the existance of
significant differences between the distribution of each mRNA in two continuous time points. The
red dashed line defines the significant level (a = 0.05).

5.2 Isolation and characterization of viral Replication Compartments.

Since viral replication compartments seem to represent a regulating hub for virus-cell interactions, a detailed study of these viral structures should allow elucidation of molecular mechanisms that govern not only the regulation of viral genome replication and expression but also of cellular activities by viral infection. Therefore, in order to study the molecular mechanisms that promote formation of replication compartments as a general viral strategy, in the present work we established a cell-free system consisting of enriched RC (RC fractions) [214] to analyze the morphology, composition and functions of RC isolated from Ad-infected cells [100, 214].

5.2.1 Morphological and biochemical analysis of RC fractions.

As described in the previous sections, the adenoviral replication cycle comprises a complex interplay between viral and cellular factors that regulate and establish optimal conditions for viral genome replication. Accumulation of newly replicated viral DNA molecules promotes late gene expression and consequently viral progeny production. Viral DNA replication and late gene expression take place in replication compartments (RC); however, a major obstacle in the study of the adenovirus replication cycle has been our limited understanding of the molecular composition of RC and the viral and cellular activities that are influenced or controlled in these compartments. Nuclear viral RC have not been isolated, perhaps due to the complexity of the nuclear architecture and absence of intranuclear membranes that would facilitate their isolation. Their study has relied instead on immunofluorescence microscopy, FISH and transmission electron microscopy. However, despite complications inherent to isolating subnuclear structures, other nuclear domains such as Cajal bodies [231], nucleoli [215] or spliceosomes [232] have been isolated from the nucleus on the basis of features, such as, size, molecular mass or density. Isolated sub-nuclear fractions have allowed a detailed characterization of the molecular composition and properties of their cognate nuclear domain.

As described in the introduction, viral and cellular proteins that modulate viral DNA replication, transcription and post-transcriptional processing, as well as components of the cellular anti-viral response are associated to RC. Nevertheless, little is known about their localization within these viral microenvironments. Since nucleoli and RC are both composed of proteins and nucleic acids, and have a diameter between 0.5-5 µm, we hypothesized that RC should also be amenable to isolation. Therefore, in order to analyze in more detail the morphology and biochemical composition of RC, we developed a fractionation protocol to isolate adenovirus RC (Fig. 12 A) [214]. To this end, we prepared sub-nuclear fractions using velocity gradients and sucrose cushions similar to procedures used to isolate

nucleoli [134] or other nuclear domains [231] and established a cell-free system that allows the study of the molecular composition and associated activities of RC. We first determined the localization of DBP and nucleolin within isolated RC particles by TIRF microscopy and the Bayesian analysis of Blinking and Bleaching (3B analysis) to obtain super-resolution images (Fig 12 D-F). This approach allowed for the first time a nanoscale analysis of isolated RC particles that can help to study their organization at a resolution of approximately 50 nm. In parallel, the intracellular distribution of DBP and nucleolin was also analyzed both by conventional immunofluorescence (IF) microscopy (Fig. 12 C) and using a 100x/1.49 numerical aperture oil-immersion objective lens with an extra 1.6x intermediate magnification lens (Fig. 12 B), as described in materials and methods. Using conventional IF microscopy DBP was seen to accumulate mostly in large foci and ring-like structures in the nuclei of Ad-infected cells, as expected (Fig.12 C a-c). Nucleolin was detected as a faint diffuse signal that was mostly nuclear with some cytoplasmic staining near the periphery of the nucleus (Fig. 12C b and c). The weak signal was overlaid with a small number of higher intensity large inclusion-like structures that were devoid of DBP (likely corresponding to nucleoli), as well as numerous structures that matched the periphery of all DBP-containing foci and rings (Fig. 12 C a-c). When the distribution of DBP was analyzed in Ad-infected cells at different times post-infection by TIRF microscopy (Fig. 12 B), the expected pattern of distribution was observed, as DBP accumulated in numerous small foci by 16 hpi, and at later time points, was distributed in ring-like and open structures that appeared to coalesce forming larger more morphologically complex structures; however, in contrast to conventional IF microscopy, each of the larger structures was overlaid with numerous small DBP foci, especially by the latter time-point analyzed (36 hpi) (Fig. 12 B). Interestingly, in contrast with the images that have been previously produced by confocal microscopy analysis of individual rings formed by DBP in Ad-infected cells using TIRF at 24 hpi (Fig. 12 D, TIRF e-g and insets d and k) or 36 hpi (Fig. 12 E, TIRF e-g and insets d and k) and processing by the 3B algorithm (Fig. 12 D or 12 E, a-c and h-j) showed that DBP occupied the periphery of these rings only partially. Moreover, while nucleolin was associated with these structures, essentially no colocalization with DBP was observed at 24 hpi (Fig. 12 D) as each protein localized with a different and separate pattern along defined regions of the rings' periphery, with nucleolin localizing mostly inside the periphery marked by DBP; in contrast with the 24 hpi time point, at 36 hpi (Fig. 12 E), colocalization of DBP and nucleolin was observed, mainly at the periphery of the ring-like structures. Isolated RC particles like those shown in the insets of Fig. 1A were then analyzed by super-resolution microscopy, both from Ad-infected cells (24 and 36 hpi) and mock-infected cells (Fig. 12 D and E l-q and F, respectively). The distribution of DBP or nucleolin in these particles was essentially the same as observed in RC within Ad-infected cells (Fig. 12 D and E a-k). Interestingly the

58

particles obtained in the RC fractions displayed abundant levels of both DBP and nucleolin, confirming that Ad-infection induces the recruitment of nucleolin to RC. RC fractions isolated at 36 hpi formed clusters (Fig. 12 E o-q), displaying a similar morphology to that observed for RC within Ad-infected cells, where higher colocalization of DBP and nucleolin at the periphery of RC could be observed.
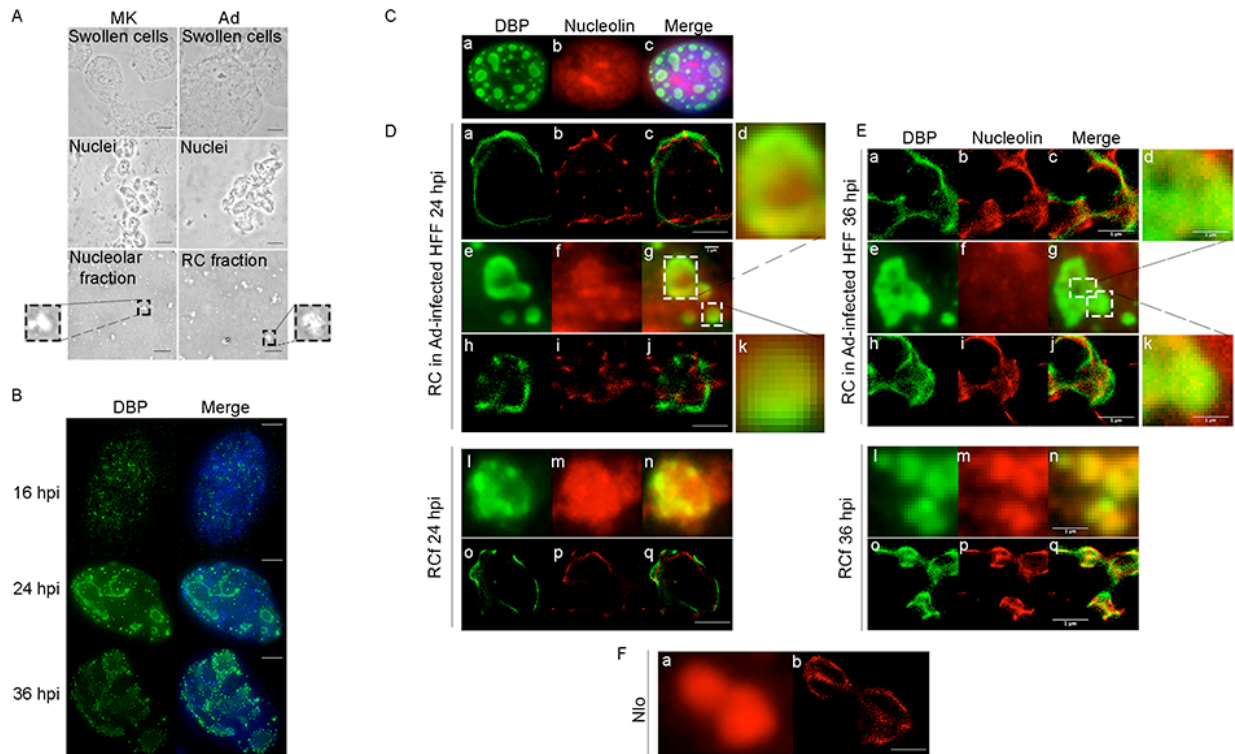
Figure 12. **Morphology of isolated RC particles and nucleoli.** A. Procedure to isolate subnuclear fractions. The bright-field micrographs taken with a 40x objective show swollen mock-infected or Ad-infected cells in hypotonic buffer and nuclei in the upper and middle panels, respectively (scale bar: 50 µm); Micrographs of RC fractions and nucleolar fractions were taken with a 63x objective (scale bar: 2 µm) and insets with a 5x zoom of RC or nucleoli of the expected size are shown. B. Micrographs of Ad-infected HFF, fixed at 16, 24 or 36 hpi (scale bar: 10 µm). DBP is shown in green and DNA in blue (DAPI). C. Immunofluorescence analysis of DBP (green) and nucleolin (red) in Ad-infected HFF, 24 hpi. D and E. Super-resolution analysis of RC fractions. TIRF images and 3B reconstructions of Ad-infected HFF, fixed 24 (D) or 36 (E) hpi and immunolabeled for DBP (green) and nucleolin (red). The TIRF images (d-g, k, l-n) represent the average of 300 micrographs. Scale bar 1 µm. Super-resolution images were obtained for RC in infected cells (a-c, h-j) and for RC fractions (o-q). F. Super-resolution analysis of nucleolar fractions (Nlo). a. The TIRF image represents the average of 300 micrographs. The super-resolution image of isolated nucleoli is shown in b. Scale bar 1 µm.

We found that *bona fide* RC components, such as the viral DNA, the DBP protein and various representative sequences of viral late mRNA from the MLTU (TPL, L2, L4 and L5 mRNA) are associated to RC fractions [214]. To confirm the association of nucleolin to RC fractions the presence of this protein was analyzed by western blots. Representative results for the analysis of nucleolin in various subcellular fractions are shown in Fig. 13. The fractions from mock-infected cells showed that

59

while nucleolin was not detectable in the cytoplasmic fraction (CYT) or total cell lysate (TL), the levels of this protein were approximately 5-fold higher in the nucleolar fraction (Nlo) compared with the nucleoplasmic (Npl) or total nuclear fractions (NL). Analysis of nucleolin from the same number of Ad-infected cells showed that the protein was redistributed from the nucleolus to all sub-cellular fractions, in agreement with IF and super-resolution microscopy (Fig. 12), and with previously reported experiments where the adenoviral pV protein induced the relocalization of nucleolin to the cytoplasm in transfection assays [233]. Apart from the redistribution of nucleolin, the protein levels were higher than in mock-infected cells and the anti-nucleolin antibody detected both higher and lower migrating bands that were more prominent in the fraction corresponding to RC (Fig. 13). The nature of the additional bands observed in the nucleolar or RC fractions for nucleolin is unknown, but they could be originated from post-translational modifications or proteolytic cleavage. Nucleolin is known to be phosphorylated and to possess auto-catalytic activity resulting in cleavage fragments with apparent molecular masses of about 100, 70, 60, and 50 kDa [234]. Such fragments closely match the bands observed in RC fractions from Ad-infected cells (Fig. 13). These results confirm that nucleolin was relocalized to RC, and suggest that its proteolytic products may also be relocalized to these sites (Fig 12C-D and Fig. 13).
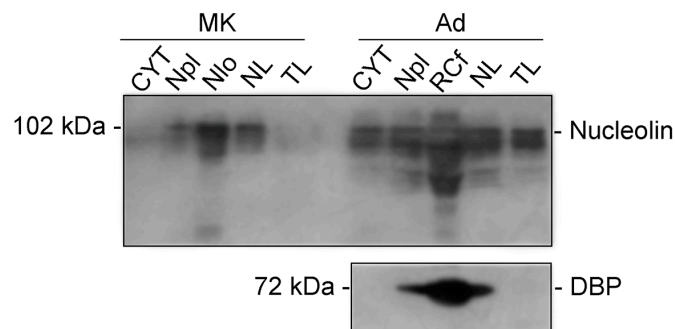
Figure 13. **Nucleolin and DBP are enriched in RC fractions.** Western blot (WB) of nucleolin and DBP in sub-nuclear fractions: Nucleolar (Nlo), replication compartment (RC fractions), Nucleoplasm (Npl), and cytoplasmic (CYT) fractions, as well as total cell lysates (TL) and total nuclear lysates (NL) were obtained from mock-infected or Ad-infected HFF at 36 hpi. The molecular masses are shown for each protein.

Taken together, these results indicate that isolated RC have similar morphology to that of RC within Ad-infected cells at different stages of the late phase of infection and that nucleolin is relocalized to the periphery of DBP in the RC, demonstrating that at this level of resolution compartmentalization of RC can be observed, as DBP and nucleolin displayed distinguishable distributions at different times post infection. These results indicate that RC fractions can be used to precisely define the spatio-temporal association of DBP, and presumably other viral and cellular molecules, to RC at different stages of the viral replication cycle.

5.2.2 Adenovirus RC fractions are functional.

Since RC are sites of viral DNA synthesis and late gene expression, in addition to viral DNA, viral mRNA and DBP [235], RC fractions could be expected to also contain other viral and cellular components that participate in these molecular processes, such as the viral E2B DNA polymerase (Ad pol), the cellular RNA polymerase II (RNA pol II), and spliceosome components. Therefore, we decided to determine if the RC fractions were functional. To this end the sub-nuclear fractions were used for *in vitro* synthesis of DNA and mRNA and to evaluate mRNA splicing activity, as described in materials and methods.

- Viral DNA synthesis in RC fractions

To determine whether viral DNA replication was associated with RC fractions, viral DNA synthesis was evaluated in fractions obtained at 16 (not shown), 24 and 36 hpi. The RC fractions were incubated in a reaction mixture in the presence of ATP and dNTP, DNA was then extracted and purified, and viral DNA was amplified by PCR and analyzed in agarose gels by densitometry as described in materials and methods. ActD was used in these assays to inhibit DNA synthesis as a control. As an example from these experiments one such gel is shown and the data from two independent experiments are included in Fig. 14. No viral DNA synthesis was detected in samples from mock-infected cells or in the absence of ATP or dNTP. Clearly detectable levels of *de novo* synthesized DNA were obtained at both times post-infection, as the level of DNA increased from input levels 1.6-fold at 24 hpi and 3.3-fold at 36 hpi. ActD treatment significantly inhibited viral DNA replication resulting in levels that were comparable to the input DNA at both times post-infection (Fig. 14A and B). Both nucleolar DNA (ribosomal DNA) and non-nucleolar DNA (U1 gene) were also measured in these experiments, when no amplification from these cellular DNA was observed (data not shown). These results clearly indicate that RC fractions contain active Ad pol that can direct *de novo* synthesis of viral DNA and that *in vitro* viral DNA synthesis is higher in RC isolated at 36 than at 24 hpi.

Figure 14. **Viral DNA replication assay in RC subnuclear fractions.** RC fractions obtained from Ad WT-infected or mock-infected HFF, harvested at 24 or 36 hpi, were incubated with ATP and dNTP; DNA was isolated and *de novo* synthesized DNA was amplified by PCR. A. Densitometry measurements of viral DNA. B. Representative gel with the viral DNA synthesized *de novo*. ActD: actinomycin (100 ng/ml). The PCR products were measured by densitometry. Data from duplicates of two independent experiments are shown. ** $p<0.01$; *** $p<0.001$; **** $p<0.0001$.

- RNA synthesis in RC fractions

RNA pol II synthesis of viral late mRNA was then measured to evaluate transcriptional activity associated to RC fractions (Figure 15 A and B). The samples were incubated in the presence of NTP to determine the *de novo* synthesis of RNA, and as before, ActD served as control to inhibit *de novo* transcription. No synthesis of viral mRNA was detected in mock-infected cells. As shown in Fig. 4, the levels of viral ML mRNA increased above the input approximately 2-fold at 24 hpi and 5-fold at 36 hpi. The synthesis was dependent on the presence of NTP, and was inhibited to input levels by ActD treatment. The same analysis was made to evaluate cellular mRNA synthesis, when no *in vitro* transcription was observed (data not shown) indicating that RNA pol II activity in RC fractions directed transcription of viral but not cellular genes.

Since nucleoli are sites where rRNA are produced, and previous work has established that isolated nucleoli maintain transcriptional activity [236], we decided to determine whether RC fractions retained RNA pol I activity. Therefore, rRNA synthesis was measured as before (Figure 15 C and D). *De novo* rRNA synthesis was observed both in mock-infected (MK) and Ad-infected cells, and was dependent on the presence of NTP. As with the RNA Pol II viral products, rRNA transcription was inhibited by ActD to input levels in mock-infected and RC fractions. Surprisingly, rRNA synthesis showed an almost 3-fold increase at 36 hpi, compared to MK.

Together, these results indicate RC fractions have both RNA pol I- and pol II-associated activity, and that such activity is higher at 36 than at 24 hpi.
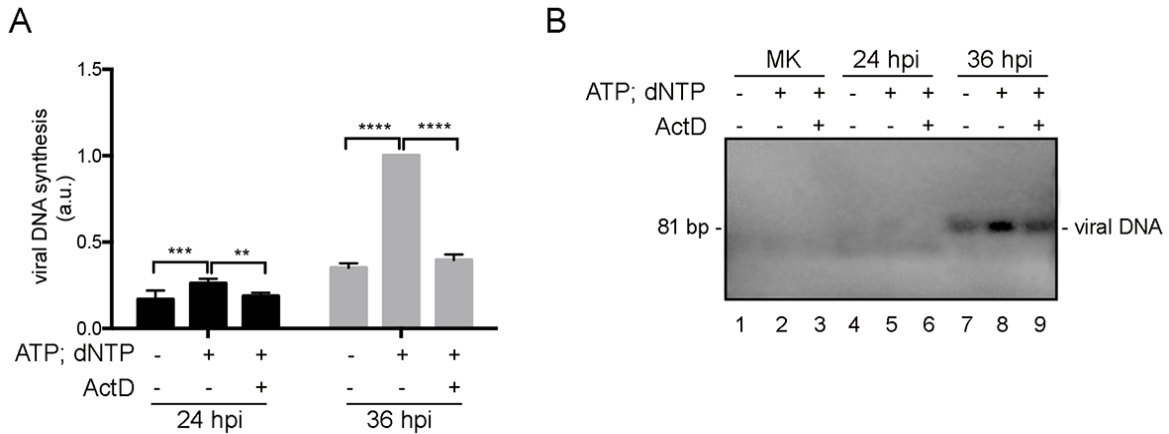
Figure 15.   Transcription assay in RC subnuclear fractions. RC fractions obtained from Ad WT-infected or mock-infected HFF, harvested at 24 or 36 hpi, were incubated with NTP; RNA was isolated and *de novo* synthesized pre-mRNA were amplified by RT-PCR. A. and C. viral late pre-mRNA (A) and cellular pre-mRNA (C). The mock-infected subnuclear fractions (MK) corresponded to nucleoli. B. and D. Representative gels with the viral (B) and cellular (D) mRNA synthesized *de novo*. ActD (25 μg/ml). The RT-PCR products were measured by densitometry. Data from duplicates of two independent experiments are shown. ** p<0.01; *** p<0.001; **** p<0.0001.

- mRNA Splicing in RC fractions

Previous reports have shown that splicing factors and snRNP are localized adjacent to DBP foci [90, 133]. ASF/SF2 as well as snRNP colocalize with viral transcription sites [142, 237-239]. Since RC fractions were transcriptionally functional, the molecules necessary to process viral pre-mRNA could be expected to be associated to this fraction. Therefore, viral late mRNA splicing was evaluated in the sub-nuclear fractions. The RC fractions were incubated in a reaction mixture in the presence of ATP and creatine phosphate. RNA was then extracted and purified, and spliced viral mRNA was analyzed by RT-PCR. As control, treatment of the samples with erythromycin was used to inhibit the formation of the spliceosome C complex, as previously reported [223].

Viral pre-mRNA splicing was dependent on the presence of ATP and creatine phosphate and no products were obtained in samples from mock-infected cells. Mature viral mRNA were detected at levels that were approximately 3-fold higher

63

than input at 36 hpi, but not at 24 hpi (Figure 16 A and B). Treatment with erythromycin significantly inhibited the post-transcriptional processing of viral transcripts. Additionally, cellular pre-mRNA splicing was evaluated (Figure 16 C and D). In nucleolar and RC fractions, cellular actin pre-mRNA splicing was observed and was dependent on ATP and creatine phosphate. In all samples, treatment with erythromycin significantly inhibited pre-mRNA processing. Furthermore, RC fractions from Ad-infected cells showed a progressive increase at the different times post-infection in the levels of spliced actin mRNA species. It is known that IG are closely associated to DBP foci [112, 239]; therefore, it is possible that IG might co-isolate with RC, which may account for *de novo* processing of cellular species of pre-mRNA in RC fractions.

Together, these results demonstrate that RC fractions are functional and should allow detailed analysis of molecular activities associated to these structures.

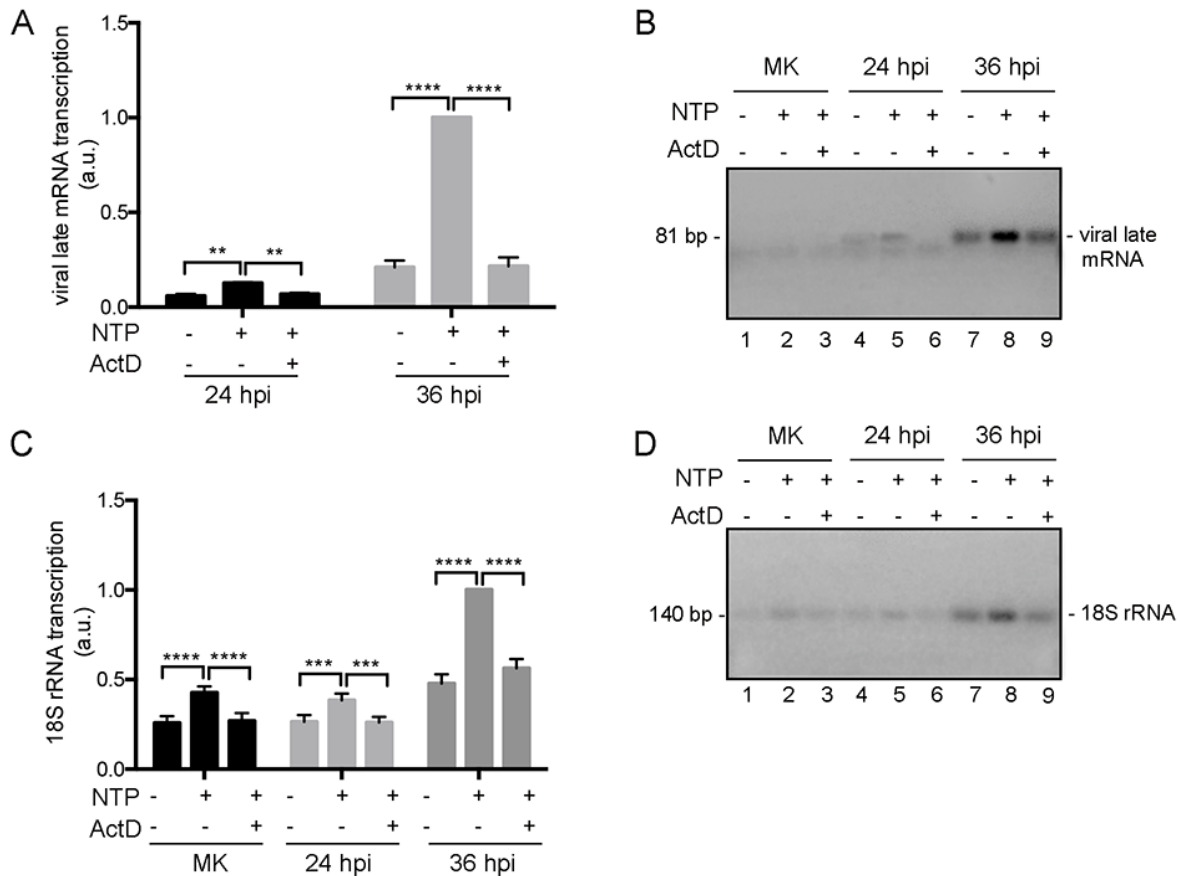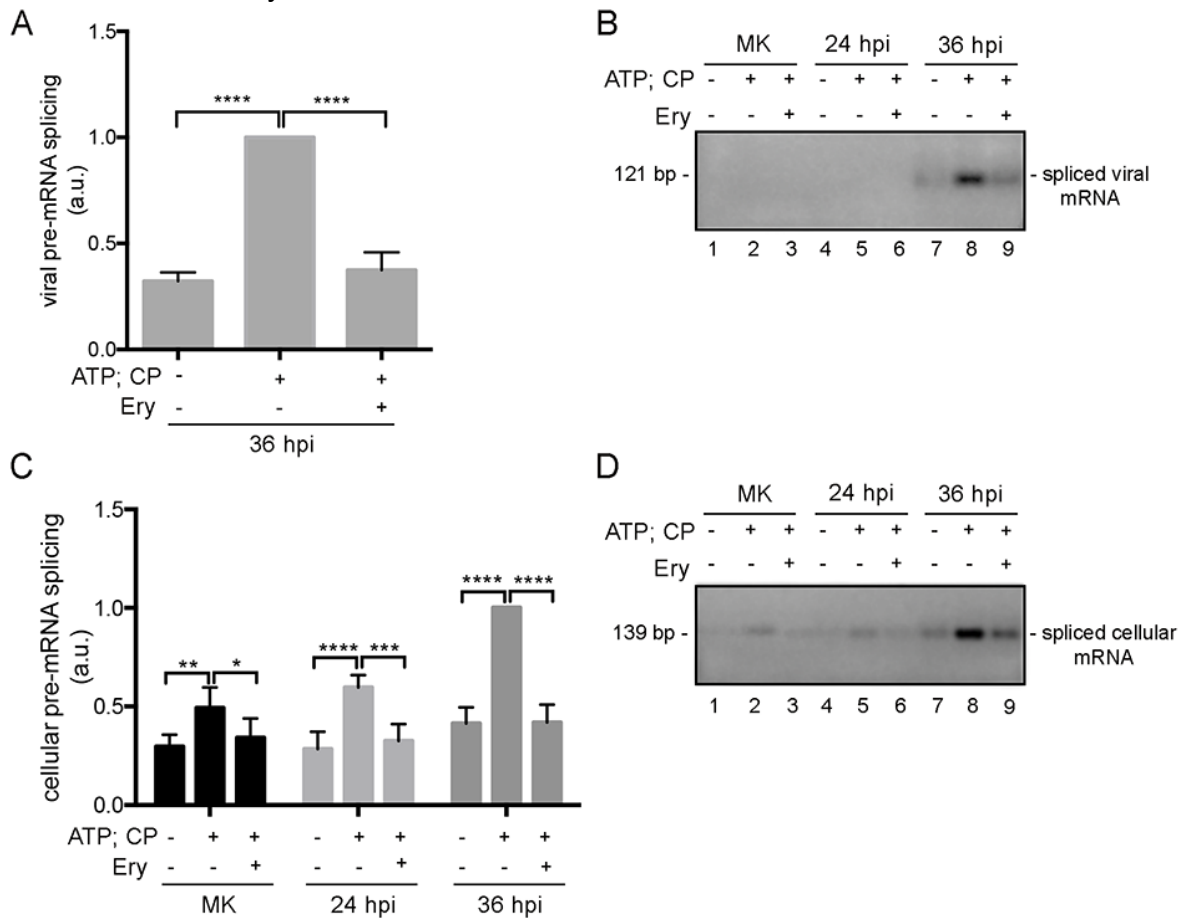**Figure 16. Splicing assay in RC subnuclear fractions.** RC fractions obtained from Ad WT-infected or mock-infected HFF, harvested at 24 or 36 hpi, were incubated with ATP and CP; RNA was isolated and spliced mRNA were amplified by RT-PCR. A. and C. Spliced viral late mRNA (A) and cellular mRNA (C). The mock-infected subnuclear fractions (MK) corresponded to nucleoli. B. and D. Representative gels with the viral (B) and cellular (D) mature mRNA spliced *in vitro* in RC fractions. Ery: erythromycin (500 μM); CP: creatine phosphate. The RT-PCR products were

64

measured by densitometry. Data from duplicates of two independent experiments are shown. * p<0.05; ** p<0.01; *** p<0.001; **** p<0.0001.

5.2.3 Quantification of viral late mRNA synthesis and splicing associated to RC fractions.

As described in the previous sections, adenovirus late gene expression proceeds through a coordinated and complex transcription program that requires initiation of viral DNA synthesis for the activation of the major late (MLP) and L4 (L4P) promoters. The complexity of the viral late gene expression program is further compounded with post-transcriptional processing of all mRNA species produced by the L1 to L5 viral late mRNA families. Although during the initial stages of the late phase both newly synthesized and spliced ML transcripts are associated with the peripheral replicative zones (PRZ) of RC [90, 240], as the late phase progresses cellular snRNP and spliced ML sequences accumulate in large clusters within surrounding IG [138, 239, 240]. Since transcription does not take place in these IG structures [92, 239], it has been suggested that post-transcriptional processing of viral late mRNA continues in these sites [90, 138, 240]. Nevertheless, it is not yet clear at which stage of post-transcriptional processing these transcripts may dissociate from RC to be transported to IG and latter exported to the cytoplasm; nor is it known whether each viral late mRNA species may be processed in the same compartments or with similar kinetics. Moreover, previous studies have all relied on immunofluorescence or electron microscopy and it is not known whether at the latter stages of viral replication IG remain a separate nuclear structure or if their components become embedded in viral RC. Since we detected a sequence within the unspliced ML TPL both in RC fractions and in Npl [235], and *de novo* splicing of a ML sequence could be detected in RC fractions (Fig. 16); we decided to measure partitioning of viral late pre-mRNA and spliced mRNA between the RC and Npl fractions at different times post-infection by quantitative RT-PCR. Therefore, RNA was isolated from RC fractions and Npl at 24 and 36 hpi as before, and primers designed to amplify sequences from the ML TPL and L5 spliced or unspliced mRNA were employed, as described in materials and methods. For these experiments we initially measured synthesis of viral late mRNA using total RNA obtained from the nucleus of Ad-infected cells at 24 and 36 hpi, and steady-state levels of all viral ML or the L5 pre-mRNA were determined. The results from representative experiments are shown in Fig. 17, where a similar increase in ML or L5 pre-mRNA was observed from 24 to 36 hpi (Fig 17 A and B). Such increments are in agreement with previous reports that have measured transcription rates for late mRNA [157, 158]. To determine the relative accumulation of spliced mRNA in the nucleus and cytoplasm steady-state levels of spliced ML and L5 mRNA were then quantified (Fig 17 C and D). The increase in nuclear mRNA from 24 to 36 hpi was higher for L5 than for ML, for which a 6-fold increase was observed.

65

Furthermore, the cytoplasmic accumulation of L5 mRNA was more efficient than ML, since at 36 hpi a greater number of spliced L5 transcripts were quantified in the cytoplasm than in the nucleus, while the number of ML transcripts was the same in both sub-cellular fractions. Since nuclear-cytoplasmic partitioning of mRNA has been traditionally used to measure export of viral late mRNA [76, 77, 241, 242], these data suggest that the export rate for L5 mRNA is higher than for all other ML mRNA; an alternative explanation, not necessarily exclusive, is that by the latter time point nuclear or cytoplasmic mRNA turnover may vary for each mRNA species.
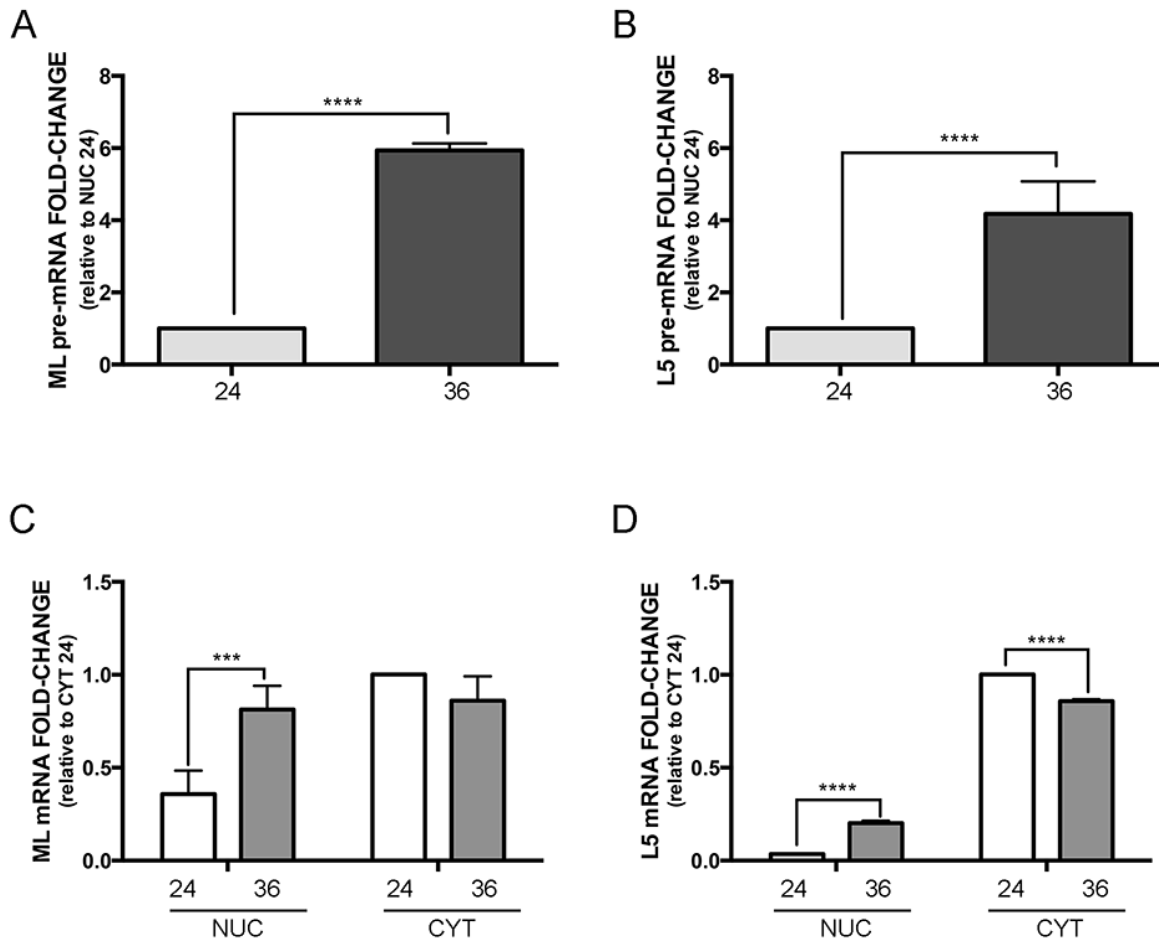
Figure 17. **Quantitative analysis of nuclear and cytoplasmic viral late mRNA.** Cytoplasmic and nuclear fractions were obtained from Ad WT-infected HFF and harvested at 24 or 36 hpi. Total RNA was isolated from each fraction and analyzed by real time RT-PCR, as described in materials and methods. A. and B. Fold-change of viral late pre-mRNA (ML pre-mRNA) (A) and L5 pre-mRNA (B) in nuclear (NUC) fractions; C. and D. fold-change of mature ML mRNA (C) and L5 mRNA (D) in cytoplasmic (CYT) and NUC fractions. No amplification of pre-mRNA was detected in cytoplasmic fractions, which indicated there was no nuclear contamination of these fractions. Standard deviations and mean fold-change values were plotted for triplicates of two independent experiments. *** p<0.001; **** p<0.0001.

66

To evaluate whether the observed differences in transcription and splicing, or in the temporal pattern of cytoplasmic accumulation of ML and L5 mRNA, were consequences of nuclear events during their biogenesis, we decided to measure partitioning of spliced and unspliced ML and L5 mRNA between RC and Npl fractions, as described in materials and methods. Representative results where the fold-change was measured in these experiments are shown in Fig. 18. At both 24 and 36 hpi all ML transcripts, unspliced (Fig. 18A) and spliced (Fig. 18B), displayed very similar distribution between RC fractions and Npl. In contrast, the unspliced L5 mRNA showed a 25-fold decrease in the RC fractions from 24 to 36 hpi (Fig. 18C), while the ratio of processed over non-processed L5 mRNA increased to a greater extent than ML mRNA in RC fractions. Since mRNA splicing activity was detected in RC fractions at 36 hpi (Fig. 16), the decrease in the quantity of spliced L5 mRNA in the nucleus (Fig. 18D) and its simultaneous accumulation in the cytoplasm at the same time point (Fig 18D) indicates that L5 mRNA splicing occurs in the RC, and that at the latter time post-infection L5 mRNA splicing and export to the cytoplasm is more efficient than the rest of ML transcripts (Fig. 18B).
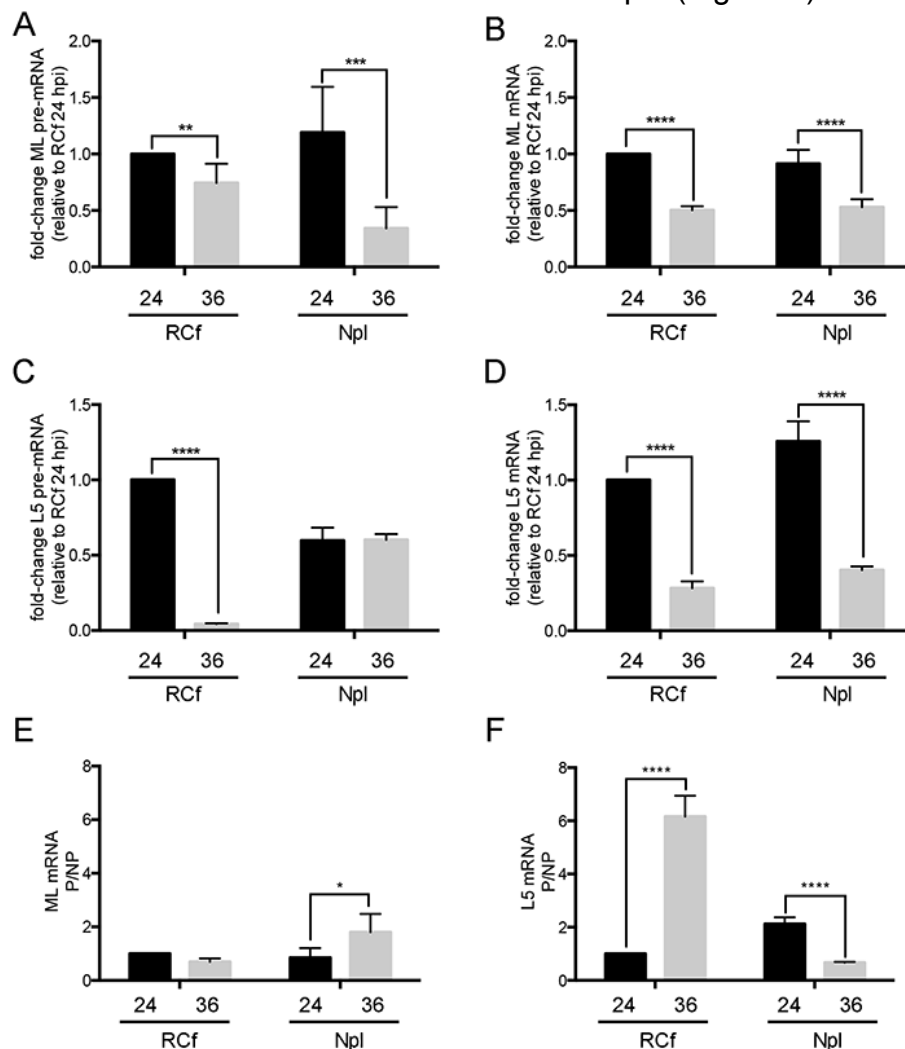
Figure 18.   Quantitative analysis of splicing and association of viral late mRNA to RC fractions at different times post-infection. RC fractions and Npl fractions were obtained from Ad WT-infected HFF and harvested at 24 or 36 hpi. Total RNA was isolated from each fraction and quantified by real time RT-PCR as described in materials and methods. A. to D. The graphs show the fold-change for viral late ML pre-mRNA (A) and ML mRNA (B), and for L5 pre-mRNA (C) and L5 mRNA (D). E. and F. The ratio of Processed/Non-Processed mRNA (P/NP) for ML (E) and L5 (F) are shown. Standard deviations and mean fold-change values were plotted for triplicates from two independent experiments. * p<0.05; ** p<0.01; *** p<0.001; **** p<0.0001.

To make a direct quantitative analysis of the unspliced and spliced forms of ML and L5 mRNA associated to RC and to further evaluate if splicing of all alternative forms of L5 mRNA occurs in RC, we made an RNA-Seq analysis of the mRNA associated to RC fractions at 36 hpi and quantified the sequences aligned to the junctions between different exons for these late transcripts (Fig. 19). Post-transcriptional processing of fiber mRNA requires splicing of an intron of close to 18 kb in length; a process that ignores at least 13 potential splice sites upstream of L5 [243, 244]. Moreover, the fiber exon can be spliced to different upstream ancillary leader exons, including the TPL and the "i" leader in combination with three other potential leaders inside the E3 region (leaders x, y and z), as shown in Fig. 19 B [243-245]. Since splice sites for the Ad genome have been reported for serotype 2 [245] but the annotation was not complete for serotype 5, we first made an *in silico* search to map all possible L5 splice sites in the Ad WT genome sequence (H5pg4100) (Fig. 19C-Table) [100]. In this viral genome a region in the E3 transcription unit that includes the 5' splice site of the z leader has been deleted, while x and y leaders remain intact. To match the regions analyzed by qRT-PCR with the RNA-Seq analysis, we quantified the reads aligned to: the leader 2-3 junction (ML P); the intron between leader 2-3 (ML NP); the leader 3-fiber junction (L5 P); and the intron right before fiber exon (L5 NP) to determine the number of spliced and unspliced mRNA from the total set of viral late mRNA (ML) and the TPL-L5 mRNA (Fig. 19 A). As shown in the graph, a greater quantity of spliced than unspliced mRNA were found for both ML and L5 at 36 hpi. As expected, the reads aligned for ML mRNA species were higher than those for L5 mRNA. Since the primers used in the qRT-PCR assays only account for TPL-fiber mRNA, we decided to quantify the RNA-Seq reads for different possible combination of fiber splice junctions (Fig. 19 C). The biological significance of the i-leader exon inclusion or exclusion has not been elucidated, but it has been shown to depend on the viral E4Orf3 and E4Orf6 proteins, respectively, and that splicing of ML mRNA at late times usually leads to its exclusion [246]. Therefore, the low number of reads covering the leader i-3 splice junction could be expected (Fig. 19 C). Alternatively, while the processing of all exon junctions leading to production of L5-fiber mRNA occur in association with RC, the i-3 splice junction may not. The x and y leaders can be spliced to E3 and L5 mRNA, so the reads aligned to the splice junction between leaders x-y could correspond to either of these two viral

68

mRNA species. Interestingly, the overall coverage pattern for reads aligned to L5 splice junctions in RC fractions closely matched those from total cell-lysates recently reported for Ad2 [245], including the high number of reads covering the splice junctions between leader 3-y indicating that the fiber mRNA that contain these exons are the most abundant both in RC fractions and total cell lysates at 36 hpi. To our knowledge a spatio-temporal change in the rate of synthesis or post-transcriptional processing of individual viral late transcripts has not been reported and the present results indicate that quantitative analysis of the differential biogenesis of individual viral late mRNA species at different times of viral replication should be performed to obtain detailed analysis of these events, and that RC fractions are amenable to perform such studies. Taken together, the results from quantitative RT-PCR assays and RNA-Seq indicate for the first time that alternative splicing of L5 mRNA occurs associated to RC and that these mRNA are spliced and accumulate in the cytoplasm more efficiently than the rest of ML mRNA at late times post-infection.
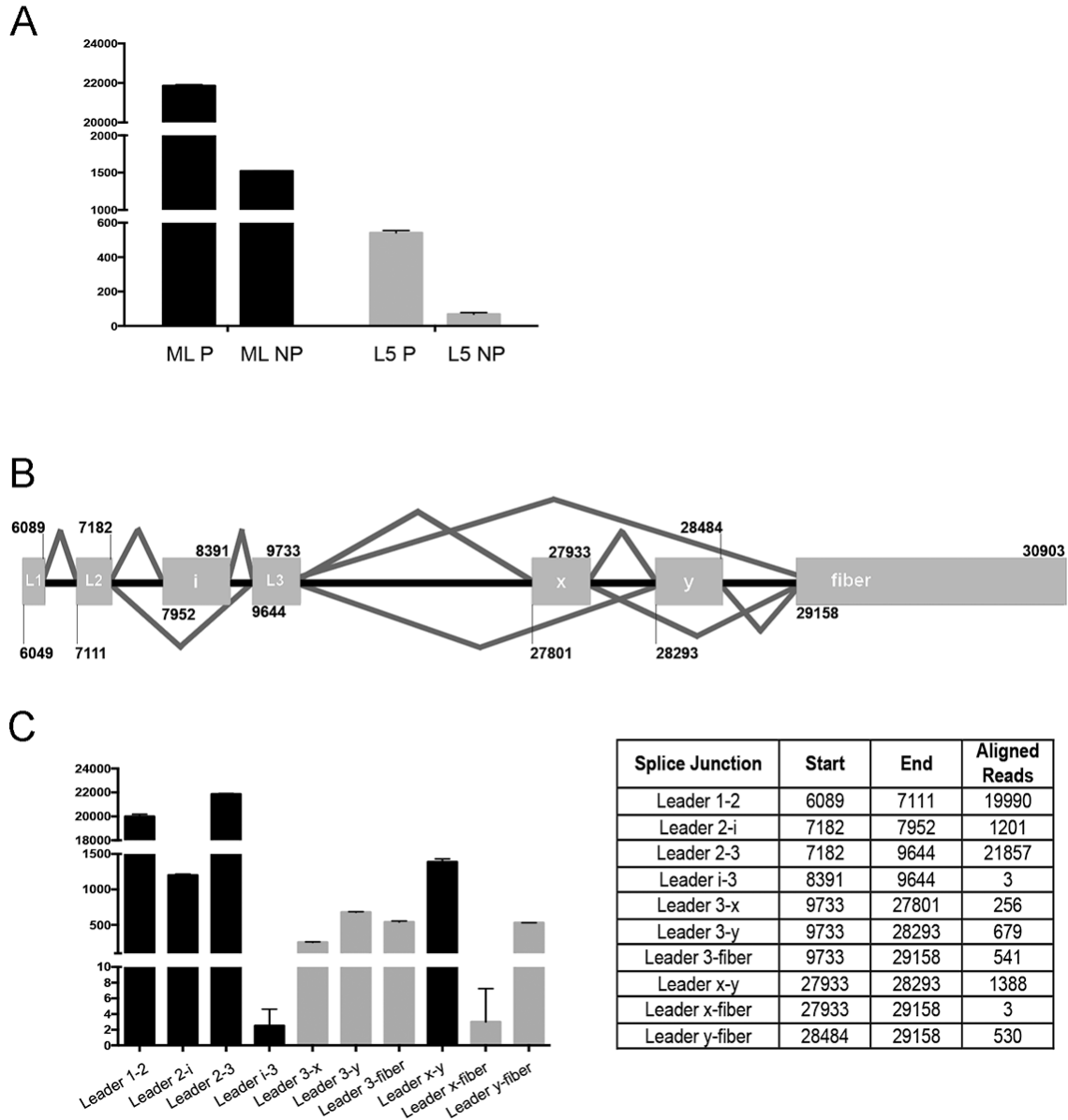
Figure 19. **RNA sequence analysis of fiber mRNA splice sites in RC fractions.** A. The graph shows the sequence reads aligned to: the leader 2-3 junction (ML P, black bars): intron between leader 2 and 3 (ML NP, black bars); leader 3-fiber junction (L5 P, grey bars); and intron region immediately upstream of fiber (L5 NP, grey bars). P: processed mRNA; NP: non-processed mRNA. B. Splice diagram of fiber mRNA splice sites in the H5pg4100 genome. The numbers indicate the 5' and 3' ends of each exon. C. The graph shows the sequence reads aligned to different potential splice sites for ML (black bars) and fiber (gray bars) mRNA. The number of sequence reads covering these splice sites as well as the nucleotides covering the splice junctions shown in the graph are listed in the table.

Splice Junction	Start	End	Aligned Reads
Leader 1-2	6089	7111	19990
Leader 2-i	7182	7952	1201
Leader 2-3	7182	9644	21857
Leader i-3	8391	9644	3
Leader 3-x	9733	27801	256
Leader 3-y	9733	28293	679
Leader 3-fiber	9733	29158	541
Leader x-y	27933	28293	1388
Leader x-fiber	27933	29158	3
Leader y-fiber	28484	29158	530

70

5.3 E1B impacts RC-associated activities

Since RC isolated from Ad-infected cells are functional [100, 214], we took advantage of this procedure and evaluated if E1B could impact *de novo* DNA replication, late gene transcription and splicing associated to RC.

5.3.1 E1B promotes efficient genome replication, as well as transcription and splicing of viral late genes in RC

Viral RC particles were isolated from Ad WT, E1B⁻ or E1B PM-infected HFF cells. These particles were incubated with ATP and dNTP to evaluate *in vitro* synthesis of viral DNA, ATP and NTP to measure viral late transcription, or ATP and Creatine Phosphate (CP) for splicing of viral late mRNA. As controls, the absence of these reagents or the addition of Actinomycin D or erythromycin for inhibition of these molecular processes, were used.

In the absence of E1B, lower levels of viral DNA were measured. However, no defect in the proportional increase between the input template and the *de novo* synthesized DNA was observed (Fig. 20 A). When synthesis of viral late mRNA was measured (Fig. 20 B), as well as for splicing (Fig. 20 C), a 2-fold decrease in RNA synthesis was observed both at 24 and 36 hpi. These results demonstrate that E1B is required for efficient viral late mRNA synthesis and splicing, associated to RC.
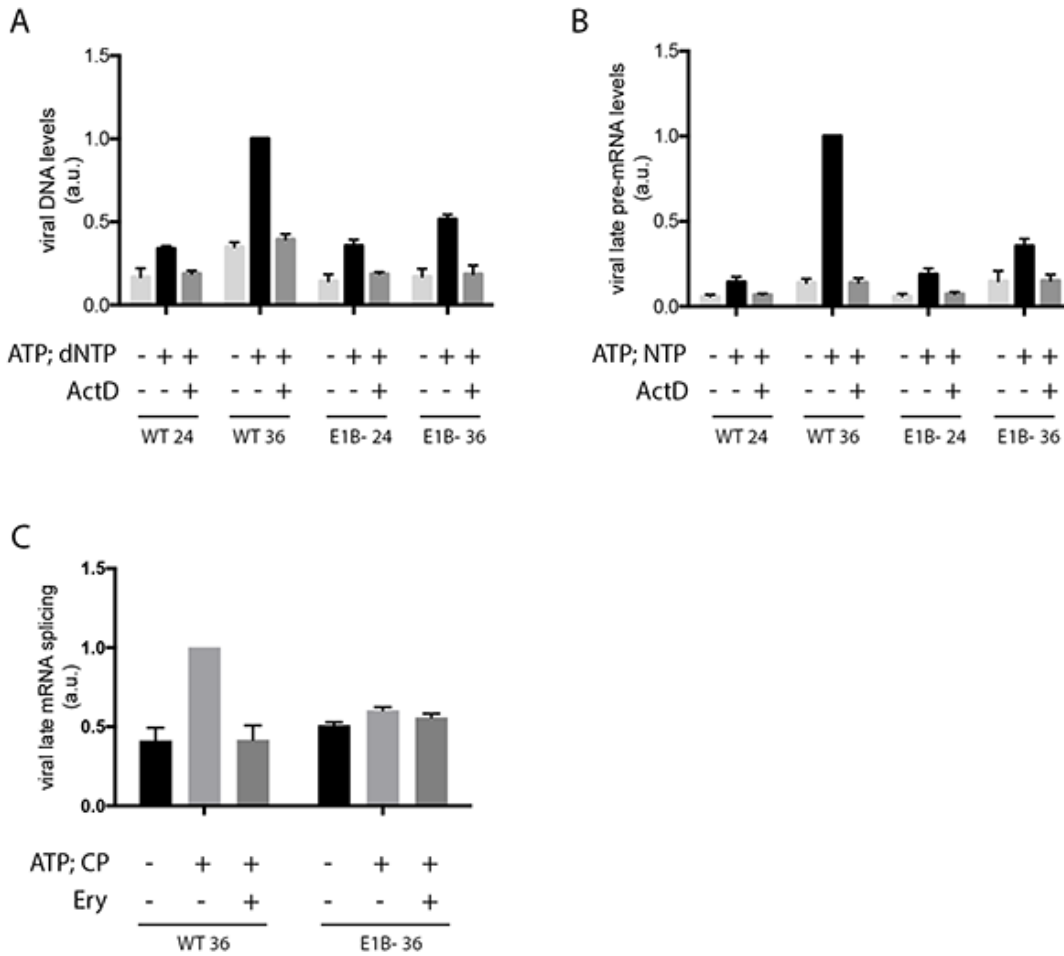
Figure 20. **Functional assays in RC fractions from Ad WT or E1B⁻ infected cells.** RC fractions from Ad WT or E1B⁻ infected cells were isolated at 24 or 36 hpi and subjected to in vitro assays to determine de novo synthesis of viral DNA, viral late mRNA and splicing.

Interestingly, in RC isolated from E1B PM-infected cells, higher levels of viral DNA and RNA were synthesized, and splicing of viral late mRNA increased, compared to Ad WT RC (Fig. 21). E1B PM resulted in higher synthesis for DNA replication and transcription assays; an almost 4-fold increase in viral DNA (Fig. 21A) was observed and a 2-fold increase for synthesis of viral late mRNA (Fig. 21B). These results showed that phosphorylation of E1B results in more efficient viral DNA replication and late gene transcription. However, although more spliced mRNA were found associated to E1B PM RC, the proportional increase between the input and the analysis of splicing in RC was comparable between Ad WT and E1B PM.
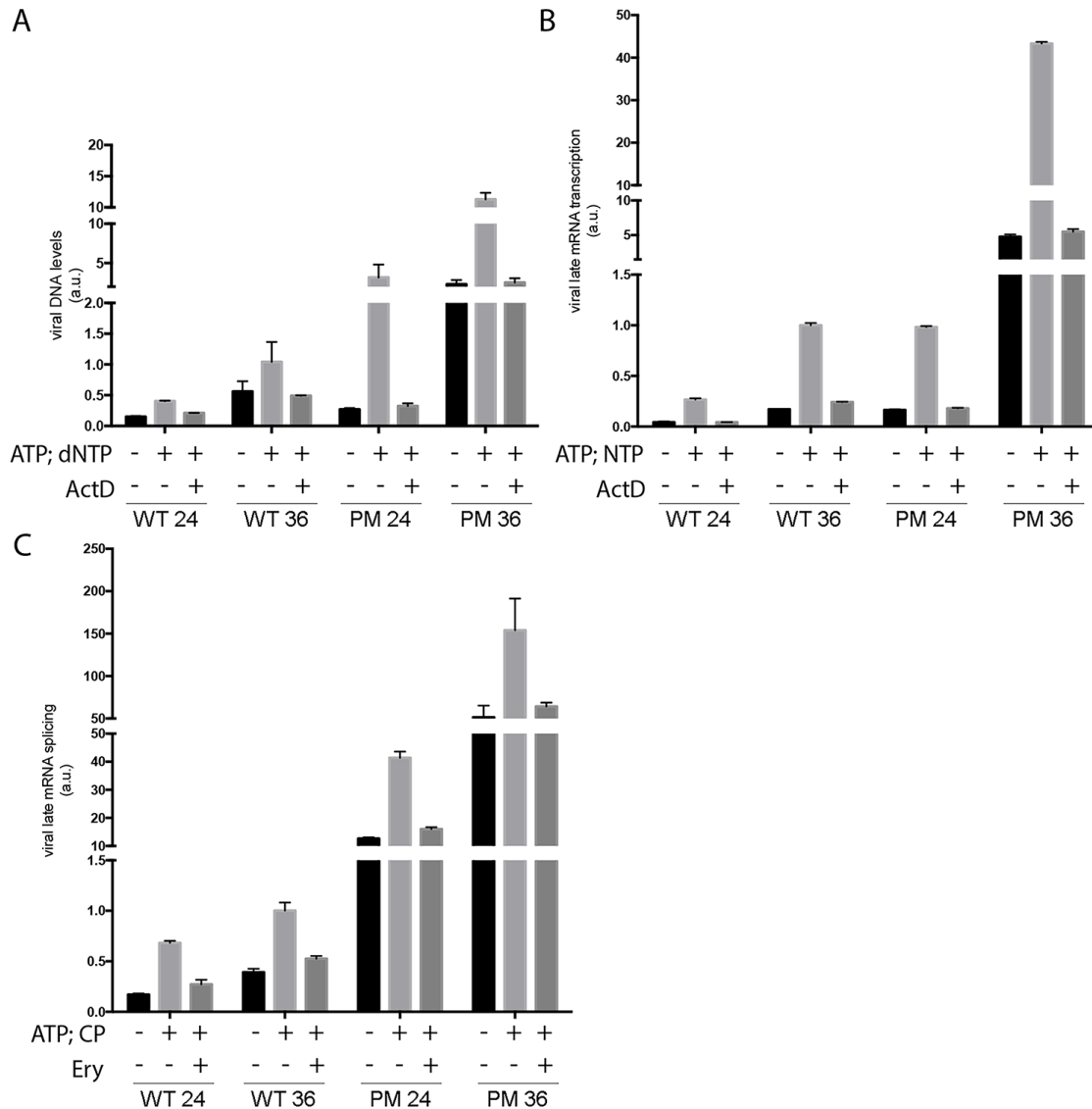
Figure 21. **Functional assays in RC fractions from Ad WT or E1B PM-infected cells.** RC fractions from Ad WT or E1B⁻ infected cells were isolated at 24 or 36 hpi and subjected to in vitro assays to determine de novo synthesis of viral DNA, viral late mRNA or splicing.

5.3.2 E1B is required for efficient production and splicing of viral late mRNA in RC and for their partitioning between RC and Npl.

To further analyze the effect of E1B on mRNA biogenesis, we performed measurements by qRT-PCR of viral late pre-mRNA and spliced mRNA between RC and nucleoplasmic (Npl) fractions obtained from cells infected with either Ad WT or the E1B⁻ mutant, at different times post-infection. Analysis of the partitioning of these RNA species in Ad WT fractions showed that L5 mRNA splicing occurs in the RC, and that at a late time post-infection L5 mRNA splicing and its accumulation in the cytoplasm was more efficient than for the rest of the ML

transcripts [100]. In RC isolated from cells infected with the E1B⁻ mutant, ML pre-mRNA exhibited 100- and 20-fold decreases at 24 and 36 hpi, respectively, compared with Ad WT, and similar defects were observed in Npl (150 and 30-fold) (Fig. 22A). When partitioning for the spliced form of ML was measured in the absence of E1B (Fig. 22C), 100- and 25-fold decreases were quantified at 24 and 36 hpi, respectively in RC; while in Npl these differences were of 150- and almost 60-fold, respectively.

When the fold-change was measured for the non-spliced form of L5 mRNA (pre-mRNA) (Fig. 22B), a 280-fold decrease and a 5-fold decrease was detected at 24 and 36 hpi, respectively in RC of E1B⁻ fractions, while in Npl the differences where 300- and 40-fold at 24 and 36 hpi, respectively.

The spliced L5 mRNA displayed a 20- and 3-fold decrease at 24 and 36 hpi, respectively in RC, while in Npl these differences were 30 (24 hpi)- and 8 (36 hpi)-fold in the absence of E1B (Fig. 22D). These data demonstrate that E1B is required for efficient production and splicing of viral late mRNA in the RC and of their partitioning between RC and Npl.
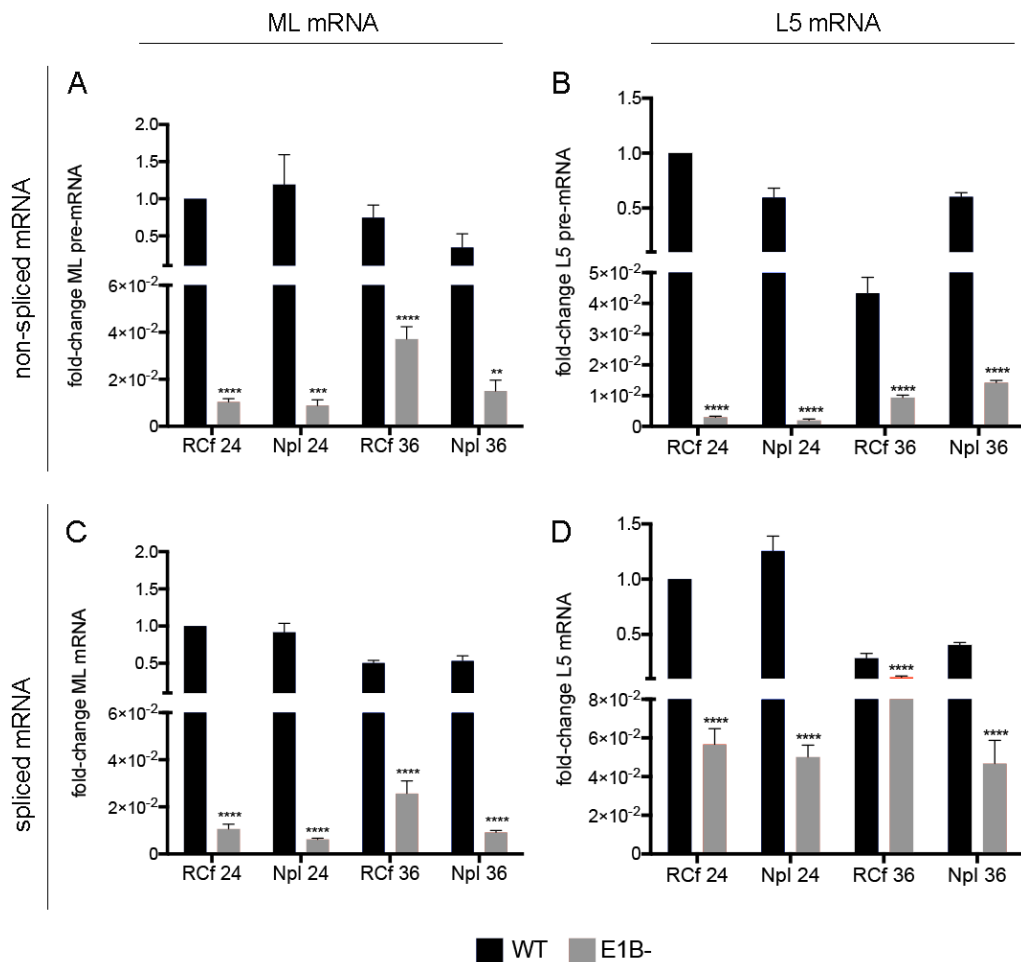
Figure 22. **RC and Npl partitioning of ML and L5 unspliced and spliced mRNA in Ad WT or E1B⁻ isolated sub-nuclear fractions.** RC and Npl fractions were obtained from Ad WT or E1B⁻

infected HFF and harvested at 24 or 36 hpi. Total RNA was isolated from each fraction and quantified by qRT-PCR. The graphs show the fold-change for viral ML pre-mRNA (A) and ML mRNA (C), and for L5 pre-mRNA (B) and L5 mRNA (D). Standard deviations and mean fold-change values were plotted for triplicates from two independent experiments. ** p<0.01; *** p<0.001; **** p<0.0001.

- E1B is required for nuclear steps of viral late mRNA biogenesis, at the level of both transcription and splicing.

The partitioning between nuclear (NUC) and cytoplasmic (CYT) fractions was then compared by qRT-PCR. Pre-mRNA species were only detected in the nuclear fraction, as expected (Fig. 23). When ML pre-mRNA were measured, defects were detected in the absence of E1B. A 7-fold and an almost 30-fold decrease in mRNA were detected at 24 and 36 hpi, respectively. In contrast, in E1B PM NUC fractions, 3- and 2-fold increases were measured at 24 and 36 hpi, respectively. When L5 pre-mRNA was measured, similar defects were found in the absence of E1B and similar increases were measured for E1B PM as well as for ML pre-mRNA. However, although more mRNA were detected with E1B PM, the increase between 24 and 36 hpi was very similar to that of Ad WT (around 5-fold increase). These observations indicate that E1B is necessary for efficient viral late transcription, but phosphorylation of E1B does not directly impact this activity of the protein.

When the ML and L5 spliced mRNA were measured, a decrease in these processed mRNA were also found in the absence of E1B, while E1B PM resulted in higher levels of mRNA compared to Ad WT. Since the increase in E1B PM was higher than that measured for Ad WT, these results suggests that phosphorylation of E1B promotes efficient viral late splicing, in agreement with the results obtained in the experiments described in section 5.3.1.
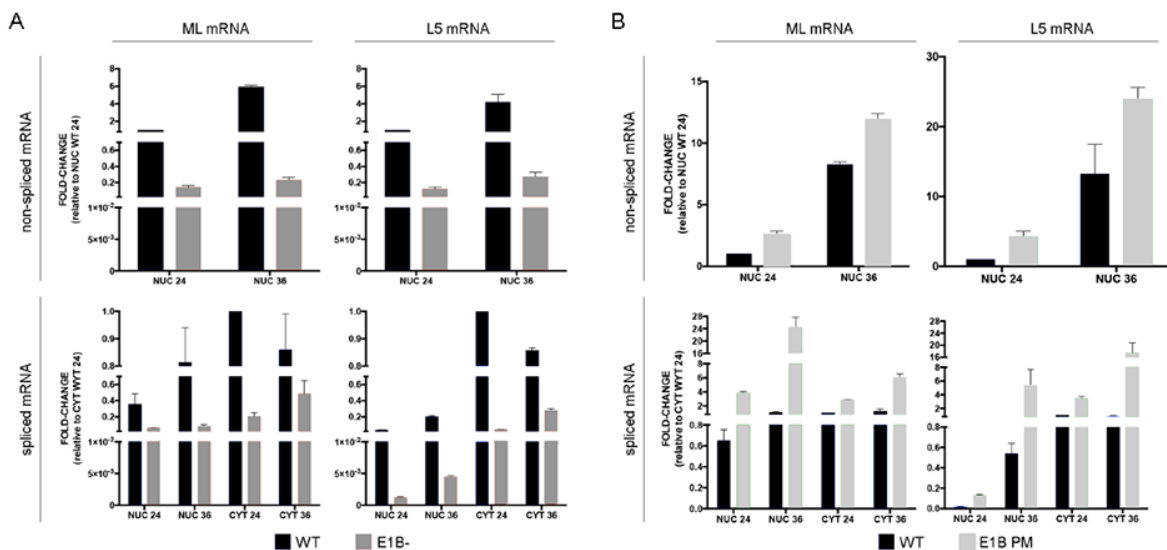

Figure 23.   NUC and CYT partitioning of ML and L5 unspliced and spliced mRNA in Ad WT, E1B⁻ or E1B PM fractions. NUC and CYT fractions were obtained from Ad WT, E1B⁻ (A) or

E1B PM (B) infected HFF and harvested at 24 or 36 hpi. Total RNA was isolated from each fraction and quantified by qRT-PCR. Standard deviations and mean fold-change values were plotted for two independent experiments performed in triplicate.

5.4 E1B promotes efficient formation, as well as adequate organization and morphology of viral Replication Compartments.

During the viral replication cycle, the E1B can be localized in the cytoplasm or in the nucleus depending on the cells used and the presence of other viral proteins [164-167]. E1B can also be localized in juxtanuclear cytoplasmic bodies similar to aggresomes [168]. In the nucleus, the protein can associate with the viral protein E4Orf3 and localize to PML-nuclear bodies [169] or with the nuclear matrix, independent from its association with E4Orf3 [170]. Additionally, E1B localizes in viral RC and this localization is enhanced by its interaction with another viral early protein, E4Orf6 [167, 171, 172]. As described in previous sections, E1B is a multifunctional protein that can be postranslationally modified by SUMOylation and phosphorylation. Although the effect of these modifications on the protein's activities is incompletely understood, phosphorylation of the E1B C-terminus is known to foster SUMO modification, which in turn promotes the association of the protein with RC [201]. The accumulated evidence indicates that different populations of the E1B protein exist in the infected cell at any one time-point of the viral replication cycle, which may be defined by both postranslational modifications or the variety of protein-protein interactions in which E1B participates, which in turn determine its spatio-temporal distribution. For example, it has been suggested that the fraction or subpopulation of E1B that participates in viral mRNA metabolism is associated to RC. In order to determine if E1B can impact biochemical and morphological aspects of RC that result in regulation of RNA biogenesis in these structures, we performed high resolution assays, using Dynamic Light Scattering (DLS) analyses, super-resolution (SR) microscopy, mass spec and RNAseq to measure the impact of E1B and of its phosphorylation on biochemical and morphological features of RC.

5.4.1 E1B affects the hydrodynamic diameter of viral Replication Compartments.

DLS is a technique classically used to measure the size of particles dispersed in a liquid, typically in the sub-micron region. The size of particles is calculated as the hydrodynamic diameter by the Stokes-Einstein equation, which takes into account the diffusion coefficient, the viscosity of the liquid and the temperature. Since, our method to isolate RC from infected cells allowed us to obtain RC particles, we decided to use this technique to measure the size of RC isolated from Ad WT, E1B⁻ or E1B PM-infected HFF cells. The RC particles were analyzed by DLS at 24 hpi

(early to late transition time point) and 36 hpi (late time point) (Fig. 24). First we compared the size of particles obtained from mock-infected (MK) cells, which correspond to nucleoli, with those from Ad WT-infected cells (Fig. 24 A). At 24 hpi, Ad WT RC were slightly larger tan nucleoli, at approximately 450 nm in hydrodynamic diameter. At 36 hpi, the size distribution increased up to 630 nm, and an additional population of smaller particles was measured at approximately 300 nm. In the E1B⁻ virus, the absence of E1B resulted in a slight decrease in the apparent hydrodynamic diameter of RC (Fig. 24B). Interestingly, for the E1B PM virus RC particles were divided into different populations, with apparent sizes ranging from 600 nm, similar to Ad WT, up to 6 µm (Fig. 24C). These results suggest that E1B is necessary for efficient formation of RC and that phosphorylation of E1B results in RC with increased dimensions and heterogeneity.
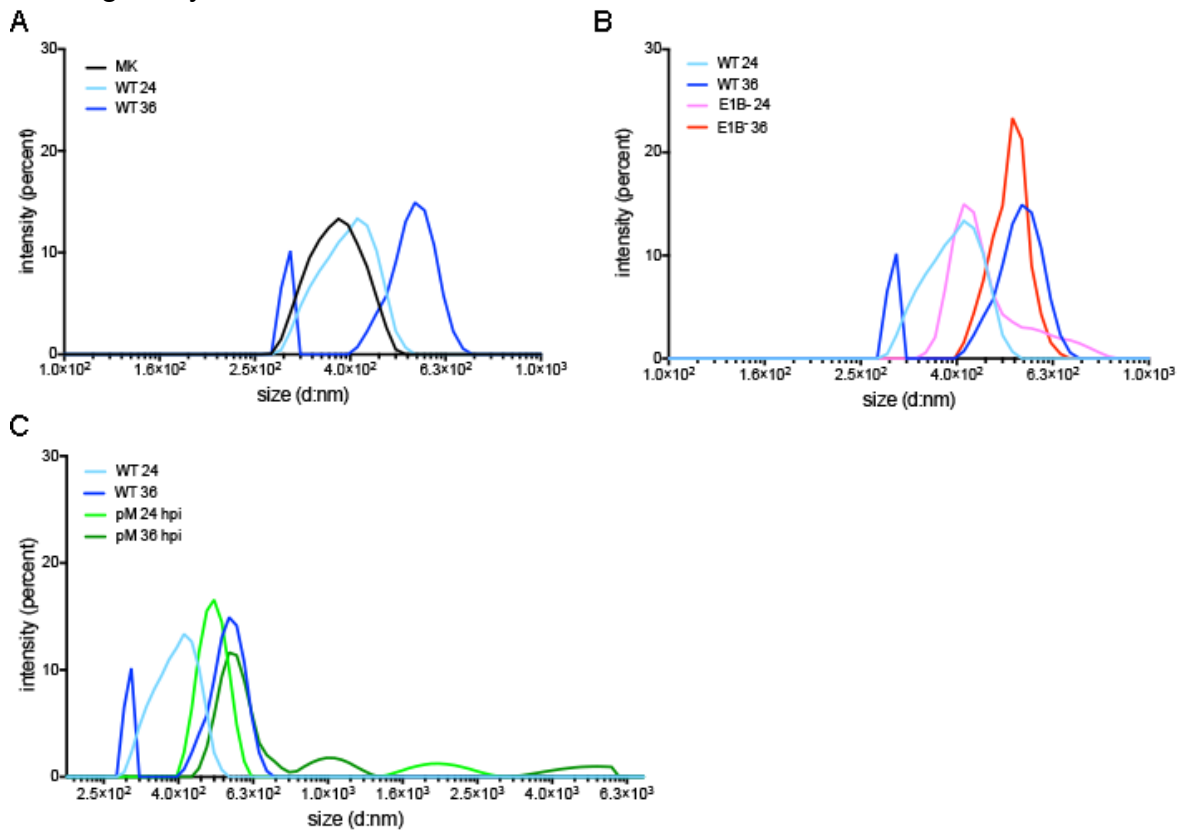
Figure 24. **Dynamic Light Scattering of RC particles isolated from MK, Ad WT, E1B⁻ or E1B PM infected HFF.** The apparent hydrodynamic diameter was calculated using a Malvern Zetasizer Nano SP instrument at 4ºC for 1 ml of each RC sample. Three measurements were performed for each sample, with 12 reads of 10 s per each measurement. The average of intensity per size (d:nm) was plotted for each sample at 24 and 36 hpi.

77

5.4.2 E1B impacts the area of viral Replication Compartments.

We recently developed a novel algorithm to perform quantitative analysis of RC in populations of Ad-infected cells using the adjustment of ellipses visualizing RC by fluorescence microscopy [224] (Fig. 25). Using this algorithm we found that in Ad WT-infected cells, RC increase in size, reaching their maximum area between 24 and 28 hpi. After 28 hpi the area of RC decreased and remained constant by 36 hpi. In contrast, cells infected with the E1B⁻ virus displayed a complex behavior, as although the area of RC in the absence of E1B was always lower than that of Ad WT RC, the area of RC increased transiently between 20 and 24 hpi, decreased between 24 and 28 hpi and increased again at the two latest time points (36 and 48 hpi) [224]. Interestingly, when RC from E1B PM-infected cells were analyzed, a faster increase in size compared with Ad WT was detected from 16 hpi, reaching a maximum area at 20 hpi, and a decrease from that point forward. For this virus, fluorescence micrographs at 36 hpi could not be analyzed due to excessive coalescence between RC, which abrogate ellipse adjustment. These data are consistent with DLS measurements, as in the absence of E1B, RC were smaller, and the E1B PM-RC were larger at earlier times than Ad WT.
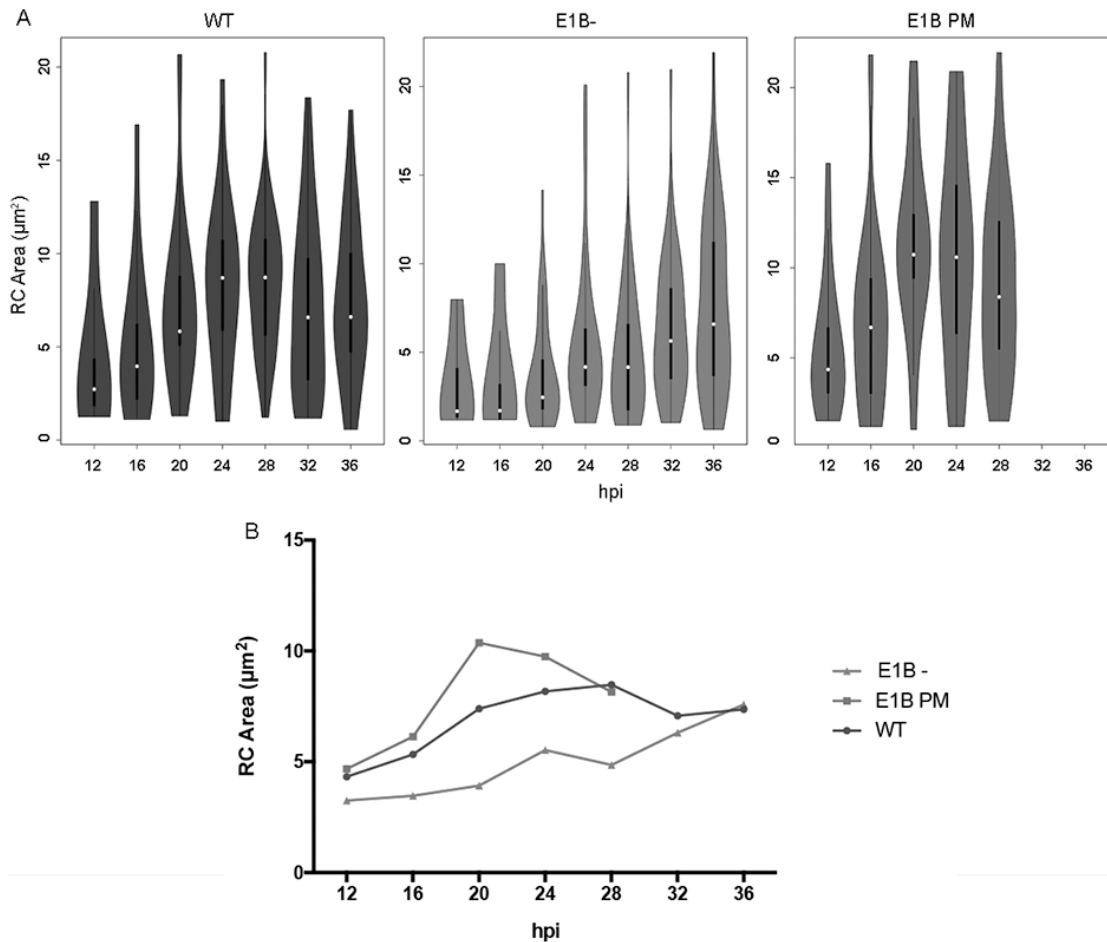
Figure 25. **Descriptive statistical analysis of the area of RC from Ad WT, E1B⁻ or E1B PM-infected HFF at different times of the viral replication cycle.** HFF cells were infected with the indicated viruses and fixed at the indicated times post infection. The cells were processed for immunofluorescence analysis and viewed using a Zeiss Axiovert 200 M inverted microscope with a 63x/1.4- numerical-aperture oil-immersion objective lens with an Axiocam MRM and Axiovision 3.1 software (Carl Zeiss, Inc.). A. Ad WT (blue), E1B⁻ (red) and E1B PM (green) RC area violin graphs. The white dot represents the mean and the bold lines are the standard deviation. B. Plot of mean area for the three viruses. The number of cells analyzed for each experimental condition was n ≥ 60. The red asterisks represent the statistical significance in the difference between the wild type and mutant viruses using the test of Kruskal-Wallis: *p-value ≤0.05; **p-value ≤0.01.

5.4.3 E1B impacts the organization and compartmentalization of viral Replication Compartments.

To examine the organization of RC and further determine if E1B affects their organization and morphology we performed super-resolution (SR) microscopy analyses of Ad WT, E1B⁻ or E1B PM-infected HFF cells at 20 and 24 hpi. The nuclear distribution of several cellular proteins that are known to colocalize with E2-DBP at RC and regulate RC-associated activities was studied in relation to E2-DBP and the E4Orf3 viral protein, which is organized in track-like structures that form adjacent to DBP and correspond to reorganized PML-nuclear bodies during the infection.

♦ E1B

The distribution of E1B was initially analyzed in these experiments, and as expected, both in Ad WT and E1B PM-infected cells the protein localized in RC, in close proximity to E2-DBP often intercalated in ring-like structures. In addition, E1B also colocalized with E4Orf3 in nuclear tracks. These findings suggest that phosphorylation of E1B may induce its localization to RC and E4Orf3-nuclear tracks, and are in agreement with previous reports described above, where phosphorylation of E1B was shown to increase the protein's SUMOylation, and its SUMOylation in turn increases the protein's localization in RC [201] (Fig. 26).
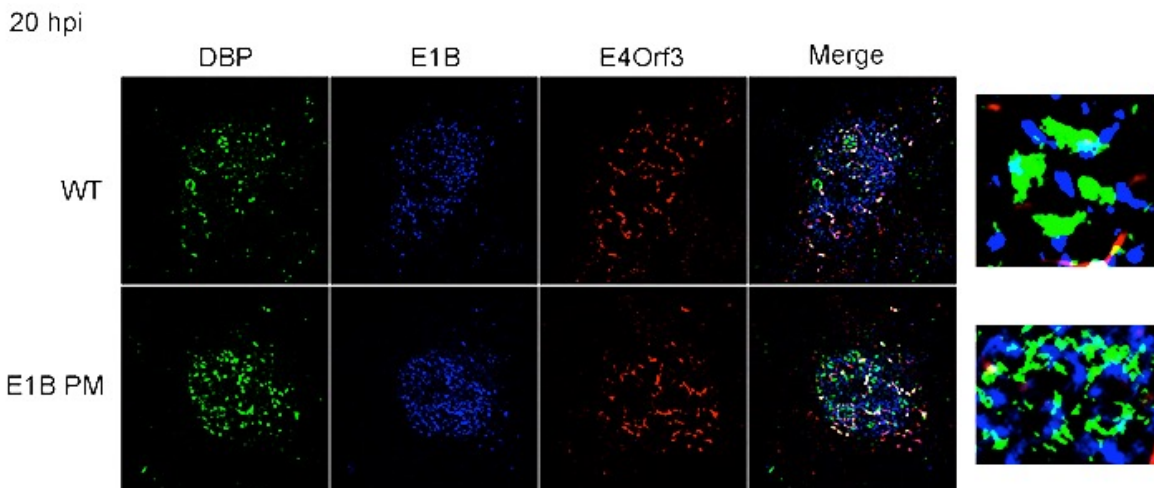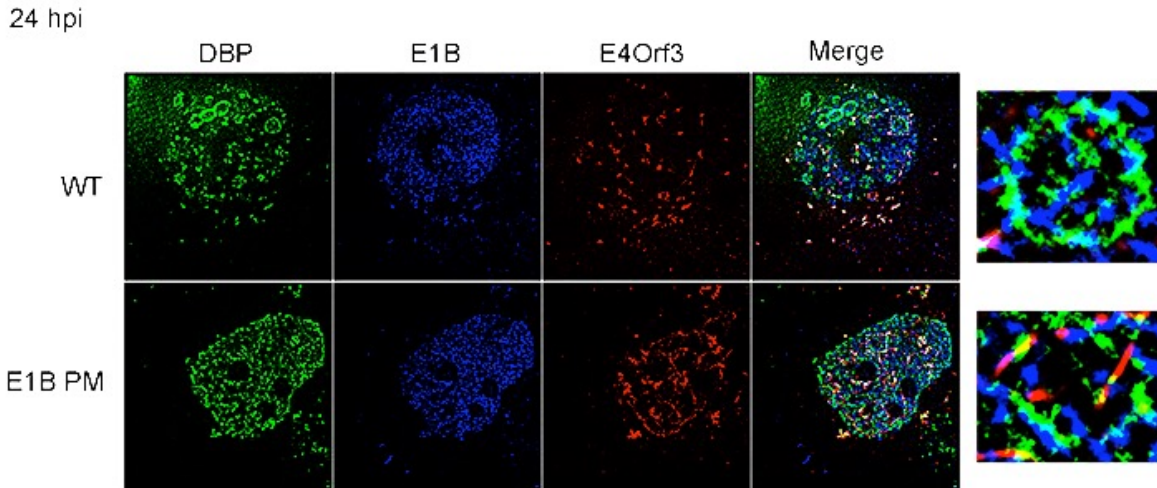
Figure 26.   **Phosphorylation of E1B induces its localization to RC and nuclear tracks**. Super-resolution microscopy images of HFF cells infected with Ad WT, E1B PM or E1B⁻ viruses and analyzed at 20 and 24 hpi. DBP (green, Alexa Fluor 405), E1B 55K (blue, Alexa Fluor 488), E4Orf3 (red, Alexa Fluor 568). The insets show the amplification of selected DBP rings to show the intercalated distribution of E1B in Ad WT and E1B PM.

♦ SUMO 2/3 and CTCF

SUMO modification of proteins has been shown to regulate formation of nuclear domains, in particular the PML-nuclear bodies [247, 248]. During adenovirus infection, the SUMOylation system is modulated and reorganized. The E1A protein associates with the E2 SUMO ligase, Ubc9 and regulates SUMOylation of target proteins [249]. E1B functions as an E3 SUMO ligase for p53 and can also interact with Ubc9. E4Orf3 induces SUMOylation of components of the DNA damage response [250]. In addition, we recently found that nearly the total pool of SUMO is relocalized to RC, and that such redistribution depends on E1B, E4Orf6 and E4Orf3 [124]. Whether the role of E1B on SUMOylation of cellular proteins may impact the formation and functional organization of RC is not known, however, these observations suggest that the adenoviral oncogenes, including E1B, induce formation of RC by recruiting cellular proteins to the viral genome [95]. CTCF is a multifunctional cellular protein implicated in the maintenance of the nuclear architecture. In Ad-infected cells CTCF is relocalized to RC where it binds viral DNA and promotes efficient viral late transcription [56, 251]. In our experiments, SUMO 2/3 and CTCF both localized in similar structures with E2-DBP, and to a lower extent with E4Orf3, in Ad WT and E1B PM-infected cells. Interestingly, the localization of SUMO 2/3 (Fig. 27) and CTCF (Fig. 28) in RC was not observed in the absence of E1B, since in cells infected with the E1B⁻ mutant virus, these cellular proteins were only observed in nuclear tracks. These results suggest that the localization of SUMO 2/3 and CTCF in nuclear tracks is independent of E1B; however, their localization to RC does depend on E1B and it is promoted by the protein's phosphorylation. These results are interesting, as they suggest that E1B

80

might promote efficient expression of viral genes by recruiting CTCF to RC. Moreover, CTCF and SUMO 2/3 could function as a scaffold for RC formation, recruiting proteins to these sites, a role that has been suggested before for these proteins in some cellular processes [252, 253].
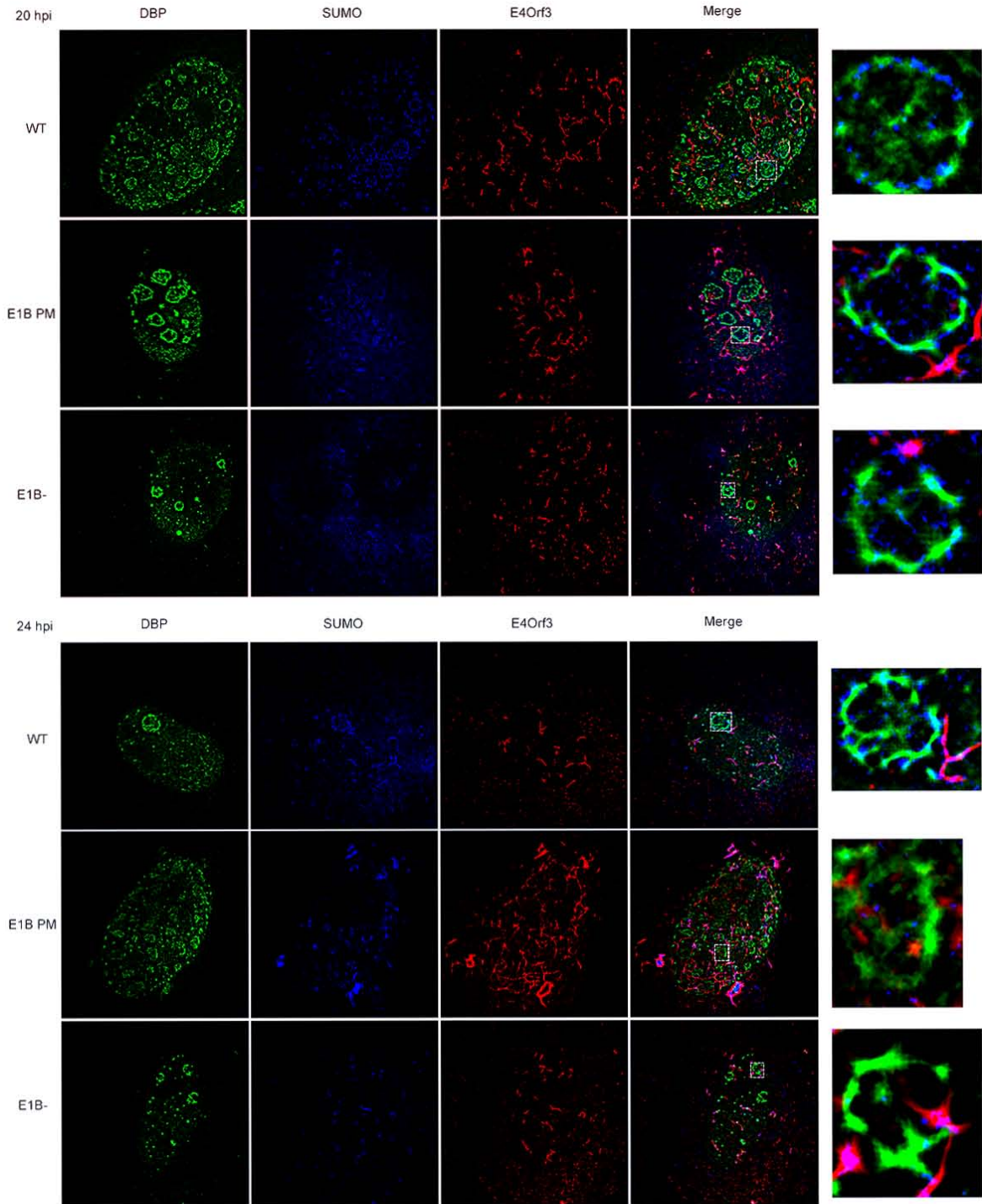
Figure 27. **SUMO2/3 molecules are recruited to RC dependent of E1B.** Super-resolution microscopy images of HFF cells infected with Ad WT, E1B PM or E1B⁻ viruses and analyzed at 20 and 24 hpi. DBP (green, Alexa Fluor 488), SUMO 2/3 (blue, Alexa Fluor 405), E4Orf3 (red, Alexa

Fluor 568). The insets show the amplification of selected DBP rings to show the intercalated distribution of SUMO 2/3 in Ad WT and E1B PM, the absence of SUMO 2/3 in E1B⁻ RC and the close proximity to E4Orf3 nuclear tracks.

Figure 28. **CTCF is recruited to RC dependent on E1B.** Super-resolution microscopy images of HFF cells infected with Ad WT, E1B PM or E1B⁻ viruses and analyzed at 20 and 24 hpi. DBP (green, Alexa Fluor 488), CTCF (blue, Alexa Fluor 405), E4Orf3 (red, Alexa Fluor 568). The insets show the amplification of selected DBP rings to show the intercalated distribution (20 hpi) or RC-

82

puncta distribution (24 hpi) of CTCF in Ad WT and E1B PM, the absence of CTCF in E1B⁻ RC and the close proximity to E4Orf3 nuclear tracks.

♦ BRCA1

BRCA1 is a tumor suppressor with antiviral activity that participates in the DNA damage response (DDR). Previous reports have shown that in HEp-2 cells infected with adenovirus, BRCA1 is localized at early times with E4Orf3-tracks and later it is relocalized to RC [119]. In Ad-infected HFF cells, we found that BRCA1 was relocalized to RC and to a lesser extent to E4Orf3-tracks independently of the presence of E1B, suggesting that E1B does not modulate BRCA1 localization in RC and that this tumor suppressor might be co-opted to participate in activities associated to RC or, since this cellular protein is an antiviral factor, it might be sequestered at RC to inhibit its antiviral activity (Fig. 29).
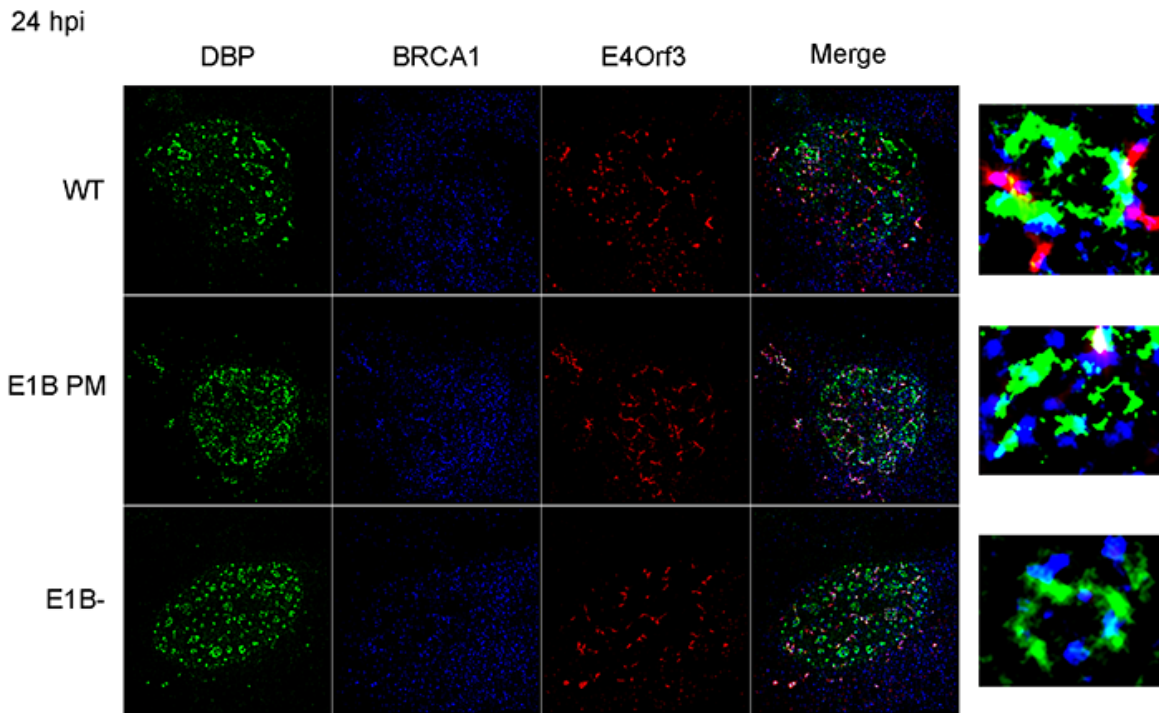
Figure 29. **BRCA1 is recruited to RC and nuclear tracks independently of E1B.** Super-resolution microscopy images of HFF cells infected with Ad WT, E1B PM or E1B⁻ viruses and analyzed at 20 and 24 hpi. DBP (green, Alexa Fluor 405), BRCA1 (blue, Alexa Fluor 488), E4Orf3 (red, Alexa Fluor 568). The insets show the amplification of selected DBP rings to show the distribution of BRCA1 in RC.

♦ YB1

YB1 is a multifunctional cellular factor that localizes preferentially in the cytoplasm in non-infected cells. When the cell is subjected to stress, YB1 is relocalized to the nucleus. During adenovirus infection of HeLa cells, YB1 has been shown to relocalize to RC. Such relocalization depends on E1B, and YB1 binds and activates the E2 viral late promoter [57]. In our experiments, in infected HFF cells YB1 was only partially relocalized to RC by 20 hpi and later (24 hpi) associated with the E4Orf3-nuclear tracks. However, we did not find changes in the viral-induced localization of YB1 in the absence of E1B, contrary to the previous report [57]. In fact, YB1 association to RC was enhanced when the E1B protein was not produced. These results indicate that relocalization of YB1 to RC is independent of E1B (Fig. 30).

84
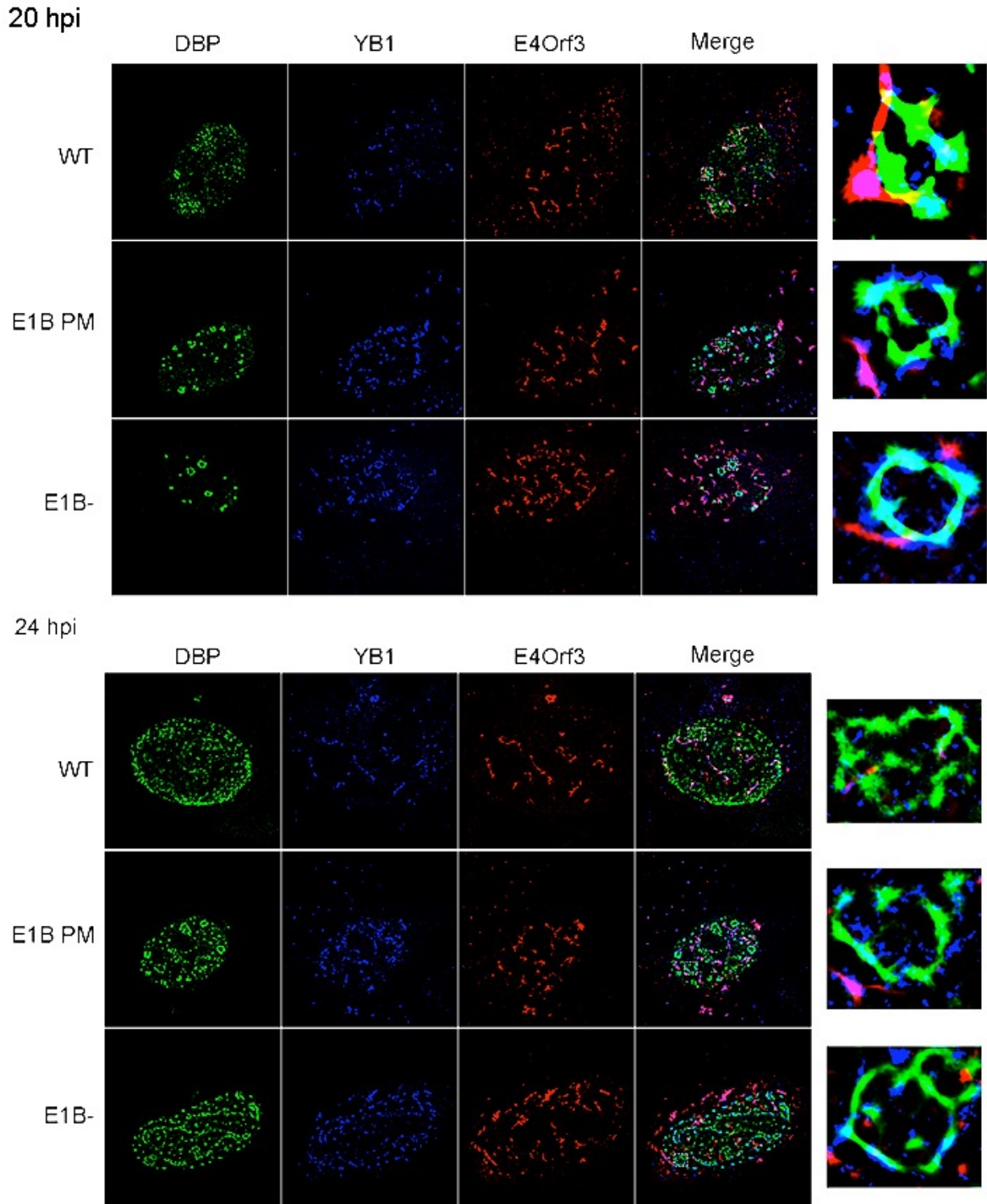
Figure 30. **Localization of YB1 to RC is independent of E1B.** Super-resolution microscopy images of HFF cells infected with Ad WT, E1B PM or E1B⁻ viruses and analyzed at 20 and 24 hpi. DBP (green, Alexa Fluor 488), YB1 (blue, Alexa Fluor 405), E4Orf3 (red, Alexa Fluor 568). The insets show the amplification of selected DBP rings to show the distribution of YB1 in RC.

♦ Tap

The cellular protein, Tap (NXF1) is the main export receptor for cellular mRNA nuclear-cytoplasmic export and is responsible for the export of viral late mRNA during the late phase of infection [78]. For this protein, as for YB1, we did not observe a modulation of its localization induced by E1B. In all conditions and all viruses analyzed, Tap was localized both in close proximity with DBP in RC and in E4Orf3-nuclear tracks. These results are consistent with the activity of Tap on the export of mRNA synthesized in RC, since this localization is an intermediate compartment in the transit of viral mRNA from their site of synthesis and processing to the nuclear envelope to be exported (Fig. 31).
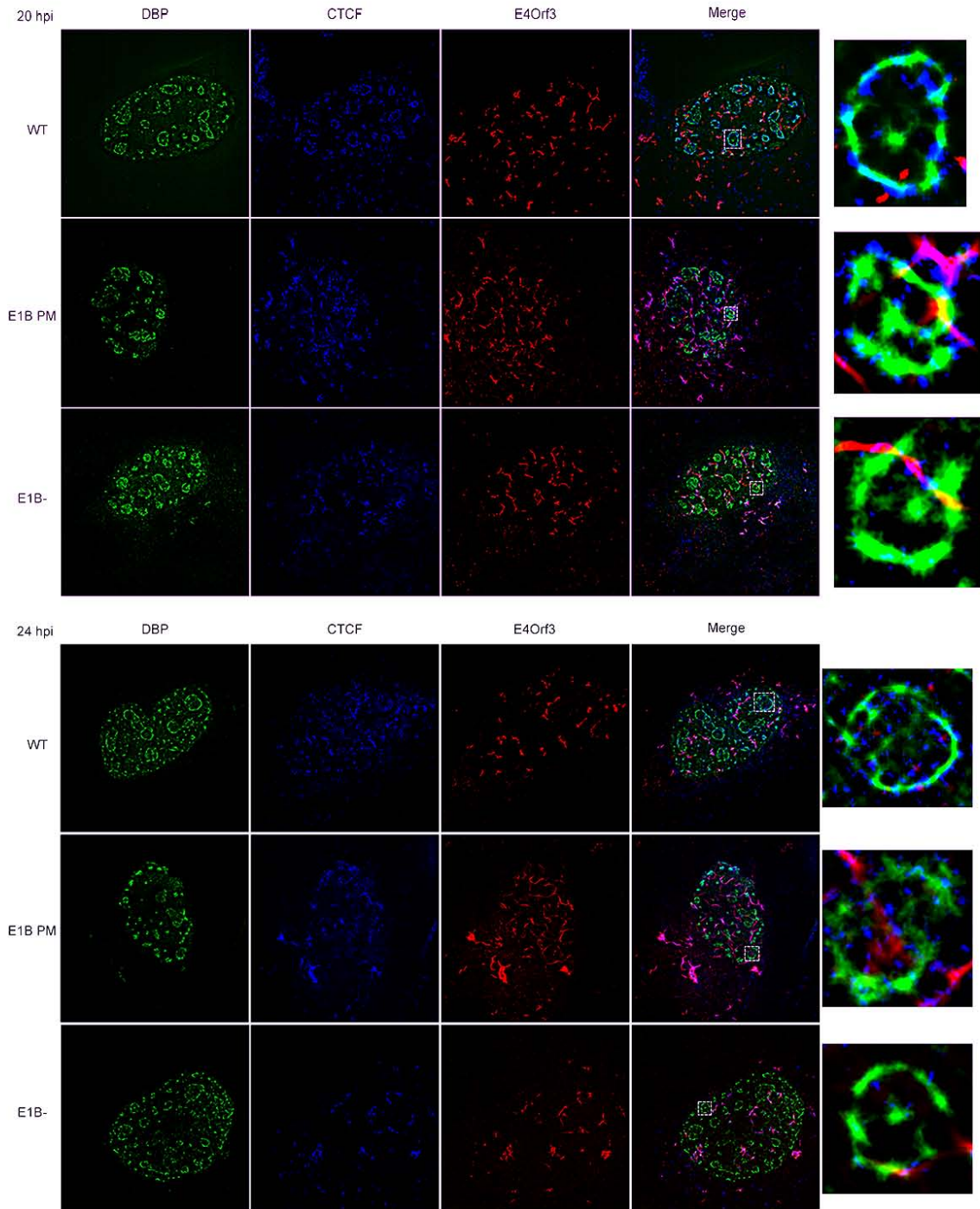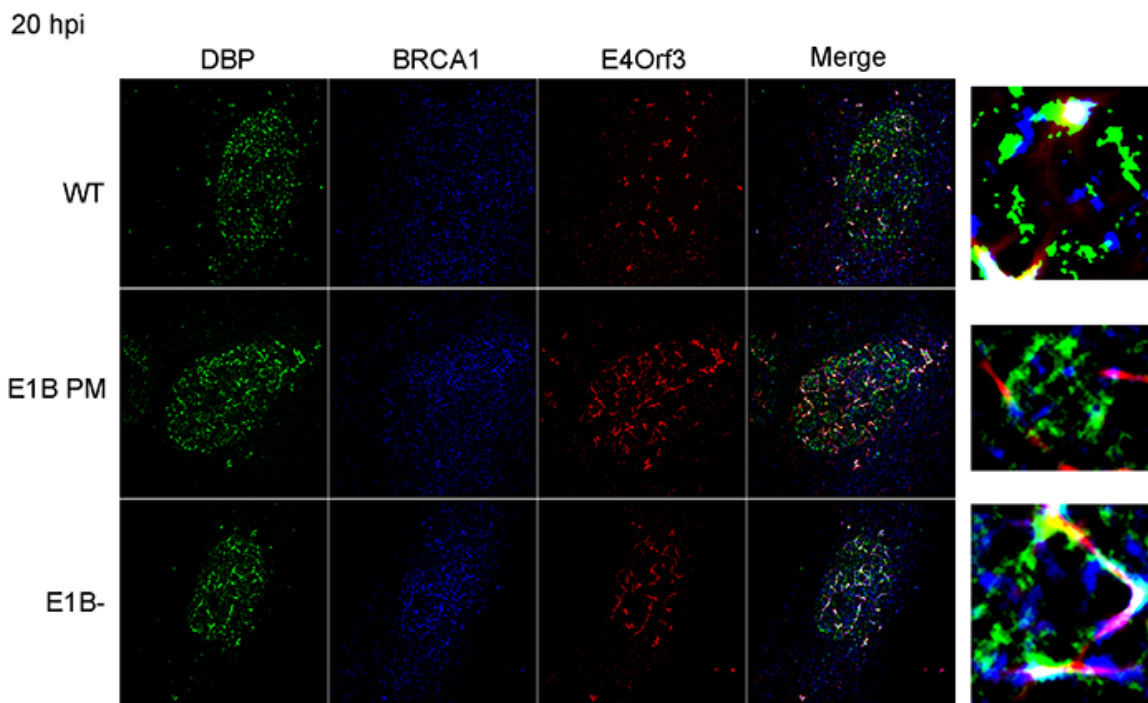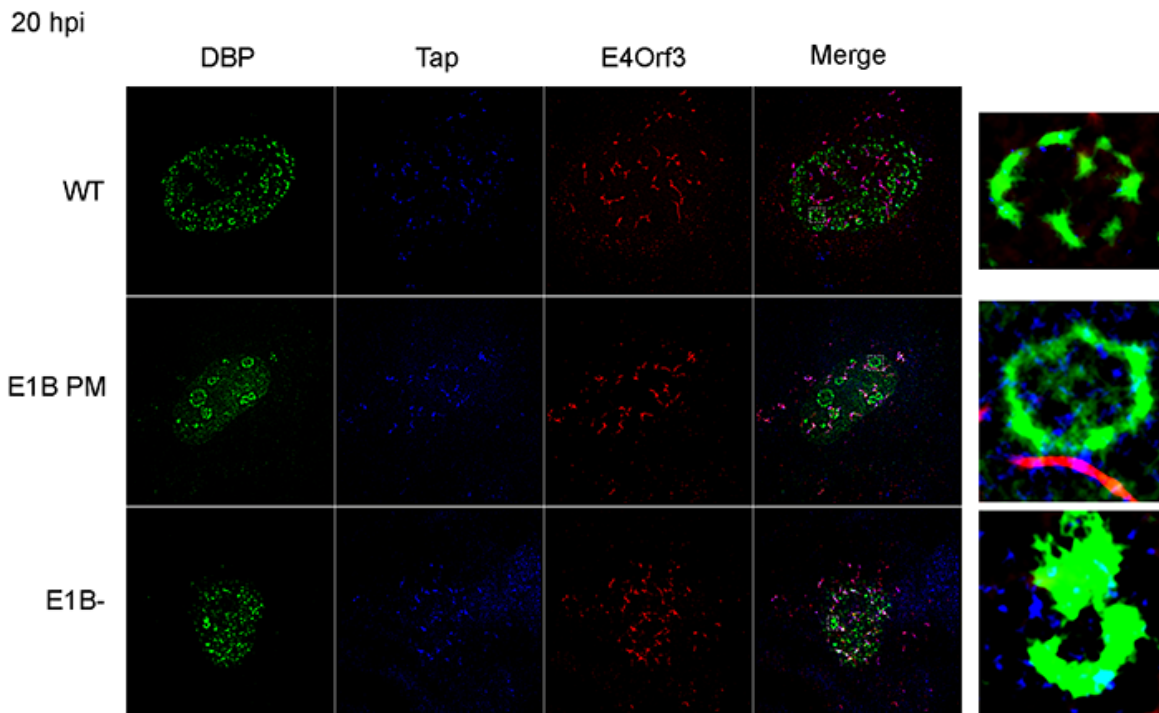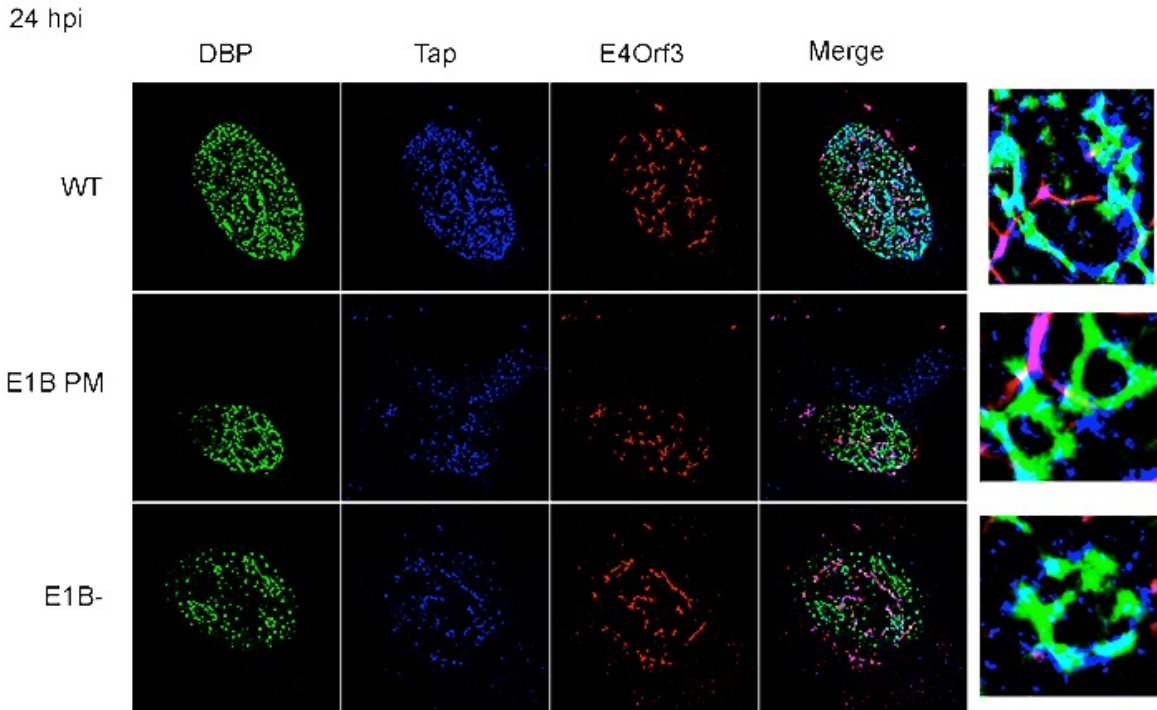
Figure 31. **Localization of Tap to the periphery of RC is independent of E1B.** Super-resolution microscopy images of HFF cells infected with Ad WT, E1B PM or E1B⁻ viruses and analyzed at 20 and 24 hpi. DBP (green, Alexa Fluor 488), Tap (blue, Alexa Fluor 405), E4Orf3 (red, Alexa Fluor 568). The insets show the amplification of selected DBP rings to show the RC localization of Tap.

These images will be further analyzed to statistically model the organization of the proteins in RC and in E4Orf3 nuclear-tracks. Taken together, the results suggest that E1B impacts the recruitment of some proteins to RC that, on the one hand, may function as scaffolds or factors that promote efficient genome replication and gene expression, and on the other, are proteins with antiviral activity that may be inhibited or co-opted in RC.

5.4.4 E1B modulates the composition of viral Replication Compartments

Proteomic and transcriptomic analyses of RC particles from Ad WT, E1B⁻ and E1B PM-infected HFF at 36 hpi were performed to explore the effect of E1B on the protein and RNA composition of RC (Fig. 32 and 33). The mass spec analysis was made using the technique of ESI-QTOF. The number of proteins identified for each RC fraction was as follows: 863 in MK (nucleoli), 509 in Ad WT, 680 in E1B⁻ and 401 in E1B PM RC. These proteins were classified according to their molecular function. Interestingly, anti-viral proteins were more abundant in Ad WT and E1B PM than in E1B⁻ RC. This observation is relevant, since it not only confirms previous reports that E1B inhibits the anti-viral interferon response [254], but it also suggests that the E1B-dependent recruitment of cellular factors to RC avoids blocking of the viral replication cycle progression. An additional observation was

87

that viral proteins were under-represented in RC in the absence of E1B. This observation correlates with the defects observed in viral gene expression in cells infected with the E1B⁻ mutant. As expected, nucleolar as well as cellular proteins that participate in RNA synthesis and processing were abundant in these fractions [146].
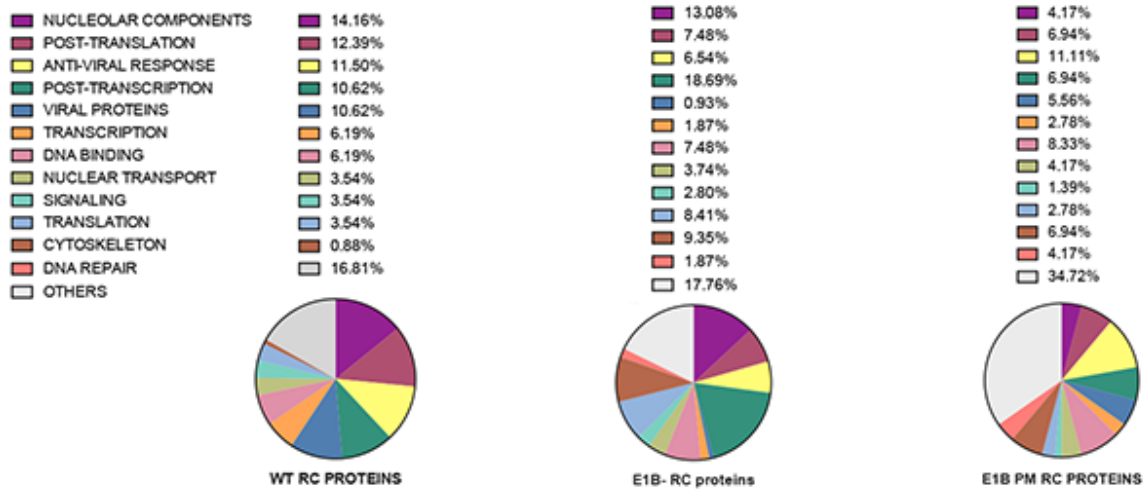
Figure 32. **Classification of proteins specific for RC from Ad WT, E1B⁻ or E1B PM-infected HFF at 36 hpi.** RC particles for each virus were analyzed by ESI-QTOF and the proteins identified were analyzed to determine those that were specific for each sample. These proteins were classified according to their molecular function.

We further analyzed the RC particles by quantitative mass spectrometry assays using TMT-tags, as described in Materials and Methods. For this purpose, we initially analyzed the proteins associated to Npl and RC fractions from HFF cells infected with Ad WT, E1B⁻ or mock-infected to define the proteins proper from RC and then compared the effect of E1B on the association of these proteins to RC (Fig. 33).
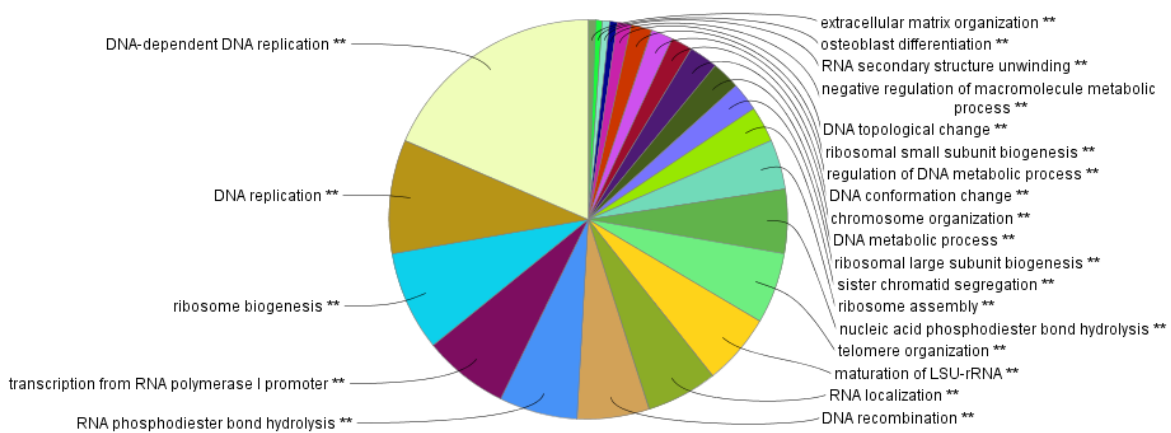
Figure 33. **Classification of proteins specific for RC from Ad WT at 24 hpi.** The proteins were classified according to their GO biological process. To determine which proteins are specific of

88

RC, an RC/Npl ratio higher than 1.3 and an RC/Nlo ratio (mock-infected RC) higher than 1.4 were considered, measuring a total of 264 proteins.

Table 6 shows the viral proteins found to be associated to Ad WT RC.

Table 6.   Viral proteins associated to RC

Accession	Protein Name	Gene
P04493	Early E3 14.5 kDa protein	E3
A8W995	U exon protein	U
P24940	Protein 33K	L4
P03265	DNA-binding protein	E2A
P03281	Hexon-interlacing protein	IX
P03271	Packaging protein 1	IVa2
P24937	Pre-protein VI	L3
P04496	Packaging protein 3 52/55K	L1
P68951	Pre-histone-like nucleoprotein VII	L2
P24938	Core-capsid bridging protein V	L2
P04499	Preterminal protein	E2B
P24933	Shutoff protein 100K	L4
P12537	Pre-hexon-linking protein IIIa	L1
P24936	Pre-hexon-linking protein VIII	L4
P12538	Penton protein III	L2
P11818	Fiber protein IV	L5
Q2KS19	I-leader protein	i-leader
P04133	Hexon protein II	L3
P04495	DNA polymerase	E2B

The E2 viral proteins DBP, pol and pTP, were found in RC particles, as expected, since these proteins are directly involved in viral DNA replication. RC protein levels were found reduced in the absence of E1B. However, these analyses are still preliminary and replicates need to be compared in order to quantitatively define the effect of E1B on RC composition.

The RNAseq assay showed that higher levels of early and late mRNA were associated to RC in E1B PM-infected cells, and in the absence of E1B the reads aligned to these transcripts were reduced nearly 20-fold (Fig. 34). These differences are in agreement with mRNA measurements using qRT-PCR assays described in this study. These results are also in agreement with our previous results, showing that phosphorylation of E1B enhances biogenesis of viral mRNA in RC.
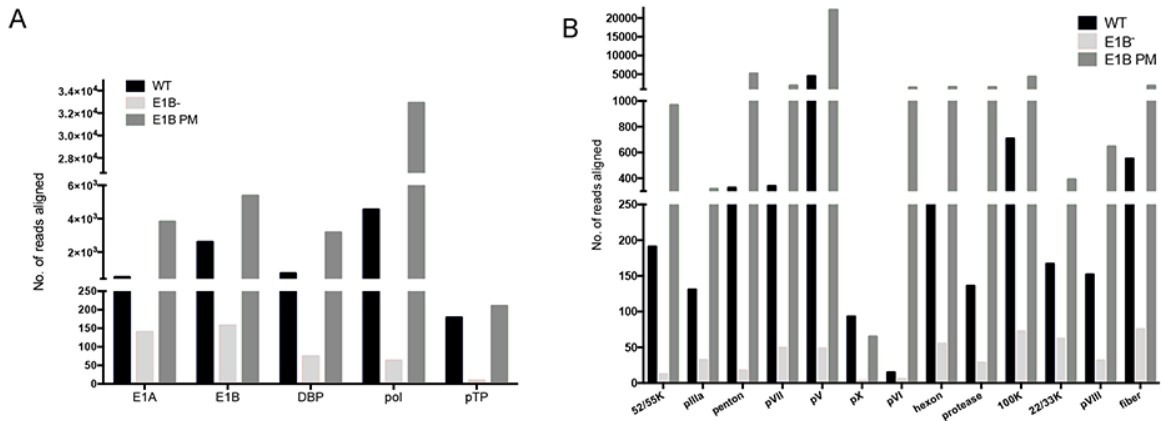
Figure 34. **RNAseq analyses of RC from Ad WT, E1B⁻ or E1B PM infected HFF at 36 hpi.**
RNA from RC particles for each virus were sequenced and the reads for early (A) and late (B) viral mRNA were plotted.

Taken together, these results indicate that E1B impacts the morphology, organization and composition of RC. The databases generated for the proteomic and transcriptomic assays will be extended and further analyzed to continue exploring the role of E1B on RC composition at several time-points of the infection cycle.

6 DISCUSSION

The E1B 55K protein (E1B) is a multifunctional phosphoprotein that plays a major role in establishing a productive adenoviral infection (as detailed in the introduction). A particular interest for the study of this protein has increased because of the potential use of adenoviruses as therapeutic vectors, since the gene that encodes E1B is deleted from adenovirus vectors used in cancer gene therapy, which allows the virus to preferentially replicate and kill tumor cells [5]. However, the molecular functions of E1B that allow a cell-selective viral replication and subserve an efficient viral replication cycle are poorly defined.

This protein assembles a Cullin 5-based E3 ubiquitin ligase complex with the viral protein E4Orf6, which polyubiquitinates and targets for proteasomal degradation cellular proteins that inhibit the efficient production of viral progeny; therefore promoting efficient viral replication [14]. E1B can also control the anti-viral response, because it may function as a repressor of transcription of interferon-inducible genes. This activity has been proposed to be linked to formation of viral replication centers and genome replication [254]. Furthermore, E1B mediates efficient viral DNA replication and viral late mRNA biogenesis, while inhibiting cytoplasmic accumulation of several cellular mRNA [76, 77, 87, 158, 163, 226].

We hypothesized that the effect of E1B on regulation of viral DNA replication and viral mRNA biogenesis depend on the role of this protein on proper formation of RC. Therefore, in order to study how E1B regulates virus-host interactions and promotes an efficient progression of the viral replication cycle, we performed a detailed analysis of the viral gene expression program in normal human cells and evaluated the role of E1B on different steps of the viral replication cycle. Moreover, we established a protocol to isolate RC from infected cells and directly evaluate the role of E1B on RC-associated activities and RC formation. For this purpose, we performed quantitative and high-resolution assays such as super-resolution (SR) microscopy, sub-cellular and sub-nuclear fractionation, quantitative PCR, next generation RNA sequencing and mass spec analyses to study RC biochemistry and morphology, viral DNA replication, and early and late gene expression of the viral genome. HeLa cells have been one of the main cell lines used to study the biology of adenoviral infections. Cell lines provide a system that supports efficient viral growth, but with a shortened viral replication cycle, compared to primary cells. Moreover, the cell cycle in cell lines is deregulated, making it difficult to study the alterations that are solely dependent on viral infection, that is, without the interference of the severely altered genetic background of the cells. Hence, primary cells were used in the present work because the periods of time for different steps of the viral replication cycle are extended in these cells, and the molecular mechanisms that regulate cell cycle progression are functional, which allow to analyze the effect of the viral infection on cellular and viral processes without interference by the genetic background of the cells, and to analyze in detail the

91

temporal changes of viral gene expression at times post-infection that comprise both early and late events of the viral replication cycle.

6.1 Analysis of the adenovirus gene expression program and its regulation by E1B

The complexity of the adenoviral replication cycle involves a gene expression program with multiple levels of regulation, from sequential regulation of transcription, to the selective export and translation of viral late mRNA that result in the progressive increase of viral late gene products (reviewed in [255]). Such increase in the expression of viral late genes depends on the accumulation of replicated viral genomes and the presence of a number of cellular and viral proteins (Table 1). Many features of the biogenesis of major late (ML) mRNA have been studied in detail [255]. However, simultaneous analysis at different times post-infection of the rate of synthesis of ML pre-mRNA, the ratio of spliced vs. unspliced RNA, partitioning of different ML RNA between nucleus and cytoplasm and between RC and Npl, as well as the impact of E1B on these processes has not been reported.

Real-time PCR is a quantitative technique with high sensitivity that has been widely employed in several areas of virology. Therefore, different aspects of viral early and late mRNA biogenesis were measured using this technique, such as synthesis, stability and steady-state levels at several time-points that comprise almost the entire adenoviral replication cycle in non-transformed HFF cells (Fig. 6-11). This study represents, to our knowledge, the most complete analysis of the viral gene expression program and should allow a detailed analysis of the regulation of gene expression, beyond the analysis performed here.

We found that some mRNA levels correlate with the functions of the proteins encoded by these transcripts. Transfection assays to evaluate the role of DBP in regulation of adenoviral promoters activities using reporter genes has shown that DBP enhanced the expression of E1A, E2-E and ML promoters, but inhibited E4 promoter expression [51]. Other reports have also shown that the E1A and IVa2 proteins also function as transcriptional activators of the ML promoter [38, 58]. Our results show that when E2A-DBP mRNA levels increased, the levels of the E4Orf6/7 mRNA started to decrease, which correlates with the activity of DBP as an E4-repressor (Fig. 6A). Moreover, the increase in the levels of E1A, E2A-DBP and IVa2 mRNA correlated in time with the beginning of the accumulation of viral late mRNA, again, correlating the pattern and level of expression of early genes that regulate viral late promoters (Fig. 6). Therefore, the study of the accumulation of viral mRNA should help to study the regulation of gene expression, since the results show that qRT-PCR kinetic studies can be used to make detailed analyses of the role of each viral gene product on regulation of gene expression.

In HeLa cells, an unknown repressor factor binds to an intragenic sequence of IVa2 inhibiting its transcription. This factor is titrated as the number of viral DNA molecules increases during DNA replication, thus restricting IVa2 expression to the late phase of infection [60]. However, our results in normal human cells, showed that the steady-state levels of IVa2 mRNA increased (8-16 hpi) before viral DNA molecules started to accumulate (16-20 hpi) (Fig. 6). These observations indicate that in primary cells, the IVa2 repressor factor may not exist or the titration-dependent transcription mechanism for IVa2 production is not established.

Additionally, the expression of viral late genes, apart from L1-52/55K, which is known to be expressed during the early phase, had been reported to be restricted to the late phase of infection. In contrast, in HFF-infected cells, L4, L5 and L1-pIIIa mRNA expression began before the onset of viral DNA replication (Fig. 6B and C). As expected, these viral mRNA increased to higher levels during the late phase of infection, which correlates with the reported increase in expression of the MLTU after the onset of viral DNA replication. Furthermore, our results showed a decrease for both early and late mRNA at the onset of viral DNA replication (20 hpi) (Fig. 6). Interestingly, previous reports where changes in cellular gene expression were measured in primary human lung fibroblasts (IMR-90) infected with Ad-2, showed that the adenovirus infectious cycle can be divided into four time periods based on the changes observed for cellular genes. From 12-24 hpi, prior to viral DNA replication, Zhao and coworkers found an upregulation of cellular genes involved in cell cycle regulation, while proliferation and anti-viral response factors were downregulated [227]. It is known that one of the main events of the early phase of infection is to induce the infected cell to enter the S phase of the cell cycle, providing an optimal environment for viral DNA replication [10, 256]. Hence, these data suggest that viral transcription could be paused, while cellular genes responsible for the progression to S-phase are expressed. Another possibility is that, at around 20 hpi, viral DNA molecules are committed to the initiation of DNA replication, suggesting there could be a preference for the DNA replication machinery rather than for the transcription machinery to bind the viral DNA. These results, together with the clustering shown in Fig. 7, provide novel insight into the complex networks that regulate viral early and late genes throughout the replication cycle and suggest that these data can be used to make specific predictions on the role early genes play on regulation of viral genome expression. For example, these data reveal a novel regulatory loop between E1B and IVa2 that results in efficient expression of viral late genes (Fig. 7). Moreover, the data also indicate that regulation of transcription depends not only on E1A, as previously reported, but that E1B can act as a transcriptional factor, an activity that has been suggested for this protein in the control of expression of immune response genes [160].

Therefore, the effect of E1B on viral gene expression was evaluated (Fig. 8). In HeLa cells, the rate of ML transcription and accumulation of viral late mRNA

becomes progressively lower in E1B-null mutant viruses than in Ad WT-infected cells during the late phase of infection [76, 87, 154, 156-158] and the stability of viral late mRNA is reduced [87, 154, 158]. Additionally, as described in the previous section, the regulation of viral late mRNA production by E1B seems to occur at an intranuclear step of viral mRNA biogenesis (Leppard and Shenk, 1989). Moreover, it has been reported that different viral late mRNA species are not equally dependent on E1B and that IVa2 transcription and accumulation is defective in the absence of E1B [156]. Our results show that IVa2 mRNA levels are dependent on E1B, as in the absence of E1B IVa2 mRNA accumulation was delayed and the levels of this intermediate mRNA were lower, compared to Ad WT. Also, this phenotype correlated with the levels of viral late mRNA, since in E1B⁻ infected cells, their accumulation was deficient.

Furthermore, we found not only that viral mRNA biogenesis is dependent on E1B, but also on the phosphorylation status of the protein. IVa2 mRNA accumulation began earlier than Ad WT in E1B PM-infected cells, which correlated with the increase in ML mRNA levels. However, phosphorylation of E1B negatively impacted the levels of E1A, E4Orf6/7, L152/55K and E2A-DBP mRNA. These results indicate that phosphorylation of E1B differentially impacts the role of E1B on efficient accumulation of viral mRNA (Fig. 8). Additionally, our results show that E1B can impact viral mRNA stability, with a greater effect on early mRNA than on late mRNA half-life (Fig. 9). This activity of E1B also correlates with E1B effect on viral mRNA steady state levels; the decrease of E1A mRNA was faster than the decrease for L5 mRNA when viral DNA synthesis began (Fig. 8).

An interesting finding was the dual role of E1B as an enhancer or repressor of various viral promoters and that these activities depend on the time post-infection and on the phosphorylation of the protein (Fig. 10 and 11). The differential effect of E1B on different viral late promoters and viral late mRNA steady-state levels is not a paradox; although it has long been believed that late gene expression begins with the transition to the late phase of infection when the activity of the MLP greatly increases to direct expression of the full set of L1-L5 gene products, it is now clear that new additional regulation mechanisms controlling viral late gene expression are established, such as regulation of the L4P [34] independently from the MLP, temporal control of the repression or activation of the MLP by different internal sequences [64] and a wide combination of factors that can regulate late gene expression and could be controlled by E1B [31, 34, 51, 56, 59, 61-67]. However, these suggestions need to be further studied to define how E1B differentially modulates each viral gene.

These data were validated by statistical analyses and by a linear regression model (Fig. 11), where the accumulation of each mRNA was measured in correlation to the accumulation of E1A, since E1A induces the activation of all viral genes. These models not only provide a tool for prediction, but also make it possible to describe

94

changes in the expression of each gene dependent on E1A at early and late times of infection.

As for E1B, other viral proteins have been reported to have a similar dual role as regulators of transcription of viral genes. For example, while E1A activates most of the viral promoters it displays a distinguishable effect on the E2 promoter, as it activates the E2 early promoter but represses the E2 late promoter [257]. Also, E1A can both enhance or suppress its own promoter [45]. In CAT reporter assays, E2A-DBP was shown to stimulate transcription of E1A, ML and E2E promoters, while repressing E4 [51]. This phenomenon is not exclusively found among the early genes, as the L4-22K protein both enhances and represses the ML promoter by binding to a downstream element (DE). L4-22K activates the ML promoter by binding the R1 region, but induces the recruitment of Sp1 to this DNA region with a repressive effect on ML transcription [64]. Finally, the E1B-19K protein represses expression of E1A but promotes expression of E1B, E2E, E3, E4, pIX and ML [44]. The data obtained in our experiments suggest that E1B could display activities as a dual viral transcriptional regulator. Furthermore, the effect of E1B on the efficient progression of the viral replication cycle can be mapped to its independent activities on efficient viral DNA replication, as well as production and stability of viral mRNA. However, the experiments performed in this work cannot be used to determine whether E1B regulates transcription directly or indirectly.

The E1B protein contains sequences that resemble motifs characteristic of a C_2H_2 zinc finger and a ribonucleoprotein (RNP) RNA-binding domain [164]. Nonetheless, it has not been established if the putative zinc finger of E1B can coordinate Zinc or if the protein is able to bind to DNA, but mutations in this sequence result in impaired viral replication [196]. In relation to the RNP domain, it has been reported that the protein can bind RNA *in vitro* [258], and in our lab, we have established that E1B is able to bind viral mRNA in the context of infection, which is necessary for efficient splicing of viral transcripts and efficient viral progeny production (Tejera, B. et al., unpublished); but whether the RNP motif is necessary for regulation of viral gene expression or how it impacts splicing is not yet clear. Moreover, although E1B structure has not been determined hitherto, it is known that the N-terminal region of the protein is intrinsically disordered and intrinsically disordered regions have been found to mediate multiple protein/protein interactions [259, 260]. In addition, E1B can be modified by phosphorylation and SUMOylation, as described before, and these posttranslational modifications could be determinant for the protein to associate to different targets, like nucleic acids or proteins. The E1B protein is known to interact with multiple viral and cellular proteins [261]. These characteristics suggest that E1B intracellular localization, in combination with its interactome could define different E1B pools that could participate in different molecular mechanisms that result in an efficient viral replication cycle.

95

The activities of E1B could depend on interactions with different molecules, for example transcription factors. E1B has been shown to interact with p53 inducing repression of p53 target genes [262] and p53 has been shown to activate the expression of the L4 promoter [62]. E1B also interacts with YB1, which in turn activates the expression of the E2 late promoter [57]. E1B binds to Daxx, a transcription repressor that can bind other transcription factors [263]. Further experiments should be performed to determine the E1B interactome and identify E1B-interacting proteins that may directly regulate viral gene expression, both at the level of transcription and mRNA processing. Moreover, since E1B possesses nucleic acid-biding activity experiments should be performed to evaluate whether the protein can also directly bind regulatory sequences to enhance or repress viral gene expression.

6.2   Isolation of RC

Since we established that E1B modulates expression of the viral genome, we then evaluated the role of E1B on regulation of RC-associated activities directly in isolated RC. With these experiments we measured replication of the viral genome, late mRNA synthesis and splicing. As described in the introduction, adenoviruses and other DNA viruses that replicate in the nucleus induce extensive reorganization of nuclear components, some of which are recruited to sites where viral RC are assembled (reviewed in [95]). These virus-induced microenvironments represent a common viral strategy that promotes a productive replication cycle, and simultaneously counteracts the antiviral cellular response. However, most aspects of the structure and function of RC remain to be explored; some of these include the relationship between their molecular components and the activities they regulate, as well as the dynamics of their assembly and the molecules involved in their structural integrity. In this study we report for the first time the use of a recently established procedure that allows the isolation of adenovirus RC particles in subnuclear fractions obtained from infected cells to perform morphological and functional studies of RC [100, 214].

Isolated adenoviral RC are morphologically similar to RC in the infected cell (Fig. 12). The distribution of DBP associated to RC within the infected cell-nucleus by conventional or confocal microscopy, like that shown in Fig. 12C, has shown that the protein forms closed circular structures that seem to coalesce giving rise to larger morphologically complex open structures (reviewed in [95]). The detailed analysis of Ad-infected cells presented here using higher magnification has shown for the first time that DBP accumulates in numerous small foci that are distributed in the periphery of the RC rings forming structures with a beads-on-a-string appearance. This complex assembly of RC is stable enough to be isolated, since the morphology of isolated particles was indistinguishable from that of RC inside

the infected-cell nuclei. Morphological analyses of RC within infected cells, as well as isolated RC and Nlo fractions by TIRF and super-resolution microscopy produced images in which both DBP and nucleolin could be seen to occupy defined areas of the particles' periphery. When TIRF images were reconstructed using the 3B algorithm, obtaining images close to 50 nm resolution, both proteins appeared as dots that accumulated in some areas of the periphery of the isolated particles indicating that, like nucleoli, RC are compartmentalized, and that DBP and other proteins occupy defined subcompartments localized mainly in the periphery of RC and only in certain areas that may correspond to PRZ. These findings indicate that the isolated particles can reveal detailed ultrastructural features of RC and studies are currently underway to determine the localization of viral and cellular proteins that are known to be associated with RC using higher resolution methods, such as transmission electron microscopy (TEM) and interferometry [264]. Also, our novel technique to isolate RC from Ad-infected cells should unravel fundamental aspects of the viral replication cycle and regulation of virus-host interactions**.**

6.3 Nucleolin is relocalized to RC in adenovirus-infected cells

As described in previous sections, during adenovirus infection, nuclear domains are extensively reorganized. One prominent example is the reorganization of nucleoli, with major effects on the biogenesis of rRNA and relocalization of nucleolar proteins. For example, in transfected cell lines, nucleolin is relocalized from the nucleus to the cytoplasm in the presence of the viral late protein pV [233]; the phosphoproteins B23.1 and B23.2 interact with viral E2 proteins and basic core proteins pV and pVII, promoting efficient DNA replication [145, 265, 266]; and accumulation of rRNA in the cytoplasm is impaired during adenovirus infection [267, 268]. Comparisons of the effect of ActD versus viral infection on the proteomic composition of nucleoli have shown no correlation since inhibiting replication and transcription with ActD treatment induced changes in more than 30% of the nucleolar proteins, while Ad-infection showed an effect in only 7% of these proteins [146, 269]. These results suggest that the effect of Ad-infection on the nucleolar proteome is specific to the infection and not due to a more general effect of non-specific cellular stress. Here we demonstrated for the first time that nucleolin is relocalized to specific compartments of adenoviral RC. Significantly, nucleolin localized to the periphery of these viral sites, in a dynamic spatio-temporal reorganization. The localization of nucleolin initially differed from that of DBP, but as the late phase progressed (by 36 hpi) both proteins colocalized in a few defined dots around RC (Fig. 12). The periphery of RC is the zone where viral DNA replication and gene expression take place [133, 138, 143, 237, 239, 240, 270, 271], hence the localization of nucleolin at the periphery of RC particles,

which likely corresponds to the PRZ, suggests this nucleolar protein could participate in adenoviral genome replication or expression. In cytomegalovirus-infected cells nucleolin interacts with viral DNA replication factors UL44 and UL84 at the periphery of viral replication compartments, maintaining the architecture of these viral sites and promoting efficient viral DNA synthesis, expression of viral late genes, and virus production [272-274]. Other proteins from RNA or DNA viruses have been shown to target nucleolar proteins to subserve viral transcription, translation and regulation of cell cycle to promote viral replication [108, 269, 272, 275]. In the case of adenovirus, the role of nucleoli during the replication cycle is incompletely understood, and it should therefore be interesting to investigate whether relocalization of nucleolin to specific subcompartments of the adenoviral RC may be required to modulate specific activities associated with viral DNA replication, gene expression or, as it does in the nucleolus, to provide structural integrity to RC. Our experiments have revealed an additional unprecedented finding, as lower and higher migrating bands that closely match proteolytic and phosphorylated products of nucleolin were generated in Ad-infected cells (Fig. 13). Nucleolin is a phosphoprotein with self-cleavage properties and its fragmentation has usually being observed during extraction procedures, indicating that its association with nuclear molecules, such as DNA, RNA or the nuclear matrix promotes the protein's stability [276]. Additionally, self-cleavage activity of nucleolin correlates with its phosphorylation and with cell cycle regulation [276, 277]. In our experiments the higher and lower migrating bands detected with the anti-nucleolin antibody were more abundant in RC than Npl or other subcellular fractions (Fig. 13A, RC), suggesting Ad-infection may mimic the conditions in the cell that induce modification and processing of nucleolin. Furthermore, nucleolin was also detected in its intact form, as the expected 102-kDa band was more abundant than the modified products, indicating that the various forms of nucleolin become associated to RC during infection. It is unlikely that the fractionation procedure accounts for the generation of the proteolytic (or post-translationally modified) products, since both RC and nucleoli were isolated using the same procedure, and these bands were almost undetectable in the nucleolar fraction from mock-infected cells (Fig. 13A, MK Nlo). Also, the procedure to obtain other sub-cellular fractions, such as CYT, NL or the TL did not result in the generation of higher or lower migrating bands for nucleolin. These data suggest that Ad infection may induce proteolysis of nucleolin and that the proteolytic products are enriched in RC. Since the isolated particles resemble the morphology of RC in Ad-infected cells, this strategy should allow determination of the impact of the post-translational modifications and relocalization of nucleolin in Ad-infected cells.

98

6.4 Effect of E1B on RC-associated activities

The accumulated evidence suggests that E1B may promote progression of the viral replication cycle by impacting on regulation of viral DNA replication or on different steps of the viral genome expression program, from transcription, posttranscriptional processes or release of viral mRNA from RC to be exported to the cytoplasm. To explore the participation of E1B in each of these molecular processes we exploited our cell-free system to measure directly RC-associated activities.

The presence of *bona fide* RC markers in RC [214] (Fig. 12 and 13) suggested these subnuclear fractions should also contain the enzymatic activities associated with these viral sites in the infected cell. This hypothesis was confirmed, as RC directed *de novo* synthesis of viral DNA and viral late RNA, as well as splicing of viral late mRNA indicating that this novel approach can help to determine the macromolecular composition of RC and unravel fundamental aspects of the viral replication cycle and virus-cell interactions (Fig. 14-16). As the infection proceeds into the late phase, IG surround the PRZ and components of Cajal bodies that participate in viral mRNA post-transcriptional processing are recruited to these sites [110, 240]. Splicing factors, such as SC-35 and snRNP, are also relocalized to IG forming clusters at the periphery of DBP where viral late mRNA enriched in exon sequences accumulate [90, 133, 143, 239, 240, 278, 279]. Since in our experiments RC could direct the splicing of both viral late and cellular mRNA, it is possible that clusters of IG may be tightly associated to RC so that they are coisolated in RC. An alternative explanation for both the RC-associated RNA Pol I activity and for the splicing of cellular mRNA could be that by late times post-infection (36 hpi) the coalescing RC may form a meshwork to which actively transcribed mRNA associate and can therefore be sedimented with the RC particles.

Taking advantage of this possibility to study RC-activities in a cell-free system, we evaluated the effect of E1B on viral DNA replication and gene expression in RC and found that the regulation of E1B by phosphorylation is necessary for the efficient and adequate morphogenesis, organization and composition of viral RC and that this early viral protein is also important for efficient viral DNA replication, mRNA synthesis and splicing in RC (Fig. 20-21). However, our results indicate that phosphorylation of E1B does not directly impact this activity of the protein. Since higher levels of viral mRNA were observed in E1B PM-infected cells (Fig. 8), these results indicate that these levels are a consequence of increased viral mRNA half-life when E1B is in a constitutive phosphorylated state (Fig. 9), rather than an increase in mRNA synthesis (Fig. 10 and 21).

This influence of E1B on RC-associated activities could be a consequence of a direct interaction of E1B with viral nucleic acids or interactions with viral or cellular

99

proteins that are known to localize to RC and promote efficient viral DNA replication or mRNA biogenesis, as described before.

6.5 Effect of E1B on viral mRNA partitioning between intranuclear compartments and the cytoplasm.

Using the RC fractions, in combination with nuclear and cytoplasmic fractions, splicing and partitioning of viral mRNA was evaluated. The study of spliced and unspliced species of all ML and that of L5 mRNA revealed that although as expected, all nuclear pre-mRNA increased as the late phase of infection progressed, the efficiency of cytoplasmic accumulation of the L5 mRNA was significantly higher than the rest of all ML RNA combined (Fig. 18). Interestingly, partitioning of the spliced vs. unspliced L5 mRNA between RC and Npl was also different from ML, and the pattern of accumulation of L5 RNA indicated that it is efficiently and completely spliced in association with RC, and that its transit from RC to cytoplasm is also more efficient than the rest of the ML mRNA. Since the L5 pre-mRNA and mRNA displayed different temporal patterns of splicing and release from RC to Npl when compared with all ML mRNA, these findings suggest that each viral late RNA family may be subject to different regulatory events during their biogenesis associated with RC. Alternatively, it is also possible that production of the L5 mRNA has unique features among the viral late mRNA, and that the splicing of the ancillary x and y exons (as described in Results) may be biologically significant, as it has been suggested to determine the virus host-range [280]. Although it has been known for some time that as the late phase of viral replication progresses splicing of longer introns of the MLTU increases, the large difference in the efficiency of splicing and export of L5 mRNA compared with the rest of ML mRNA observed in these experiments had not been reported. The RNA-Seq analysis of viral late mRNA in RC indicates that production of the different species of fiber mRNA is established at adenovirus RC (Fig. 19). These findings are in agreement with previous reports that have shown both introns and exons from the MLTU are present in PRZ and in IG, suggesting that splicing may occur in both compartments [90, 92, 111, 112, 138, 140, 142, 239, 240, 270, 278, 281].

Using a fractionation scheme that relied on stepwise extraction of RNA with different salt concentrations, ionic and non-ionic detergents, and DNase I, Leppard & Shenk determined that viral late mRNA were synthesized in a nuclear matrix-associated fraction, and were then transported to a nuclear soluble fraction before reaching the nuclear membrane and finally a cytoplasmic fraction. Moreover, they found that E1B facilitates RNA metabolism at an intranuclear step, regulating dissociation of viral mRNA from their sites of synthesis but before their export to the cytoplasm [157]. Interestingly, our experiments have shown not only a similar pattern of mRNA partitioning between subnuclear compartments and the cytoplasm, but also, we showed that efficient accumulation of viral early and late

100

mRNA depends on the presence of E1B (Fig. 22-23). We found that mRNA were efficiently and completely spliced in association with RC, and that late mRNA splicing was inefficient in the absence of E1B. These results are interesting because they substantiate the possibility that E1B may regulate directly not only viral DNA replication, but also downstream events, such as viral transcription, as well as splicing, and that the effects on the latter mechanisms do not only depend on the accumulation of viral DNA molecules.

6.6 Impact of E1B on RC organization

From the observations of the super-resolution micrographies, a dynamic interplay in the localization of the proteins analyzed between the E4Orf3 nuclear-tracks and the DBP structures was apparent (Fig. 26-31). As it was described before, E1B can be localized with E4Orf3 at nuclear tracks and at RC. Binding of E1B to E4Orf3 and E4Orf6 results in efficient recruitment of E1B to RC [76, 167, 169]. E4Orf3 is also required for efficient formation of RC and recruitment of cellular antiviral factors to nuclear tracks, such as PML and the MRN complex [114, 130]. PML and E4Orf3 could facilitate formation of a scaffold favorable for RC formation and regulation of protein-protein and protein-nucleic acid interactions. Previous reports have shown that PML IV can assemble in cage-like structures [282, 283]. In the case of E4Orf3, this early protein can oligomerize in linear and branched chains that form a polymer network that has been described to partition the nuclear volume [284]. It will be interesting to determine whether these and other viral and cellular proteins participate in the formation and maintenance of the structural integrity and activities of RC.

The presence of E1B in RC seems to be necessary to recruit cellular proteins that are inhibited during infection [57, 117, 157, 174]. As described above, in HeLa cells infected with WT adenovirus, YB1 is relocalized from the cytoplasm to the nucleus. YB1 facilitates DNA replication by binding to the E2-late (E2L) promoter and activating the expression of the E2 genes. Nuclear YB1 colocalized with a major viral component of RC, the early protein E2A-DBP (DBP) and with E1B. Nevertheless, when the cells were infected with an E1B null-mutant virus, Ad338, DBP displayed a diffuse nuclear pattern and YB1 remained in the cytoplasm. These results suggest that targeting of YB1 by E1B to RC favors viral DNA replication at late times of infection, when the E2L promoter is active [57]. It has been demonstrated that E1B is necessary for the localization of p53 in RC. Moreover, in HFF infected either with an E1B-null mutant virus (Hr6) or a virus that expresses an E1B unable to bind p53, viral DNA replication is inefficient [117]. These observations suggest that the reorganization of the cell nucleus that results in formation of RC and later promote efficient genome replication and expression, may underlie the mechanism(s) by which E1B regulates cellular activities and promotes efficient progression of the viral replication cycle. In the present work, we

101

showed that E1B could impact the temporal localization of proteins necessary for efficient viral DNA replication and transcription, as well as antiviral factors, with E4Orf3 or with DBP structures. Some of these cellular proteins could also function as scaffolds for RC formation, such as CTCF and SUMO2/3, as described in the introduction.

Several E4Orf3 targets regulate gene expression, linking E4Orf3 to transcriptional control, and it has been demonstrated that E4Orf3 induces the reorganization of nuclear components impacting regulation of transcription [285]. These results suggest a cross-talk between DBP-accumulation sites and E4Orf3 nuclear tracks regulated by E1B that could result in efficient viral genome replication and expression. Moreover, these results suggest that the nuclear tracks could form part of viral RC.

Because of the importance of E1B in the development of oncolytic vectors, it is necessary to understand in detail the activities of this protein and its role in regulation of virus-host interactions in order to make a rational design of oncolytic therapies. This work highlights the importance of E1B in establishing an efficient viral replication cycle and modulating virus-host interactions, from reorganization of the cell nucleus, to expression of viral genes and control of the anti-viral response. Although the experiments performed in the present work do not define molecular mechanisms for E1B activities, they show that the multifunctional E1B protein impacts viral DNA replication, viral late gene transcription, early and late mRNA stability, temporal viral promoter enhancement or repression, efficiency of splicing and release of viral late mRNA from RC, and formation of RC. Our results suggest a role of E1B on RC formation that could be determinant for RC-associated activities. For example, the functional assays using the RC cell-free system suggest that the impact of E1B on RC formation underlies the lower levels of viral DNA synthesized when E1B is not present, since the increase from the input DNA was similar between Ad WT and E1B⁻ samples (Fig. 20A). However, this does not seem to be the case for transcription, as 2-fold lower levels of viral late mRNA were synthesized in the absence of E1B (Fig. 20B). Therefore, a detailed characterization of RC composition, ultrastructure and activities should help further define E1B molecular mechanisms that result in an efficient progression of viral replication.

7 CONCLUSIONS

- The data obtained provide the most complete analysis hitherto of the program of expression of the adenoviral genome.
- RC can be isolated and contain viral DNA, RNA and proteins.
- Isolated RC are morphologically similar to RC in the cell nucleus.
- Nucleolin is relocalized to RC.
- RC are functional, since they direct *de novo* synthesis of viral DNA and late mRNA, as well as splicing of viral late mRNA.
- E1B timely regulates accumulation of viral early and late mRNA.
- E1B increases viral mRNA stability and may act as a differential transcriptional repressor or enhancer on viral early and late promoters, and these activities depend on the time post-infection, and on the modification of the protein by phosphorylation.
- E1B-PM promotes efficient DNA synthesis, transcription and splicing in RC.
- CTCF and SUMO2/3 recruitment to RC depends on the presence of E1B.
- E1B impacts the recruitment of some proteins to RC that, on the one hand, promote efficient genome replication and gene expression, and on the other, co-opt proteins with antiviral activity that may be inhibited at RC.

8 PERSPECTIVES

- Perform ultrastructural analyses of RC to study in detail architectural features and organization of these virus-induced structures.
- In our lab we have found that E1B is able to bind RNA and that this activity correlates with efficient splicing of viral late mRNA and progeny production (Tejera, B., et al., unpublished). Therefore, we wish to define whether E1B is able to bind DNA, at promoter or regulatory regions and directly modulate replication or transcription, or if its activity is indirect by interacting with other viral and/or cellular proteins that regulate these molecular mechanisms.
- Determine the interactome of E1B and identify which viral or cellular proteins participate in viral DNA replication or gene expression.
- Model the compartmentalization of different RC-components over different times post-infection and the effect of E1B on this compartmentalization.
- Determine viral protein levels that could correlate with the mRNA levels measured in the present work.
- Quantitative analyses of the effect of E1B on the proteomic composition and further transcriptomic analyses of RC are underway and will help to identify viral and cellular proteins and nucleic acids that associate with or are processed in these structures and should provide detailed insights into the viral replication cycle and virus-cell interaction.

103

9 REFERENCES

1. Rowe, W.P., et al., *Isolation of a cytopathogenic agent from human adenoids undergoing spontaneous degeneration in tissue culture.* Proc Soc Exp Biol Med, 1953. **84**(3): p. 570-3.

2. Fields, B.N., D.M. Knipe, and P.M. Howley, *Fields Virology*. 2007: Wolters Kluwer Health/Lippincott Williams & Wilkins.

3. Esposito, S., et al., *Adenovirus 36 infection and obesity.* J Clin Virol, 2012. **55**(2): p. 95-100.

4. Trentin, J.J., Y. Yabe, and G. Taylor, *The quest for human cancer viruses.* Science, 1962. **137**: p. 835-41.

5. Wold, W.S. and K. Toth, *Adenovirus vectors for gene therapy, vaccination and cancer gene therapy.* Curr Gene Ther, 2013. **13**(6): p. 421-33.

6. Hodge, L.D. and M.D. Scharff, *Effect of adenovirus on host cell DNA synthesis in synchronized cells.* Virology, 1969. **37**(4): p. 554-64.

7. Beltz, G.A. and S.J. Flint, *Inhibition of HeLa cell protein synthesis during adenovirus infection. Restriction of cellular messenger RNA sequences to the nucleus.* J Mol Biol, 1979. **131**(2): p. 353-73.

8. Dolph, P.J., et al., *The adenovirus tripartite leader may eliminate the requirement for cap-binding protein complex during translation initiation.* J Virol, 1988. **62**(6): p. 2059-66.

9. Huang, J.T. and R.J. Schneider, *Adenovirus inhibition of cellular protein synthesis involves inactivation of cap-binding protein.* Cell, 1991. **65**(2): p. 271-80.

10. Berk, A.J., *Recent lessons in gene expression, cell cycle control, and cell biology from adenovirus.* Oncogene, 2005. **24**(52): p. 7673-85.

11. Bridge, E. and U. Pettersson, *Nuclear organization of replication and gene expression in adenovirus-infected cells.* Curr Top Microbiol Immunol, 1995. **199 (Pt 1)**: p. 99-117.

12. Miller, D.L., et al., *Adenovirus type 5 exerts genome-wide control over cellular programs governing proliferation, quiescence, and survival.* Genome Biol, 2007. **8**(4): p. R58.

13. Davison, A.J., M. Benko, and B. Harrach, *Genetic content and evolution of adenoviruses.* J Gen Virol, 2003. **84**(Pt 11): p. 2895-908.

14. Schreiner, S., P. Wimmer, and T. Dobner, *Adenovirus degradation of cellular proteins.* Future Microbiol, 2012. **7**(2): p. 211-25.

104

15.   Shenk, T.E., *Adenoviridae: The Viruses and Their Replication*. 2001.

16.   Perez-Berna, A.J., et al., *Structure and uncoating of immature adenovirus.* J Mol Biol, 2009. **392**(2): p. 547-57.

17.   Nemerow, G.R., et al., *Insights into adenovirus host cell interactions from structural studies.* Virology, 2009. **384**(2): p. 380-8.

18.   Fessler, S.P. and C.S. Young, *Control of adenovirus early gene expression during the late phase of infection.* J Virol, 1998. **72**(5): p. 4049-56.

19.   Shaw, A.R. and E.B. Ziff, *Transcripts from the adenovirus-2 major late promoter yield a single early family of 3' coterminal mRNAs and five late families.* Cell, 1980. **22**(3): p. 905-16.

20.   White, E., *Regulation of the cell cycle and apoptosis by the oncogenes of adenovirus.* Oncogene, 2001. **20**(54): p. 7836-46.

21.   Steegenga, W.T., et al., *Adenovirus E1A proteins inhibit activation of transcription by p53.* Mol Cell Biol, 1996. **16**(5): p. 2101-9.

22.   Gooding, L.R., et al., *The adenovirus E3-14.7K protein is a general inhibitor of tumor necrosis factor-mediated cytolysis.* J Immunol, 1990. **145**(9): p. 3080-6.

23.   Hoeben, R.C. and T.G. Uil, *Adenovirus DNA replication.* Cold Spring Harb Perspect Biol, 2013. **5**(3): p. a013003.

24.   Chow, L.T., T.R. Broker, and J.B. Lewis, *Complex splicing patterns of RNAs from the early regions of adenovirus-2.* J Mol Biol, 1979. **134**(2): p. 265-303.

25.   Stillman, B.W., et al., *Identification of the gene and mRNA for the adenovirus terminal protein precursor.* Cell, 1981. **23**(2): p. 497-508.

26.   Stillman, B.W., *Adenovirus DNA replication in vitro: a protein linked to the 5' end of nascent DNA strands.* J Virol, 1981. **37**(1): p. 139-47.

27.   Smart, J.E. and B.W. Stillman, *Adenovirus terminal protein precursor. Partial amino acid sequence and the site of covalent linkage to virus DNA.* J Biol Chem, 1982. **257**(22): p. 13499-506.

28.   Tamanoi, F. and B.W. Stillman, *Function of adenovirus terminal protein in the initiation of DNA replication.* Proc Natl Acad Sci U S A, 1982. **79**(7): p. 2221-5.

29.   Lutz, P. and C. Kedinger, *Properties of the adenovirus IVa2 gene product, an effector of late-phase-dependent activation of the major late promoter.* J Virol, 1996. **70**(3): p. 1396-405.

30.   Boulanger, P., et al., *Characterization of adenovirus protein IX.* J Gen Virol, 1979. **44**(3): p. 783-800.

31.   Lutz, P., M. Rosa-Calatrava, and C. Kedinger, *The product of the adenovirus intermediate gene IX is a transcriptional activator.* J Virol, 1997. **71**(7): p. 5102-9.

32.   Winter, N. and J.C. D'Halluin, *Regulation of the biosynthesis of subgroup C adenovirus protein IVa2.* J Virol, 1991. **65**(10): p. 5250-9.

33.   Venkatesh, L.K. and G. Chinnadurai, *Activation of the adenovirus 2 protein IX promoter by DNA replication in a transient expression assay.* Nucleic Acids Res, 1987. **15**(5): p. 2235-50.

34.   Morris, S.J., G.E. Scott, and K.N. Leppard, *Adenovirus late-phase infection is controlled by a novel L4 promoter.* J Virol, 2010. **84**(14): p. 7096-104.

35.   Morris, S.J. and K.N. Leppard, *Adenovirus serotype 5 L4-22K and L4-33K proteins have distinct functions in regulating late gene expression.* J Virol, 2009. **83**(7): p. 3049-58.

36.   Tribouley, C., et al., *The product of the adenovirus intermediate gene IVa2 is a transcriptional activator of the major late promoter.* J Virol, 1994. **68**(7): p. 4450-7.

37.   Nevins, J.R., et al., *Regulation of the primary expression of the early adenovirus transcription units.* J Virol, 1979. **32**(3): p. 727-33.

38.   Berk, A.J., *Adenovirus promoters and E1A transactivation.* Annu Rev Genet, 1986. **20**: p. 45-79.

39.   Vijayalingam, S. and G. Chinnadurai, *Adenovirus L-E1A activates transcription through mediator complex-dependent recruitment of the super elongation complex.* J Virol, 2013. **87**(6): p. 3425-34.

40.   Pelka, P., et al., *Identification of a second independent binding site for the pCAF acetyltransferase in adenovirus E1A.* Virology, 2009. **391**(1): p. 90-8.

41.   Pelka, P., et al., *Transcriptional control by adenovirus E1A conserved region 3 via p300/CBP.* Nucleic Acids Res, 2009. **37**(4): p. 1095-106.

42.   Schaack, J., et al., *Adenovirus E1A protein activates transcription of the E1A gene subsequent to transcription complex formation.* J Virol, 1991. **65**(4): p. 1687-94.

43.   Engel, D.A., S. Hardy, and T. Shenk, *cAMP acts in synergy with E1A protein to activate transcription of the adenovirus early genes E4 and E1A.* Genes Dev, 1988. **2**(12A): p. 1517-28.

44.   White, E., A. Denton, and B. Stillman, *Role of the adenovirus E1B 19,000-dalton tumor antigen in regulating early gene expression.* J Virol, 1988. **62**(9): p. 3445-54.

45.   Borrelli, E., R. Hen, and P. Chambon, *Adenovirus-2 E1A products repress enhancer-induced stimulation of transcription.* Nature, 1984. **312**(5995): p. 608-12.

46.   Maxfield, L.F. and D.J. Spector, *Readthrough activation of early adenovirus E1b gene transcription.* J Virol, 1997. **71**(11): p. 8321-9.

47.   Jones, C. and K.A. Lee, *E1A-mediated activation of the adenovirus E4 promoter can occur independently of the cellular transcription factor E4F.* Mol Cell Biol, 1991. **11**(9): p. 4297-305.

48.   Bondesson, M., et al., *Adenovirus E4 open reading frame 4 protein autoregulates E4 transcription by inhibiting E1A transactivation of the E4 promoter.* J Virol, 1996. **70**(6): p. 3844-51.

49.   Kornuc, M., et al., *Adenovirus early region 3 promoter regulation by E1A/E1B is independent of alterations in DNA binding and gene activation of CREB/ATF and AP1.* J Virol, 1990. **64**(5): p. 2004-13.

50.   Deryckere, F. and H.G. Burgert, *Tumor necrosis factor alpha induces the adenovirus early 3 promoter by activation of NF-kappaB.* J Biol Chem, 1996. **271**(47): p. 30249-55.

51.   Chang, L.S. and T. Shenk, *The adenovirus DNA-binding protein stimulates the rate of transcription directed by adenovirus and adeno-associated virus promoters.* J Virol, 1990. **64**(5): p. 2103-9.

52.   Berscheminski, J., et al., *The adenoviral oncogene E1A-13S interacts with a specific isoform of the tumor suppressor PML to enhance viral transcription.* J Virol, 2013. **87**(2): p. 965-77.

107

53. Neill, S.D., et al., *An adenovirus E4 gene product trans-activates E2 transcription and stimulates stable E2F binding through a direct association with E2F.* Proc Natl Acad Sci U S A, 1990. **87**(5): p. 2008-12.

54. Yen, R. and M. Hung, *Complex regulation of the adenovirus e2 promoter by the viral oncoproteins e1a and e7 and tumor-suppressor rb.* Int J Oncol, 1994. **4**(1): p. 109-15.

55. Swaminathan, S. and B. Thimmapaya, *Transactivation of adenovirus E2-early promoter by E1A and E4 6/7 in the context of viral chromosome.* J Mol Biol, 1996. **258**(5): p. 736-46.

56. Komatsu, T., T. Sekiya, and K. Nagata, *DNA replication-dependent binding of CTCF plays a critical role in adenovirus genome functions.* Sci Rep, 2013. **3**: p. 2187.

57. Holm, P.S., et al., *YB-1 relocates to the nucleus in adenovirus-infected cells and facilitates viral replication by inducing E2 gene expression through the E2 late promoter.* J Biol Chem, 2002. **277**(12): p. 10427-34.

58. Pardo-Mateos, A. and C.S. Young, *Adenovirus IVa2 protein plays an important role in transcription from the major late promoter in vivo.* Virology, 2004. **327**(1): p. 50-9.

59. Carcamo, J., et al., *Factors involved in specific transcription by mammalian RNA polymerase II. Role of factors IID and MLTF in transcription from the adenovirus major late and IVa2 promoters.* J Biol Chem, 1989. **264**(13): p. 7704-14.

60. Lin, H.J. and S.J. Flint, *Identification of a cellular repressor of transcription of the adenoviral late IVa(2) gene that is unaltered in activity in infected cells.* Virology, 2000. **277**(2): p. 397-410.

61. Wright, J., et al., *The Human Adenovirus Type 5 L4 Promoter Is Negatively Regulated by TFII-I and L4-33K.* J Virol, 2015. **89**(14): p. 7053-63.

62. Wright, J. and K.N. Leppard, *The human adenovirus 5 L4 promoter is activated by cellular stress response protein p53.* J Virol, 2013. **87**(21): p. 11617-25.

63. Ali, H., et al., *The adenovirus L4 33-kilodalton protein binds to intragenic sequences of the major late promoter required for late phase-specific stimulation of transcription.* J Virol, 2007. **81**(3): p. 1327-38.

64. Lan, S., et al., *A suppressive effect of Sp1 recruitment to the first leader 5' splice site region on L4-22K-mediated activation of the adenovirus major late promoter.* Virus Res, 2015. **210**: p. 133-40.

65.   Lan, S., et al., *The adenovirus L4-22K protein regulates transcription and RNA splicing via a sequence-specific single-stranded RNA binding.* Nucleic Acids Res, 2017. **45**(4): p. 1731-1742.

66.   Parks, C.L. and T. Shenk, *Activation of the adenovirus major late promoter by transcription factors MAZ and Sp1.* J Virol, 1997. **71**(12): p. 9600-7.

67.   Toth, M., W. Doerfler, and T. Shenk, *Adenovirus DNA replication facilitates binding of the MLTF/USF transcription factor to the viral major late promoter within infected cells.* Nucleic Acids Res, 1992. **20**(19): p. 5143-8.

68.   Berk, A.J., et al., *Pre-early adenovirus 5 gene product regulates synthesis of early viral messenger RNAs.* Cell, 1979. **17**(4): p. 935-44.

69.   Jones, N. and T. Shenk, *An adenovirus type 5 early gene function regulates expression of other early viral genes.* Proc Natl Acad Sci U S A, 1979. **76**(8): p. 3665-9.

70.   Flint, J., *The topography and transcription of the adenovirus genome.* Cell, 1977. **10**(2): p. 153-66.

71.   Kovesdi, I., R. Reichel, and J.R. Nevins, *Identification of a cellular transcription factor involved in E1A trans-activation.* Cell, 1986. **45**(2): p. 219-28.

72.   Kovesdi, I., R. Reichel, and J.R. Nevins, *E1A transcription induction: enhanced binding of a factor to upstream promoter sequences.* Science, 1986. **231**(4739): p. 719-22.

73.   Thomas, G.P. and M.B. Mathews, *DNA replication and the early to late transition in adenovirus infection.* Cell, 1980. **22**(2 Pt 2): p. 523-33.

74.   Iftode, C. and S.J. Flint, *Viral DNA synthesis-dependent titration of a cellular repressor activates transcription of the human adenovirus type 2 IVa2 gene.* Proc Natl Acad Sci U S A, 2004. **101**(51): p. 17831-6.

75.   Flint, S.J., *Regulation of adenovirus mRNA formation.* Adv Virus Res, 1986. **31**: p. 169-228.

76.   Gonzalez, R.A. and S.J. Flint, *Effects of mutations in the adenoviral E1B 55-kilodalton protein coding sequence on viral late mRNA metabolism.* J Virol, 2002. **76**(9): p. 4507-19.

77.   Gonzalez, R., et al., *Adenovirus E1B 55-kilodalton protein is required for both regulation of mRNA export and efficient entry into the late phase of infection in normal human fibroblasts.* J Virol, 2006. **80**(2): p. 964-74.

78.   Yatherajam, G., W. Huang, and S.J. Flint, *Export of adenoviral late mRNA from the nucleus requires the Nxf1/Tap export receptor.* J Virol, 2011. **85**(4): p. 1429-38.

79.   Hayes, B.W., et al., *The adenovirus L4 100-kilodalton protein is necessary for efficient translation of viral late mRNA species.* J Virol, 1990. **64**(6): p. 2732-42.

80.   Schneider, R.J. and I. Mohr, *Translation initiation and viral tricks.* Trends Biochem Sci, 2003. **28**(3): p. 130-6.

81.   Cuesta, R., Q. Xi, and R.J. Schneider, *Preferential translation of adenovirus mRNAs in infected cells.* Cold Spring Harb Symp Quant Biol, 2001. **66**: p. 259-67.

82.   Mathews, M.B. and T. Shenk, *Adenovirus virus-associated RNA and translation control.* J Virol, 1991. **65**(11): p. 5657-62.

83.   Yueh, A. and R.J. Schneider, *Selective translation initiation by ribosome jumping in adenovirus-infected and heat-shocked cells.* Genes Dev, 1996. **10**(12): p. 1557-67.

84.   Yueh, A. and R.J. Schneider, *Translation by ribosome shunting on adenovirus and hsp70 mRNAs facilitated by complementarity to 18S rRNA.* Genes Dev, 2000. **14**(4): p. 414-21.

85.   Flint, S.J., et al., *Principles of Virology, 3rd Edition, Volume I: Molecular Biology.* 2009: ASM Press.

86.   Babich, A. and J.R. Nevins, *The stability of early adenovirus mRNA is controlled by the viral 72 kd DNA-binding protein.* Cell, 1981. **26**(3 Pt 1): p. 371-9.

87.   Babiss, L.E., H.S. Ginsberg, and J.E. Darnell, Jr., *Adenovirus E1B proteins are required for accumulation of late viral mRNA and for effects on cellular mRNA translation and transport.* Mol Cell Biol, 1985. **5**(10): p. 2552-8.

88.   Bridge, E., C. Hemstrom, and U. Pettersson, *Differential regulation of adenovirus late transcriptional units by the products of early region.* Virology, 1991. **183**(1): p. 260-6.

89.   Huang, M.M. and P. Hearing, *Adenovirus early region 4 encodes two gene products with redundant effects in lytic infection.* J Virol, 1989. **63**(6): p. 2605-15.

90.   Aspegren, A., C. Rabino, and E. Bridge, *Organization of splicing factors in adenovirus-infected cells reflects changes in gene expression during the early to late phase transition.* Exp Cell Res, 1998. **245**(1): p. 203-13.

110

91.   Everett, R.D., *The spatial organization of DNA virus genomes in the nucleus.* PLoS Pathog, 2013. **9**(6): p. e1003386.

92.   Puvion-Dutilleul, F. and E. Pichard, *Segregation of viral double-stranded and single-stranded DNA molecules in nuclei of adenovirus infected cells as revealed by electron microscope in situ hybridization.* Biol Cell, 1992. **76**(2): p. 139-50.

93.   Netherton, C., et al., *A guide to viral inclusions, membrane rearrangements, factories, and viroplasm produced during virus replication.* Adv Virus Res, 2007. **70**: p. 101-82.

94.   Netherton, C.L. and T. Wileman, *Virus factories, double membrane vesicles and viroplasm generated in animal cells.* Curr Opin Virol, 2011. **1**(5): p. 381-7.

95.   Schmid, M., et al., *DNA virus replication compartments.* J Virol, 2014. **88**(3): p. 1404-20.

96.   Puvion-Dutilleul, F. and E. Puvion, *Replicating single-stranded adenovirus type 5 DNA molecules accumulate within well-delimited intranuclear areas of lytically infected HeLa cells.* Eur J Cell Biol, 1990. **52**(2): p. 379-88.

97.   Puvion-Dutilleul, F. and E. Puvion, *Analysis by in situ hybridization and autoradiography of sites of replication and storage of single- and double-stranded adenovirus type 5 DNA in lytically infected HeLa cells.* J Struct Biol, 1990. **103**(3): p. 280-9.

98.   Zhang, G., et al., *Localization of pre-mRNA splicing in mammalian nuclei.* Nature, 1994. **372**(6508): p. 809-12.

99.   Hidalgo, P., R. Gonzalez, and A. n, *Isolation of Viral Replication Compartment-enriched Sub-nuclear Fractions from Adenovirus-infected Normal Human Cells.* 2015(105): p. e53296.

100.   Hidalgo, P., et al., *Morphological, Biochemical, and Functional Study of Viral Replication Compartments Isolated from Adenovirus-Infected Cells.* J Virol, 2016. **90**(7): p. 3411-27.

101.   Uchil, P.D. and V. Satchidanandam, *Architecture of the flaviviral replication complex. Protease, nuclease, and detergents reveal encasement within double-layered membrane compartments.* J Biol Chem, 2003. **278**(27): p. 24388-98.

102.   Mazzolini, L., et al., *Strand-specific viral DNA synthesis in purified viroplasms isolated from turnip leaves infected with cauliflower mosaic virus.* Virology, 1985. **145**(2): p. 293-303.

103. Paul, D., et al., *Morphological and biochemical characterization of the membranous hepatitis C virus replication compartment.* J Virol, 2013. **87**(19): p. 10612-27.

104. Lallemand-Breitenbach, V. and H. de The, *PML nuclear bodies.* Cold Spring Harb Perspect Biol, 2010. **2**(5): p. a000661.

105. Wang, L., et al., *The nucleolus and viral infection.* Virol Sin, 2010. **25**(3): p. 151-7.

106. Spector, D.L. and A.I. Lamond, *Nuclear speckles.* Cold Spring Harb Perspect Biol, 2011. **3**(2).

107. Ishov, A.M. and G.G. Maul, *The periphery of nuclear domain 10 (ND10) as site of DNA virus deposition.* J Cell Biol, 1996. **134**(4): p. 815-26.

108. Hiscox, J.A., *The nucleolus--a gateway to viral infection?* Arch Virol, 2002. **147**(6): p. 1077-89.

109. Rodrigues, S.H., et al., *The behavior of the coiled body in cells infected with adenovirus in vitro.* Mol Biol Rep, 1996. **23**(3-4): p. 183-9.

110. James, N.J., et al., *The role of Cajal bodies in the expression of late phase adenovirus proteins.* Virology, 2010. **399**(2): p. 299-311.

111. Besse, S. and F. Puvion-Dutilleul, *Anchorage of adenoviral RNAs to clusters of interchromatin granules.* Gene Expr, 1995. **5**(2): p. 79-92.

112. Bridge, E., et al., *Dynamic organization of splicing factors in adenovirus-infected cells.* J Virol, 1995. **69**(1): p. 281-90.

113. Blackford, A.N., et al., *A role for E1B-AP5 in ATR signaling pathways during adenovirus infection.* J Virol, 2008. **82**(15): p. 7640-52.

114. Evans, J.D. and P. Hearing, *Relocalization of the Mre11-Rad50-Nbs1 complex by the adenovirus E4 ORF3 protein is required for viral replication.* J Virol, 2005. **79**(10): p. 6207-15.

115. Carson, C.T., et al., *Mislocalization of the MRN complex prevents ATR signaling during adenovirus infection.* EMBO J, 2009. **28**(6): p. 652-62.

116. Sohn, S.Y. and P. Hearing, *Adenovirus sequesters phosphorylated STAT1 at viral replication centers and inhibits STAT dephosphorylation.* J Virol, 2011. **85**(15): p. 7555-62.

112

117. Cardoso, F.M., et al., *An early function of the adenoviral E1B 55 kDa protein is required for the nuclear relocalization of the cellular p53 protein in adenovirus-infected normal human cells.* Virology, 2008. **378**(2): p. 339-46.

118. Rosa-Calatrava, M., et al., *Adenovirus protein IX sequesters host-cell promyelocytic leukaemia protein and contributes to efficient viral proliferation.* EMBO Rep, 2003. **4**(10): p. 969-75.

119. Maul, G.G., et al., *Nuclear redistribution of BRCA1 during viral infection.* Cell Growth Differ, 1998. **9**(9): p. 743-55.

120. Everett, R.D., *DNA viruses and viral proteins that interact with PML nuclear bodies.* Oncogene, 2001. **20**(49): p. 7266-73.

121. Everett, R.D., *Interactions between DNA viruses, ND10 and the DNA damage response.* Cell Microbiol, 2006. **8**(3): p. 365-74.

122. Geoffroy, M.C. and M.K. Chelbi-Alix, *Role of promyelocytic leukemia protein in host antiviral defense.* J Interferon Cytokine Res, 2011. **31**(1): p. 145-58.

123. Kite, G.L. and R. Chambers, Jr., *Vital Staining of Chromosomes and the Function and Structure of the Nucleus.* Science, 1912. **36**(932): p. 639-41.

124. Castillo-Villanueva, E., et al., *The Mre11 Cellular Protein Is Modified by Conjugation of Both SUMO-1 and SUMO-2/3 during Adenovirus Infection.* ISRN Virology, 2014. **2014**: p. 14.

125. Cherubini, G., et al., *The FANC pathway is activated by adenovirus infection and promotes viral replication-dependent recombination.* Nucleic Acids Res, 2011. **39**(13): p. 5459-73.

126. Komatsu, T. and K. Nagata, *Replication-uncoupled histone deposition during adenovirus DNA replication.* J Virol, 2012. **86**(12): p. 6701-11.

127. Ching, W., et al., *A ubiquitin-specific protease possesses a decisive role for adenovirus replication and oncogene-mediated transformation.* PLoS Pathog, 2013. **9**(3): p. e1003273.

128. Schreiner, S., et al., *SPOC1-mediated antiviral host cell response is antagonized early in human adenovirus type 5 infection.* PLoS Pathog, 2013. **9**(11): p. e1003775.

129. Reyes, E.D., et al., *Identifying host factors associated with DNA replicated during virus infection.* Mol Cell Proteomics, 2017.

130.   Doucas, V., et al., *Adenovirus replication is coupled with the dynamic properties of the PML nuclear structure.* Genes Dev, 1996. **10**(2): p. 196-207.

131.   Navarro, M., *Activación de IRF3 (Factor de Regulación de Interferón 3) por la infección con adenovirus en células humanas no transformadas.*, in *Facultad de Ciencias, UAEM*2011, Universidad Autónoma del Estado de Morelos: Cuernavaca, Morelos.

132.   Souquere-Besse, S., et al., *Adenovirus infection targets the cellular protein kinase CK2 and RNA-activated protein kinase (PKR) into viral inclusions of the cell nucleus.* Microsc Res Tech, 2002. **56**(6): p. 465-78.

133.   Pombo, A., et al., *Adenovirus replication and transcription sites are spatially separated in the nucleus of infected cells.* EMBO J, 1994. **13**(21): p. 5075-85.

134.   Lam, Y.W., L. Trinkle-Mulcahy, and A.I. Lamond, *The nucleolus.* J Cell Sci, 2005. **118**(Pt 7): p. 1335-7.

135.   Schwarzacher, H.G. and W. Mosgoeller, *Ribosome biogenesis in man: current views on nucleolar structures and function.* Cytogenet Cell Genet, 2000. **91**(1-4): p. 243-52.

136.   Hutten, S., et al., *An intranucleolar body associated with rDNA.* Chromosoma, 2011. **120**(5): p. 481-99.

137.   Murti, K.G., D.S. Davis, and G.R. Kitchingman, *Localization of adenovirus-encoded DNA replication proteins in the nucleus by immunogold electron microscopy.* J Gen Virol, 1990. **71 (Pt 12)**: p. 2847-57.

138.   Puvion-Dutilleul, F., et al., *Rearrangements of intranuclear structures involved in RNA processing in response to adenovirus infection.* J Cell Sci, 1994. **107 (Pt 6)**: p. 1457-68.

139.   Lang, M., et al., *Three-dimensional organization of promyelocytic leukemia nuclear bodies.* J Cell Sci, 2010. **123**(Pt 3): p. 392-400.

140.   Puvion-Dutilleul, F., R. Roussev, and E. Puvion, *Distribution of viral RNA molecules during the adenovirus type 5 infectious cycle in HeLa cells.* J Struct Biol, 1992. **108**(3): p. 209-20.

141.   Besse, S. and F. Puvion-Dutilleul, *Compartmentalization of cellular and viral DNAs in adenovirus type 5 infection as revealed by ultrastructural in situ hybridization.* Chromosome Res, 1994. **2**(2): p. 123-35.

142.   Aspegren, A. and E. Bridge, *Release of snRNP and RNA from transcription sites in adenovirus-infected cells.* Exp Cell Res, 2002. **276**(2): p. 273-83.

143.   Rebelo, L., et al., *The dynamics of coiled bodies in the nucleus of adenovirus-infected cells.* Mol Biol Cell, 1996. **7**(7): p. 1137-51.

144.   Lawrence, F.J., B. McStay, and D.A. Matthews, *Nucleolar protein upstream binding factor is sequestered into adenovirus DNA replication centres during infection without affecting RNA polymerase I location or ablating rRNA synthesis.* J Cell Sci, 2006. **119**(Pt 12): p. 2621-31.

145.   Hindley, C.E., A.D. Davidson, and D.A. Matthews, *Relationship between adenovirus DNA replication proteins and nucleolar proteins B23.1 and B23.2.* J Gen Virol, 2007. **88**(Pt 12): p. 3244-8.

146.   Lam, Y.W., et al., *Proteomics analysis of the nucleolus in adenovirus-infected cells.* Mol Cell Proteomics, 2010. **9**(1): p. 117-30.

147.   Thiry, M. and F. Puvion-Dutilleul, *Differential distribution of single-stranded DNA, double-stranded DNA, and RNA in adenovirus-induced intranuclear regions of HeLa cells.* J Histochem Cytochem, 1995. **43**(8): p. 749-59.

148.   Rosa-Calatrava, M., et al., *Functional analysis of adenovirus protein IX identifies domains involved in capsid stability, transcriptional activity, and nuclear reorganization.* J Virol, 2001. **75**(15): p. 7131-41.

149.   Franqueville, L., et al., *Protein crystals in Adenovirus type 5-infected cells: requirements for intranuclear crystallogenesis, structural and functional analysis.* PLoS One, 2008. **3**(8): p. e2894.

150.   Marusyk, R., E. Norrby, and H. Marusyk, *The relationship of adenovirus-induced paracrystalline structures of the virus core protein(s).* J Gen Virol, 1972. **14**(3): p. 261-70.

151.   Endter, C., et al., *SUMO-1 modification required for transformation by adenovirus type 5 early region 1B 55-kDa oncoprotein.* Proc Natl Acad Sci U S A, 2001. **98**(20): p. 11312-7.

152.   Teodoro, J.G., et al., *Phosphorylation at the carboxy terminus of the 55-kilodalton adenovirus type 5 E1B protein regulates transforming activity.* J Virol, 1994. **68**(2): p. 776-86.

115

153. Querido, E., et al., *Degradation of p53 by adenovirus E4orf6 and E1B55K proteins occurs via a novel mechanism involving a Cullin-containing complex.* Genes Dev, 2001. **15**(23): p. 3104-17.

154. Bridge, E. and G. Ketner, *Interaction of adenoviral E4 and E1b products in late gene expression.* Virology, 1990. **174**(2): p. 345-53.

155. Chahal, J.S. and S.J. Flint, *Timely synthesis of the adenovirus type 5 E1B 55-kilodalton protein is required for efficient genome replication in normal human cells.* J Virol, 2012. **86**(6): p. 3064-72.

156. Leppard, K.N., *Selective effects on adenovirus late gene expression of deleting the E1b 55K protein.* J Gen Virol, 1993. **74 (Pt 4)**: p. 575-82.

157. Leppard, K.N. and T. Shenk, *The adenovirus E1B 55 kd protein influences mRNA transport via an intranuclear effect on RNA metabolism.* EMBO J, 1989. **8**(8): p. 2329-36.

158. Pilder, S., et al., *The adenovirus E1B-55K transforming polypeptide modulates transport or cytoplasmic stabilization of viral and host cell mRNAs.* Mol Cell Biol, 1986. **6**(2): p. 470-6.

159. Woo, J.L. and A.J. Berk, *Adenovirus ubiquitin-protein ligase stimulates viral late mRNA nuclear export.* J Virol, 2007. **81**(2): p. 575-87.

160. Miller, D.L., et al., *The adenoviral E1B 55-kilodalton protein controls expression of immune response genes but not p53-dependent transcription.* J Virol, 2009. **83**(8): p. 3591-603.

161. Spurgeon, M.E. and D.A. Ornelles, *The adenovirus E1B 55-kilodalton and E4 open reading frame 6 proteins limit phosphorylation of eIF2alpha during the late phase of infection.* J Virol, 2009. **83**(19): p. 9970-82.

162. Harada, J.N. and A.J. Berk, *p53-Independent and -dependent requirements for E1B-55K in adenovirus type 5 replication.* J Virol, 1999. **73**(7): p. 5333-44.

163. Babiss, L.E. and H.S. Ginsberg, *Adenovirus type 5 early region 1b gene product is required for efficient shutoff of host protein synthesis.* J Virol, 1984. **50**(1): p. 202-12.

164. Blackford, A.N. and R.J. Grand, *Adenovirus E1B 55-kilodalton protein: multiple roles in viral infection and cell transformation.* J Virol, 2009. **83**(9): p. 4000-12.

165. Rubenwolf, S., et al., *Structural analysis of the adenovirus type 5 E1B 55-kilodalton-E4orf6 protein complex.* J Virol, 1997. **71**(2): p. 1115-23.

116

166. Zantema, A., et al., *Localization of the E1B proteins of adenovirus 5 in transformed cells, as revealed by interaction with monoclonal antibodies.* Virology, 1985. **142**(1): p. 44-58.

167. Ornelles, D.A. and T. Shenk, *Localization of the adenovirus early region 1B 55-kilodalton protein during lytic infection: association with nuclear viral inclusions requires the early region 4 34-kilodalton protein.* J Virol, 1991. **65**(1): p. 424-9.

168. Liu, Y., et al., *Adenovirus exploits the cellular aggresome response to accelerate inactivation of the MRN complex.* J Virol, 2005. **79**(22): p. 14004-16.

169. Leppard, K.N. and R.D. Everett, *The adenovirus type 5 E1b 55K and E4 Orf3 proteins associate in infected cells and affect ND10 components.* J Gen Virol, 1999. **80 (Pt 4)**: p. 997-1008.

170. Lethbridge, K.J., G.E. Scott, and K.N. Leppard, *Nuclear matrix localization and SUMO-1 modification of adenovirus type 5 E1b 55K protein are controlled by E4 Orf6 protein.* J Gen Virol, 2003. **84**(Pt 2): p. 259-68.

171. Dobbelstein, M., et al., *Nuclear export of the E1B 55-kDa and E4 34-kDa adenoviral oncoproteins mediated by a rev-like signal sequence.* Embo J, 1997. **16**(14): p. 4276-84.

172. Goodrum, F.D., T. Shenk, and D.A. Ornelles, *Adenovirus early region 4 34-kilodalton protein directs the nuclear localization of the early region 1B 55-kilodalton protein in primate cells.* J Virol, 1996. **70**(9): p. 6323-35.

173. Marshall, L.J., et al., *RUNX1 permits E4orf6-directed nuclear localization of the adenovirus E1B-55K protein and associates with centers of viral DNA and RNA synthesis.* J Virol, 2008. **82**(13): p. 6395-408.

174. Zheng, X., et al., *Adenovirus E1B55K region is required to enhance cyclin E expression for efficient viral DNA replication.* J Virol, 2008. **82**(7): p. 3415-27.

175. Denome, R.M., E.A. Werner, and R.J. Patterson, *RNA metabolism in nuclei: adenovirus and heat shock alter intranuclear RNA compartmentalization.* Nucleic Acids Res, 1989. **17**(5): p. 2081-98.

176. Ciejek, E.M., et al., *Ribonucleic acid precursors are associated with the chick oviduct nuclear matrix.* Biochemistry, 1982. **21**(20): p. 4945-53.

177. Robinson, S.I., B.D. Nelkin, and B. Vogelstein, *The ovalbumin gene is associated with the nuclear matrix of chicken oviduct cells.* Cell, 1982. **28**(1): p. 99-106.

117

178. Ross, D.A., R.W. Yen, and C.B. Chae, *Association of globin ribonucleic acid and its precursors with the chicken erythroblast nuclear matrix.* Biochemistry, 1982. **21**(4): p. 764-71.

179. Pardoll, D.M., B. Vogelstein, and D.S. Coffey, *A fixed site of DNA replication in eucaryotic cells.* Cell, 1980. **19**(2): p. 527-36.

180. Zeitlin, S., et al., *Pre-mRNA splicing and the nuclear matrix.* Mol Cell Biol, 1987. **7**(1): p. 111-20.

181. Gabler, S., et al., *E1B 55-kilodalton-associated protein: a cellular protein with RNA-binding activity implicated in nucleocytoplasmic transport of adenovirus and cellular mRNAs.* J Virol, 1998. **72**(10): p. 7960-71.

182. Bachi, A., et al., *The C-terminal domain of TAP interacts with the nuclear pore complex and promotes export of specific CTE-bearing RNA substrates.* RNA, 2000. **6**(1): p. 136-58.

183. Eliseeva, I.A., et al., *Y-box-binding protein 1 (YB-1) and its functions.* Biochemistry (Mosc), 2011. **76**(13): p. 1402-33.

184. Evdokimova, V., L.P. Ovchinnikov, and P.H. Sorensen, *Y-box binding protein 1: providing a new angle on translational regulation.* Cell Cycle, 2006. **5**(11): p. 1143-7.

185. Evdokimova, V., et al., *The major mRNA-associated protein YB-1 is a potent 5' cap-dependent mRNA stabilizer.* EMBO J, 2001. **20**(19): p. 5491-502.

186. Janz, M., et al., *Y-box factor YB-1 predicts drug resistance and patient outcome in breast cancer independent of clinically relevant tumor biologic factors HER2, uPA and PAI-1.* Int J Cancer, 2002. **97**(3): p. 278-82.

187. Gimenez-Bonafe, P., et al., *YB-1 is upregulated during prostate cancer tumor progression and increases P-glycoprotein activity.* Prostate, 2004. **59**(3): p. 337-49.

188. Dahl, E., et al., *Nuclear detection of Y-box protein-1 (YB-1) closely associates with progesterone receptor negativity and is a strong adverse survival factor in human breast cancer.* BMC Cancer, 2009. **9**: p. 410.

189. Das, S., et al., *Stimulation of NEIL2-mediated oxidized base excision repair via YB-1 interaction during oxidative stress.* J Biol Chem, 2007. **282**(39): p. 28474-84.

118

190.   Zhang, Y.F., et al., *Nuclear localization of Y-box factor YB1 requires wild-type p53.* Oncogene, 2003. **22**(18): p. 2782-94.

191.   Chansky, H.A., et al., *Oncogenic TLS/ERG and EWS/Fli-1 fusion proteins inhibit RNA splicing mediated by YB-1 protein.* Cancer Res, 2001. **61**(9): p. 3586-90.

192.   Holm, P.S., et al., *Multidrug-resistant cancer cells facilitate E1-independent adenoviral replication: impact for cancer gene therapy.* Cancer Res, 2004. **64**(1): p. 322-8.

193.   Sarnow, P., et al., *Adenovirus E1b-58kd tumor antigen and SV40 large tumor antigen are physically associated with the same 54 kd cellular protein in transformed cells.* Cell, 1982. **28**(2): p. 387-94.

194.   Querido, E., et al., *Regulation of p53 levels by the E1B 55-kilodalton protein and E4orf6 in adenovirus-infected cells.* J Virol, 1997. **71**(5): p. 3788-98.

195.   Kao, C.C., P.R. Yew, and A.J. Berk, *Domains required for in vitro association between the cellular p53 and the adenovirus 2 E1B 55K proteins.* Virology, 1990. **179**(2): p. 806-14.

196.   Yew, P.R., C.C. Kao, and A.J. Berk, *Dissection of functional domains in the adenovirus 2 early 1B 55K polypeptide by suppressor-linker insertional mutagenesis.* Virology, 1990. **179**(2): p. 795-805.

197.   Barral, P.M., et al., *The interaction of the hnRNP family member E1B-AP5 with p53.* FEBS Lett, 2005. **579**(13): p. 2752-8.

198.   Okamoto, T., et al., *Direct interaction of p53 with the Y-box binding protein, YB-1: a mechanism for regulation of human gene expression.* Oncogene, 2000. **19**(54): p. 6194-202.

199.   Jones, N. and T. Shenk, *Isolation of adenovirus type 5 host range deletion mutants defective for transformation of rat embryo cells.* Cell, 1979. **17**(3): p. 683-9.

200.   Groitl, P. and T. Dobner, *Construction of adenovirus type 5 early region 1 and 4 virus mutants.* Methods Mol Med, 2007. **130**: p. 29-39.

201.   Wimmer, P., et al., *Cross-talk between phosphorylation and SUMOylation regulates transforming activities of an adenoviral oncoprotein.* Oncogene, 2013. **32**(13): p. 1626-37.

202.   Blanchette, P., et al., *Control of mRNA export by adenovirus E4orf6 and E1B55K proteins during productive infection requires E4orf6 ubiquitin ligase activity.* J Virol, 2008. **82**(6): p. 2642-51.

203.   Reich, N.C., et al., *Monoclonal antibodies which recognize native and denatured forms of the adenovirus DNA-binding protein.* Virology, 1983. **128**(2): p. 480-4.

204.   Sarnow, P., C.A. Sullivan, and A.J. Levine, *A monoclonal antibody detecting the adenovirus type 5-E1b-58Kd tumor antigen: characterization of the E1b-58Kd tumor antigen in adenovirus-infected and -transformed cells.* Virology, 1982. **120**(2): p. 510-7.

205.   Schneider, C.A., W.S. Rasband, and K.W. Eliceiri, *NIH Image to ImageJ: 25 years of image analysis.* Nat Methods, 2012. **9**(7): p. 671-5.

206.   Quackenbush, J., *Microarray data normalization and transformation.* Nat Genet, 2002. **32 Suppl**: p. 496-501.

207.   Kolmogorov, A.N., *Sulla determinazione empirica di una legge di distribuzione.* Giornale dell'Istituto Italiano degli Attuari, 1933. **4**: p. 83-91.

208.   Wilk, S.S.S.a.M.B., *An Analysis of Variance Test for Normality (Complete Samples).* Biometrika, 1965. **52**(3/4): p. 591-611.

209.   Levene, H., *Robust tests for equality of variances.* In Contributions to Probability and Statistics: Essays in Honor of Harold Hotelling, I. Olkin et al. eds., Stanford University Press, 1960: p. 278-292.

210.   Cohen, J., Cohen P., West, S.G., & Aiken, L.S. , *Applied multiple regression/correlation analysis for the behavioral sciences. .* Journal of the Royal Statistical Society Series D (The Statistician). Lawrence Erlbaum Associates. , 2002. **52**(4).

211.   Nevels, M., et al., *"Hit-and-run" transformation by adenovirus oncogenes.* J Virol, 2001. **75**(7): p. 3089-94.

212.   Wimmer, P., et al., *PML isoforms IV and V contribute to adenovirus-mediated oncogenic transformation by functionally inhibiting the tumor-suppressor p53.* Oncogene, 2016. **35**(1): p. 69-82.

213.   Schreiner, S., et al., *Control of human adenovirus type 5 gene expression by cellular Daxx/ATRX chromatin-associated complexes.* Nucleic Acids Res, 2013. **41**(6): p. 3532-50.

214. Hidalgo, P. and R.A. Gonzalez, *Isolation of Viral Replication Compartment-enriched Sub-nuclear Fractions from Adenovirus-infected Normal Human Cells.* J Vis Exp, 2015(105).

215. Busch, H., et al., *Isolation of Nucleoli.* Exp Cell Res, 1963. **24**: p. SUPPL9:150-63.

216. Andersen, J.S., et al., *Directed proteomic analysis of the human nucleolus.* Curr Biol, 2002. **12**(1): p. 1-11.

217. Cox, S., et al., *Bayesian localization microscopy reveals nanoscale podosome dynamics.* Nat Methods, 2012. **9**(2): p. 195-200.

218. Rosten, E., G.E. Jones, and S. Cox, *ImageJ plug-in for Bayesian analysis of blinking and bleaching.* Nat Methods, 2013. **10**(2): p. 97-8.

219. Hernández, H.O.H., P.; Wood, C.D.; González, R. A.; Guerrero, A. , *Parallelizing the Bayesian Analysis of Blinking and Bleaching for Super-Resolution Microscopy*, in *High Performance Computer Applications. ISUM 2015. Communications in Computer and Information Science*, K.J. Gitler I., Editor 2016, Springer, Cham.

220. Brison, O., C. Kedinger, and J. Wilhelm, *Enzymatic properties of viral replication complexes isolated from adenovirus type 2-infected HeLa cell nuclei.* J Virol, 1977. **24**(2): p. 423-35.

221. Wilhelm, J., et al., *Characterization of adenovirus type 2 transcriptional complexes isolated from infected HeLa cell nuclei.* J Virol, 1976. **19**(1): p. 61-81.

222. Hicks, M.J., B.J. Lam, and K.J. Hertel, *Analyzing mechanisms of alternative pre-mRNA splicing using in vitro splicing assays.* Methods, 2005. **37**(4): p. 306-13.

223. Hertweck, M., R. Hiller, and M.W. Mueller, *Inhibition of nuclear pre-mRNA splicing by antibiotics in vitro.* Eur J Biochem, 2002. **269**(1): p. 175-83.

224. Garces, Y., et al., *Automatic detection and measurement of viral replication compartments by ellipse adjustment.* Sci Rep, 2016. **6**: p. 36505.

225. Langmead, B. and S.L. Salzberg, *Fast gapped-read alignment with Bowtie 2.* Nat Methods, 2012. **9**(4): p. 357-9.

226. Dobner, T. and J. Kzhyshkowska, *Nuclear export of adenovirus RNA.* Curr Top Microbiol Immunol, 2001. **259**: p. 25-54.

227. Zhao, H., F. Granberg, and U. Pettersson, *How adenovirus strives to control cellular gene expression.* Virology, 2007. **363**(2): p. 357-75.

228. Crossland, L.D. and H.J. Raskas, *Identification of adenovirus genes that require template replication for expression.* J Virol, 1983. **46**(3): p. 737-48.

229. Binger, M.H. and S.J. Flint, *Accumulation of early and intermediate mRNA species during subgroup C adenovirus productive infections.* Virology, 1984. **136**(2): p. 387-403.

230. Smirnov, N., *Table for Estimating the Goodness of Fit of Empirical Distributions.* The Annals of Mathematical Statistics, 1948. **19**(2): p. 279-281.

231. Lam, Y.W., C.E. Lyon, and A.I. Lamond, *Large-scale isolation of Cajal bodies from HeLa cells.* Mol Biol Cell, 2002. **13**(7): p. 2461-73.

232. Lindsey, L.A. and M.A. Garcia-Blanco, *Prespliceosome and spliceosome isolation and analysis.* Methods Mol Biol, 1999. **118**: p. 351-64.

233. Matthews, D.A., *Adenovirus protein V induces redistribution of nucleolin and B23 from nucleolus to cytoplasm.* J Virol, 2001. **75**(2): p. 1031-8.

234. Fang, S.H. and N.H. Yeh, *The self-cleaving activity of nucleolin determines its molecular dynamics in relation to cell proliferation.* Exp Cell Res, 1993. **208**(1): p. 48-53.

235. Hidalgo, P. and R.A. Gonzalez, *Isolation of Viral Replication Compartment-Enriched Sub-Nuclear Fractions from Adenovirus-Infected Normal Human Cells.* J Vis Exp, 2015. **In press**.

236. Cheutin, T., et al., *Three-dimensional organization of active rRNA genes within the nucleolus.* J Cell Sci, 2002. **115**(Pt 16): p. 3297-307.

237. Lindberg, A., et al., *A single RNA recognition motif in splicing factor ASF/SF2 directs it to nuclear sites of adenovirus transcription.* J Gen Virol, 2004. **85**(Pt 3): p. 603-8.

238. Gama-Carvalho, M., I. Condado, and M. Carmo-Fonseca, *Regulation of adenovirus alternative RNA splicing correlates with a reorganization of splicing factors in the nucleus.* Exp Cell Res, 2003. **289**(1): p. 77-85.

239. Bridge, E., et al., *Nuclear organization of splicing small nuclear ribonucleoproteins in adenovirus-infected cells.* J Virol, 1993. **67**(10): p. 5792-802.

240. Bridge, E. and U. Pettersson, *Nuclear organization of adenovirus RNA biogenesis.* Exp Cell Res, 1996. **229**(2): p. 233-9.

241. O'Shea, C.C., et al., *Late viral RNA export, rather than p53 inactivation, determines ONYX-015 tumor selectivity.* Cancer Cell, 2004. **6**(6): p. 611-23.

242. Flint, S.J., et al., *A peptide inhibitor of exportin1 blocks shuttling of the adenoviral E1B 55 kDa protein but not export of viral late mRNAs.* Virology, 2005. **337**(1): p. 7-17.

243. Uhlen, M., et al., *Leader arrangement in the adenovirus fiber mRNA.* EMBO J, 1982. **1**(2): p. 249-54.

244. Leppard, K.N., *Regulated RNA Processing and RNA Transport during Adenovirus Infection.* Seminars in Virology, 1998. **8**(4): p. 301-307.

245. Zhao, H., M. Chen, and U. Pettersson, *A new look at adenovirus splicing.* Virology, 2014. **456-457**: p. 329-41.

246. Nordqvist, K., K. Ohman, and G. Akusjarvi, *Human adenovirus encodes two proteins which have opposite effects on accumulation of alternatively spliced mRNAs.* Mol Cell Biol, 1994. **14**(1): p. 437-45.

247. Seeler, J.S. and A. Dejean, *SUMO: of branched proteins and nuclear bodies.* Oncogene, 2001. **20**(49): p. 7243-9.

248. Van Damme, E., et al., *A manually curated network of the PML nuclear body interactome reveals an important role for PML-NBs in SUMOylation dynamics.* Int J Biol Sci, 2010. **6**(1): p. 51-67.

249. Yousef, A.F., et al., *Identification of a molecular recognition feature in the E1A oncoprotein that binds the SUMO conjugase UBC9 and likely interferes with polySUMOylation.* Oncogene, 2010. **29**(33): p. 4693-704.

250. Sohn, S.Y. and P. Hearing, *Adenovirus Early Proteins and Host Sumoylation.* MBio, 2016. **7**(5).

251. Williams, A. and R.A. Flavell, *The role of CTCF in regulating nuclear organization.* J Exp Med, 2008. **205**(4): p. 747-50.

252. Hilmi, K., et al., *CTCF facilitates DNA double-strand break repair by enhancing homologous recombination repair.* Sci Adv, 2017. **3**(5): p. e1601898.

253. Ghosh, H., et al., *Several posttranslational modifications act in concert to regulate gephyrin scaffolding and GABAergic transmission.* Nat Commun, 2016. **7**: p. 13365.

254. Chahal, J.S., J. Qi, and S.J. Flint, *The human adenovirus type 5 E1B 55 kDa protein obstructs inhibition of viral replication by type I interferon in normal human cells.* PLoS Pathog, 2012. **8**(8): p. e1002853.

255. Imperiale, M.J., G. Akusjärvi, and K.N. Leppard, *Post-transcriptional control of adenovirus gene expression.* Curr Top Microbiol Immunol, 1995. **199 (Pt 2)**: p. 139-71.

256. Ben-Israel, H. and T. Kleinberger, *Adenovirus and cell cycle control.* Front Biosci, 2002. **7**: p. d1369-95.

257. Guilfoyle, R.A., W.P. Osheroff, and M. Rossini, *Two functions encoded by adenovirus early region 1A are responsible for the activation and repression of the DNA-binding protein gene.* Embo J, 1985. **4**(3): p. 707-13.

258. Horridge, J.J. and K.N. Leppard, *RNA-binding activity of the E1B 55-kilodalton protein from human adenovirus type 5.* J Virol, 1998. **72**(11): p. 9374-9.

259. Dyson, H.J. and P.E. Wright, *Insights into the structure and dynamics of unfolded proteins from nuclear magnetic resonance.* Adv Protein Chem, 2002. **62**: p. 311-40.

260. Sieber, T., et al., *Intrinsic disorder in the common N-terminus of human adenovirus 5 E1B-55K and its related E1BN proteins indicated by studies on E1B-93R.* Virology, 2011. **418**(2): p. 133-43.

261. Hung, G. and S.J. Flint, *Normal human cell proteins that interact with the adenovirus type 5 E1B 55kDa protein.* Virology, 2017. **504**: p. 12-24.

262. Roth, J. and M. Dobbelstein, *Interaction of p53 with the adenovirus E1B-55 kDa protein.* Methods Mol Biol, 2003. **234**: p. 135-49.

263. Zhao, L.Y., et al., *Adenovirus E1B 55-kilodalton oncoprotein binds to Daxx and eliminates enhancement of p53-dependent transcription by Daxx.* J Virol, 2003. **77**(21): p. 11809-21.

264. Handwerger, K.E., J.A. Cordero, and J.G. Gall, *Cajal bodies, nucleoli, and speckles in the Xenopus oocyte nucleus have a low-density, sponge-like structure.* Mol Biol Cell, 2005. **16**(1): p. 202-11.

124

265. Samad, M.A., et al., *B23/nucleophosmin is involved in regulation of adenovirus chromatin structure at late infection stages, but not in virus replication and transcription.* J Gen Virol, 2012. **93**(Pt 6): p. 1328-38.

266. Samad, M.A., et al., *Physical and functional interaction between a nucleolar protein nucleophosmin/B23 and adenovirus basic core proteins.* FEBS Lett, 2007. **581**(17): p. 3283-8.

267. Castiglia, C.L. and S.J. Flint, *Effects of adenovirus infection on rRNA synthesis and maturation in HeLa cells.* Mol Cell Biol, 1983. **3**(4): p. 662-71.

268. Ledinko, N., *Nucleolar ribosomal precursor RNA and protein metabolism in human embryo kidney cultures infected with adenovirus 12.* Virology, 1972. **49**(1): p. 79-89.

269. Hiscox, J.A., A. Whitehouse, and D.A. Matthews, *Nucleolar proteomics and viral infection.* Proteomics, 2010. **10**(22): p. 4077-86.

270. Puvion-Dutilleul, F. and E. Puvion, *Sites of transcription of adenovirus type 5 genomes in relation to early viral DNA replication in infected HeLa cells. A high resolution in situ hybridization and autoradiographical study.* Biol Cell, 1991. **71**(1-2): p. 135-47.

271. Puvion-Dutilleul, F., *Protocol of electron microscope in situ nucleic acid hybridization for the exclusive detection of double-stranded DNA sequences in cells containing large amounts of homologous single-stranded DNA and RNA sequences: application to adenovirus type 5 infected HeLa cells.* Microsc Res Tech, 1993. **25**(1): p. 2-11.

272. Strang, B.L., et al., *Host cell nucleolin is required to maintain the architecture of human cytomegalovirus replication compartments.* MBio, 2012. **3**(1).

273. Bender, B.J., D.M. Coen, and B.L. Strang, *Dynamic and nucleolin-dependent localization of human cytomegalovirus UL84 to the periphery of viral replication compartments and nucleoli.* J Virol, 2014. **88**(20): p. 11738-47.

274. Strang, B.L., S. Boulant, and D.M. Coen, *Nucleolin associates with the human cytomegalovirus DNA polymerase accessory subunit UL44 and is necessary for efficient viral replication.* J Virol, 2010. **84**(4): p. 1771-84.

275. Malik-Soni, N. and L. Frappier, *Nucleophosmin contributes to the transcriptional activation function of the Epstein-Barr virus EBNA1 protein.* J Virol, 2014. **88**(4): p. 2323-6.

125

276. Chen, C.M., S.Y. Chiang, and N.H. Yeh, *Increased stability of nucleolin in proliferating cells by inhibition of its self-cleaving activity.* J Biol Chem, 1991. **266**(12): p. 7754-8.

277. Warrener, P. and R. Petryshyn, *Phosphorylation and proteolytic degradation of nucleolin from 3T3-F442A cells.* Biochem Biophys Res Commun, 1991. **180**(2): p. 716-23.

278. Bridge, E., et al., *Spliced exons of adenovirus late RNAs colocalize with snRNP in a specific nuclear domain.* J Cell Biol, 1996. **135**(2): p. 303-14.

279. Jimenez-Garcia, L.F. and D.L. Spector, *In vivo evidence that transcription and splicing are coordinated by a recruiting mechanism.* Cell, 1993. **73**(1): p. 47-59.

280. Anderson, K.P. and D.F. Klessig, *Altered mRNA splicing in monkey cells abortively infected with human adenovirus may be responsible for inefficient synthesis of the virion fiber polypeptide.* Proc Natl Acad Sci U S A, 1984. **81**(13): p. 4023-7.

281. Berget, S.M., C. Moore, and P.A. Sharp, *Spliced segments at the 5' terminus of adenovirus 2 late mRNA.* Proc Natl Acad Sci U S A, 1977. **74**(8): p. 3171-5.

282. Reichelt, M., et al., *3D reconstruction of VZV infected cell nuclei and PML nuclear cages by serial section array scanning electron microscopy and electron tomography.* PLoS Pathog, 2012. **8**(6): p. e1002740.

283. Reichelt, M., et al., *Entrapment of viral capsids in nuclear PML cages is an intrinsic antiviral host defense against varicella-zoster virus.* PLoS Pathog, 2011. **7**(2): p. e1001266.

284. Ou, H.D., et al., *A structural basis for the assembly and functions of a viral polymer that inactivates multiple tumor suppressors.* Cell, 2012. **151**(2): p. 304-19.

285. Vink, E.I., et al., *Impact of Adenovirus E4-ORF3 Oligomerization and Protein Localization on Cellular Gene Expression.* Viruses, 2015. **7**(5): p. 2428-49.

126

10 ANNEXES

Supplementary information and Published articles.

E1B 55K REGULATES EXPRESSION OF VIRAL EARLY AND LATE GENES

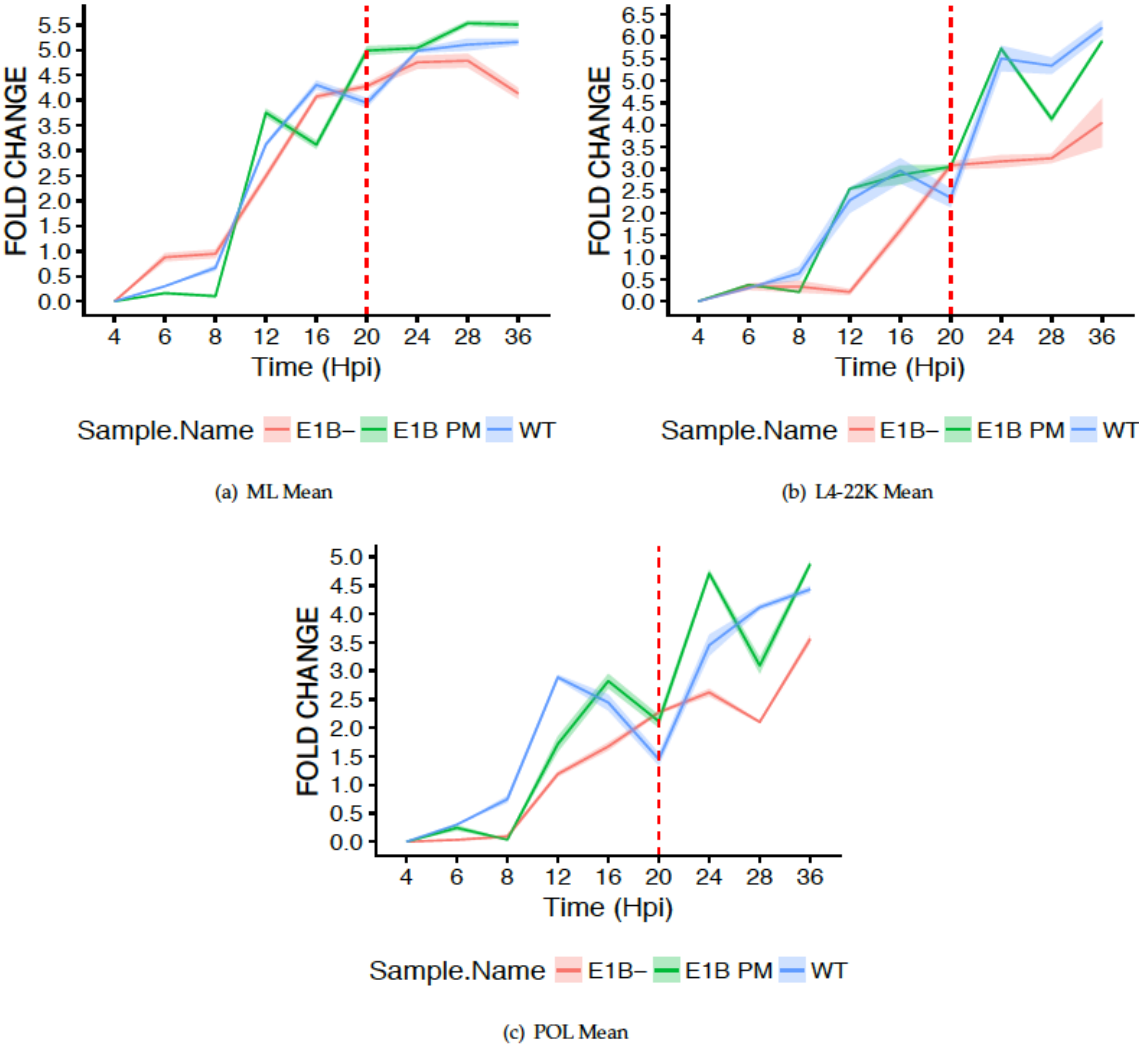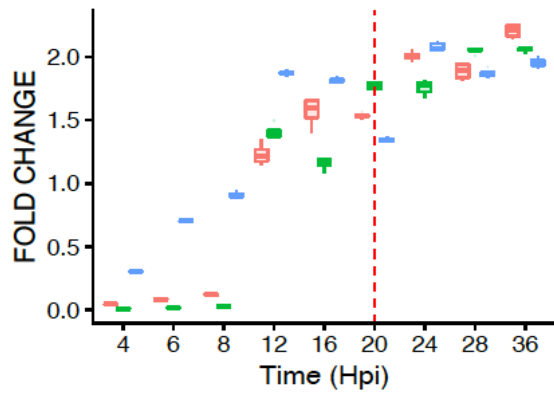(a) ML Mean
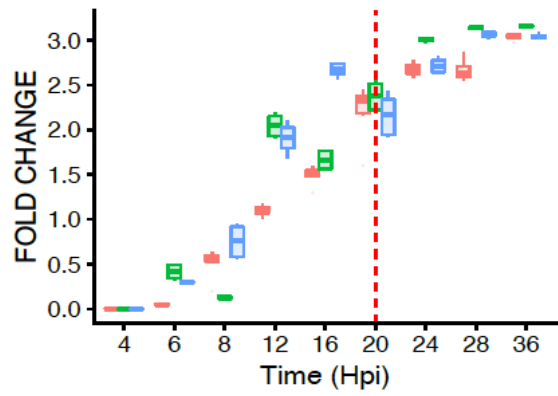
(b) L4-22K Mean

(c) POL Mean

Figure S2. Kinetics of viral early and late mRNA through different times of the replication cycle. Total RNA from HFF infected with Ad WT, E1B⁻ or E1B PM viruses was used to quantify the indicated viral transcripts at different times post-infection.

(a) E1A Boxplot

(b) E1B Boxplot

Figure S3. Kinetics of viral early and late mRNA through different times of the replication cycle. Box plots of viral early mRNA at various time-points.
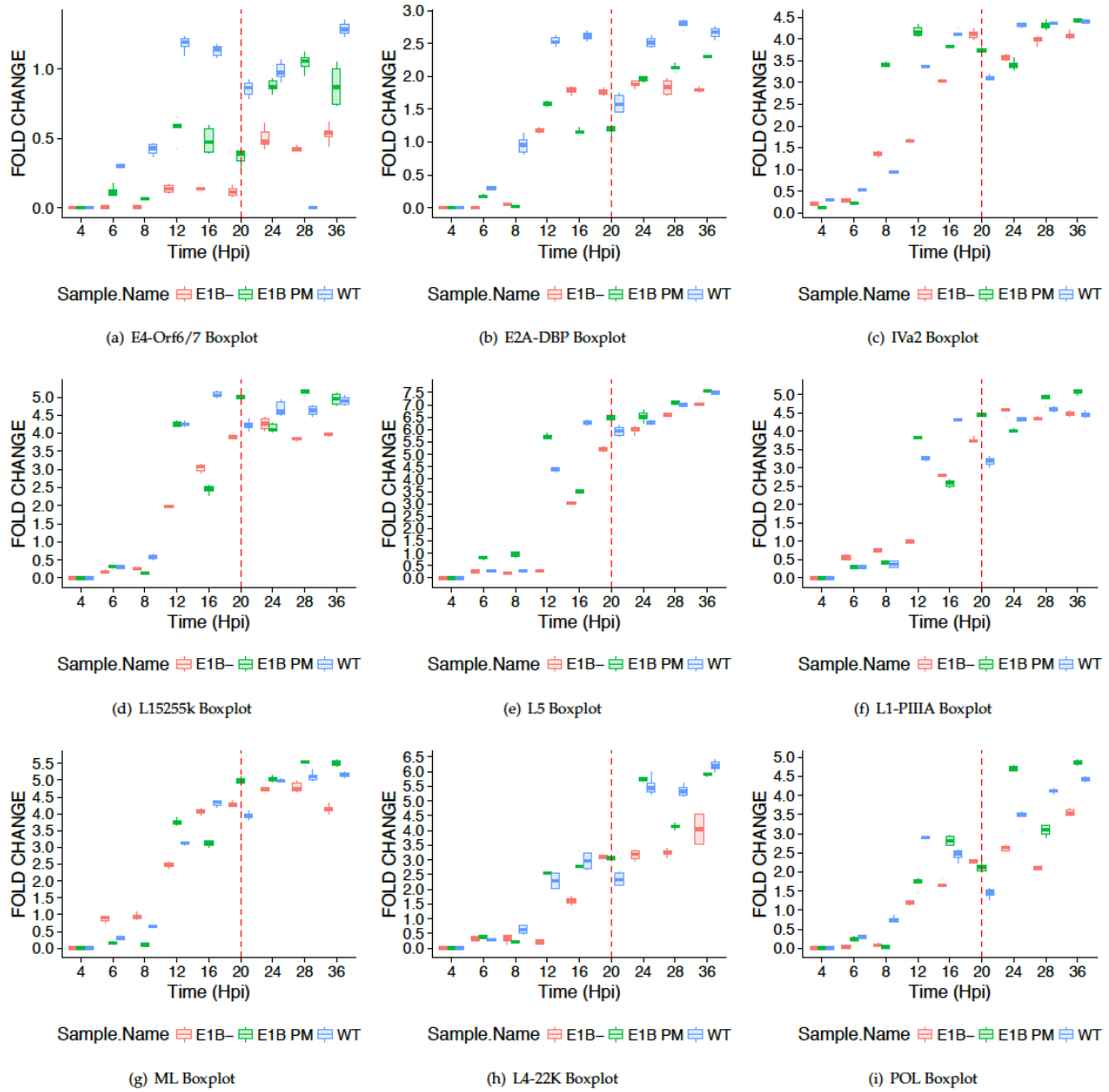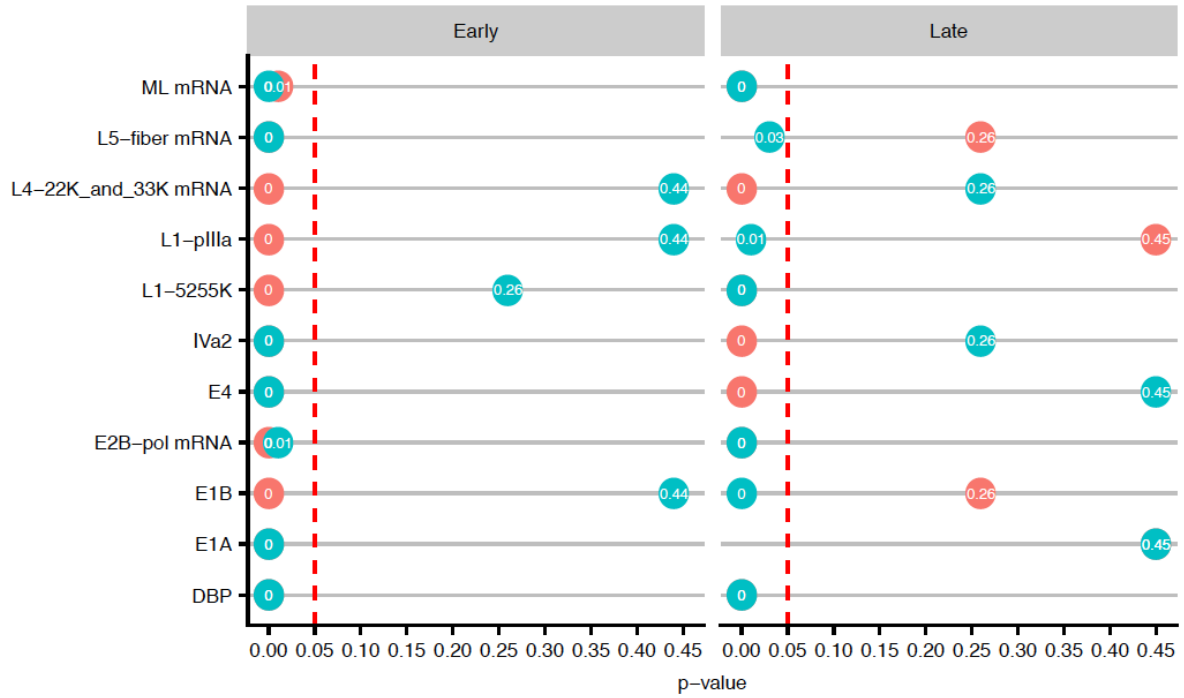
Figure S4. Kinetics of viral early and late mRNA through different times of the replication cycle. Box plots of viral early mRNA at various time-points.

Figure S5. P-value of the Kolmogorov-Smirnov test for Ad WT, E1B⁻ and E1B PM. The hypothesis test evaluates the existance of significant differences between the distribution of each mRNA in two continuous time points. The red dashed line defines the significant level (a = 0.05).

E1B 55K CAN EITHER REPRESS OR ENHANCE VIRAL GENE EXPRESSION AT DIFFERENT TIME-POINTS OF THE VIRAL REPLICATION CYCLE.
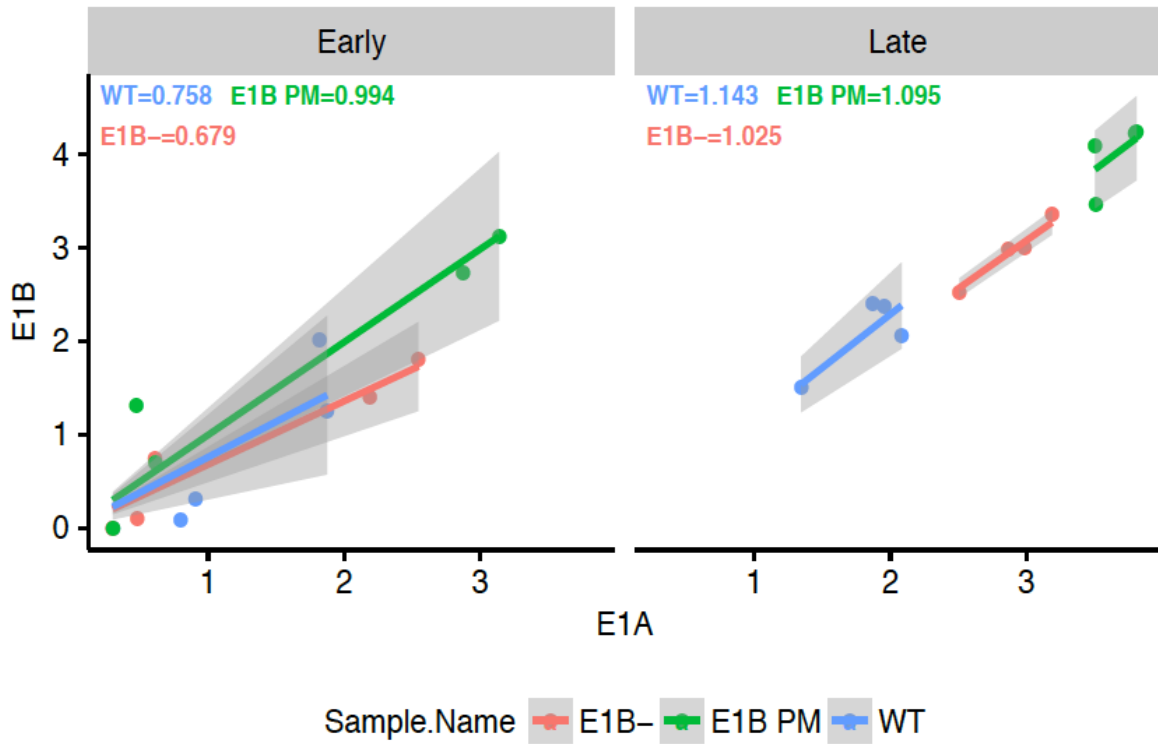

Figure S6. E1A vs. E1B
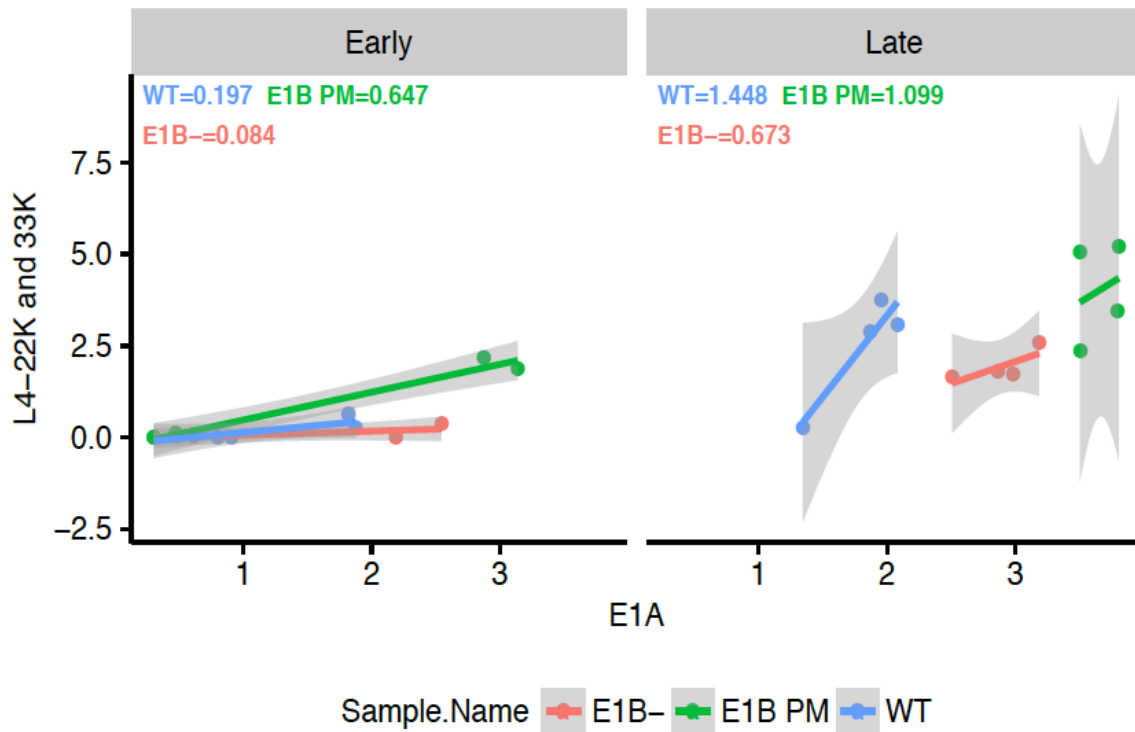
Figure S7. E1A vs L4-22K and 33K

Figure S8. E1A vs. ML

Figure S9. Slope and standard deviation: E1A vs. E1B

Figure S10. Slope and standard deviation: E1A vs. E4Orf6/7

Figure S11. Slope and standard deviation: E1A vs. DBP

Figure S12. Slope and standard deviation: E1A vs. pol

Figure S13. Slope and standard deviation: E1A vs. IVa2

Figure S14. Slope and standard deviation: E1A vs. L1-52/55K

Figure S15. Slope and standard deviation: E1A vs. L5-fiber

Figure S16. Slope and standard deviation: E1A vs. L1-pIIIa

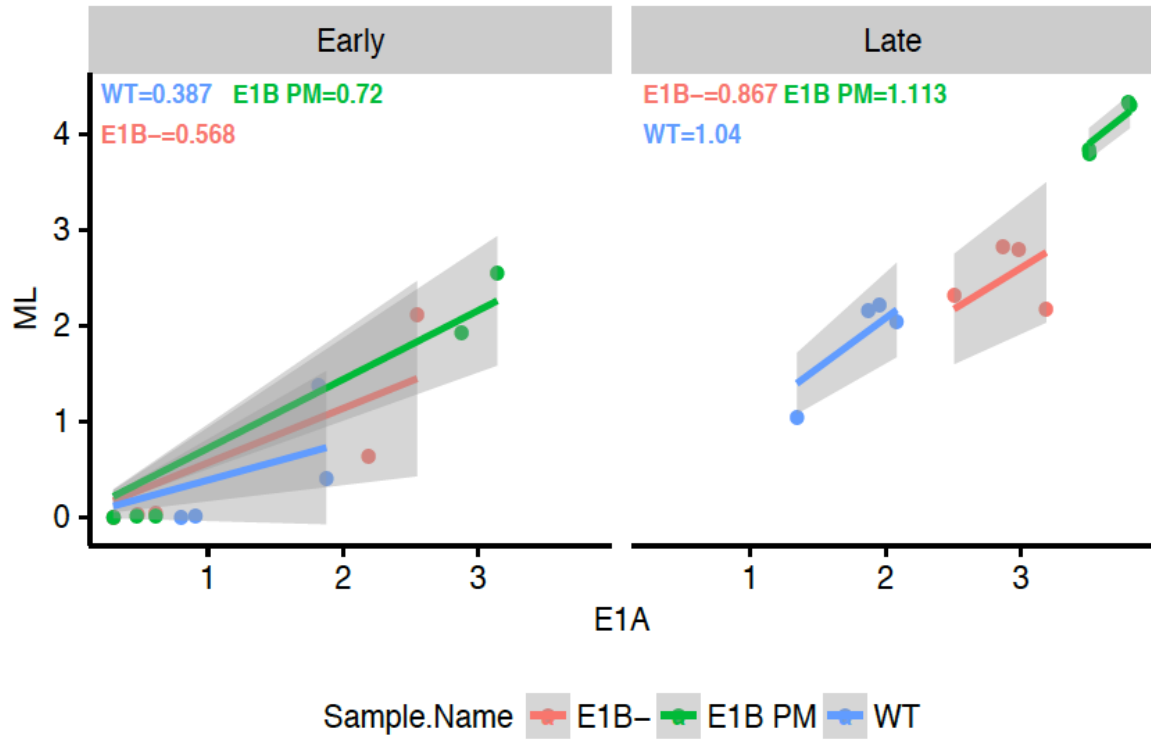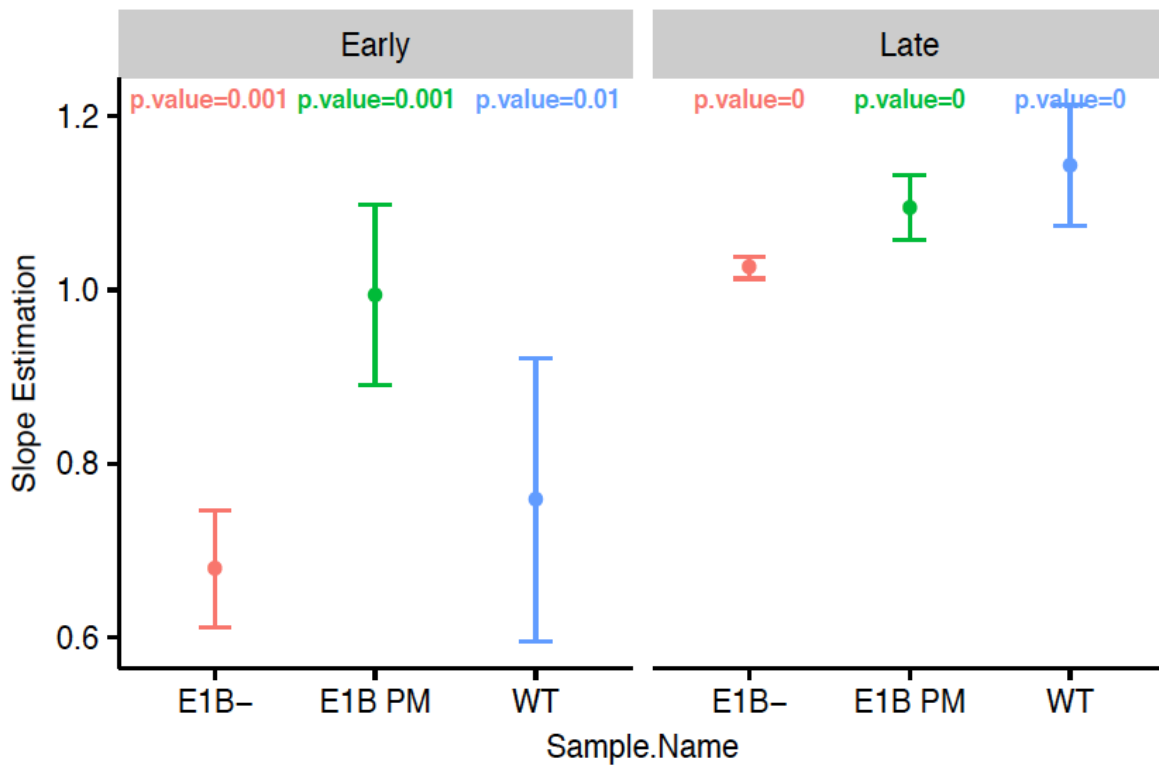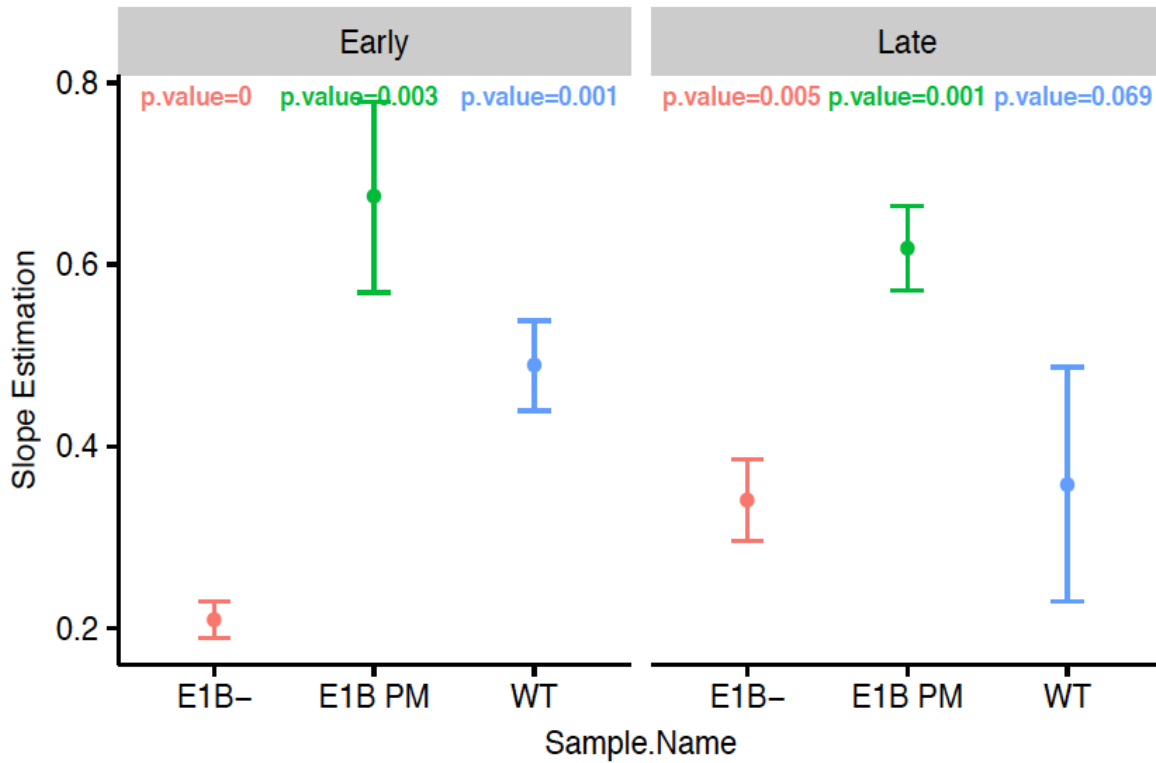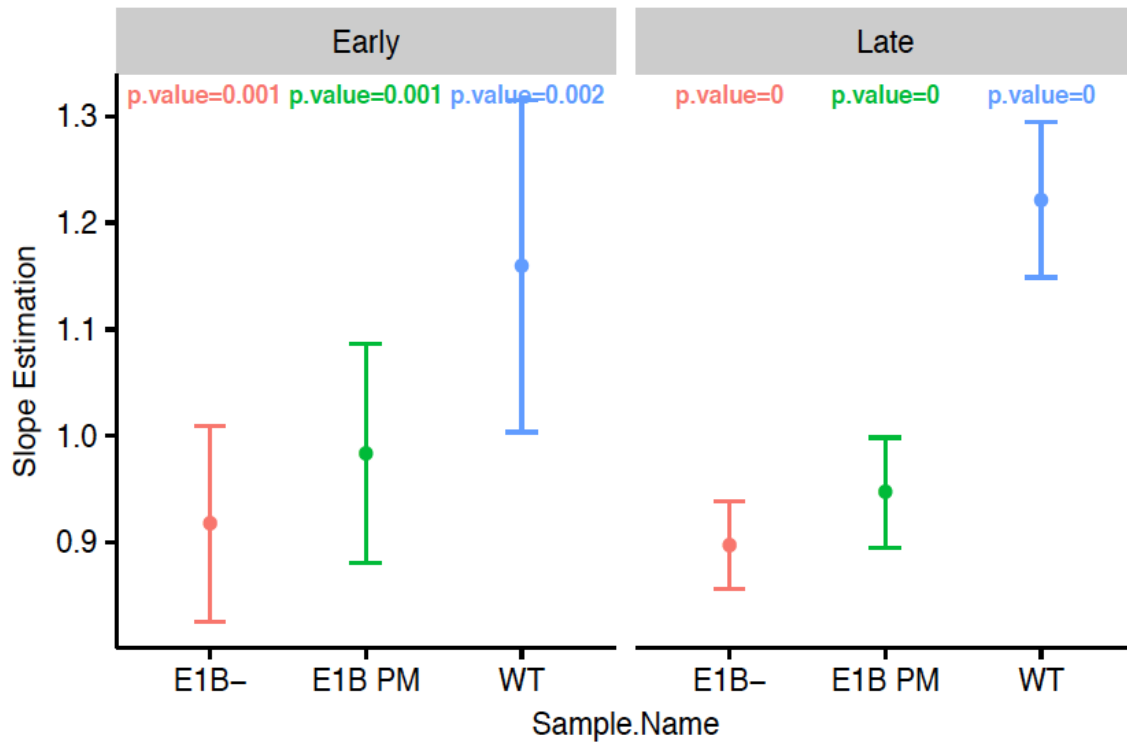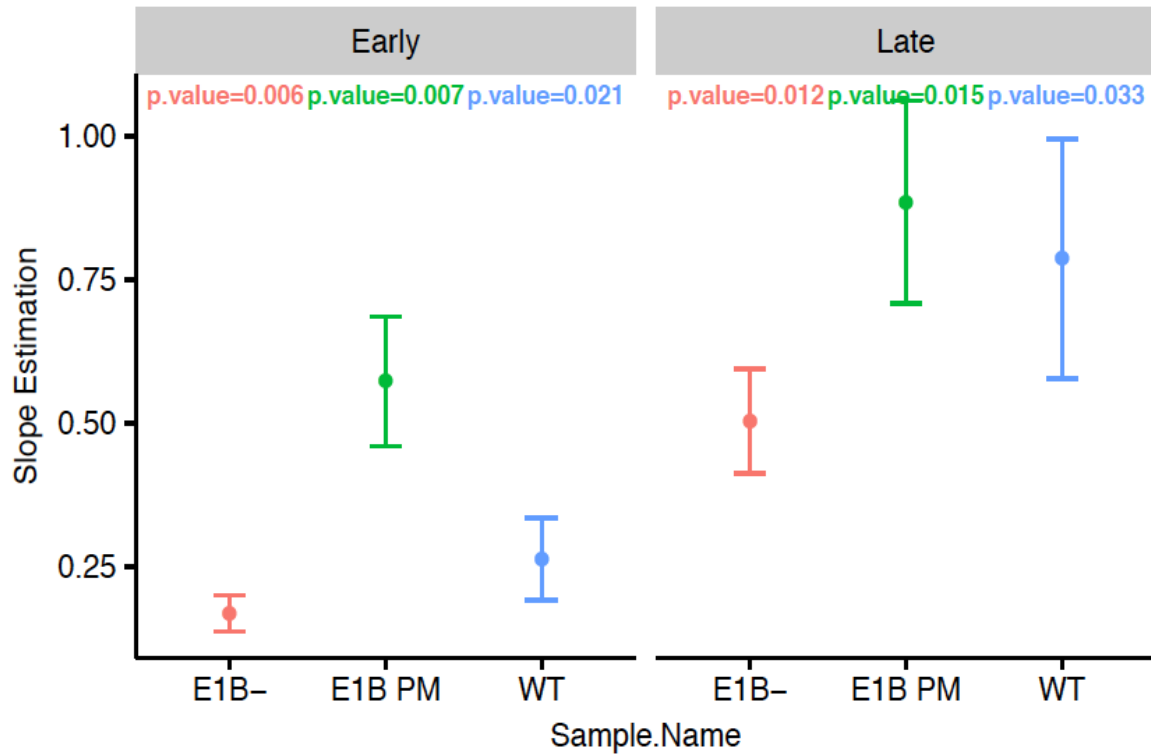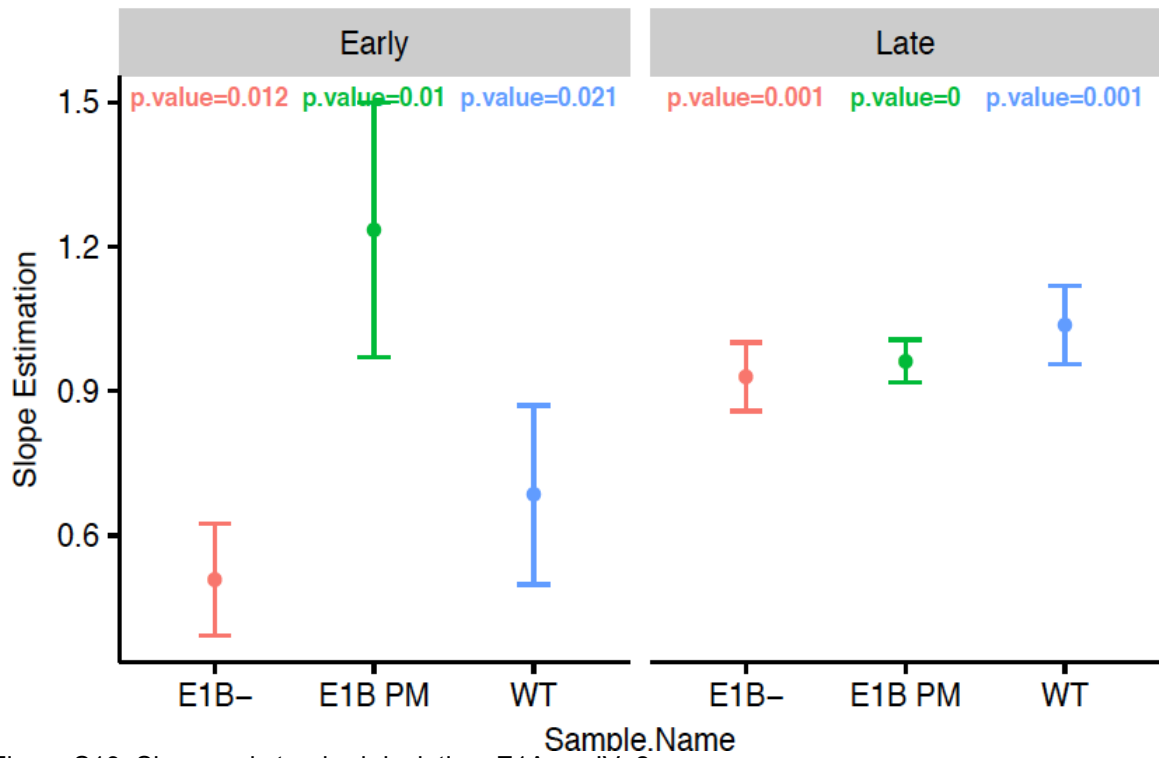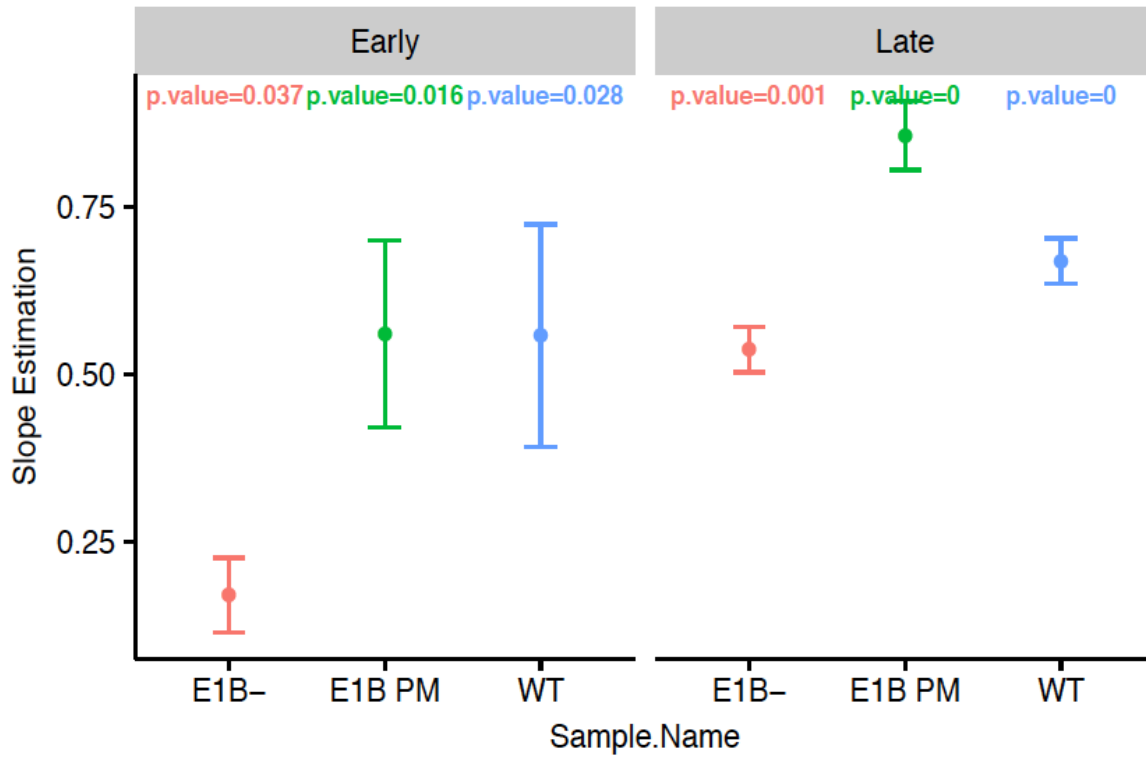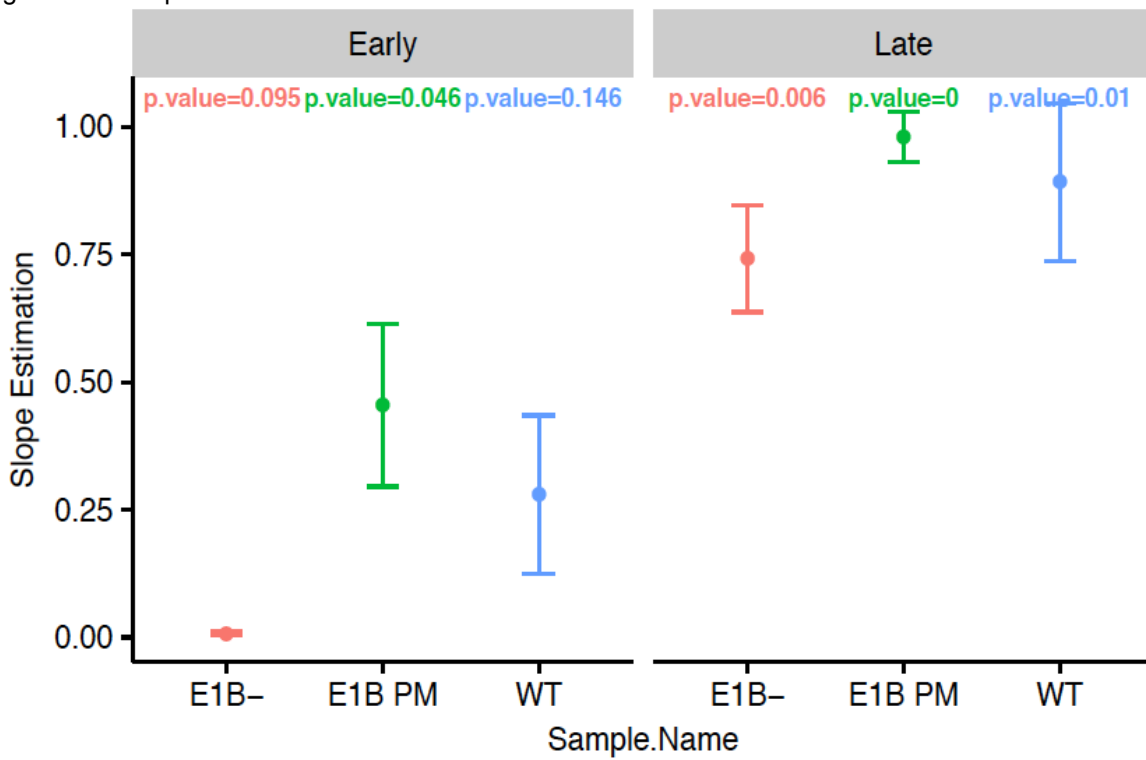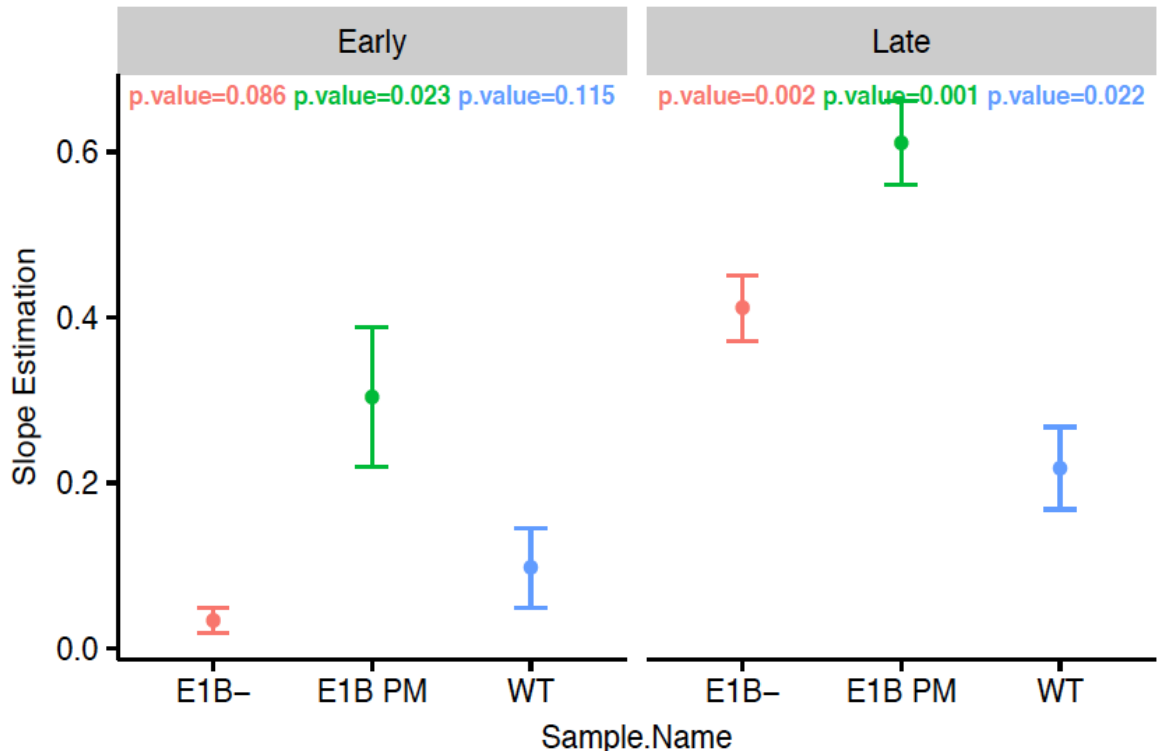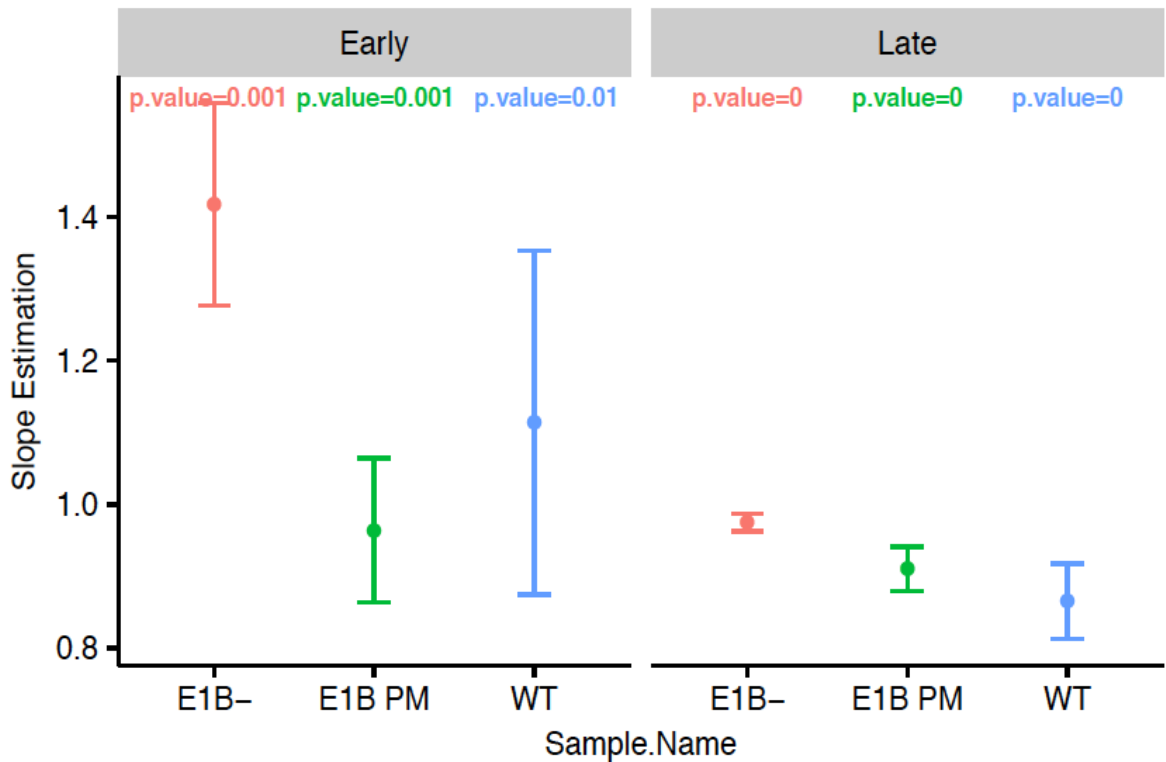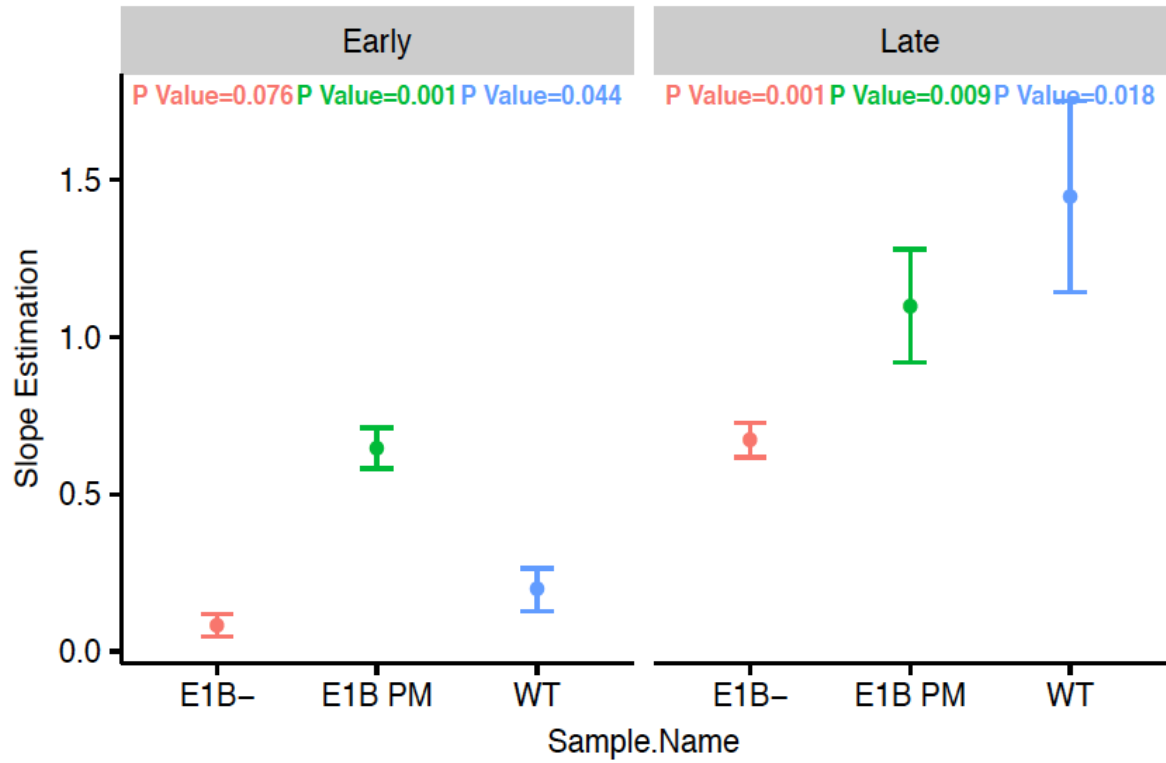Figure S17. Slope and standard deviation: E1B vs. E1A

Figure S18. Slope and standard deviation: E1A vs. L4-22K and 33K
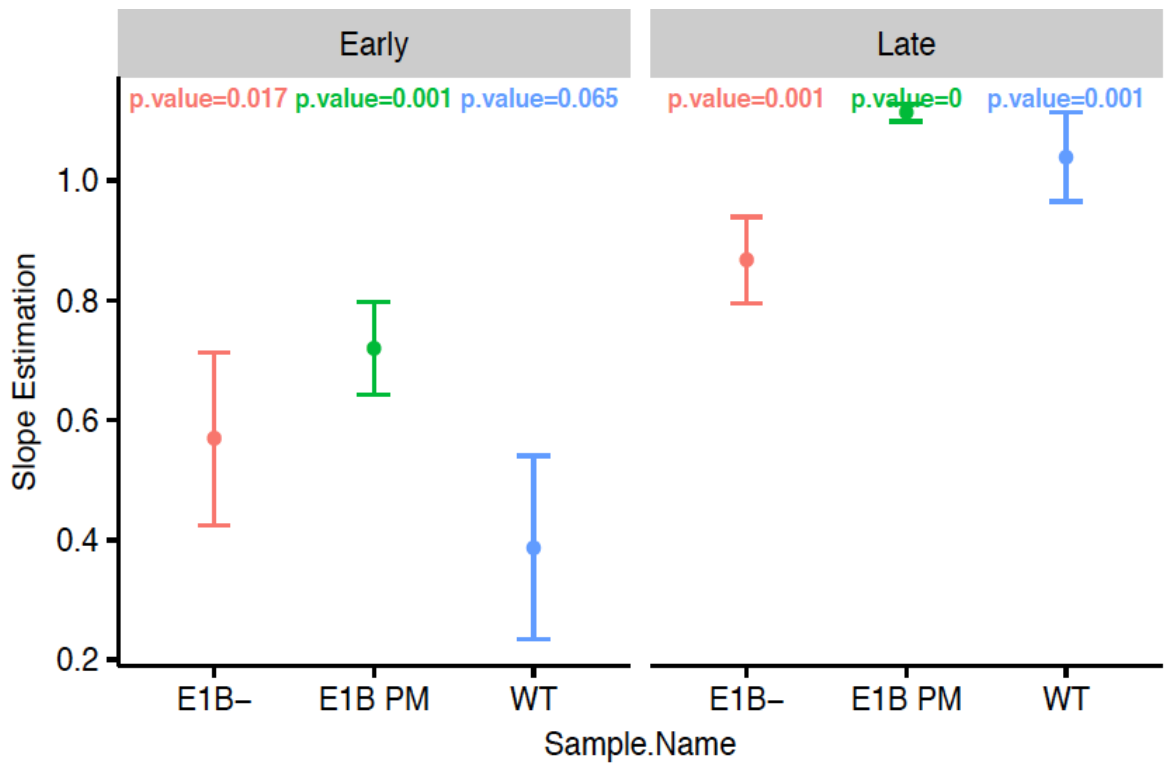

Figure S19. Slope and standard deviation: E1A vs. L4-22K and ML

			E1A~E1B	E1B	E4Orf6/7	E2A-DBP	E2B-pol	IVa2	L1-52/55K	L5-fiber	L1-pIIIa	L4-22K&33K	ML
WT	Early	RSE	0.76	0.67	0.38	0.67	0.45	0.73	0.69	0.67	0.37	0.44	0.67
		R^2	0.84	0.84	0.96	0.93	0.77	0.77	0.74	0.45	0.5	0.68	0.61
	Late	RSE	0.47	0.5	0.69	0.51	0.88	0.55	0.35	0.75	0.43	1.06	0.52
		R^2	0.99	0.99	0.72	0.99	0.83	0.98	0.99	0.92	0.87	0.88	0.98
E1B-	Early	RSE	0.58	0.48	0.26	0.56	0.33	0.63	0.44	0.11	0.23	0.35	0.7
		R^2	0.96	0.96	0.96	0.96	0.88	0.83	0.7	0.54	0.56	0.59	0.8
	Late	RSE	0.27	0.27	0.51	0.49	0.73	0.64	0.44	0.78	0.48	0.56	0.65
		R^2	1	1	0.95	0.99	0.91	0.98	0.99	0.94	0.97	0.98	0.98
E1B PM	Early	RSE	0.66	0.67	0.67	0.67	0.7	1.07	0.79	0.83	0.6	0.53	0.58
		R^2	0.96	0.96	0.91	0.96	0.87	0.84	0.8	0.67	0.76	0.96	0.96
	Late	RSE	0.5	0.52	0.58	0.61	1.14	0.57	0.63	0.6	0.61	1.15	0.32
		R^2	1	1	0.98	0.99	0.9	0.99	0.99	0.99	0.98	0.93	1

Table S1. "Residual Standard Error" (RES) and "R Squared" (R2) for each linear regression model.

General Model	Virus	Early Phase	Late Phase
E1A~E1B	WT	E1A=1.113506912×E1B	E1A=0.865263093×E1B
	E1B-	E1A=1.417437374×E1B	E1A=0.974761926×E1B
	E1B PM	E1A=0.964052421×E1B	E1A=0.910107241×E1B
E1B~E1A	WT	E1B=0.758098925×E1A	E1B=1.142996226×E1A
	E1B-	E1B=0.678763925×E1A	E1B=1.02540422×9E1A
	E1B PM	E1B=0.994213435×E1A	E1B=1.094982108×E1A
E4Orf6/7~E1A	WT	E4Orf6/7=0.488939957×E1A	No Fitting
	E1B-	E4Orf6/7=0.209663594×E1A	E4Orf6/7=0.341166788×E1A
	E1B PM	E4Orf6/7=0.674330192×E1A	E4Orf6/7=0.618134827×E1A
E2A-DBP~E1A	WT	E2A-DBP=1.159123447×E1A	E2A-DBP=1.221559185×E1A
	E1B-	E2A-DBP=0.917190710×E1A	E2A-DBP=0.896860672×E1A
	E1B PM	E2A-DBP=0.983355810×E1A	E2A-DBP=0.946439204×E1A
E2B-pol~E1A	WT	E2B-pol=0.263225036×E1A	E2B-pol=0.786533312×E1A
	E1B-	E2B-pol=0.168992928×E1A	E2B-pol=0.503435744×E1A
	E1B PM	E2B-pol=0.572673808×E1A	E2B-pol=0.885270472×E1A
IVa2~E1A	WT	IVa2=0.683716860×E1A	IVa2=1.036749318×E1A
	E1B-	IVa2=0.507753937×E1A	IVa2=0.929936355×E1A
	E1B PM	IVa2=1.234066552×E1A	IVa2=0.962228552×E1A
L1-52/55K~E1A	WT	L1-52/55K=0.558422247×E1A	L1-52/55K=0.669409405×E1A
	E1B-	L1-52/55K=0.170859945×E1A	L1-52/55K=0.537088752×E1A
	E1B PM	L1-52/55K=0.560601102×E1A	L1-52/55K=0.856723101×E1A
L5-fiber~E1A	WT	L5-fiber=0.279511542×E1A	L5-fiber=0.891380847×E1A
	E1B-	No Fitting	L5-fiber=0.742102193×E1A
	E1B PM	L5-fiber=0.454466027×E1A	L5-fiber=0.980950698×E1A
L1-pIIIa~E1A	WT	L1-pIIIa=0.097106128×E1A	L1-pIIIa=0.217843584×E1A
	E1B-	No Fitting	L1-pIIIa=0.410758076×E1A
	E1B PM	L1-pIIIa=0.304182051×E1A	L1-pIIIa=0.611181673×E1A
L4-22K&33K~E1A	WT	No Fitting	L4-22K&33K=1.448102954×E1A
	E1B-	No Fitting	L4-22K&33K=0.672866475×E1A
	E1B PM	L4-22K&33K=0.646894238×E1A	L4-22K=1.098926630×E1A
ML~E1A	WT	No Fitting	ML=1.039526812×E1A
	E1B-	ML=0.568165189×E1A	ML=0.867233793×E1A
	E1B PM	ML=0.719560349×E1A	ML=1.113207992×E1A

Table S2. Explicit form of the linear regression models. All the coefficients of the models in this table have a statistical significance level under 0.05. The "General Model" column specify the model that was adjusted by a simple linear regression approach ("Dependent variable"_"Independent variable").

REFERENCES
1. J. C. Kiefer, INTRODUCTION TO STATISTICAL INFERENCE (Springer New York, 1987).

La Universidad Autónoma del Estado
de Morelos y la Secretaría de Investigación /
Dirección General de Publicaciones
de Investigación

invitan a la presentación del número 21
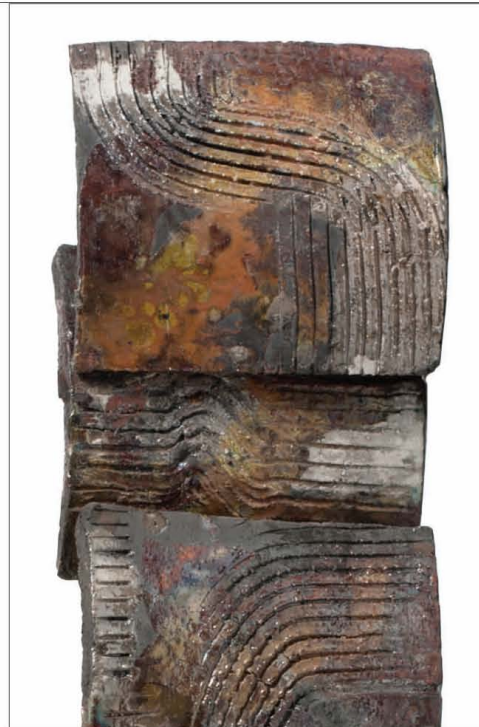de la revista *Inventio*, nueva época

Sala de Rectores
Jueves 28 de agosto, 13:00 horas

Presentan: Gustavo Urquiza, Lydia Elizalde
Álvaro Zamudio y Alfonso Valenzuela

Lectura de poesía: Luis Enrique Aguirre

Obra escultórica: Eduardo Chávez. *Tejas* (fragmento).
Barro de Zacatecas, 60 x 20 cm, 2011

ÍNDICE DE REVISTAS MEXICANAS
CONACYT DE DIVULGACIÓN CIENTÍFICA Y TECNOLÓGICA

LAS PROTEÍNAS DE UNIÓN A *ARN*

Moléculas integradoras de la expresión génica

➢ *El ARN es una molécula central en los procesos biológicos*

Todos los seres vivos están constituidos por los mismos tipos de biomoléculas. Entre ellas están los ácidos nucleicos y las proteínas, que son moléculas *informacionales*. En el caso de las proteínas este término se refiere al hecho que la secuencia de aminoácidos que compone a cada proteína determina el arreglo tridimensional que adopta la cadena polipeptídica y consecuentemente su conformación tridimensional y su función. Para los ácidos nucleicos, el ADN (ácido desoxirribonucleico) y el ARN (ácido ribonucleico), son moléculas informacionales porque portan en las secuencias de nucleótidos que las componen la información genética de cada organismo. En el caso del ARN, se trata además de una molécula que puede tener actividad catalítica. En la molécula de ARN, la secuencia de nucleótidos determina no sólo la información genética sino que también determina la forma y la función de la molécula; en otras palabras, la molécula de ARN puede representar tanto un genotipo como un fenotipo[1].

La identidad de cada célula y las actividades que puede desempeñar dependen de los genes que se expresan a partir de la información contenida en su genoma. La secuencia de nucleótidos en una molécula de ADN es utilizada como un molde para *transcribirse* y sintetizar una molécula de ARN. La secuencia de nucleótidos de esta molécula de ARN es después *traducida* resultando en la síntesis de una proteína; es decir, una cadena de aminoácidos organizada en una secuencia que corresponde directamente a la secuencia de nucleótidos en el ARN, pero traducida a un lenguaje molecular diferente.

El ARN es una biomolécula formada por azúcares (ribosa), bases nitrogenadas (adenina, uracilo, guanina o citosina) y fosfatos, constituyendo nucleótidos que forman los bloques que construyen el ARN. Esta molécula puede encontrarse en forma de cadena sencilla o doble, formando estructuras (secundarias y terciarias) topológicamente

---

[1] Cech, T. R. "The RNA worlds in context", *Cold Spring Harbor Perspectives in Biology,* vol. **4**, 2012, pp. 1-5.

complejas. La organización tridimensional de estas estructuras depende de la secuencia del ARN, de su longitud, de modificaciones químicas a las que está sujeto y de proteínas que se le asocian.

Existen muchos tipos de ARN, con tamaños, estructuras y funciones diversas. Los tres más conocidos, por ser los primeros en identificarse, son los ARN mensajeros (ARNm), los de transferencia (ARNt) y los ribosomales (ARNr). No obstante, en los últimos años se han encontrado muchos otros tipos de ARN. En la tabla 1, se incluyen algunos de los ARN que se encuentran en todos los metazoarios.

Tabla 1. Principales tipos de ARN presentes en metazoarios.

Tipo de ARN	Función
ARNm	ARN que codifica para una proteína.
ARNt	ARN que aporta cada aminoácido en la síntesis de proteínas.
ARNr	ARN que forma parte estructural y catalítica de los ribosomas.
ARNsi	ARN de 20-25 nucleótidos de longitud, que regula la traducción de un ARNm.
miR	ARN de 21-22 nucleótidos de longitud, que regula la traducción de un ARNm.
ARNnc	ARN que no codifica para una proteína.
ARN pequeños nucleares	ARN estructural y catalítico del "spliceosoma" en el procesamiento de ARNm.
ARN pequeños nucleolares	ARN que participa en el procesamiento de ARNr y en el ensamblaje de ribosomas.

ARNlnc	ARN largos no codificantes que regulan la expresión génica.
ARNpi	ARN derivados de transcritos largos que regulan transposones.

El ARN es una molécula central en la regulación de la expresión génica y el funcionamiento de la célula y puede actuar como integradora de las diferentes funciones biológicas de una célula. No obstante, el ARN no se encuentra libre en una célula, ya que a lo largo de su biogénesis –desde el inicio de su síntesis hasta su degradación- cada ARN está físicamente asociado a diferentes proteínas. A estas proteínas se les llama RBP (por sus siglas en inglés "RNA-Binding-Proteins" o Proteínas de unión a ARN) y, dado que toda molécula de ARN está siempre asociada a una o más RBP, entonces funcional y estructuralmente, los ARN pueden ser considerados ribonucleoproteínas o RNP. Las proteínas de unión a ARN (RBP) son determinantes en la estabilidad de la molécula de ARN, su localización celular, su forma y su función. Las RBP funcionan como integradoras de las actividades celulares, desde la organización estructural del ADN en el núcleo de una célula, hasta cada paso de la regulación de la expresión de los genes.

En la última década los hallazgos que han permitido aprender sobre la estructura y función de los ARN y las proteínas que se les asocian, han mostrado que las RBP son esenciales en el funcionamiento normal de la célula. Este tipo de proteínas son moléculas clave en el flujo y expresión de la información genética. En los últimos años se ha encontrado que mutaciones que afectan el funcionamiento de ARN y las RBP están ligadas a una gran variedad de enfermedades (en la Tabla 1 se incluyen sólo algunos ejemplos). En este artículo hacemos una descripción breve de algunas de las principales actividades celulares que dependen de RBP y cómo estas actividades pueden ser alteradas en enfermedades.

Tabla 1[2]. Ejemplos de enfermedades causadas por fallas en ARN y RBP

---

[2] Modificado de: Thomas A. Cooper, Lili Wan, Gideon Dreyfuss. "RNA and Disease", Cell, vol. 136(4), 2009, pp. 777-793.

ENFERMEDAD	FUNCIÓN ALTERADA
Síndrome de Prader Willi	biogénesis de ribosoma
Eritroblastopenia congénita de Blackfan-Diamond	biogénesis de ribosoma
Síndrome de Shwachman-Diamond	biogénesis de ribosoma
Síndrome de Treacher-Collins	biogénesis de ribosoma
Cáncer de Próstata	biogénesis de ribosoma
Esclerosis lateral amiotrófica	splicing, transcripción
Atrofia muscular espinal	splicing
Retinosis pigmentaria	splicing
Síndrome X Frágil	traducción
Síndrome de Charcot–Marie–Tooth	traducción
Discapacidad congnitiva ligada a X	traducción/NMRDA
Autismo	RNA no codificante
Cáncer	splicing/traducción/exportación

➢ *Las RBP, Proteínas de Unión a ARN*

❖ Aspectos estructurales y funcionales

Las RBP se unen a ARN a través de una o más regiones de la cadena polipeptídica, conocidas como *dominios*. Los dominios son regiones de una proteína que pueden adoptar una conformación estructural y funcional de forma autónoma. Se han encontrado múltiples tipos de dominios en las proteínas, que son responsables de su interacción con ARN. En la Tabla 2 se enlistan los principales dominios que se conocen en la actualidad.

Tabla 2. Tipos de dominios proteicos de unión a ARN

Dominios de unión a ARN	Topología	Tipo de ARN que une	Ejemplo
Dominio KH	tipo I: βαββα tipo II: αββαβ	ARNcs	hnRNP K
PAZ	Barril β	ARNcd	Ago
Dominio rico en argininas	-------	ARNcd, ARNcs	SC35, ASF/SF2
Dominio dedo de zinc	Bβα	ARNcd	BRCA-1, Complejo Polycomb
RRM	Bαββαβ	ARNcs	U1, U2, Aly, Tap
CSD	Barril β	ARNcs	eIF2α
dsRBD	Aββα	ARNcd	PKR
PIWI	5 hojas β rodeadas por una α hélice	ARNcd	Ago

ARNcs, ARN de cadena sencilla; ARNcd, ARN de cadena doble; KH, dominio con homología a proteína K; RRM, motivo de reconocimiento de ARN; CSD, dominio "cold

shock"; dsRBD, dominio de unión a ARN de cadena doble; PAZ, dominio PIWI-Argonauta-Zille; PIWI, dominio P-element induced "wimpy testis".

Las RBP pueden reconocer secuencias de nucleótidos y/o estructuras específicas en el ARN y la presencia de varios dominios de unión a ARN en una misma proteína incrementa la afinidad y especificidad por su ARN blanco.

Las funciones de las RBP a nivel molecular son tan variadas como las actividades en las que están involucradas, pero para describirlas las dividimos aquí en cinco grandes grupos. I) **Las ARN polimerasas**, son las RBP encargadas de la síntesis de ARN. Estas RBP son enzimas polimerasas (polimerasas de ARN celulares; replicasas y transcriptasas de ARN virales) que reconocen una secuencia de ADN como molde (o ARN en los genomas virales compuestos por esta molécula) y dirigen la formación de enlaces fosfodiéster entre grupos 3' OH de un nucleótido y el extremo 5' fosforilado del nucleótido entrante. II) **Las ARNasas o ribonucleasas**, son enzimas que cortan enlaces entre los nucleótidos del ARN. Se han identificado al menos 20 tipos diferentes que reconocen distintas formas de ARN. Algunas reconocen secuencias específicas de nucleótidos y otras reconocen arreglos estructurales en la molécula del ARN. Las ARNasas pueden reconocer moléculas de ARN de cadena sencilla o doble, o híbridos de ARN/ADN; algunas cortan enlaces en los extremos (exorribonucleasas) y otras, enlaces internos (endorribonucleasas) de un ARN. III) **Las helicasas de ARN**, son RBP encargadas de inducir cambios conformacionales del ARN; en estos casos una enzima helicasa reconoce una secuencia o estructura en el ARN y cambia su torsión y arreglo estructural, por la remoción de puentes de hidrógeno. IV) **Las enzimas modificadoras de ARN**. Entre estas RBP se puede incluir un número muy grande de enzimas que comprenden todas aquellas que pueden hacer cambios químicos a los nucleótidos que forman un ARN, sin alterar su secuencia. V) **Las ribonucleoproteínas (RNP)**. Este es el grupo más extenso de las RBP; éstas participan en el contacto de una molécula de ARN con otras proteínas, formando complejos de ribonucleoproteínas. En un complejo de RNP pueden estar incluidas proteínas de cualquiera de los cuatro grupos anteriores. Las RNP pueden estar formadas por un ARN y una RBP, o pueden llevar a la formación de complejos macromoleculares en los que las RBP se asocian a moléculas de ARN y permiten la interacción de otras proteínas formando

estructuras multiméricas complejas. Entre ellas, están dos de los complejos macromoleculares de mayor tamaño y complejidad de la célula: el "spliceosoma" y el ribosoma. Ambos son ensamblajes de ARN y RBP que cumplen funciones estructurales y enzimáticas, e incluso acompañan la actividad catalítica del ARN.

❖ Las RBP en la regulación de la expresión de los genes

▪ **Estabilidad y organización de la cromatina**

Dentro de un núcleo celular, el ADN se organiza en arreglos que tienen diferentes grados de compactación. Estos grados de compactación dependen de las histonas (un conjunto de proteínas que se encargan de organizar y compactar a las moléculas de ADN) y de modificaciones químicas a las que están sujetas, tanto las histonas (metilación y acetilación) como el ADN (metilación). La forma más compactada del ADN se conoce como heterocromatina, mientras que a la menos compactada se le llama eucromatina. En las regiones del genoma menos compactados -en la eucromatina- generalmente se encuentran genes activos; es decir, éstas son regiones de ADN que están (temporalmente) accesibles a la maquinaria celular encargada de expresar los genes. Estas regiones pueden ser activamente transcritas y son reconocidas por las enzimas celulares encargadas de sintetizar las moléculas de ARN codificadas en cada gen.

Las RBP tienen un papel crucial en la estabilidad de los cromosomas. Tal es el caso del supresor tumoral BRCA-1. Esta RBP es un componente de la maquinaria de reparación de daño al ADN (DDR de "DNA Damage Repair"); funciona como factor transcripcional e interacciona con complejos remodeladores de la cromatina, entre muchas funciones más. BRCA-1 ayuda a reparar ADN dañado por cortes de doble cadena e induce la muerte de las células en las que el genoma dañado no puede ser reparado. Por otra parte se asocia al dominio carboxilo terminal de la ARN polimerasa II (descrito más adelante) y a complejos de desacetilación de histonas, participando en el control de la transcripción a través de la modulación de la cromatina. Recientemente se identificó a BRCA-1 como una RBP que reconoce estructuras secundarias de ARN y se une directamente a miR a través de un

dominio de dedo de zinc. Esta función se ha asociado a su mecanismo como supresor tumoral y en el mantenimiento de la estabilidad cromosómica. Mutaciones en el gen que codifica para BRCA-1 están estrechamente asociadas al desarrollo de cáncer, principalmente el cáncer de mama.

Durante la remodelación de la cromatina, el papel de las RBP también es fundamental. Esta actividad de las RBP es novedosa, ya que no se conocían RBP que pudieran participar en la remodelación de la cromatina. Dos grupos de RBP ejemplifican este caso; la familia de proteínas Argonauta y la proteína heterogénea nuclear (hn) hnRNP K. Las proteínas Argonauta se encuentran en organismos de los tres dominios de la vida (Eukarya, Bacteria y Archaea) y sus secuencias están muy conservadas a lo largo de la evolución. Las Argonauta unen ARN a través de un dominio PAZ (Piwi/argonauta/Zwille) y participan principalmente en la regulación de la traducción de ARNm mediante el silenciamiento que depende de ARN cortos, conocidos como ARNsi (RNA pequeños interferentes o silenciadores). Recientemente se ha observado que al asociarse con algunos ARN, las Argonauta se pueden unir al ADN y favorecer su compactación en heterocromatina. En el caso de la hnRNP K, la conexión entre diferentes actividades es aún más notable. Esta RBP funciona como un conector entre la remodelación de la cromatina y varios pasos de la regulación de la expresión de genes. La hnRNP K se une a proteínas del grupo Policomb (PcG) para permitir la compactación de la cromatina, inhibiendo la expresión de genes. Además, participa en la activación de la transcripción de genes, como el gen c-myc (un factor que regula el crecimiento celular) y eIF4E (un factor esencial en la traducción de ARNm). Adicionalmente, esta RBP participa en el procesamiento postranscripcional al regular a SRp20, otro conector de actividades celulares ya que es un proto-oncogen que participa en el "splicing", exportación y traducción de ARNm. La hnRNP K se encuentra sobrexpresada o tiene una localización intracelular aberrante en cáncer colorectal, cáncer de próstata, hepático, de mama y en leucemias.

❖ Las RBP en la regulación de la expresión de los genes

▪ **Transcripción**

8

El primer paso en la expresión de un gen es el proceso llamado *transcripción*, que se describió anteriormente. Durante la transcripción de un gen, se reclutan varios factores a la molécula de ADN que se ensamblan sobre secuencias específicas de nucleótidos que permiten que se una la ARN polimerasa II (RPII). Esta última, es una RBP formada por 12 subunidades, que utiliza ADN como templado para sintetizar ARN. La RPII tiene una secuencia en el carboxilo terminal conocida como CTD, el cual es modificado por fosforilación para regular su actividad, así como su asociación con otras proteínas; entre ellas, RBP que participan en la biogénesis del ARNm (por ejemplo TAF15, un componente del factor de inicio de la transcripción, TFIID). Por lo tanto, el CTD de la RPII funciona como un sitio de andamiaje para el reclutamiento de RBP durante el proceso transcripcional y postranscripcional, permitiendo el acoplamiento de ambos eventos.

- **Procesamiento de ARN**

Durante su síntesis, la molécula de ARN sufre diferentes modificaciones; éstas incluyen la adición de un nucleótido en el extremo de la molécula en el que inicia su síntesis (extremo 5'), conocido como estructura de "caperuza" o "cap"; la adición de una secuencia de poli-Adeninas en el extremo opuesto de la molécula (extremo 3'); y la remoción de secuencias de la molécula de ARN por un mecanismo muy complejo, conocido como corte y empalme o "splicing", en el que se unen secuencias de ARN, conocidas como exones y, se eliminan secuencias, conocidas como intrones, resultando en el ARNm maduro que puede ser exportado a citoplasma y traducido a proteína.

Gran parte de las RBP son proteínas multifuncionales; es decir que participan en diferentes actividades biológicas, lo que les permite funcionar como acopladores entre diferentes procesos celulares. Además de los citados en la sección anterior, otro ejemplo de RBP multifuncional es el de los factores de "splicing" conocidos como SC-35 y ASF/SF2. Estas son proteínas SR (factores de "splicing" llamados así por tener secuencias ricas en los aminoácidos serina (S) y arginina (R)) que modifican el ARNm al unírsele mediante dominios RRM. Estas proteínas participan en la transcripción, procesamiento postranscripcional, exportación, estabilidad y traducción del ARNm. En otras palabras, en cada uno de los eventos moleculares en la expresión de un gen. SC-35 y ASF/SF2

reconocen secuencias específicas del ARN, conocidas como mejoradores (o "enhancers"). Ambas funcionan como promotoras del procesamiento de ARNm por "splicing". Además, SC-35 promueve la transcripción de algunos genes al favorecer la fosforilación del CTD de la RPII. Por lo tanto, SC-35 permite el acoplamiento de la transcripción con el procesamiento postranscripcional. Además, se ha sugerido que SC-35 participa en el transporte de ARNm favoreciendo su exportación a citoplasma. Por otro lado, estas dos proteínas también están asociadas a la degradación de ARNm por un mecanismo conocido como NMD (degradación de ARN mediado por sin-sentido, "nonsense-mediated ARNm decay"), proceso que se describirá más adelante.

Para el procesamiento de ARNm por "splicing", es esencial la formación del mayor complejo de ribonucleoproteínas en la célula mencionado antes, llamado "spliceosoma". Este complejo está conformado por ARN pequeños nucleares (U1, U2, U4, U5, U6, U4$_{atac}$, U6$_{atac}$, U11 o U12), y subconjuntos de alrededor de 100 proteínas RBP con actividades de helicasas, nucleasas y RBP accesorias, como las proteínas Sm (o Lsm en el caso del ARN U6), que dirigen el reconocimiento de secuencias entre los ARN pequeños nucleares y el ARNm. Las proteínas Sm forman un anillo que envuelve al ARN y son esenciales para la biogénesis, el transporte y la actividad de las RNP pequeñas nucleares. Los ARN pequeños nucleares se unen al ARNm recién sintetizado en un orden específico (U1 y U2, seguidas por U4, U5 y U6) para marcar las regiones del ARNm que serán cortadas por la actividad catalítica del complejo formado por U4 y U6, para unir los exones, escindir los intrones y formar ARNm maduros listos para ser exportados a citoplasma.

Las alteraciones en la localización y función de estas RBP se han asociado con el desarrollo de cáncer, específicamente de leucemias y, de una variedad de otras enfermedades. Se piensa que esto podría deberse a que el mal funcionamiento de estas proteínas puede afectar la fidelidad de la expresión génica y por cambios en la organización o ensamblaje de la maquinaria involucrada en la transcripción de genes y procesamiento postranscripcional de los ARNm. Además, la producción de formas aberrantes de ARNm por alteraciones en el procesamiento por "splicing" podría favorecer la transformación oncogénica de la célula debido a la síntesis de variantes de ARNm con potencial

oncogénico, como en el caso del síndrome mielodisplásico y de la leucemia mieloide aguda.

- **Exportación núcleo-citoplásmica de ARNm**

Los pasos posteriores del procesamiento postranscripcional de ARNm ocurren hacia la periferia del interior del núcleo y una vez que los ARNm salieron al citoplasma. Las células eucariontes poseen una compartimentalización que les permite separar y regular diferentes funciones biológicas en microambientes definidos. A pesar de esta separación física, los procesos que ocurren en el núcleo y citoplasma no están desconectados, ya que moléculas como las RBP y los ARN a los que se asocian permiten integrar las actividades celulares. Además, existen estructuras que funcionan como comunicadores entre estos microambientes. En el caso del núcleo, éste se comunica con el citoplasma a través de un canal de comunicación conocido como Complejo del Poro Nuclear (NPC). Las proteínas que lo componen hacen contacto con RBP que participan en la organización de la cromatina en el núcleo, en la regulación de la transcripción, el procesamiento postranscripcional de ARN, y activamente seleccionan ARNm correctamente procesados, permitiendo su exportación al citoplasma en donde pueden ser traducidos a proteínas por los ribosomas. El NPC es entonces, no sólo un canal que permite el paso regulado de moléculas, sino que participa activamente en la regulación de la expresión de los genes.

La exportación de los ARNm está mediada por la maquinaria compuesta por las RBP ALY/REF y Tap. Estas se unen a otras RBP y al NPC para asociarse al ARNm y translocarlo al citoplasma. La síntesis, procesamiento, empaquetamiento y exportación del ARNm asociado a las RBP requieren de mecanismos muy finos de control de calidad, ya que cualquier falla puede originar ARNm aberrantes que, si son exportados al citoplasma y traducidos a proteínas, pueden tener efectos deletéreos sobre la célula y favorecer el desarrollo de enfermedades. Uno de estos mecanismos es la vigilancia dependiente de SUMO y exosoma, establecido desde el NPC. Asociados a la cara nuclera del NPC, se encuentran factores de vigilancia que participan en el control de calidad de los ARNm. Los transcritos que no son correctamente procesados son rápidamente degradados por el

exosoma, un complejo de exonucleasas y ARN helicasas. El complejo TRAMP, formado por un ensamblaje de varias RBP, se asocia al NPC y participa en este proceso. TRAMP poliadenila ARNm aberrantes, marcándolos para ser procesados correctamente o degradados por el exosoma. Un mecanismo de control de calidad de los ARNm es el conocido como "degradación de ARN mediado por sin-sentido", NMD ("Non-Sense Mediated RNA Decay"), en el cual los ARNm con codones de paro prematuros son reconocidos y degradados para impedir la síntesis de una proteína incompleta que pueda tener efectos deletéreos sobre el funcionamiento celular. Este mecanismo de control de calidad es principalmente citoplásmico, pero se ha observado que proteínas SR, como SC-35 y ASF/SF2 pueden promover esta respuesta en el núcleo. Estos datos indican que existe una función adicional para estos factores de "splicing", actuando no sólo sobre el procesamiento de ARNm (como se describió antes), sino también en la regulación de su estabilidad. Se ha observado que en tumores el mecanismo de NMD se encuentra inhibido, lo que permite una desregulación génica favorable para la tumorogénesis.

- **Traducción**

La traducción es un proceso en el que a partir de una molécula de ARNm (en un lenguaje de nucleótidos) se sintetiza una cadena polipeptídica (traducido a un lenguaje de aminoácidos). La maquinaria celular encargada de la traducción de un ARNm es el segundo RNP de mayor tamaño y complejidad en la célula, el ribosoma. Los ribosomas constan de dos subunidades que están compuestas por cuatro moléculas de ARNr y alrededor de 80 proteínas ribosomales. Las proteínas S forman a la subunidad pequeña y las L a la subunidad grande. La mayoría de estas proteínas tienen topología tipo barril β o sandwich α/β. La integridad y estabilidad del ribosoma depende de interacciones proteína-ARN y proteína-proteína. Estas interacciones electrostáticas dependen del acoplamiento conformacional entre ARN y proteínas, lo que asegura la especificidad de la interacción. Las proteínas que forman parte de la superficie del ribosoma son las que están más directamente involucradas en la interacción con ARN. En este sentido, se sabe que las proteínas de la superficie del ribosoma S2, S16, L1, L2 y L3 son responsables de las principales interacciones entre el ARNm y el ribosoma. Estas interacciones son imprescindibles para el reconocimiento correcto del ARNm por parte del ribosoma, ya que

permiten que se ensamble el complejo de inicio de la traducción, formado a su vez por varias otras RBP. Para el inicio de la traducción es necesario el reconocimiento de la estructura de "cap" y secuencias específicas en el ARNm, por una serie de RBP que se conocen como factores de inicio de la traducción eucariotes, eIF ("eukaryotic Initiation Factor"), como eIF4F que está constituido por eIF4E, eIF4A y eIF4G, los cuales hacen contacto con al menos otras 6 RBP. Estos factores de inicio de la traducción favorecen la interacción correcta entre el ARNm y las subunidades del ribosoma para su traducción. La alteración de cualquiera de los pasos, desde el ensamblaje del ribosoma hasta la traducción de un ARNm está asociada a diversas enfermedades; particularmente cáncer y enfermedades neurodegenerativas.

➤ Conclusiones

En las últimas dos décadas, las evidencias experimentales acumuladas han dejado claro que la molécula de ARN es central en el funcionamiento de todos los procesos biológicos; consecuentemente, las proteínas que se asocian a ARN juegan un papel igualmente esencial en la biología. Hemos hecho aquí una breve descripción de algunas de las actividades celulares que por depender de algún tipo de ARN, dependen de las proteínas que se asocian a ARN y definen su forma, procesamiento, estabilidad y función. Estas proteínas y los mecanismos celulares en los que participan están alterados en enfermedades. La participación de RBP en cada aspecto del funcionamiento celular, desde la organización estructural y funcional del núcleo, hasta la regulación de la expresión de genes, permite suponer que en los próximos años se seguirán encontrando nuevas RBP y que aprender sobre las funciones de RBP permitirá, por una parte, entender mejor el funcionamiento de la célula y por otra, desarrollar nuevas estrategias terapéuticas para interferir o utilizar ARN y RBP en el tratamiento de un número creciente de enfermedades.

Paloma Hidalgo Ocampo
hopr@ibt.unam.mx
3297020
02 de septiembre de 2013
Av. Universidad 1001, Cuernavaca, Morelos 62209
Facultad de Ciencias, UAEM
Estudiante de la Maestría en Ciencias Bioquímicas, IBT/UNAM.

Berto Tejera Hernández
bertotejera48@yahoo.com.mx
3297020
02 de septiembre de 2013
Av. Universidad 1001, Cuernavaca, Morelos 62209
Facultad de Ciencias, UAEM
Estudiante del Doctorado en Ciencias, Facultad de Ciencias, UAEM.

Ramón A. Gonzalez*
rgonzalez@uaem.mx
3297020
02 de septiembre de 2013
Av. Universidad 1001, Cuernavaca, Morelos 62209
Facultad de Ciencias, UAEM
Profesor de tiempo completo, Titular A.

*Autor de correspondencia.

Número de caracteres: 25,713

14

Research Article

The Mre11 Cellular Protein Is Modified by Conjugation of Both SUMO-1 and SUMO-2/3 during Adenovirus Infection

Elizabeth Castillo-Villanueva,[1] Grisel Ballesteros,[1] Melanie Schmid,[2,3] Paloma Hidalgo,[1] Sabrina Schreiner,[2] Thomas Dobner,[2] and Ramon A. Gonzalez[1]

[1] *Facultad de Ciencias, Universidad Autónoma del Estado de Morelos, Avenida Universidad 1001, 62209 Cuernavaca, MOR, Mexico*
[2] *Heinrich Pette Institute, Leibniz Institute for Experimental Virology, Martinistrasse 52, 20251 Hamburg, Germany*
[3] *European Molecular Biology Laboratory, Meyerhofstrasse 1, 69117 Heidelberg, Germany*

Correspondence should be addressed to Ramon A. Gonzalez; rgonzalez@uaem.mx

The adenovirus type 5 (Ad5) E1B 55 kDa and E4 Orf6 proteins assemble a Cullin 5-E3 ubiquitin (Ub) ligase that targets, among other cellular proteins, p53 and the Mre11-Rad50-Nbs1 (MRN) complex for degradation. The latter is also inhibited by the E4 Orf3 protein, which promotes the recruitment of Mre11 into specific nuclear sites to promote viral DNA replication. The activities associated with the E1B 55 kDa and E4 Orf6 viral proteins depend mostly on the assembly of this E3-Ub ligase. However, E1B 55 kDa can also function as an E3-SUMO ligase, suggesting not only that regulation of cellular proteins by these viral early proteins may depend on polyubiquitination and proteasomal degradation but also that SUMOylation of target proteins may play a key role in their activities. Since Mre11 is a target of both the E1B/E4 Orf6 complex and E4 Orf3, we decided to determine whether Mre11 displayed similar properties to those of other cellular targets, in Ad5-infected cells. We have found that during Ad5-infection, Mre11 is modified by SUMO-1 and SUMO-2/3 conjugation. Unexpectedly, SUMOylation of Mre11 is not exclusively dependent on E1B 55 kDa, E4 Orf6, or E4 Orf3, rather it seems to be influenced by a molecular interplay that involves each of these viral early proteins.

1. Introduction

The adenoviral E1B 55 kDa, E4 Orf6, and E4 Orf3 early proteins are necessary to complete an efficient viral replication cycle. E1B 55 kDa and E4 Orf6 form a complex that associates with an adenovirus-infected cell-specific Cullin 5-containing E3 ubiquitin (Ub) ligase that induces polyubiquitination and degradation of various cellular targets, namely, the tumor suppressor p53, the Mre11-Rad50-Nbs1 (MRN) complex, DNA ligase IV, bloom helicase, ATRX, Tip60, SPOC1, and integrin α3 [1–12]. The activity of the E1B/E4 Orf6 E3-Ub ligase is required for viral late mRNA export [4, 13], and it has been suggested that most activities associated with E1B 55 kDa and E4 Orf6 depend on formation of this E3-Ub ligase [14]. However, during adenovirus infection of normal human cells (human foreskin fibroblasts, HFF), complete degradation of one of these cellular substrates, the p53

protein, is not attained and reduction of its steady state levels initiates only late during infection [15, 16]. Furthermore, the accumulation of p53 does not lead to apoptosis, and efficient viral replication correlates with the E1B 55 kDa-dependent nuclear localization of p53 to viral replication centers where these proteins colocalize [16–18]. An additional key target of the E1B/E4 Orf6 E3-Ub ligase is the DNA double-strand break repair (DSBR) complex, MRN [5, 8, 19]. Inhibition of DSBR is necessary to avoid concatemerization of the viral genome and to promote efficient viral DNA replication [20–24]. These activities also depend on the E4 Orf3 protein, another early gene product that interacts with E1B 55 kDa as well as the isoform II of the promyelocytic leukemia protein (PML). Thereby E4 Orf3 initiates the reorganization of PML nuclear bodies (PML NBs) and formation of nuclear sites where the viral genome is replicated and expressed [8, 22, 23, 25–29].

The PML protein is modified by the small ubiquitin-like modifier (SUMO) system, and this modification is critical for the formation and regulation of PML NBs [30–36]. Like PML many proteins that localize in PML NBs are SUMOylated [31, 36]. The SUMO system is responsible for the modification of a large pool of cellular proteins [30, 32, 37, 38]. Modification of proteins by SUMO-1 or by SUMO-2 or -3, which display a high degree of similarity to each other and form a family distinct from SUMO-1, achieves a diverse range of effects from cellular stress responses to regulating subcellular localization, transcription factor activity, and protein stability [37–41]. SUMO modification is operated by an enzymatic pathway consisting of an E1 activating enzyme (SAE-2/1), a unique E2 conjugating enzyme (Ubc9), and a number of E3 ligases (reviewed in [30]). While Ubc9 is capable of directly modifying substrates through interaction with a SUMO conjugation motif (ΨKXD/E, where Ψ is a large hydrophobic amino acid and X is any amino acid), E3 ligases add specificity and increase the efficiency of the conjugation reaction. In contrast to SUMO-1, both SUMO-2 and -3 possess an N-terminal SUMO conjugation motif (VKTE) that allows their polymerization to form SUMO chains [42, 43], while conjugation of SUMO-1 to a SUMO-2/3 moiety leads to chain termination [44]. An important role of SUMO modification is to protect modified proteins from proteasomal degradation or conversely to promote their polyubiquitination and degradation [40, 42, 45–48].

During adenovirus infection the E1B 55 kDa protein undergoes SUMO-1 and SUMO-2/3 [49] modification resulting in regulation of its nucleocytoplasmic shuttling and intranuclear targeting [49–53]. Significantly, E1B 55 kDa not only stimulates SUMOylation of p53 in the PML NBs [54] but also functions as an E3 SUMO-1 ligase for this cellular protein; a modification that contributes to relocalization and maximal transcriptional repression of p53 [55].

These observations confirmed that regulation of p53 in Ad5-infected cells is achieved by processes that do not depend solely on its polyubiquitination and degradation [16–18], suggesting that other cellular targets of the early adenoviral proteins may be regulated by SUMOylation. Therefore, we decided to investigate whether Mre11 is modified by SUMO-1 and/or SUMO-2/3 in Ad5-infected cells. We found that during Ad5 infection of nontumor cells (HFF) Mre11 degradation was not complete and initiated very late during infection, similar to previous observations on p53 [16]. As expected, Mre11 was relocalized to E4 Orf3- and PML-containing structures, where these proteins could be seen throughout viral replication. Significantly, we have found not only that Mre11 was subject to SUMO-2/3-modification [56] but also that the protein was modified by SUMO-1. The redistribution of Mre11 in adenovirus-infected cells correlated with changes in the nuclear localization of the SUMO-1 and SUMO-2/3 cellular pools, and the protein colocalized extensively but displayed distinct SUMO-paralogue colocalization in PML NBs. In contrast to p53 [55], Mre11 SUMOylation was not dependent solely on E1B 55 kDa; rather, our data indicate that during adenovirus infection of nontumor cells, Mre11 is modified by the addition of both SUMO-1 and SUMO-2/3

paralogues and that these modifications depend on concerted activities of the E1B 55 kDa, E4 Orf6, and E4 Orf3 proteins.

2. Materials and Methods

2.1. Cells and Viruses. H1299, HeLa, HEK-293, and human foreskin fibroblast (HFF) cells were grown as monolayer cultures in Dulbecco's modified Eagle's medium (DMEM) supplemented with 5% or 10% fetal bovine serum. The E1B 55 kDa mutant virus A143, carrying a linker insertion in the hybrid Ad2/Ad5 E1B gene, has been described previously [57]. The Ad5 mutant Hr6 carries a frameshift mutation in the E1B coding sequence leading to an E1B 55 kDa null mutant virus [58]. The RF6 mutant carries a point mutation that inhibits E1B 55 kDa binding to Mre11 [59]. The Ad5 wild-type *dl*309 virus [60] and E1B mutants were propagated in monolayers of HeLa and HEK-293 cells, respectively. Viruses were titered by plaque assay on HEK-293 cells as described [61]. The H5*pm*4149 virus carries four stop codons in the E1B 55 kDa open reading frame and does not express the E1B 55 kDa protein [62]; H5*pm*4154 does not express the E4 Orf6 protein and H5*pm*4150 does not express the E4 Orf3 protein [13]. The three latter virus mutants were propagated in 2E2 cells and titered as fluorescent forming units (FFU) in HEK-293 cells [63].

2.2. Antibodies. Primary antibodies specific for Ad5 proteins included the anti-E1B 55 kDa mouse monoclonal antibody (mAb) 2A6 [64], anti-DBP mouse mAb B6-8 [65], anti-E4 Orf6 mouse mAb RSA3 [66], and anti-E4 Orf3 rat mAb 6A11 [67]. Primary antibodies specific for cellular proteins included the anti-Mre11 mouse mAb 12D7 (GTX70212) (GeneTex, Inc), anti-Nbs1 mouse mAb (GTX70222) (Gene-Tex, Inc.), anti-Rad50 mouse mAb (GTX70228) (GeneTex, Inc.), anti-Mre11 rabbit polyclonal antibody (pAB) (pNB 100-142) (Novus Biologicals, Ltd., Cambridge, UK), anti-ß-actin mouse mAb AC-15 (Sigma-Aldrich, Inc.), anti-actin mouse mAb AC-40 (Sigma-Aldrich, Inc.), anti-Ubc9 mouse mAb (610748) (BD Transduction Laboratories), anti-SUMO-1 rabbit mAb (4930) (Cell Signaling), anti-SUMO-2/3 rabbit mAb (4971) (Cell Signaling), anti-HA rat mAb (clone 3F10) (Roche Applied Science), and anti-vimentin rabbit pAb (a gift from Pavel Isa).

2.3. Immunoblotting. To analyze the steady-state concentrations of the cellular Mre11 protein, H1299 and HFF cells at approximately 80–90% confluence were infected with Ad5 or the E1B 55 kDa mutants at 30 plaque forming units (PFU)/cell. For immunoblotting, cells were harvested at indicated times after infection, washed with phosphate-buffered saline (PBS), and extracted with 25 mM Tris-HCl, pH 8.0, 50 mM NaCl, 0.5% (w/v) sodium deoxycholate, 0.5% (v/v) Nonidet P-40 (NP-40), and 1 mM phenylmethylsulfonyl fluoride for 30 min at 4°C. Cell debris was removed by centrifugation at 10,000 g at 4°C for 5 min. The extracts were analyzed by sodium dodecyl sulfate (SDS)-polyacrylamide gel electrophoresis and immunoblotting. For immunoblotting equal amounts of total protein were separated by

SDS-PAGE, transferred to nitrocellulose membranes, and incubated as described previously [68]. The bands were visualized by enhanced chemiluminescence as recommended by the manufacturer (Pierce, Thermo Fisher Scientific, Bonn, Germany) on X-ray films (CEA RP, medical X-ray film). Autoradiograms were scanned and cropped using Adobe Photoshop Elements 8.0.

2.4. Immunoprecipitation. To analyze the SUMOylated forms of the Mre11 protein, HFF cells at approximately 80–90% confluence were infected with Ad5 or the E1B 55 kDa mutants at 30 PFU/cell. For immunoprecipitation, all protein extracts were prepared in RIPA buffer (50 mM Tris-HCl/pH 8.0, 150 mM NaCl, 5 mM EDTA, 0.5% (w/v) sodium deoxycholate, 1% (v/v) Nonidet P-40 (NP-40), 1% (v/v) phenylmethylsulfonyl fluoride (PMSF), 0.1% (v/v) aprotinin, 1 mg/mL leupeptin, 1 mg/mL pepstatin, 25 mM iodacetamide, and 25 mM N-ethylmaleimide) and kept on ice for 30 min. Cell debris was removed by centrifugation at 10,000 g at 4°C for 5 min. For immunoprecipitation (IP) protein A-sepharose was incubated with 1 μg of anti-Mre11 mAb (12D7) (Gene-Tex, Inc.) for 1 h at 4°C. The antibody-coupled protein A-sepharose was added to pansorbin (50 μL/lysate; Calbiochem, Merck Chemicals Ltd., Nottingham, UK) precleared cellular extracts and incubated with constant rotation for 2 h at 4°C. Proteins bound to the antibody-coupled protein A-sepharose were sedimented by centrifugation, washed three times, boiled for 3 min at 95°C in 2x Laemmli buffer [69], and analyzed by immunoblotting.

2.5. Percentage of Mre11 SUMOylation. To measure *in vivo* SUMOylation of Mre11 in Ad infected cells, the EpiSeeker Global Protein SUMOylation Assay Kit (Abcam) was used as described by the manufacturer. Briefly, HFF cells were infected with Ad5 wt or the A143, E4 Orf3-, E4 Orf6-, or E1B 55 K-mutants. Cells were harvested at 16 and 28 h p.i. and nuclei were isolated using nonidet NP-40 as described previously [15]. Nuclear extracts were incubated with the anti-Mre11 rabbit pAB (pNB 100-142) (Novus Biologicals, Ltd., Cambridge, UK) in 8-well assay microwell strips, and SUMO was measured with the anti-SUMO antibody included in the kit by colorimetry. Positive and negative controls included in the kit were used. To calculate SUMOylation of Mre11, the $OD_{450\,nm}$ values from the negative control were subtracted from the values obtained for extracts from infected cells and were compared to the level of mock-infected cells. Values are expressed as the percentage of SUMO-conjugated Mre11 normalized to the values obtained for Ad5 wt-infected cells. The error bars indicate the standard deviation of the duplicates of two independent measurements.

2.6. Plasmid and Transient Transfection. The expression vectors pcDNA3-empty, pcDNA3-E1B 55 kDa wt [70], pcDNA3-HA-Ubc9, pcDNA3-E4 Orf6 wt, and pcDNA3-E4 Orf3 wt were used for the transfection assays. One hour before transfection, the medium was replaced by DMEM without antibiotics. For transient transfection, the transfection solution containing 1 μL DNA (1 μg/μL), 10 μL of 25 kDa linear polyethylenimine (PEI; Polysciences Inc., Eppelheim, Germany), and 100 μL DMEM was incubated for 30 min at room temperature. After application of the solution, cells were incubated for 6 h before replacing the medium with standard culture medium.

2.7. Immunofluorescence. HFF cells grown on coverslips to approximately 90% confluence were mock-infected or infected with Ad5 wt or E1B 55 kDa, E4 Orf6, or E4 Orf3 null mutant viruses. Cells were processed for immunofluorescence as described previously [68]. After application of specific primary antibodies, cells were incubated with secondary antibodies (Alexa-Fluor 488, 568, and 680, Invitrogen). The coverslips were mounted on glass slides in 10% glycerol and samples were examined by optical section microscopy (Apotome. Zeiss Axiovert 200 M). Images were taken with an Axiocam MRM using Axiovision 3.1 software (Carl Zeiss, Inc.). Images were assembled using Adobe Photoshop Elements 8.0.

3. Results

3.1. The Mre11 Protein Is not Efficiently Degraded and Is Posttranslationally Modified in Ad5-Infected Normal Human Cells. During Ad5-infection of cultured human cells the DNA damage response (DDR) is initially inhibited by the E4 Orf3 protein, which disrupts PML nuclear bodies (PML NBs) and induces the intracellular redistribution of Mre11 to these sites, prior to its targeted polyubiquitination and proteasomal degradation directed by E1B 55 kDa and E4 Orf6 [8, 14, 22–24, 71]. A similar order of events occurs to regulate p53. In addition, this cellular protein is SUMOylated by E1B 55 kDa and relocalized to nuclear structures [54], where p53 and E1B 55 kDa colocalize [16, 55].

In order to investigate if Mre11 is subject to similar processes, we decided to analyze whether degradation of Mre11 is induced in Ad5-infected human foreskin fibroblasts (HFF). Therefore, we analyzed soluble extracts of Ad5-infected HFF cells by immunoblotting. Adenovirus infection reduced the Mre11 protein levels; however, such reductions could only be observed at time points corresponding to the late phase of infection in HFF cells (28 h postinfection (p.i.)) (Figure 1). Since Mre11 degradation requires association of E1B 55 kDa with E4 Orf6, we examined Mre11 protein levels in cells infected with the E1B 55 kDa insertion mutant (A143) and the E1B 55 kDa null mutant Hr6 [58]. The A143 mutant virus carries a small insertion in the E1B 55 kDa coding sequence [57], which impairs binding to the E4 Orf6 protein [72]. A band of 55 kDa corresponding to E1B 55 kDa was detectable in Ad5 wild-type (wt) and A143-infected cells after immunostaining with the anti-E1B 55 kDa monoclonal antibody (mAb) 2A6. Additionally, we observed bands of higher molecular mass that correspond to the previously observed pattern for the SUMOylated forms of E1B 55 kDa [49, 51–53, 73]. In agreement with previous findings [52], absence of the E1B 55 kDa-E4 Orf6 interaction during infection with the A143 mutant led to more abundant E1B 55 kDa-SUMOylation than during Ad5 infection (Figure 1). Higher levels of Mre11
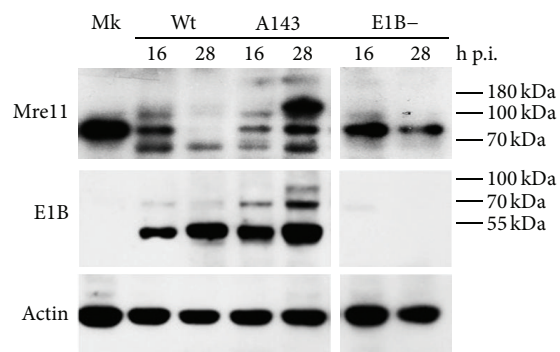
Figure 1: Degradation of Mre11 is not efficiently induced in Ad infected normal human cells. Degradation of the Mre11 cellular protein over the time course of Ad5 infection was analyzed in HFF cells infected with Ad5 and E1B 55 kDa mutants. Cell lysates were prepared at the indicated times postinfection for analysis by Western blot with antibodies directed to E1B 55 kDa (2A6), Mre11 (12D7. GeneTex), or actin (AC-40. Sigma). Actin served as a loading control.

could be observed in cells infected with the E1B 55 kDa mutants compared to the Ad5 wt virus, indicating that, as expected, degradation of the Mre11 protein was impaired by each of the mutations (Figure 1). This effect on Mre11 protein levels was significantly more pronounced late in infection. In agreement with previous reports, we thus observed that degradation of Mre11 in HFF cells depends on formation of the E1B/E4 Orf6 complex. However, a clear difference in the Mre11 protein pattern, which was particularly noticeable for Mre11 in response to Ad5 and A143 infection compared to the mock-infected control, could be observed in these cells (Figure 1). After immunostaining with the anti-Mre11 mAb (12D7), both Ad5 and A143-infected cell lysates showed additional bands with higher molecular mass (approximately 100 kDa and 200 kDa) than the corresponding Mre11 protein band (81 kDa). These high molecular weight bands were present at low levels in Ad5-infected cells and at significantly increased levels in A143-infected cells. The accumulation of slower-migrating bands detected by the anti-Mre11 mAb suggests this protein may be posttranslationally modified in the course of Ad5 infection.

3.2. The Mre11 Protein Colocalizes with E4 Orf3 and E1B 55 kDa in Nuclear and Cytoplasmic Structures throughout the Ad5 Replication Cycle. The inactivation of MRN during the early phase of infection correlates with the E4 Orf3-induced relocalization of Mre11 to nuclear sites adjacent or juxtaposed to PML NBs [23]. During the late phase Mre11 is redistributed to the cytoplasm where it has been described to colocalize with the viral E1B 55 kDa, E4 Orf6, and E4 Orf3 proteins, as well as cellular aggresome components, in a cage-like structure formed by the reorganization of vimentin filaments [8, 23, 27, 74]. Since the degradation of Mre11 was not efficiently induced in Ad5-infected HFFs (Figure 1), we decided to analyze the intracellular distribution of Mre11 and the intermediate filament protein, vimentin, as well as the viral proteins E1B 55 kDa and E4 Orf3

(Figures 2(a) and 2(b)) in these cells, at early and late times postinfection. Therefore, immunfluorescence analyses were performed as described in Section 2. In mock-infected cells, the Mre11 protein was diffusely distributed throughout the nucleoplasm (Figure 2(a)), in agreement with previous reports [23, 71]. After Ad5-infection the Mre11 protein was mostly relocalized to a number of nuclear speckles or tracks during the early phase, displaying extensive colocalization with E4 Orf3 (Figure 2(a)). Interestingly, in HFF cells the Mre11 and E4 Orf3 proteins also colocalized in numerous punctuate cytoplasmic structures (Figure 2(a)). Significantly, in contrast to the staining pattern reported in Ad5-infected cell lines, such as HeLa, a different staining pattern was observed during the late phase of infection by 28 and 48 h p.i., as the Mre11 protein was still prominently detected in nuclear dots colocalizing with the adenoviral E4 Orf3 protein (Figure 2(a)). We also examined the intracellular distribution of the E1B 55 kDa and E4 Orf3 proteins (Figure 2(b)) during the viral replication cycle and their localization resembled the patterns previously described for Ad5-infected HeLa and HFF cells [68]. Interestingly, since the Mre11 protein was clearly detected at late times postinfection, these results suggest that inhibition of nuclear Mre11, by E4 Orf3 or additional mechanisms, should be sustained well into the late phase.

3.3. The Mre11 Protein Is Modified by Addition of Both SUMO-1 and SUMO-2/3 in Ad5 Infection. In order to determine whether the Mre11 protein is SUMOylated during adenovirus infection, we decided to test the addition of SUMO paralogues to Mre11. To evaluate whether the protein can be modified by SUMO-1 and SUMO-2/3 we performed immunoprecipitation assays at different times postinfection (10, 16, 28, and 36 h p.i.) from extracts of cells infected with Ad5, the E1B 55 kDa insertion mutant A143, or virus mutants that do not express either E1B 55 kDa, E4 Orf6, or E4 Orf3. For the pull down assays anti-Mre11 was used, and subsequent Western blot analyses were performed using monoclonal antibodies directed specifically to SUMO-1 or SUMO-2/3 (Figure 3(a)) thus allowing us to distinguish SUMO-1 from SUMO-2/3 paralogues.

Immunoprecipitated Mre11 and subsequent SUMO-2/3 immunostaining showed bands with molecular masses of approximately 130 kDa, 180 kDa, and 250 kDa, which correspond to different forms of poly-SUMO-2/3 chains covalently attached to Mre11. As shown in Figure 3(a), the pattern of SUMO-2/3-modified Mre11 bands was very dynamic throughout the Ad5 replication cycle. The SUMO-2/3 forms of Mre11 were present from the early phase (10 and 16 h p.i.) and remained well into the late phase (28 and 36 h p.i.), in agreement with the sustained nuclear Mre11 signal observed by immunofluorescence analysis (Figure 2). Interestingly, different patterns were observed between the Ad5 and mutant viruses. The 130 kDa band was the most abundant form of SUMO-2/3-Mre11 detected during infection with either Ad5 or A143 (Figure 3(a)), where this band was detected throughout infection. In contrast to Ad5-infected cells, where the 250 kDa band was only observed late during infection (36 h p.i.), in A143-infected cells this band was present from
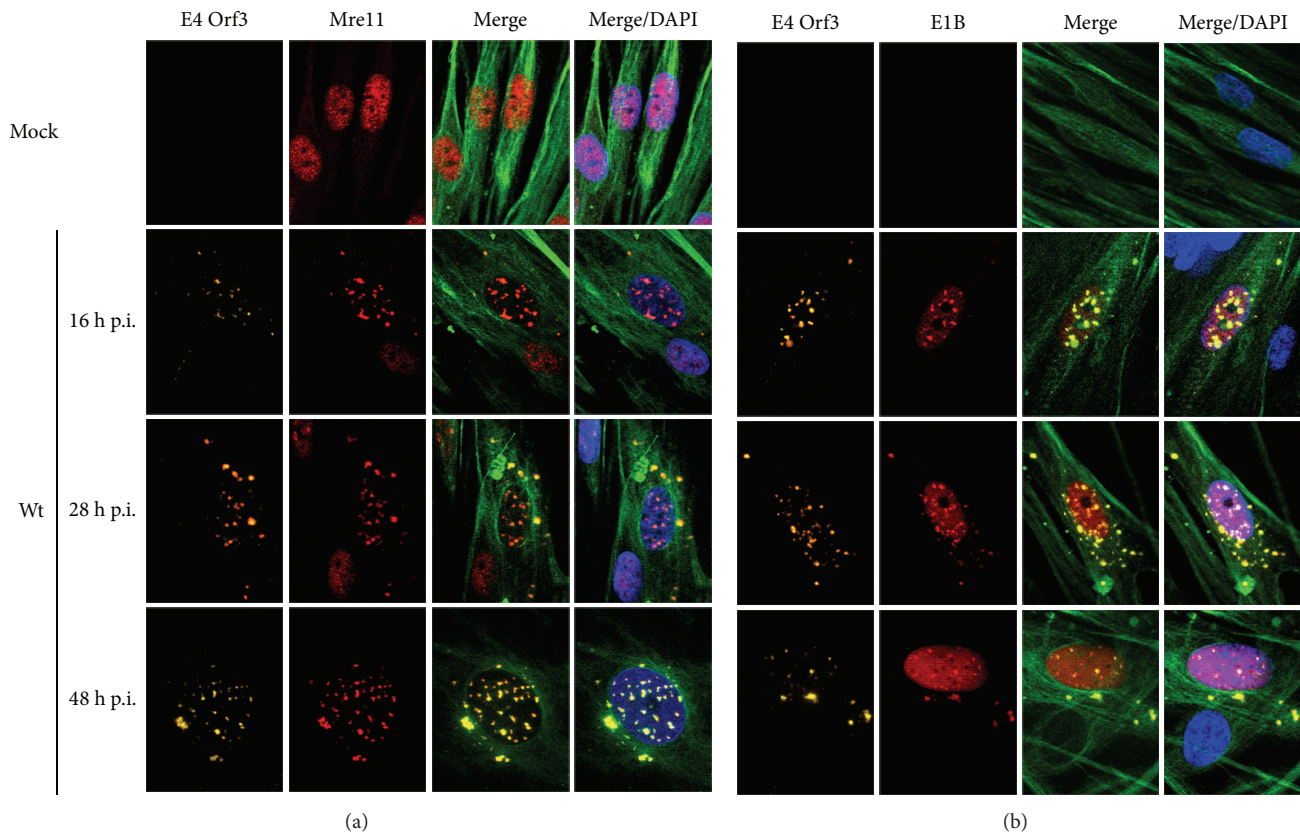
FIGURE 2: The Mre11 protein colocalizes with E4 Orf3 and E1B 55 kDa in nuclear and cytoplasmic structures throughout the Ad5 replication cycle. The intracellular distribution of (a) E4 Orf3 (6A11), Mre11 (12D7-GeneTex), and vimentin and (b) E4 Orf3 (6A11), E1B 55 kDa (2A6), and vimentin was analyzed in mock-infected and Ad5-infected HFF cells at various times after infection. The cells were processed for immunofluorescence and E4 Orf3, Mre11, E1B 55 kDa, and vimentin were visualized as described in Section 2. The E4 Orf3 protein signal is shown in yellow, Mre11 (a) or E1B 55 kDa (b) in red, vimentin in green, and DAPI-stained nuclei in blue.

the early phase of the viral replication cycle (16 h p.i.). Throughout infection, this 250 kDa band was significantly more abundant in cells infected with the E1B 55 kDa- or E4 Orf3 null mutants. In addition a 180 kDa band which was observed in cells infected with A143, as well as with the E1B 55 kDa- or E4 Orf3-minus mutant viruses, was not detected during infection with Ad5 wt (Figure 3(a)). A clear difference in the pattern and a higher overall abundance of SUMOylated bands was observed in cells infected with the E4 Orf6 null mutant, where multiple SUMO-2/3 forms of Mre11 were detected and a band with a molecular weight higher than 250 kDa was prominent. As control for total Mre11 input levels the same samples were also analyzed by Western blot using the anti-Mre11 (Mre11 long exposure). These results clearly show that Mre11 is modified by addition of SUMO-2/3, in agreement with recently published results [56]. However, these data also demonstrate that during infection the SUMO-2/3 modification of Mre11 can occur in the absence of either E1B 55 kDa, E4 Orf6, or E4 Orf3. Nevertheless, since we observed a clear difference in the pattern of Mre11-SUMO-2/3 bands between Ad5 and the different mutant viruses (Figure 3(a)), these data suggest that all three proteins have the ability to modulate SUMOylation of Mre11 in the context of infection. We then decided to test the addition of SUMO-1

to Mre11. In mock-infected cells, we observed a 110 kDa band that corresponded to SUMO-1-modified Mre11 (Figure 3(a)). The SUMO-1-modified Mre11 was also clearly visible during infection with the Ad5, A143, or the E1B 55 kDa, E4 Orf6, or E4 Orf3 null mutant viruses. However, during Ad5 infection, the level of SUMO-1-modified Mre11 decreased as the viral replication cycle progressed, displaying significantly reduced levels by 36 h p.i. Such reduction of SUMO-1-Mre11 levels was not observed in cells infected with any of the mutant viruses; rather, the level of SUMO-1-Mre11 increased by 36 h p.i. in the absence of E1B or E4 Orf3. These data indicate that Mre11 can be modified by SUMO-1 and furthermore suggest that during adenovirus infection the E1B 55 K, E4 Orf6, and E4 Orf3 proteins can each modulate SUMO-1 addition to Mre11.

In order to further explore the relative impact of E1B 55 kDa, E4 Orf3, E4 Orf6, and the E1B/E4 Orf6 complex on SUMOylation of Mre11 during virus infection, we decided to measure total levels of Mre11 SUMOylation, detecting SUMO-1 as well as SUMO-2 and -3-modified forms, at different times postinfection (16 and 28 h p.i.). Using nuclear extracts of infected HFF cells, anti-Mre11 and anti-SUMO antibodies were used to measure the modified form of Mre11 through the signal reporter-color development system, as described in Section 2. As expected, in Ad5-infected cells,
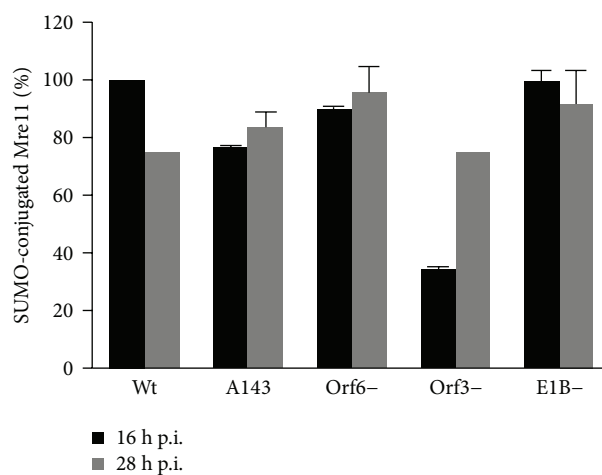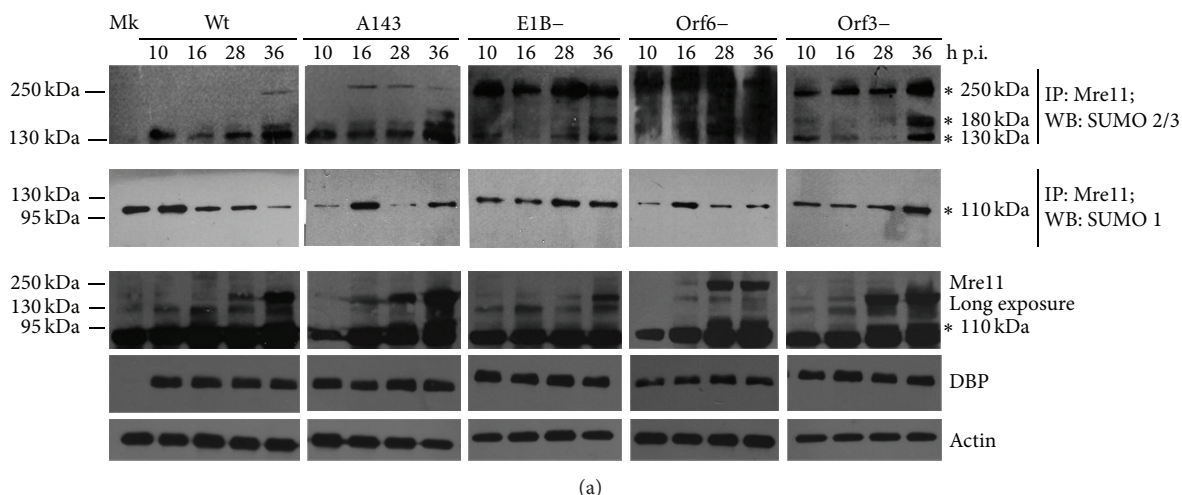
(a)

(b)

FIGURE 3: The Mre11 protein is modified by addition of both SUMO-1 and SUMO-2/3 during Ad5 infection. (a) HFF cells either mock-infected or infected with Ad5, the E1B 55 kDa insertion mutant A143, or E1B 55 kDa, E4 Orf6, or E4 Orf3 null mutants were harvested at different times postinfection (10, 16, 28, and 36 h p.i.), and lysates were analyzed by immunoprecipitation and Western blot. The immunoprecipitation of Mre11 was performed using anti-Mre11, resolved on 10% SDS-PAGE, and visualized by immunoblotting using anti-SUMO-2/3 or anti-SUMO-1 mAbs. Specific Mre11-SUMO-2/3 or -SUMO-1 bands are indicated by (∗). Western blotting was performed using anti-Mre11 as input control. DBP and actin were included as infection control and internal loading control, respectively. (b) Quantification of total SUMO-Mre11 protein. Nuclear extracts of HFF cells either mock-infected or infected with Ad5, A143, or virus null mutants (E1B 55 kDa, E4 Orf6, or E4 Orf3) were obtained at two different times postinfection (16 and 28 h p.i.). Nuclear extracts were incubated with the anti-Mre11, and SUMO was detected by a colorimetric assay, as described in Section 2.

we observed approximately 20% decrease in the total level of SUMO-modified Mre11 in the late phase of infection compared with the early phase (Figure 3(b)). This is consistent with the lower levels of SUMO-1-Mre11, which are more prominent in Ad5 infection than the SUMO-2 and -3 modified protein, detected at 36 h p.i. (Figure 3(a)) and with the degradation of Mre11 induced during the late phase of the replication cycle. To compare the relative effect of E1B 55 kDa, E4 Orf3, E4 Orf6, and the E1B/E4 Orf6 complex, the SUMO-Mre11 values obtained for each mutant virus were normalized to Ad5 levels, which were set to 100% at 16 h p.i. (Figure 3(b)). Lower levels of SUMOylated Mre11 were observed in the A143, E4 Orf6, and E4 Orf3 mutants at 16 h p.i. Interestingly, in contrast to the decrease observed

for Ad5, during A143 infection, when the E1B/E4 Orf6 E3-Ub complex does not assemble and Mre11 degradation is not induced, we observed a slight increase in the level of total SUMO-Mre11 levels in the late phase versus the early phase of infection. A similar increase was observed during infection with the E1B- or E4 Orf6-null mutants. In contrast to Ad5, during infection with the E4 Orf3 null mutant, the levels of SUMO-Mre11 displayed a marked decrease at 16 h p.i.; however, by 28 h p.i. SUMO-Mre11 levels were comparable to those of Ad5. These data suggest that while E4 Orf3 may be necessary to induce SUMO addition to Mre11 during the early phase of infection, it is dispensable during the late phase, when E1B 55 kDa and E4 Orf6 seem to have a compensatory effect in the SUMOylation of Mre11
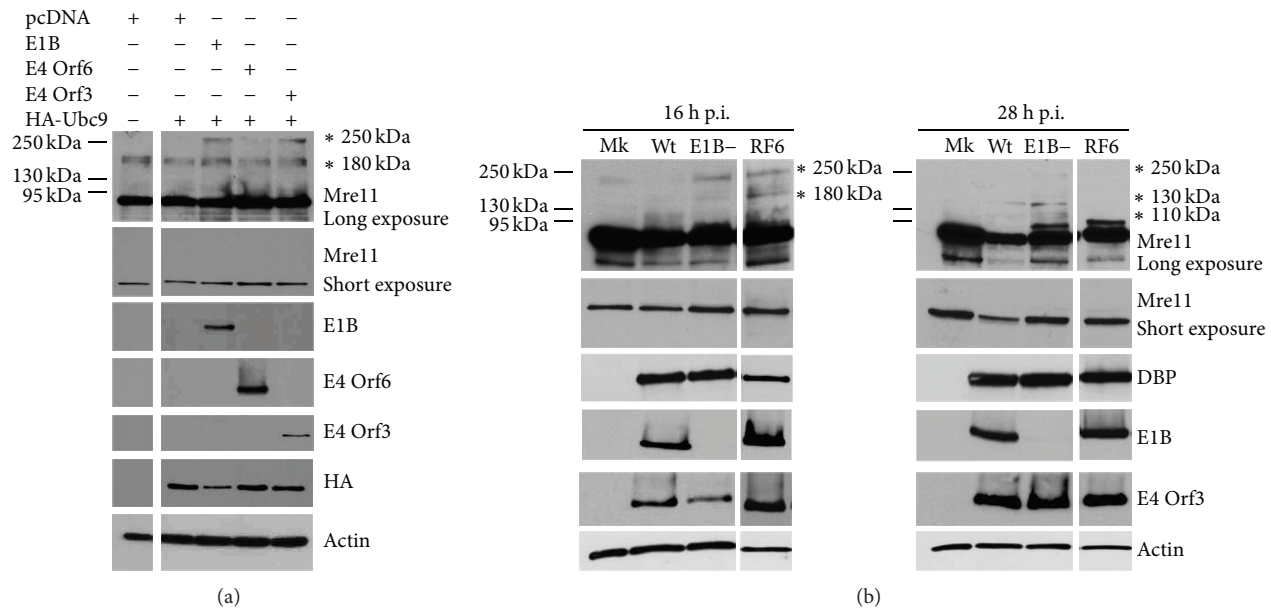
FIGURE 4: The addition of SUMO to Mre11 is influenced by E1B 55 kDa, E4 Orf6, and E4 Orf3, but none of these viral early proteins is absolutely required. (a) H1299 cells were transfected with pcDNA3-empty, pcDNA3-E1B 55 kDa wt, pcDNA3-E4 Orf6 wt, pcDNA3-E4 Orf3 wt, and/or pcDNA3-HA-Ubc9. Cells were harvested and total cell extracts were prepared at 28 h posttransfection, as described in Section 2. Protein samples (20 μg) were separated on 10% SDS-PAGE followed by immunoblotting with anti-Mre11, anti-E1B 55 kDa, anti-E4 Orf6, anti-E4 Orf3, anti-HA, and anti-actin mAbs. (b) H1299 cells were either mock-infected or infected with Ad5, RF6, or the E1B 55 kDa null mutant. Cells were harvested at 16 and 28 h p.i. for analysis by Western blot with anti-Mre11 rabbit pAb (NB100-142. Novus Biologicals), anti-E4 Orf6, anti-DBP, anti-E1B 55 kDa, and anti-actin mouse mAb (AC-15. Sigma-Aldrich, Inc.). Bands with molecular masses corresponding to Mre11-SUMO-1 and Mre11-SUMO-2/3 are indicated by (∗).

(Figure 3(b)). The higher levels of SUMO-Mre11 observed in the absence of E1B 55 kDa or E4 Orf6 cannot be attributed to decreased deconjugation of SUMO, since similar higher percentages of SUMO-Mre11 were obtained in A143-infected cells, when both proteins are produced. However, consistently a functional E1B/E4 Orf6 E3-Ub ligase could be involved in the regulation of SUMO-modified Mre11. Taken together, these data indicate that Mre11 is SUMOylated by covalent addition of both SUMO-1 and SUMO-2/3 paralogues during Ad5-infection (Figure 3(a)). In addition, our data show that the modification of Mre11 by SUMO is highly dynamic and displays different requirements for E1B, E4 Orf3, and E4 Orf6 during the early and late phases of infection (Figures 3(a) and 3(b)).

3.4. The E1B 55 kDa, E4 Orf6, and E4 Orf3 Proteins Can Each Modulate Mre11 SUMOylation during Adenovirus Infection. To further investigate the role of E1B 55 kDa, E4 Orf6, or E4 Orf3 in Mre11-SUMOylation, we decided to determine whether any one of these viral early proteins was sufficient to induce SUMO addition to Mre11 independent of an adenoviral infection environment. We overexpressed each of these viral proteins independently (E1B 55 kDa, E4 Orf6, and E4 Orf3) and in combination with Ubc9. For these experiments we transfected H1299 cells with either an empty vector or a plasmid encoding HA-Ubc9 as controls or plasmids encoding E1B 55 kDa, E4 Orf6, or E4 Orf3 plus the HA-Ubc9 plasmid. The soluble extracts of the transfected cells were analyzed by

Western blot (Figure 4(a)). Significantly, when we transfected an empty pcDNA plasmid or pcDNA in combination with the HA-Ubc9 plasmid, as controls, we observed a higher molecular weight band of approximately 180 kDa, matching the molecular mass of one of the SUMO-2/3-Mre11 bands observed in previous experiments (Figure 3(a)). This observation suggested that the stress caused by the transfection assays was enough to induce formation of the 180 kDa form of SUMO-2/3-Mre11. When each of the viral early proteins was overexpressed in combination with the HA-Ubc9 protein, we detected an additional band of higher molecular mass of approximately 250 kDa (Figure 4(a)). No differences in the pattern of bands corresponding to SUMO-2/3-Mre11 were observed between cells transfected with any of the three viral early proteins, suggesting that outside the context of virus infection and when Ubc9 is overexpressed E1B 55 kDa, E4 Orf6, and E4 Orf3 can each induce addition of SUMO-2/3 to Mre11 to form the 250 kDa SUMO-2/3-modified Mre11 independently of one another.

As described in the introduction, the E1B 55 kDa protein can function as an E3 SUMO-ligase for p53, and it provides target specificity to the Cullin 5-E3 ubiquitin ligase inducing degradation of p53 and other targets, including Mre11. To explore whether the interaction between E1B 55 kDa and Mre11 may be directly implicated in its SUMOylation, we analyzed the SUMO status of Mre11 in cells infected with the RF6 mutant, which carries a point mutation that abrogates binding of E1B 55 kDa to Mre11 [59, 75]. H1299 cells

(a)   (b)   (c)
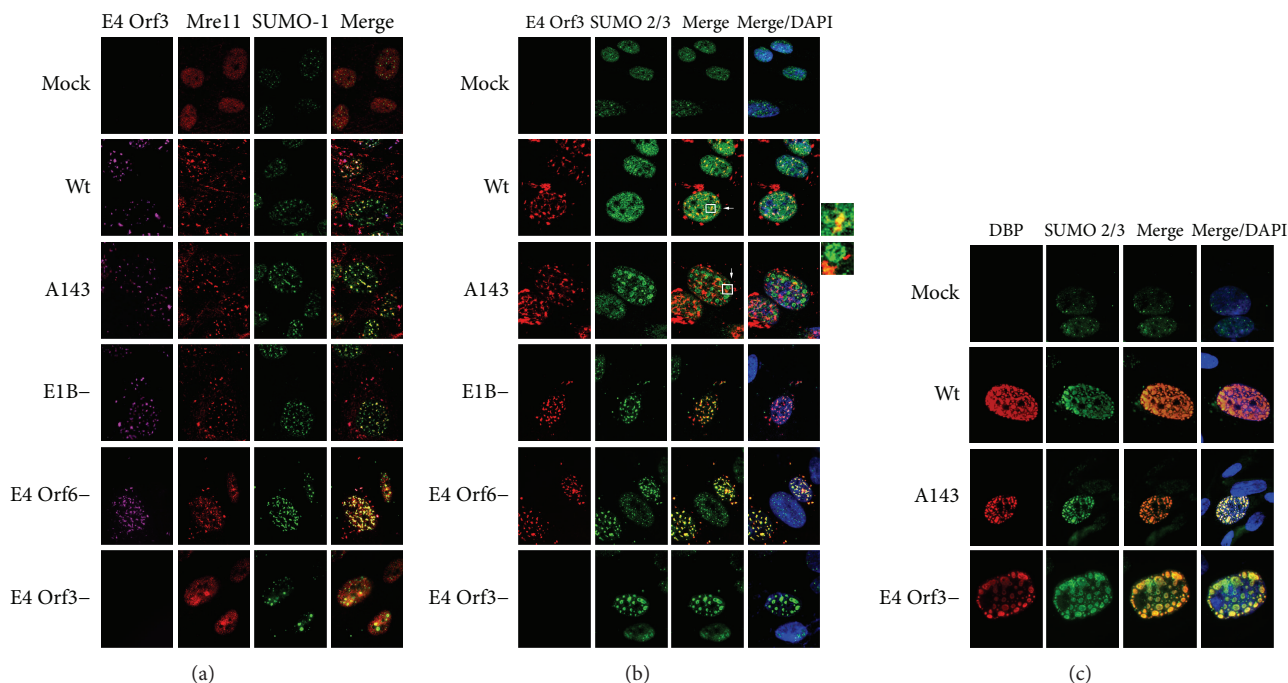
FIGURE 5: Ad5-infection induces the nuclear reorganization of SUMO-1 and SUMO-2/3 paralogues. (a) The intracellular distribution of E4 Orf3, Mre11, and SUMO-1 was analyzed in HFF cells infected with Ad5, the A143, or the E1B 55 kDa, E4 Orf6, or E4 Orf3 null mutants at 28 h p.i. After infection cells were processed for immunofluorescence as described in Section 2. E4 Orf3 is shown in magenta, Mre11 in red, and SUMO-1 in green. (b) The intracellular distribution of E4 Orf3 and SUMO-2/3 was analyzed in HFF cells infected with Ad5, A143, or the null mutants for E1B 55 kDa, E4 Orf6, or E4 Orf3. E4 Orf3 is shown in red and SUMO-2/3 in green; DAPI-stained nuclei are shown in blue. Insets were enlarged 5X to show the localization of SUMO-2/3 in ring-like structures, adjacent to E4 Orf3 tracks. (c) The intracellular distribution of DBP and SUMO-2/3 was analyzed in HFF cells infected with the Ad5, A143, or the null mutants for E1B 55 kDa or E4 Orf3 viruses, at 28 h p.i. DBP is shown in red and SUMO-2/3 in green; DAPI-stained nuclei are shown in blue.

were infected with Ad5, the E1B 55 kDa null, or the RF6 mutant virus, and infected-cell extracts were analyzed by Western blot (Figure 4(b)). As expected, both E1B 55 kDa virus mutants failed to induce decreased levels of Mre11 compared to Ad5 wt, since they either do not form the E3-Ub ligase (E1B-) or cannot recruit Mre11 for ubiquitination (RF6) [53, 76]. Interestingly, the patterns of bands observed during the early and late phase of infection were different between the Ad5 wt and E1B 55 kDa mutants. At 16 h p.i. two high molecular mass bands of approximately 180 kDa and 250 kDa were observed in extracts of cells infected with either of the E1B 55 kDa mutants. In contrast, during late infection with each of the E1B 55 kDa mutants (28 h p.i.), the 110 kDa form of Mre11 accumulated to higher levels than in Ad5 wt infection, indicating that the levels of SUMO-1 modified Mre11 increased during the late phase of infection in the absence of the E1B 55 kDa protein or the E1B 55 kDa-Mre11 interaction. In addition, during late infection with RF6 only the 110 kDa band was visible; infection with the E1B 55 kDa null mutant resulted in the appearance of both the 110 kDa and 130 kDa bands that correspond to SUMO-1 and SUMO-2/3 forms of Mre11, respectively (Figure 4(b)). These results suggest that a different SUMOylation pattern of Mre11 was induced in the absence of E1B 55 kDa and that the E1B 55 kDa-Mre11 interaction may be necessary for SUMO-2/3 addition to Mre11 only in the late phase of infection. Taken together

these data indicate that although E1B 55 kDa is not absolutely required to induce SUMOylation of Mre11 in infected cells, it can influence the level and pattern of SUMO addition to this cellular protein at different times during the viral replication cycle.

3.5. Ad5-Infection Induces Reorganization of SUMO-1 and SUMO-2/3 Paralogues. SUMOylation of PML plays an important role for the scaffold function of this protein in functional PML NB organization. Furthermore, SUMO-1 or SUMO-2/3 attachment to PML is responsible for the correct localization of PML in the PML NBs [36]. SUMO paralogues display distinct localization in the PML NBs when analyzed by immunofluorescence microscopy. While SUMO-1 modified proteins are located in the periphery of PML NBs forming a shell-like appearance, SUMO-2/3 proteins seem to occupy the interior of these structures [33]. We decided to investigate whether Ad5-infection induces the nuclear redistribution of SUMO-1 and SUMO-2/3. We therefore performed immunofluorescence analysis of the intracellular distribution of SUMO-1, SUMO-2/3, Mre11, and E4 Orf3 in HFF cells infected with Ad5 wt, A143, or the E1B 55 kDa, E4 Orf6, or E4 Orf3 null mutants (Figure 5). Besides a slight increase in the SUMO-1 and SUMO-2/3 signals upon adenovirus infection, we observed that SUMO-1 was redistributed from small nuclear dots in mock-infected

cells to speck- or track-like structures in the cell nucleus of Ad5 wt-infected HFF (90% of all cells examined, $n > 60$). The redistribution of SUMO-1 seemed to be independent of the association between E1B 55 kDa and E4 Orf6 or the presence of either of these viral proteins, since it was also induced in cells infected with the A143, E1B 55 kDa-, or E4 Orf6-mutant virus (Figure 5(a)). As expected Mre11 colocalized with E4 Orf3 [27], and the staining pattern of both of these proteins overlapped with SUMO-1 in the majority of nuclear track-like structures in cells infected with either Ad5 wt, A143, E1B 55 kDa-null, or E4 Orf6-null mutants (90% of all cells examined, $n > 60$) (Figure 5(a)). During infection with the E4 Orf3 null mutant, however, we found that neither Mre11 nor SUMO-1 was reorganized into nuclear tracks but relocalized to large dot-like structures showing a stronger Mre11 and SUMO-1 staining pattern. These data demonstrate that while E1B 55 kDa and E4 Orf6 are dispensable, E4 Orf3 is necessary for the nuclear reorganization of both Mre11 and SUMO-1 to tracks, consistent with previous observations [23, 27, 56, 71].

We next analyzed the intracellular distribution of SUMO-2/3 during infection with Ad5 and the viral mutants using the same setup as before (Figures 5(b) and 5(c)). In mock-infected cells, we observed a diffuse SUMO-2/3 distribution throughout the nucleoplasm, with small dots displaying a slightly stronger signal. In Ad5 wt-infected cells, the SUMO-2/3 signal was reorganized into a reticular distribution where the protein accumulated in ring-like spherical structures (Figures 5(b)-insets and 5(c)). These structures were closely associated and displayed partial colocalization with adjacent E4 Orf3 tracks (80% of all cells examined, $n > 30$) (Figure 5(b)). Furthermore, this distribution of SUMO-2/3 was similar to viral replication centers marked by the E2 DNA-binding protein (DBP) (Figure 5(c)), which was additionally juxtaposed with E4 Orf3 (Figure 5(b)) or PML tracks (not shown). During infection with the E1B 55 kDa or E4 Orf6 null mutants, SUMO-2/3 was reorganized into nuclear tracks and colocalized with E4 Orf3 (Figure 5(b)). In contrast, during infection with the A143 or the E4 Orf3 null mutant viruses, SUMO-2/3 colocalized more extensively with DBP (Figure 5(c)). Interestingly, relocalization of SUMO-2/3 to sites of viral DNA replication (marked by DBP) was enhanced in the absence of a functional E1B/E4 Orf6 complex (A143) or the absence of E4 Orf3 (Figure 5(c)). These data indicate that in contrast to SUMO-1, whose reorganization and colocalization depends on E4 Orf3, the extensive relocalization of SUMO-2/3 to viral replication centers is dependent on the presence of both E1B 55 kDa and E4 Orf6 (Figures 5(b) and 5(c)). Altogether, these observations suggest a compensatory effect between the three viral proteins in the modulation of the SUMO paralogues during infection. Moreover, the localization of SUMO-1 was influenced by E4 Orf3 and unaffected by E1B 55 kDa or E4 Orf6, while SUMO-2/3 relocalization to viral replication centers was dependent on E1B 55 kDa and E4 Orf6. These results suggest that a complex molecular interplay between the E1B 55 kDa, E4 Orf6, and E4 Orf3 proteins is responsible for the concerted regulation and modification of protein targets with the different SUMO paralogues during adenovirus infection.

4. Discussion

Various components of the DDR are regulated by posttranslational modifications, including phosphorylation, ubiquitylation, acetylation, methylation, NEDDylation, and SUMOylation [77]. Following DNA damage, several DNA repair factors transit to and from PML NBs, and the PML NBs themselves colocalize with sites of unscheduled DNA synthesis [78–80]. In the case of Mre11, its phosphorylation and methylation have been studied in detail [81–87], and the protein is known to shuttle to PML NBs in response to DNA damage, in an arginine methylation-dependent manner [86, 88]. However, although Mre11 is predicted to possess up to two potential SUMOylation sites, the role of this modification in the regulation of the protein's activities is not known [80, 89].

Here we have shown that Mre11 is modified by both SUMO-1 and SUMO-2/3 during infection with Ad5. The SUMOylated forms of Mre11 reproducibly displayed a complex pattern of well-defined bands in Western blot analyses that varied depending on the presence of the E1B 55 kDa, E4 Orf6, or E4 Orf3 proteins and on the ability of E1B 55 kDa to interact with E4 Orf6 or Mre11. The pulldown of Mre11 and the use of antibodies directed against either the SUMO-1 or SUMO-2/3 paralogues yielded bands with approximate molecular masses of 110, 130, 180, and 250 kDa. The 110 kDa band was observed only with antibodies directed against SUMO-1, suggesting that Mre11 was monoSUMOylated with this paralogue during infection. Prediction of potential SUMOylation sites in the Mre11 sequence has shown that there exist two putative lysines within consensus SUMO motifs (lysines 255 and 661) [90]. We do not yet know whether only one putative lysine or each lysine may be modified, with the latter resulting in a combined population of Mre11 proteins monoSUMOylated in different lysines. In contrast, higher molecular weight bands were observed only with the anti-SUMO-2/3 antibody, indicating that modification by both mono- and poly-SUMO-2/3 can occur either on one or more lysines.

As described in the introduction, E1B 55 kDa, E4 Orf6, and E4 Orf3 are required to inhibit the antiviral cellular defenses and to promote the expression of viral late genes, resulting in efficient viral replication [91]. Two key processes they modulate are the relocalization and the proteasomal degradation of cellular targets that would otherwise interfere with viral replication [2, 7–9, 14, 22, 23]. Interestingly, these viral early proteins inhibit an overlapping, but nonidentical, set of cellular target proteins. All three participate in degradation of cellular targets. Protein ubiquitination by E1B 55 kDa and E4 Orf6 depends on Cul5 or Cul2 containing E3-ubiquitin ligases whose assembly is directed by E4 Orf6, while E1B 55 kDa provides specificity for substrate recognition [2, 92]. In addition, E1B 55 kDa can induce degradation of the cellular transcription repressor, Daxx, independently of E4 Orf6 [93], and the E4 Orf3 protein can mediate turnover of the transcriptional intermediary factor 1γ (TIF 1γ), in the absence of either E4 Orf6 or E1B 55 kDa [94], suggesting that each can modulate ubiquitination of cellular targets by both common and independent mechanisms. Interestingly, E1B 55 kDa and E4 Orf3 can also modulate the SUMOylation

machinery, suggesting that regulation of cellular proteins by these viral gene products is likely to be influenced by a crosstalk between ubiquitination and SUMOylation. The data presented here now show that addition of SUMO to Mre11 during adenoviral infection is highly dynamic. The absence of E1B 55 kDa, E4 Orf6, or E4 Orf3, when neither degradation (by the E1B/E4 Orf6 complex) nor relocalization (by E4 Orf3) of Mre11 can be induced, led to the accumulation of slower migrating SUMO-modified Mre11 forms already early during infection and increased as infection progressed. However, infection with the Ad5 and each of the virus mutants produced different patterns of SUMOylated Mre11 bands, indicating that each of these proteins can differentially modulate the cellular SUMOylation system.

During infection, different adenoviral proteins modulate the cellular SUMO machinery. In the early phase, E1A interacts with Ubc9 interfering with polySUMOylation of cellular substrates, while monoSUMOylation is unaffected [95]. In the case of E1B 55 kDa, the protein is targeted by both, SUMO-1 and SUMO-2/3 addition [73], and in addition the E1B 55 kDa protein can act as an E3-SUMO-1-ligase for p53 [55]. E1B 55 kDa also interacts with Ubc9, and the degradation of p53 and Mre11 are both independent of the SUMOylation or phosphorylation status of E1B 55 kDa [49]. The SUMOylated form of E1B 55 kDa seems to be associated with an insoluble nuclear matrix fraction early during infection, when the protein associates with PML isoform IV in the PML NBs [52]. E1B 55 kDa can also interact with E4 Orf3 favoring its association with PML [26]. Upon formation of the E1B/E4 Orf6 complex E4 Orf6 has been suggested to displace E1B 55 kDa from E4 Orf3 and from the insoluble fraction, resulting in a soluble complex that associates with viral replication centers or the Cul5-E3-Ubiquitin ligase [49, 52]. A crucial player in the reorganization of PML NBs during infection is the E4 Orf3 protein, which can also impact the SUMOylation machinery [56]. Intriguingly, our results have shown that SUMOylation of Mre11 is influenced by the E1B 55 kDa, E4 Orf6, and E4 Orf3 proteins. Transient expression of each of these viral early proteins was sufficient to induce SUMO addition to Mre11, while in the context of a viral infection none of them was absolutely required for Mre11 SUMOylation. Rather, the pattern of SUMOylated bands observed during the early and late phases of infection indicated that a temporal regulation of SUMO addition was influenced by a dynamic molecular interplay that involves each of these viral early proteins.

Our data showed that, as expected, the relocalization of Mre11 to E4 Orf3 and PML containing tracks (Figure 2; data not shown) was independent of E1B 55 kDa or E4 Orf6 or formation of the E1B/E4 Orf6 complex (Figures 2 and 5(a)) and that E4 Orf3 was necessary to induce the relocalization of both Mre11 and SUMO-1 to PML tracks in infected cells (Figure 5(a)). Intriguingly, the colocalization of E4 Orf3 with SUMO-2/3 was not as abundant, as the latter accumulated mostly in ring-like spherical structures that colocalized with DBP in viral replication centers (Figure 5(c)). The distribution of SUMO-1 and SUMO-2/3 associated to PML NBs is highly dynamic but has been shown to display distinct patterns, where SUMO-1 appears as a spherical shell that

surrounds PML NBs and colocalizes with PML and SP100, while SUMO-2/3 can be located in the interior of the spherical PML NBs [33]. Our findings therefore suggest that SUMO-1 may be retained in the E4 Orf3-reorganized PML tracks that form adjacent to the viral replication centers, while SUMO-2/3 colocalizes only partially with these tracks and is instead mostly relocated to sites of viral DNA replication. The colocalization of SUMO-2/3 with DBP in these spherical structures suggests that SUMO-2/3 may be localized to the interior of the viral replication centers where it could function as a scaffold as it does in the PML NBs [33]. The more extensive recruitment of SUMO-2/3 to the interior of viral replication centers occurred only in the absence of E4 Orf3 or in the presence of both E1B 55 kDa and E4 Orf6, regardless of whether the E1B/E4 Orf6 complex can form, suggesting that each of these proteins is required for the concerted recruitment of SUMO-2/3 to the viral replication centers. These findings suggest that these three viral early proteins modulate the relocalization of SUMO paralogues to counteract antiviral host defenses that are coordinated by the PML NBs. Since other components of DDR are known to be modified by SUMO [77], it will be interesting to determine whether the different SUMO paralogues are used in Ad infected cells to modify and regulate specific DDR proteins in the PML NBs or viral replication centers.

The SUMO-modified forms of E1B 55 kDa were also more readily observed with the A143 mutant than with the Ad5 wt (Figure 1). This was in agreement with previous findings showing that E1B 55 kDa SUMOylation increases in the absence of E4 Orf6, when association of E1B 55 kDa with E4 Orf3 and PML NBs is enhanced [52]. Interestingly, in the absence of the E3-Ub ligase, the SUMO-modified forms of both E1B 55 kDa and Mre11 accumulated to a higher extent during the late phase of infection. Taken together these findings indicate that the SUMOylated forms of Mre11 increase when degradation of the protein is precluded, suggesting that SUMOylation may be induced as a cellular mechanism that protects Mre11 from degradation. An alternative possibility is that addition of SUMO-2/3 modulates Mre11 polyubiquitination. Interestingly, while SUMO-1 addition does not correlate extensively with polyubiquitination and protein degradation, SUMO-2-conjugated proteins are more commonly ubiquitylated, linking SUMO-2 modification to the ubiquitin-proteasome system [42]. In our experiments, the pattern of SUMO-modified Mre11 bands changed as viral replication progressed. While during infection with Ad5, when Mre11 degradation can be induced, slower migrating bands corresponding to the highest SUMO-2/3 modified Mre11 forms were noticeable at early times postinfection; these bands decreased by the late phase correlating with the decrease in Mre11 levels. In contrast, these bands increased in intensity in the absence of E1B 55 kDa or when E1B 55 kDa cannot interact with Mre11 (RF6), when degradation of Mre11 cannot be induced (Figure 4(b)). Interestingly at late times, the pattern of multi-SUMO-modified Mre11 switched from the slower migrating 180 and 250 kDa bands to the faster migrating, 110 and 130 kDa bands, which correspond to monoSUMO-1 and monoSUMO-2/3, respectively (Figure 4(b)). Therefore, it will be interesting to investigate whether E1B 55 kDa, E4 Orf6, and

E4 Orf3 may be responsible for the temporal regulation of the SUMO-ubiquitin switch.

Sohn and Hearing recently reported [56] that Ad infection induces modification of Mre11 by SUMO-2 conjugation and of Nbs1 by both SUMO-1 and -2 in HeLa cells. In their experiments E4 Orf3 was shown to be necessary and sufficient for this modification, while deconjugation of SUMO from Nbs1 and not Mre11 was influenced by E1B 55 kDa or E4 Orf6 [56]. Our results now confirm that Mre11 SUMOylation is induced in Ad infected normal HFF and in transformed H1299 cells. However, we have demonstrated that Mre11 is also modified by the addition of SUMO-1. The reason for the difference in the SUMO-1 modification of Mre11 is not clear and should be explored to determine whether it may depend on experimental conditions. However, while Sohn and Hearing [56] used transfected HeLa cells and overexpression of both SUMO paralogues and E4 Orf3, in our experiments SUMO-1 conjugation to Mre11 was observed in normal human foreskin fibroblast infected cells. More importantly our results now show that E1B 55 kDa and the E1B/E4 Orf6 complex influence the redistribution of SUMO-2/3 in the cell nucleus as well as SUMOylation of Mre11. Therefore, these data indicate for the first time that each of these proteins can modulate SUMO modification or degradation of cellular substrates underscoring the complexity of the molecular interplay that underlies the activities of the E1B 55 kDa, E4 Orf6, and E4 Orf3 proteins in regulation of SUMOylation and ubiquitination during Ad infection.

Conflict of Interests

The authors declare that there is no conflict of interests regarding the publication of this paper.

Acknowledgments

References

[1] J. Boyer, K. Rohleder, and G. Ketner, "Adenovirus E4 34k and E4 11k inhibit double strand break repair and are physically associated with the cellular DNA-dependent protein kinase," *Virology*, vol. 263, no. 2, pp. 307–312, 1999.

[2] P. Blanchette, Y. C. Chi, Q. Yan et al., "Both BC-box motifs of adenovirus protein E4orf6 are required to efficiently assemble an E3 ligase complex that degrades p53," *Molecular and Cellular Biology*, vol. 24, no. 21, pp. 9619–9629, 2004.

[3] J. N. Harada, A. Shevchenko, A. Shevchenko, D. C. Pallas, and A. J. Berk, "Analysis of the adenovirus E1B-55K-anchored proteome reveals its link to ubiquitination machinery," *Journal of Virology*, vol. 76, no. 18, pp. 9194–9206, 2002.

[4] J. L. Woo and A. J. Berk, "Adenovirus ubiquitin-protein ligase stimulates viral late mRNA nuclear export," *Journal of Virology*, vol. 81, no. 2, pp. 575–587, 2007.

[5] T. H. Stracker, C. T. Carson, and M. D. Weilzman, "Adenovirus oncoproteins inactivate the Mre11-Rad50-NBs1 DNA repair complex," *Nature*, vol. 418, no. 6895, pp. 348–352, 2002.

[6] S. Schreiner, P. Wimmer, and T. Dobner, "Adenovirus degradation of cellular proteins," *Future Microbiology*, vol. 7, no. 2, pp. 211–225, 2012.

[7] N. I. Orazio, C. M. Naeger, J. Karlseder, and M. D. Weitzman, "The adenovirus E1b55K/E4orf6 complex induces degradation of the bloom helicase during infection," *Journal of Virology*, vol. 85, no. 4, pp. 1887–1892, 2011.

[8] Y. Liu, A. Shevchenko, A. Shevchenko, and A. J. Berk, "Adenovirus exploits the cellular aggresome response to accelerate inactivation of the MRN complex," *Journal of Virology*, vol. 79, no. 22, pp. 14004–14016, 2005.

[9] F. Dallaire, P. Blanchette, P. Groitl, T. Dobner, and P. E. Branton, "Identification of integrin α3 as a new substrate of the adenovirus E4orf6/E1B 55-kilodalton E3 ubiquitin ligase complex," *Journal of Virology*, vol. 83, no. 11, pp. 5329–5338, 2009.

[10] N. A. Forrester, G. G. Sedgwick, A. Thomas et al., "Serotype-specific inactivation of the cellular DNA damage response during adenovirus infection," *Journal of Virology*, vol. 85, no. 5, pp. 2201–2211, 2011.

[11] S. Schreiner, C. Bürck, M. Glass et al., "Control of human adenovirus type 5 gene expression by cellular Daxx/ATRX chromatin-associated complexes," *Nucleic Acids Research*, vol. 41, no. 6, pp. 3532–3550, 2013.

[12] A. Gupta, S. Jha, D. A. Engel, D. A. Ornelles, and A. Dutta, "Tip60 degradation by adenovirus relieves transcriptional repression of viral transcriptional activator EIA," *Oncogene*, vol. 32, no. 42, pp. 5017–5025, 2013.

[13] P. Blanchette, K. Kindsmüller, P. Groitl et al., "Control of mRNA export by adenovirus E4orf6 and E1B55K proteins during productive infection requires E4orf6 ubiquitin ligase activity," *Journal of Virology*, vol. 82, no. 6, pp. 2642–2651, 2008.

[14] R. A. Schwartz, S. S. Lakdawala, H. D. Eshleman, M. R. Russell, C. T. Carson, and M. D. Weitzman, "Distinct requirements of adenovirus E1b55K protein for degradation of cellular substrates," *Journal of Virology*, vol. 82, no. 18, pp. 9043–9055, 2008.

[15] R. Gonzalez, W. Huang, R. Finnen, C. Bragg, and S. J. Flint, "Adenovirus E1B 55-kilodalton protein is required for both regulation of mRNA export and efficient entry into the late phase of infection in normal human fibroblasts," *Journal of Virology*, vol. 80, no. 2, pp. 964–974, 2006.

[16] F. M. Cardoso, S. E. M. Kato, W. Huang, S. J. Flint, and R. A. Gonzalez, "An early function of the adenoviral E1B 55 kDa protein is required for the nuclear relocalization of the cellular p53 protein in adenovirus-infected normal human cells," *Virology*, vol. 378, no. 2, pp. 339–346, 2008.

[17] J. G. Teodoro and P. E. Branton, "Regulation of p53-dependent apoptosis, transcriptional repression, and cell transformation

by phosphorylation of the 55-kilodalton E1B protein of human adenovirus type 5," *Journal of Virology*, vol. 71, no. 5, pp. 3620–3627, 1997.

[18] P. R. Yew and A. J. Berk, "Inhibition of p53 transactivation required for transformation by adenovirus early 1B protein," *Nature*, vol. 357, no. 6373, pp. 82–85, 1992.

[19] M. D. Weitzman and D. A. Ornelles, "Inactivating intracellular antiviral responses during adenovirus infection," *Oncogene*, vol. 24, no. 52, pp. 7686–7696, 2005.

[20] M. D. Weiden and H. S. Ginsberg, "Deletion of the E4 region of the genome produces adenovirus DNA concatemers," *Proceedings of the National Academy of Sciences of the United States of America*, vol. 91, no. 1, pp. 153–157, 1994.

[21] S. S. Lakdawala, R. A. Schwartz, K. Ferenchak et al., "Differential requirements of the C terminus of Nbs1 in suppressing adenovirus DNA replication and promoting concatemer formation," *Journal of Virology*, vol. 82, no. 17, pp. 8362–8372, 2008.

[22] J. D. Evans and P. Hearing, "Distinct roles of the adenovirus E4 ORF3 protein in viral DNA replication and inhibition of genome concatenation," *Journal of Virology*, vol. 77, no. 9, pp. 5295–5304, 2003.

[23] J. D. Evans and P. Hearing, "Relocalization of the Mre11-Rad50-Nbs1 complex by the adenovirus E4 ORF3 protein is required for viral replication," *Journal of Virology*, vol. 79, no. 10, pp. 6207–6215, 2005.

[24] K. A. Karen, P. J. Hoey, C. S. H. Young, and P. Hearing, "Temporal regulation of the Mre11-Rad50-Nbs1 complex during adenovirus infection," *Journal of Virology*, vol. 83, no. 9, pp. 4565–4573, 2009.

[25] V. Doucas, A. M. Ishov, A. Romo et al., "Adenovirus replication is coupled with the dynamic properties of the PML nuclear structure," *Genes and Development*, vol. 10, no. 2, pp. 196–207, 1996.

[26] K. N. Leppard and R. D. Everett, "The adenovirus type 5 E1b 55K and E4 Orf3 proteins associate in infected cells and affect ND10 components," *Journal of General Virology*, vol. 80, part 4, pp. 997–1008, 1999.

[27] F. D. Araujo, T. H. Stracker, C. T. Carson, D. V. Lee, and M. D. Weitzman, "Adenovirus type 5 E4orf3 protein targets the Mre11 complex to cytoplasmic aggresomes," *Journal of Virology*, vol. 79, no. 17, pp. 11382–11391, 2005.

[28] A. Hoppe, S. J. Beech, J. Dimmock, and K. N. Leppard, "Interaction of the adenovirus type 5 E4 Orf3 protein with promyelocytic leukemia protein isoform II is required for ND10 disruption," *Journal of Virology*, vol. 80, no. 6, pp. 3042–3049, 2006.

[29] K. N. Leppard, E. Emmott, M. S. Cortese, and T. Rich, "Adenovirus type 5 E4 Orf3 protein targets promyelocytic leukaemia (PML) protein nuclear domains for disruption via a sequence in PML isoform II that is predicted as a protein interaction site by bioinformatic analysis," *Journal of General Virology*, vol. 90, part 1, pp. 95–104, 2009.

[30] J.-S. Seeler and A. Dejean, "Sumo: of branched proteins and nuclear bodies," *Oncogene*, vol. 20, no. 49, pp. 7243–7249, 2001.

[31] R. Bernardi and P. P. Pandolfi, "Structure, dynamics and functions of promyelocytic leukaemia nuclear bodies," *Nature Reviews Molecular Cell Biology*, vol. 8, no. 12, pp. 1006–1016, 2007.

[32] V. Lallemand-Breitenbach and H. de Thé, "PML nuclear bodies," *Cold Spring Harbor Perspectives in Biology*, vol. 2, no. 5, Article ID a000661, 2010.

[33] M. Lang, T. Jegou, I. Chung et al., "Three-dimensional organization of promyelocytic leukemia nuclear bodies," *Journal of Cell Science*, vol. 123, part 3, pp. 392–400, 2010.

[34] S. Zhong, P. Salomoni, and P. P. Pandolfi, "The transcription role of PML and the nuclear body," *Nature Cell Biology*, vol. 2, no. 5, pp. E85–E90, 2000.

[35] P. Brand, T. Lenser, and P. Hemmerich, "Assembly dynamics of PML nuclear bodies in living cells," *PMC Biophysics*, vol. 3, no. 1, article 3, 2010.

[36] E. van Damme, K. Laukens, T. H. Dang, and X. van Ostade, "A manually curated network of the pml nuclear body interactome reveals an important role for PML-NBs in SUMOylation dynamics," *International Journal of Biological Sciences*, vol. 6, no. 1, pp. 51–67, 2010.

[37] P. Heun, "SUMOrganization of the nucleus," *Current Opinion in Cell Biology*, vol. 19, no. 3, pp. 350–355, 2007.

[38] B. Liu and K. Shuai, "Regulation of the sumoylation system in gene expression," *Current Opinion in Cell Biology*, vol. 20, no. 3, pp. 288–293, 2008.

[39] R. Jürgen Dohmen, "SUMO protein modification," *Biochimica et Biophysica Acta—Molecular Cell Research*, vol. 1695, no. 1—3, pp. 113–131, 2004.

[40] A. M. Andreou and N. Tavernarakis, "SUMOylation and cell signalling," *Biotechnology Journal*, vol. 4, no. 12, pp. 1740–1752, 2009.

[41] Z. Hannoun, S. Greenhough, E. Jaffray, R. T. Hay, and D. C. Hay, "Post-translational modification by SUMO," *Toxicology*, vol. 278, no. 3, pp. 288–293, 2010.

[42] J. Schimmel, K. M. Larsen, I. Matic et al., "The ubiquitin-proteasome system is a key component of the SUMO-2/3 cycle," *Molecular and Cellular Proteomics*, vol. 7, no. 11, pp. 2107–2122, 2008.

[43] M. H. Tatham, E. Jaffray, O. A. Vaughan et al., "Polymeric chains of SUMO-2 and SUMO-3 are conjugated to protein substrates by SAE1/SAE2 and Ubc9," *Journal of Biological Chemistry*, vol. 276, no. 38, pp. 35368–35374, 2001.

[44] I. Matic, M. van Hagen, J. Schimmel et al., "In vivo identification of human small ubiquitin-like modifier polymerization sites by high accuracy mass spectrometry and an in vitro to in vivo strategy," *Molecular and Cellular Proteomics*, vol. 7, no. 1, pp. 132–144, 2008.

[45] A. C. O. Vertegaal, "Small ubiquitin-related modifiers in chains," *Biochemical Society Transactions*, vol. 35, part 6, pp. 1422–1423, 2007.

[46] T. Hunter and H. Sun, "Crosstalk between the SUMO and ubiquitin pathways," *Ernst Schering Foundation symposium proceedings*, no. 1, pp. 1–16, 2008.

[47] A. Denuc and G. Marfany, "SUMO and ubiquitin paths converge," *Biochemical Society Transactions*, vol. 38, part 1, pp. 34–39, 2010.

[48] G. J. K. Praefcke, K. Hofmann, and R. J. Dohmen, "SUMO playing tag with ubiquitin," *Trends in Biochemical Sciences*, vol. 37, no. 1, pp. 23–31, 2012.

[49] P. Wimmer, P. Blanchette, S. Schreiner et al., "Cross-talk between phosphorylation and SUMOylation regulates transforming activities of an adenoviral oncoprotein," *Oncogene*, vol. 32, no. 13, pp. 1626–1637, 2013.

[50] P. Wimmer, S. Schreiner, and T. Dobner, "Human pathogens and the host cell sumoylation system," *Journal of Virology*, vol. 86, no. 2, pp. 642–654, 2012.

[51] C. Endter, J. Kzhyshkowska, R. Stauber, and T. Dobner, "SUMO-1 modification required for transformation by adenovirus type 5 early region 1B 55-kDa oncoprotein," *Proceedings of the National Academy of Sciences of the United States of America*, vol. 98, no. 20, pp. 11312–11317, 2001.

[52] K. J. Lethbridge, G. E. Scott, and K. N. Leppard, "Nuclear matrix localization and SUMO-1 modification of adenovirus type 5 E1b 55K protein are controlled by E4 Orf6 protein," *Journal of General Virology*, vol. 84, part 2, pp. 259–268, 2003.

[53] K. Kindsmüller, P. Groitl, B. Härtl, P. Blanchette, J. Hauber, and T. Dobner, "Intranuclear targeting and nuclear export of the adenovirus E1B-55K protein are regulated by SUMO1 conjugation," *Proceedings of the National Academy of Sciences of the United States of America*, vol. 104, no. 16, pp. 6684–6689, 2007.

[54] S. Muller and T. Dobner, "The adenovirus E1B-55K oncoprotein induces SUMO modification of p53," *Cell Cycle*, vol. 7, no. 6, pp. 754–758, 2008.

[55] M. A. Pennella, Y. Liu, J. L. Woo, C. A. Kim, and A. J. Berk, "Adenovirus E1B 55-kilodalton protein is a p53-SUMO1 E3 ligase that represses p53 and stimulates its nuclear export through interactions with promyelocytic leukemia nuclear bodies," *Journal of Virology*, vol. 84, no. 23, pp. 12210–12225, 2010.

[56] S. Y. Sohn and P. Hearing, "Adenovirus regulates sumoylation of Mre11-Rad50-Nbs1 components through a paralog-specific mechanism," *Journal of Virology*, vol. 86, no. 18, pp. 9656–9665, 2012.

[57] P. R. Yew, C. C. Kao, and A. J. Berk, "Dissection of functional domains in the adenovirus 2 early 1B 55K polypeptide by suppressor-linked insertional mutagenesis," *Virology*, vol. 179, no. 2, pp. 795–805, 1990.

[58] T. Harrison, F. Graham, and J. Williams, "Host range mutants of adenovirus type 5 defective for growth in HeLa cells," *Virology*, vol. 77, no. 1, pp. 319–329, 1977.

[59] B. Härtl, T. Zeller, P. Blanchette, E. Kremmer, and T. Dobner, "Adenovirus type 5 early region 1B 55-kDa oncoprotein can promote cell transformation by a mechanism independent from blocking p53-activated transcription," *Oncogene*, vol. 27, no. 26, pp. 3673–3684, 2008.

[60] A. J. Bett, V. Krougliak, and F. L. Graham, "DNA sequence of the deletion/insertion in early region 3 of Ad5 dl309," *Virus Research*, vol. 39, no. 1, pp. 75–82, 1995.

[61] J. F. Williams, "Oncogenic transformation of hamster embryo cells in vitro by adenovirus type 5," *Nature*, vol. 243, no. 5403, pp. 162–163, 1973.

[62] K. Kindsmüller, S. Schreiner, F. Leinenkugel, P. Groitl, E. Kremmer, and T. Dobner, "A 49-kilodalton isoform of the adenovirus type 5 early region 1B 55-kilodalton protein is sufficient to support virus replication," *Journal of Virology*, vol. 83, no. 18, pp. 9045–9056, 2009.

[63] P. Groitl and T. Dobner, "Construction of adenovirus type 5 early region 1 and 4 virus mutants," *Methods in molecular medicine*, vol. 130, pp. 29–39, 2007.

[64] P. Sarnow, P. Hearing, and C. W. Anderson, "Adenovirus early region 1B 58,000-dalton tumor antigen is physically associated with an early region 4 25,000-dalton protein in productively infected cells," *Journal of Virology*, vol. 49, no. 3, pp. 692–700, 1984.

[65] C. C. Kao, P. R. Yew, and A. J. Berk, "Domains required for in vitro association between the cellular p53 and the adenovirus 2 E1 B 55K proteins," *Virology*, vol. 179, no. 2, pp. 806–814, 1990.

[66] M. J. Marton, S. B. Baim, D. A. Ornelles, and T. Shenk, "The adenovirus E4 17-kilodalton protein complexes with the cellular transcription factor E2F, altering its DNA-binding properties and stimulating E1A-independent accumulation of E2 mRNA," *Journal of Virology*, vol. 64, no. 5, pp. 2345–2359, 1990.

[67] M. Nevels, B. Täuber, E. Kremmer, T. Spruss, H. Wolf, and T. Dobner, "Transforming potential of the adenovirus type 5 E4orf3 protein," *Journal of Virology*, vol. 73, no. 2, pp. 1591–1600, 1999.

[68] R. A. Gonzalez and S. J. Flint, "Effects of mutations in the adenoviral E1B 55-kilodalton protein coding sequence on viral late mRNA metabolism," *Journal of Virology*, vol. 76, no. 9, pp. 4507–4519, 2002.

[69] U. K. Laemmli, "Cleavage of structural proteins during the assembly of the head of bacteriophage T4," *Nature*, vol. 227, no. 5259, pp. 680–685, 1970.

[70] M. Nevels, B. Täuber, T. Spruss, H. Wolf, and T. Dobner, "'Hit-and-run' transformation by adenovirus oncogenes," *Journal of Virology*, vol. 75, no. 7, pp. 3089–3094, 2001.

[71] T. H. Stracker, D. V. Lee, C. T. Carson, F. D. Araujo, D. A. Ornelles, and M. D. Weitzman, "Serotype-specific reorganization of the Mre11 complex by adenoviral E4orf3 proteins," *Journal of Virology*, vol. 79, no. 11, pp. 6664–6673, 2005.

[72] S. Rubenwolf, H. Schütt, M. Nevels, H. Wolf, and T. Dobner, "Structural analysis of the adenovirus type 5 E1B 55-kilodalton-E4orf6 protein complex," *Journal of Virology*, vol. 71, no. 2, pp. 1115–1123, 1997.

[73] P. Wimmer, S. Schreiner, R. D. Everett, H. Sirma, P. Groitl, and T. Dobner, "SUMO modification of E1B-55K oncoprotein regulates isoform-specific binding to the tumour suppressor protein PML," *Oncogene*, vol. 29, no. 40, pp. 5511–5522, 2010.

[74] P. Blanchette, P. Wimmer, F. Dallaire, C. Y. Cheng, and P. E. Branton, "Aggresome formation by the adenoviral protein E1B55K is not conserved among adenovirus species and is not required for efficient degradation of nuclear substrates," *Journal of Virology*, vol. 87, no. 9, pp. 4872–4881, 2013.

[75] S. Schreiner, P. Wimmer, P. Groitl et al., "Adenovirus type 5 early region 1B 55K oncoprotein-dependent degradation of cellular factor Daxx is required for efficient transformation of primary rodent cells," *Journal of Virology*, vol. 85, no. 17, pp. 8752–8765, 2011.

[76] M. Schmid, K. Kindsmüller, P. Wimmer, P. Groitl, R. A. Gonzalez, and T. Dobner, "The E3 ubiquitin ligase activity associated with the adenoviral E1B-55K-E4orf6 complex does not require CRM1-dependent export," *Journal of Virology*, vol. 85, no. 14, pp. 7081–7094, 2011.

[77] C. Oberle and C. Blattner, "Regulation of the DNA damage response to DSBs by post-translational modifications," *Current Genomics*, vol. 11, no. 3, pp. 184–198, 2010.

[78] C. H. Eskiw, G. Dellaire, and D. P. Bazett-Jones, "Chromatin contributes to structural integrity of promyelocytic leukemia bodies through a SUMO-1-independent mechanism," *Journal of Biological Chemistry*, vol. 279, no. 10, pp. 9577–9585, 2004.

[79] G. Dellaire, R. W. Ching, K. Ahmed et al., "Promyelocytic leukemia nuclear bodies behave as DNA damage sensors whose response to DNA double-strand breaks is regulated by NBS1 and the kinases ATM, Chk2, and ATR," *Journal of Cell Biology*, vol. 175, no. 1, pp. 55–66, 2006.

[80] S. Bergink and S. Jentsch, "Principles of ubiquitin and SUMO modifications in DNA repair," *Nature*, vol. 458, no. 7237, pp. 461–467, 2009.

[81] M. P. Stokes, J. Rush, J. MacNeill et al., "Profiling of UV-induced ATM/ATR signaling pathways," *Proceedings of the National Academy of Sciences of the United States of America*, vol. 104, no. 50, pp. 19855–19860, 2007.

[82] M. di Virgilio, C. Y. Ying, and J. Gautier, "PIKK-dependent phosphorylation of Mre11 induces MRN complex inactivation by disassembly from chromatin," *DNA Repair*, vol. 8, no. 11, pp. 1311–1320, 2009.

[83] H. Takemura, V. A. Rao, O. Sordet et al., "Defective Mre11-dependent activation of Chk2 by ataxia telangiectasia mutated in colorectal carcinoma cells in response to replication-dependent DNA double strand breaks," *Journal of Biological Chemistry*, vol. 281, no. 41, pp. 30814–30823, 2006.

[84] P. Langerak and P. Russell, "Regulatory networks integrating cell cycle control with DNA damage checkpoints and double-strand break repair," *Philosophical Transactions of the Royal Society B: Biological Sciences*, vol. 366, no. 1584, pp. 3562–3571, 2011.

[85] F.-M. Boisvert, U. Déry, J.-Y. Masson, and S. Richard, "Arginine methylation of MRE11 by PRMT1 is required for DNA damage checkpoint control," *Genes and Development*, vol. 19, no. 6, pp. 671–676, 2005.

[86] F.-M. Boisvert, M. J. Hendzel, J.-Y. Masson, and S. Richard, "Methylation of MRE11 regulates its nuclear compartmentalization," *Cell Cycle*, vol. 4, no. 7, pp. 981–989, 2005.

[87] G. J. Williams, S. P. Lees-Miller, and J. A. Tainer, "Mre11-Rad50-Nbs1 conformations and the control of sensing, signaling, and effector responses at DNA double-strand breaks," *DNA Repair*, vol. 9, no. 12, pp. 1299–1306, 2010.

[88] G. Dellaire, R. Kepkay, and D. P. Bazett-Jones, "High resolution imaging of changes in the structure and spatial organization of chromatin, γ-H2A.X and the MRN complex within etoposide-induced DNA repair foci," *Cell Cycle*, vol. 8, no. 22, pp. 3750–3769, 2009.

[89] C. A. Cremona, P. Sarangi, Y. Yang, L. E. Hang, S. Rahman, and X. Zhao, "Extensive DNA damage-induced sumoylation contributes to replication and repair and acts in addition to the Mec1 checkpoint," *Molecular Cell*, vol. 45, no. 3, pp. 422–432, 2012.

[90] Y. Xue, F. Zhou, C. Fu, Y. Xu, and X. Yao, "SUMOsp: a web server for sumoylation site prediction," *Nucleic Acids Research*, vol. 34, pp. W254–W257, 2006.

[91] A. J. Berk, "Recent lessons in gene expression, cell cycle control, and cell biology from adenovirus," *Oncogene*, vol. 24, no. 52, pp. 7673–7685, 2005.

[92] C. Y. Cheng, T. Gilson, P. Wimmer et al., "The role of E1B55K in E4orf6/E1B55K E3 ligase complexes formed by different human adenovirus serotypes," *Journal of Virology*, vol. 87, no. 11, pp. 6232–6245, 2013.

[93] S. Schreiner, P. Wimmer, H. Sirma et al., "Proteasome-dependent degradation of Daxx by the viral E1B-55K protein in human adenovirus-infected cells," *Journal of Virology*, vol. 84, no. 14, pp. 7029–7038, 2010.

[94] N. A. Forrester, R. N. Patel, T. Speiseder et al., "Adenovirus E4orf3 targets transcriptional intermediary factor 1 for proteasome-dependent degradation during infection," *Journal of Virology*, vol. 86, no. 6, pp. 3167–3179, 2012.

[95] A. F. Yousef, G. J. Fonseca, P. Pelka et al., "Identification of a molecular recognition feature in the E1A oncoprotein that binds the SUMO conjugase UBC9 and likely interferes with polySUMOylation," *Oncogene*, vol. 29, no. 33, pp. 4693–4704, 2010.

Video Article

Isolation of Viral Replication Compartment-enriched Sub-nuclear Fractions from Adenovirus-infected Normal Human Cells

Paloma Hidalgo[1,2], Ramón A. Gonzalez[1]

[1]Centro de Investigación en Dinámica Celular, Instituto de Investigación en Ciencias Básicas y Aplicadas, Universidad Autónoma del Estado de Morelos

[2]Instituto de Biotecnologìa, Universidad Nacional Autónoma de México

Correspondence to: Ramón A. Gonzalez at rgonzalez@uaem.mx

Abstract

During infection of human cells by adenovirus (Ad), the host cell nucleus is dramatically reorganized, leading to formation of nuclear microenvironments through the recruitment of viral and cellular proteins to sites occupied by the viral genome. These sites, called replication compartments (RC), can be considered viral-induced nuclear domains where the viral genome is localized and viral and cellular proteins that participate in replication, transcription and post-transcriptional processing are recruited. Moreover, cellular proteins involved in the antiviral response, such as tumor suppressor proteins, DNA damage response (DDR) components and innate immune response factors are also co-opted to RC. Although RC seem to play a crucial role to promote an efficient and productive replication cycle, a detailed analysis of their composition and associated activities has not been made. To facilitate the study of adenoviral RC and potentially those from other DNA viruses that replicate in the cell nucleus, we adapted a simple procedure based on velocity gradients to isolate Ad RC and established a cell-free system amenable to conduct morphological, functional and compositional studies of these virus-induced subnuclear structures, as well as to study their impact on host-cell interactions.

Video Link

The video component of this article can be found at http://www.jove.com/video/53296/

Introduction

Adenoviruses contain a double-stranded DNA genome that replicates in the infected cell nucleus. When the viral DNA enters the nucleus, it localizes adjacent to PML nuclear bodies[1]. Following viral early gene expression, the nuclear architecture is dramatically reorganized, inducing formation of viral microenvironments, termed viral Replication Compartments (RC)[2]. Since adenovirus (Ad) RC are sites where viral genome replication and expression of viral late genes take place, they provide an environment for recruitment of all the necessary viral and cellular factors that participate in these processes. Interestingly, a variety of cellular proteins responsible for the cellular antiviral response, such as the DNA damage response, the innate immune response and tumor suppression are co-opted to these viral sites[2]. Hence, Ad RC can be considered regulatory hubs that promote efficient viral replication while concomitantly regulating the cellular antiviral response, indicating that these structures are key to the understanding of virus-host cell interactions. Nevertheless, the molecular mechanisms of RC formation, their composition and associated activities are poorly understood.

Adenoviral RC, as well as RC from other DNA viruses that replicate in the nucleus are not associated to membranes, in contrast to cytoplasmic RC[3]. Moreover, these virus-induced structures are likely to be composed entirely of proteins and nucleic acids. RC formed in cells infected with RNA viruses (usually termed viral factories) have been isolated, taking advantage of their cytoplasmic localization and membrane-bound status, which has facilitated their detailed morphological, functional and biochemical characterization[4].

To our knowledge, nuclear viral RC have not been isolated, perhaps due to the complexity of the nuclear architecture and absence of intranuclear membranes that would facilitate their isolation. Their study has relied instead on immunofluorescence microscopy, FISH and transmission electron microscopy. However, despite complications inherent to isolating subnuclear structures, other nuclear domains such as nucleoli and Cajal Bodies have been isolated before [5,6]. Since nucleoli and RC are both composed of proteins and nucleic acids, and have a diameter between 0.5 - 5 µm, we hypothesized that RC should also be amenable to isolation. Therefore, in order to more precisely characterize the molecular composition and functions associated to RC, we established a novel method to isolate subnuclear fractions enriched with RC. To this end, we prepared sub-nuclear fractions using velocity gradients and sucrose cushions similar to procedures used to isolate nucleoli[7] or other nuclear domains[6] and established a cell-free system that allows the study of the molecular composition and associated activities of RC. This technique should therefore advance the understanding of virus-host cell interactions and represents a powerful tool that should also facilitate the detailed analysis of RC from other viruses that replicate in the nucleus and induce formation of replication compartments of similar dimensions to those formed in adenovirus-infected-cells, such as, herpesviruses, papillomaviruses or polyomaviruses.

Protocol

1. HFF Cell Culture and Ad-infection

1. Propagate Ad5 WT virus in monolayers of HEK-293 cells and titer as fluorescent forming units (FFU) on HFF cells as described previously[8].
2. Grow Human Foreskin fibroblasts (HFF) in 10 ml of DMEM/10% Fetal Bovine Serum (FBS) in sterile culture 100 mm dishes at 37 °C and 5% CO_2 in a humidified incubator. Determine the cell number using a Neubauer chamber by counting cells in the four 16-square sets. The cell number per ml is obtained by calculating the average number of cells in the four 16-square sets and multiplying this number by 10^4. For each time post-infection included in step 1.3, use 1×10^7 HFF cells.
3. Mock-infect or infect HFF cells with adenovirus type 5 (Ad5) wild-type (WT) (H5pg4100[8]) in 100 mm tissue culture dishes using 1 ml of Ad5 in DMEM per dish at an MOI of 30 Focus Forming Unit, or FFU, per cell. Incubate for 2 hr in a humidified cell culture incubator at 37 °C and 5% CO_2, carefully rocking the dishes every 15 min to ensure homogeneous distribution of the virus inoculum over the cells. After this time, remove the medium and add fresh DMEM supplemented with 10% FBS and incubate for 16, 24 or 36 hr in a humidified cell culture incubator at 37 °C and 5% CO_2. Proceed to step 2.1.

2. Preparation of Sub-nuclear Fractions Enriched with Adenovirus RC

1. Harvest Ad5-infected or mock-infected HFF cells with a cell scrapper and collect the cells in sterile centrifuge tubes. Determine the cell number as in step 1.2. Use 1×10^7 cells for each time post-infection specified in step 1.3.
2. Centrifuge the cells at 220 x g, 4 °C for 5 min.
3. Resuspend the cell pellet in ice-cold PBS (137 mM NaCl, 2.7 mM KCl, 10 mM Na_2HPO_4 and 1.8 mM KH_2PO_4). Wash cell pellets 3 times using 5 ml of ice-cold PBS per wash. For this purpose, centrifuge the cells at 220 x g, 4 °C for 5 min, decant and discard the supernatant (SN), and resuspend the cell pellet by gentle pipetting.
4. To disrupt the plasma membrane, resuspend the cell pellet in 700 µl of ice-cold hypotonic buffer (10 mM HEPES pH 7.9, 10 mM KCl, 1.5 mM $MgCl_2$, 0.5 mM DTT, 20 µg/ml phenylmethylsulfonyl fluoride (PMSF), a mixture of cysteine, serine, threonine and aspartyl protease inhibitors including 10 µg/ml bovine pancreatic trypsin inhibitor, 10 µg/ml pepstatin A and 10 µg/ml N-acetyl-L-leucyl-L-leucyl-L-argininal) and let the cells swell on ice for 3 hr.
5. Lyse the cells using a homogenizer with a loose-fitting A type teflon pestle. Perform 80 dounce strokes and monitor samples every 20 strokes by bright field microscopy to ensure that all cells have been lysed, but that nuclei have not been damaged or ruptured.
6. Centrifuge the cell homogenate at 300 x g, 4 °C for 5 min. Store the SN as the cytoplasmic fraction at -20 °C in a centrifuge tube.
7. To remove cellular debris from nuclei, resuspend the pellet in 750 µl of solution 1 (S1) (0.25 M sucrose, 10 mM $MgCl_2$ 20 µg/ml PMSF, a mixture of cysteine, serine, threonine and aspartyl protease inhibitors including 10 µg/ml bovine pancreatic trypsin inhibitor, 10 µg/ml pepstatin A and 10 µg/ml N-acetyl-L-leucyl-L-leucyl-L-argininal) and layer over an equal volume of solution 2 (S2) (0.35 M sucrose, 0.5 mM $MgCl_2$, 20 µg/ml PMSF, a mixture of cysteine, serine, threonine and aspartyl protease inhibitors including 10 µg/ml bovine pancreatic trypsin inhibitor, 10 µg/ml pepstatin A and 10 µg/ml N-acetyl-L-leucyl-L-leucyl-L-argininal). Centrifuge at 1,400 x g, 4 °C for 5 min.
8. Discard the SN using a micropipette. Avoid disturbing the pellet.
9. Resuspend the pellet containing isolated nuclei in 750 µl of S2.
10. To isolate subnuclear fractions enriched with adenovirus RC (RCf), sonicate resuspended nuclei with an ultrasonic bath, using two 5 min pulses, or until all nuclei are lysed as observed by bright field microscopy. Use ice in ultrasonic bath as needed to keep samples at or below 4 °C.
11. Layer the sonicated nuclei over an equal volume of solution 3 (S3) (0.88 M sucrose, 0.5 mM $MgCl_2$) and centrifuge at 3,000 x g, 4 °C for 10 min. Store the 1.5 ml supernatant as the nucleoplasmic fraction (Npl) at -70 °C. Resuspend the pellet in 700 µl of S2 and store as RCf at -70 °C.

3. Western Blot Analyses of RCf

NOTE: For Western Blot analysis of Npl and RCf fractions set aside 640 µl for Npl and 300 µl for RCf from the total volume obtained in step 2.11.

1. Mix 15 µl of each subnuclear fraction in Laemmli buffer 2x (4% SDS, 20% glycerol, 10% 2-mercaptoethanol, 0.004% bromophenol blue, 0.125 M Tris HCl pH 6.8) and boil at 95 °C for 5 min. Load the samples in a 10% sodium dodecyl sulfate-polyacrylamide gel electrophoresis (SDS-PAGE) denaturing gel and separate proteins for 1.5 hr, at 20 milliamperes (mA).
2. Transfer proteins by electroblotting for 1.5 hr at 400 mA onto polyvinylidene difluoride (PVDF) membranes.
3. Block membrane for 2 hr at RT using 3% nonfat dry milk in PBS.
4. Incubate O/N at 4 °C with primary antibody against viral E2A DNA-binding protein (B6-8[9]) at a 1:500 dilution in PBS/0.3% nonfat dry milk.
5. Wash membrane 3 times with PBS/0.1% Tween 20 for 10 min.
6. Incubate the membrane with mouse anti IgG secondary antibody coupled to horse-radish peroxidase (HRP) at a 1:10,000 dilution in PBS for 2 hr at RT.
7. Wash the membrane 3 times with PBS/0.1% Tween 20 for 10 min.
8. Develop the membrane using enhanced chemiluminescence and X-ray films.

4. Viral DNA Detection in RCf

NOTE: For DNA isolation from both Npl and RCf fractions, use 210 µl for Npl and 100 µl for RCf of the total volume obtained in step 2.11.

1. Incubate sub-nuclear fractions for 1 hr at 55 ºC with 1 mg/ml of proteinase K and 0.5% Tween 20.
2. Inactivate proteinase K by incubating the samples for 10 min at 95 °C.
3. Centrifuge the samples at 20,000 x g, at RT for 2 min.
4. Collect the SN. Precipitate the DNA with 1/10 volume of 3M sodium acetate and one volume of isopropanol, O/N at 4 °C.
5. Centrifuge the samples at 20,000 x g, at RT for 10 min.
6. Discard the SN using a micropipette. Wash the pellet with 70% ethanol and centrifuge at 20,000 x g, 4 °C for 5 min.
7. Resuspend the DNA in 10 μl of 10 mM Tris-HCl pH 7.4
8. Quantify DNA using a spectrophotometer by measuring the optical density (OD) at 260 nm.
9. To amplify viral DNA, use 100 ng of DNA from each subnuclear fraction in a standard PCR reaction using Taq DNA polymerase in 25 μl of reaction volume with primers that allow the amplification of a region within the Major Late transcription unit, from nucleotide 7273 to nucleotide 7353 (81 bp) (Fw: GAGCGAGGTGTGGGTGAGC; Rv: GGATGCGACGACACTGACTTCA). Use the following cycle conditions: Initial denaturation for 3 min at 95 ºC, followed by 20 cycles of amplification (1 min at 95 ºC, annealing for 1 min at 62 ºC and extension for 30 sec at 72 ºC) and a final extension step for 3 min at 72 ºC.
10. Run the PCR product in 2% agarose gels, at 90 V. Stain with ethidium bromide at 0.5 μg/ml final concentration and visualize DNA to corroborate viral DNA enrichment in the RCf. Handle ethidium bromide with extreme caution and always make sure to wear gloves, as this compound is a potent mutagen. Dispose ethidium bromide according to institutional guidelines.

5. Late Viral mRNA Detection in RCf

NOTE: For RNA isolation from both Npl and RCf fractions, use 640 μl for Npl and 300 μl for RCf from the total volume obtained in step 2.11.

1. Isolate RNA from subnuclear fractions using Trizol according with the manufacturer's instructions. Resuspend the RNA in 50 μl of DEPC (diethilpyrocarbonate)-treated water.
2. Quantify the RNA using a spectrophotometer to measure the OD at 260 nm (approximately 3 μg are obtained). Store the RNA in 50 ng/μl aliquots at -70 ºC.
3. Check purified RNA for the absence of DNA contamination by performing a control PCR reaction in the absence of reverse transcriptase (RT), using 5 ng of total RNA and the cycle conditions described in step 4.9.
    1. If DNA contamination is absent no amplicon should be produced. If DNA contamination is present, incubate the samples with 10 U DNase I, 10 U of Rnase inhibitor, 0.1 M Tris-HCl pH 8.3, 0.5 M KCl and 15 mM MgCl$_2$ for 30 min at 37 ºC. Proceed to re-isolate RNA as in step 5.1.
4. To analyze viral mRNA associated to RCf, amplify 100 ng of RNA from each subnuclear fraction by RT-PCR using primers designed to detect adenoviral late mRNA from different gene families (**Table 1**).
    1. For reverse transcription (RT), use 100 ng of RNA, from each subnuclear fraction in a standard RT reaction using M-MuLV RT enzyme in 20 μl of reaction volume for 1 hr at 42 ºC and 10 min at 70 ºC.
    2. For amplification, use 1 μl of the cDNA in PCR reactions, as in step 4.9. Use the following cycle conditions: Initial denaturation for 3 min at 95 ºC, followed by 25 cycles of amplification (1 min at 95 ºC, annealing for 1 min at the temperature specified in **Table 1** and extension for 30 sec at 72 ºC) and a final extension step for 3 min at 72 ºC.
5. Run the RT-PCR products in 2% agarose gels, at 90 V. Stain gels with ethidium bromide at 0.5 μg/ml final concentration and visualize to corroborate viral late mRNA association to the RCf. Handle ethidium bromide as indicated in step 4.10.

6. Immunofluorescence Visualization of RCf

NOTE: Carry-out this procedure under a laminar flow cabinet to avoid contamination of the samples with any dust particles, and filter all solutions before use.

1. Spot 5 μl of the RCf fraction obtained in step 2.10 directly on a silane-coated slide.
2. Let the spot dry for about 5 min at RT.
3. Re-hydrate by slowly and indirectly pipetting 500 μl of PBS in a drop beside the RCf spot and letting it flow by tilting the slide. Drain off the excess PBS from the side.
4. Block by covering the sample with 500 μl of PBS/5% bovine serum albumin (BSA) for 2 hr at RT.
5. Wash the slide 3 times by gently and indirectly pipetting 500 μl of PBS onto the sample. Tilt the slide to drain off the excess PBS.
6. Incubate the sample with primary antibody against viral E2A DNA-binding protein (B6-8[9]) at a 1:500 dilution in PBS for 2 hr at RT. Cover the spotted sample with 20 μl of the antibody solution and incubate in a humid chamber to avoid drying.
7. Wash the sample 3 times with PBS/0.02% Tween 20 by gently and indirectly pipetting 500 μl of PBS onto the sample. Tilt the slide to drain off the excess wash solution.
8. Incubate the samples with mouse anti IgG secondary antibody coupled to a fluorophore that is excited at 488 nm at a 1:2,000 dilution in PBS, for 1 hr at 4 ºC. Cover the spotted sample with 20 μl of the antibody solution and incubate in a humid chamber to avoid drying.
9. Wash the sample 3 times with PBS/0.02% Tween 20 by gently and indirectly pipetting 500 μl of PBS onto the sample. Tilt the slide to drain off the excess wash solution.
10. Cover the spotted sample on the slide with a coverslip using 2 μl PBS/10% glycerol as mounting medium. Seal with clear nail polish and store al -20 ºC.
11. Analyze the samples using a fluorescence microscope, with a 63x objective and a 1.4 Numeric Aperture (NA) at a wavelength of 488 nm.

Representative Results

Since viral replication compartments (RC) are subnuclear viral-induced structures composed of proteins and nucleic acids, similar to other nuclear domains, they proved to be amenable to isolation by velocity gradients based on biochemical features. Critical steps in the fractionation protocol are illustrated in **Figure 1.** At each step the samples need to be monitored by bright field microscopy to ensure integrity of the different sub-cellular fractions. For example, when swelling the cells, incubation time in the hypotonic buffer needs to be standardized in order to swell the cytoplasm avoiding damage to the nuclei. After cell homogenization, intact nuclei, free of cytoplasmic components including endoplasmic reticulum membranes, need to be obtained. Also, sonication time needs to be standardized in order to rupture the nuclear membrane of all cells without disrupting RC.

After obtaining the sub-nuclear fractions, key controls need to be included to determine the association and enrichment of *bona fide* RC markers in the RCf. Adenoviral RC are commonly visualized in infected cells by immunofluorescence using antibodies against the viral E2A-72K protein (DBP). DBP is a viral protein that participates directly in viral genome replication; therefore, the presence of DBP in particles enriched in the RCf demonstrates the direct association of this viral protein with the isolated particles, as shown in **Figure 1**. Furthermore, detection of DBP in RCf by Western Blot confirms the association of this protein to the isolated RC. In **Figure 2** it is shown that by late times post-infection (36 hpi), DBP is enriched in the RCf compared to the nucleoplasmic fraction (Npl), demonstrating that RC obtained with this procedure at different times post-infection reflect the expected temporal pattern of DBP association to RC. An essential viral component of RC is the viral DNA itself. In experiments like that shown in **Figure 3** we demonstrate that increasing amounts of viral DNA associate with RCf as the replication cycle of the virus progresses, indicating that, as for DBP, the temporal pattern of DNA replication in these fractions can also be studied.

Besides containing viral proteins and the viral genome, RC are also sites of viral late gene expression. In **Figure 4** we present representative results of experiments designed to measure by RT-PCR the level of various species of viral late mRNA and their segregation between RCf and Npl at 36 hpi. Viral late mRNA are synthesized in RC and their postranscriptional processing initiates in these sites; later these viral mRNA dissociate from RC, are liberated to the nucleoplasm, and are subsequently exported to the cytoplasm. The total pool of mature viral late mRNA (ML mRNA) was measured using primers that amplify an exon junction of the tripartite leader, a sequence that constitutes the 5' of all adenoviral late mRNA (**Figure 4A**). Exon junctions in the mRNA of specific mature transcripts of the L2, L4 and L5 families were also measured. It has been established that as the late phase of the viral replication cycle progresses, increasing amounts of viral late mRNA are exported to the cytoplasm; however, by late times production of the L5 mRNA species increases further in comparison with the other late mRNA families. In the representative results sown in **Figure 4** an approximately 2.5-fold difference in ML mRNA is observed in Npl compared with RCf, as expected. Interestingly when we compare mRNA from specific families, both L2 and L4 mRNA appear to be distributed in similar levels between both subnuclear fractions (**Figure 4B and C**, respectively), while in contrast, the L5 mRNA showed an almost 2-fold increase in Npl compared to RCf. These results suggest a differential pattern in the synthesis and liberation of the different viral late mRNA species from adenoviral RC (as has been suggested before[10]). Significantly, these results also demonstrate that precise measurements of the different steps in the biogenesis of the viral mRNA can be performed using isolated RC with this novel procedure.
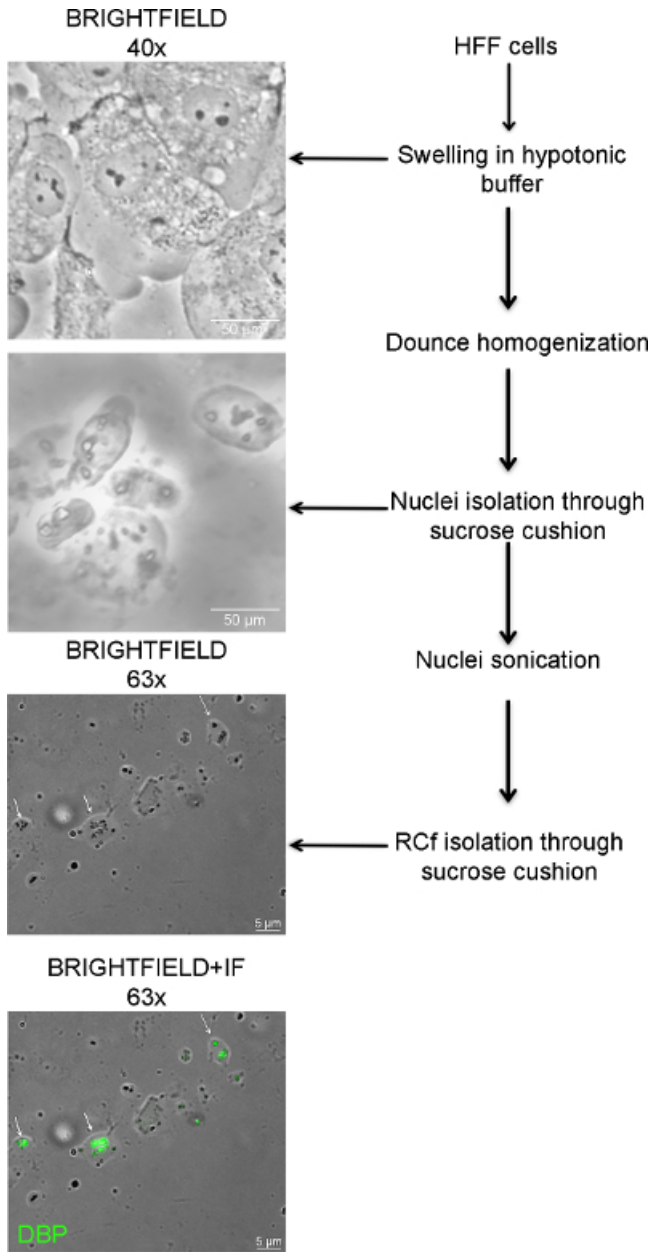
Figure 1. Bright Field Microscopy of Different Steps during the Fractionation Procedure. During the isolation of RC, the samples need to be monitored by an optical microscope to ensure integrity of sub-cellular fractions. The figure shows the steps used in the procedure to obtain RCf, from the swelling of HFF cells, to separation of nuclei and isolation of RCf through sucrose cushions. 40x micrographs: scale bar 50 μm; 63x micrographs: scale bar 5 μm; DBP is shown in green. Please click here to view a larger version of this figure.
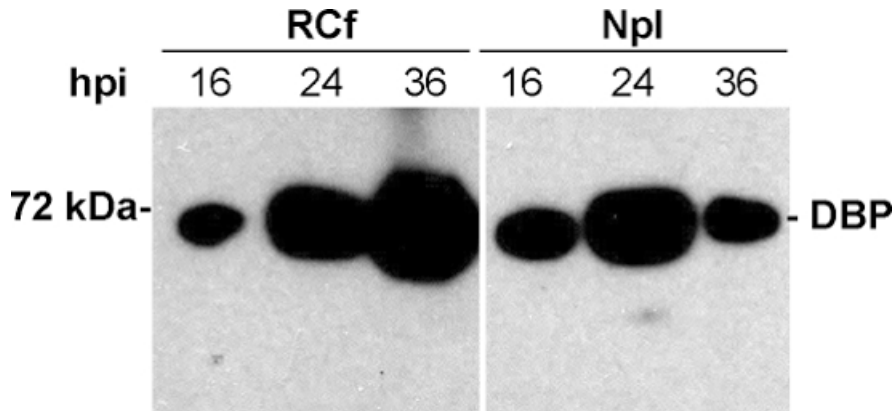
Figure 2. Western Blot against DBP. The samples are analyzed by SDS-PAGE and processed for western blot against DBP, a *bona fide* marker of viral RC. To determine the enrichment of the protein in RCf, it is useful to compare the presence and relative abundance of DBP in both RCf and Npl at different times post-infection. In HFF cells 16 hpi represents an early time during the adenoviral replication cycle; 24 hpi marks the transition to the late phase of infection as viral DNA synthesis begins; 36 hpi represents a late time post-infection. The expected molecular mass of DBP is shown. Please click here to view a larger version of this figure.

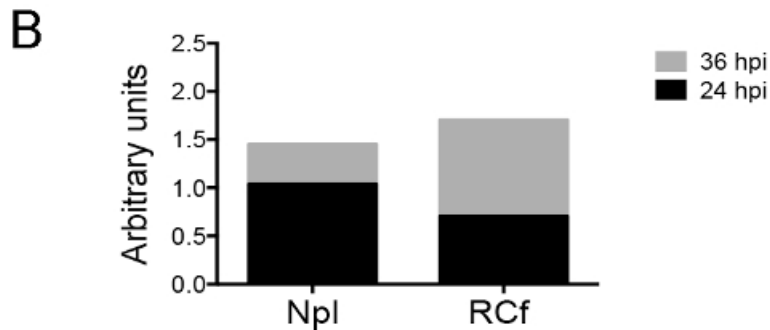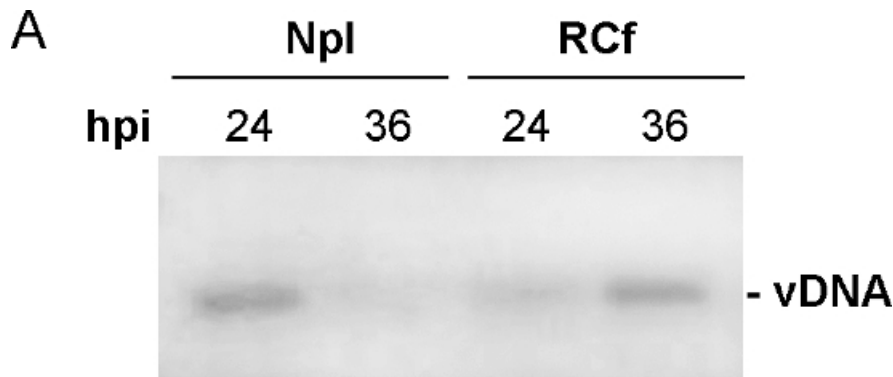**Figure 3. PCR Assay to Detect Viral DNA (vDNA) in RCf.** DNA was purified from RCf and Npl at 24 and 36 hpi. Viral DNA was amplified by PCR using primers specific for the viral genome. The graph shows the enrichment of viral DNA in RCf at 36 hpi. Please click here to view a larger version of this figure.
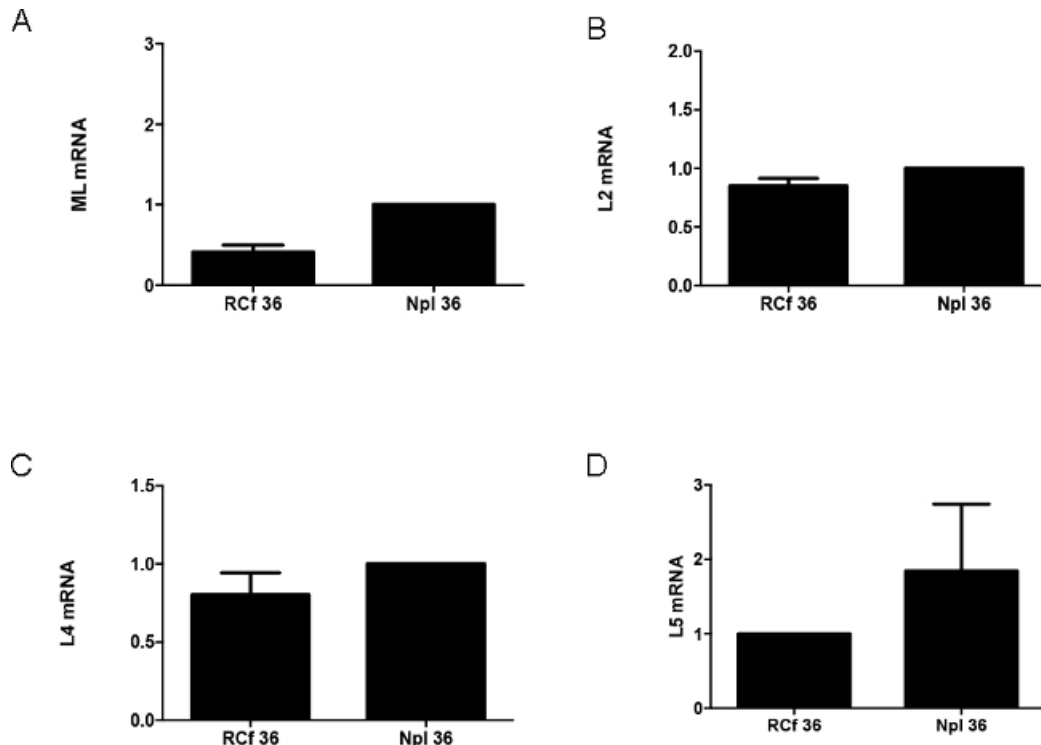
Figure 4. Analysis of Viral Late mRNA. RNA was isolated from RCf and Npl and analyzed by RT-PCR to detect specific viral late mRNA. **(A)** Total Viral Late mRNA (ML: Major Late); **(B)** mRNA from the L2 Family; **(C)** mRNA from the L4 Family; **(D)** mRNA from the L5 Family. Values represent mean ± standard deviation of triplicate samples. Please click here to view a larger version of this figure.

Name	Forward primer sequence (5'-3')	Reverse primer sequence (5'-3')	Annealing temperature
ML mRNA	GCCTCCGAACGGTACTCCGCC	CGCCACGGTGCTCAGCCTACC	60 ºC
L2 mRNA	GTCACAGTCGCAAGATGTCC-AAGC	GCAACGCCAGCATGTCCTTA-TGC	58 ºC
L4 mRNA	CCTCCGAACGGTACTCCGC	CCTTGCTCATCTTGCGACTGTG	58 ºC
L5 mRNA	GTCACAGTCGCAAGATGAAGCG	GGTAACTAGAGGTTCGGATA-GGCG	60 ºC

Table 1. Primers Used for Viral Late mRNA Amplification. ML mRNA: these primers allow the amplification of a region within the tripartite leader, the 5' sequence that is common to all viral late mRNA; L2 mRNA primers allow the amplification of a specific region within the pV mRNA; L4 mRNA primers allow the amplification of a specific region within the 100 K mRNA; L5 mRNA allows the amplification of a region within the fiber mRNA. The sequence and annealing temperatures for each primer are shown.

Discussion

In order to elucidate the molecular mechanisms that govern regulation of cellular activities by viral infection understanding the composition and activities associated with RC would be instrumental. Therefore, to make a detailed analysis of RC, we established a cell-free system that takes advantage of the size and biochemical composition of these virus-induced structures, to isolate subnuclear fractions enriched with RC using a simple procedure that relies on velocity gradients with sucrose cushions. Critical steps of the procedure that require standardization depending on the cell type used are: i) standardization of the times used for cell swelling to avoid disruption of nuclei; ii) formation of the sucrose gradients so that fractions can be properly separated; iii) constant monitoring of the samples throughout the procedure by bright field microscopy; iv) sonication time and intensity to ensure that all nuclei are lysed but RC are not disrupted; v) all fractionation steps should be carried out on ice to avoid disruption of nuclear structures.

Limitations of the technique that can be encountered or can be anticipated are: i) that nucleoli and perhaps other subnuclear structures or domains that share similar dimensions and biochemical composition are coisolated in the RC fraction, making the relative abundance of replication compartments versus other similar nuclear bodies variable depending on the virus, cell type and time post-infection used for their isolation; ii) it is possible that just as the size and composition of RC changes as the replication cycle of the virus progresses, the compactness of the RC particles may also change, making it necessary to perform experiments designed to determine detailed ultrastructural changes of the RC particles at different times post-infection to evaluate not only changes in the particles composition and activities, but whether their stability may vary. While these issues may limit the characterization of RC composition and activities at various different times post-infection, as less stable RC obtained by this procedure may not recapitulate their counterpart in the infected cell nucleus, such limitations may be overcome by using

higher multiplicities of infection or by determining the times post-infection at which viral RC have attained a minimum size and abundance in the infected cell nucleus. These potential limitations notwithstanding, the technique reported here provides several advantages over the analysis that has hitherto solely relied on microscopy; namely that the precise biochemical and functional analysis of RC can be performed using this novel approach.

We show here that the RC-fractions (RCf) obtained are enriched with *bona fide* RC markers, such as the viral E2-72K DBP protein, viral DNA and RNA. Using biochemical analysis by immunoblotting and PCR, we have confirmed that this approach facilitates the detailed analysis of components and activities associated to RC and should help unravel molecular mechanisms that regulate virus-host cell interactions in the infected-cell nucleus.

It is well established that DNA replication, transcription and post-transcriptional processing of viral late mRNA are closely associated to viral replication compartments, events that lead to viral progeny production[2,11,12]. In adenovirus-infected cells the onset of viral DNA replication marks the transition to the late phase of infection and results in the activation of the Major Late promoter, which directs the production of high quantities of viral late transcripts. However, the L4 genes are expressed through a novel promoter (L4P) that is independent from the MLP[13,14]. Besides this complex program of late promoter activation, the selection of 3' splice sites for longer introns is progressively favored as the late phase proceeds. In addition, production of these transcripts is regulated by their selective release from the site of synthesis and by selective export to the cytoplasm.

However, regulation of the late promoters and molecular events that lead to the selective production of viral late mRNA is incompletely understood. Therefore, as a proof of concept for the procedure reported here, we demonstrate that viral DNA and viral late mRNA can be isolated in RCf, suggesting that these subnuclear fractions can be used to determine the pattern of synthesis and partitioning of different species of viral late mRNA, hence allowing the use of quantitative techniques and potentially advancing the detailed study of the complex pattern of viral late mRNA biogenesis.

Furthermore, this technique can be used to study the molecular mechanisms that are responsible for the efficient replication of the viral genome, regulation of the complex program of viral gene transcription and cellular factors that are co-opted in RC, as well as morphological and ultrastructural studies of these viral induced structures. Moreover this system should be easily adapted to isolate RC from other nuclear replicating viruses, and should help unravel viral mechanisms that govern virus-cell interactions.

Disclosures

The authors have nothing to disclose.

Acknowledgements

References

1. Doucas, V. *et al.* Adenovirus replication is coupled with the dynamic properties of the PML nuclear structure. *Gene., and Dev.* **10**, 196-207, (1996).
2. Schmid, M., Speiseder, T., Dobner, T., & Gonzalez, R. A. DNA virus replication compartments. *J. Virol.* **88**, 1404-1420, (2014).
3. Boon, J.A., Diaz, A., & Ahlquist, P. Cytoplasmic viral replication complexes. *Cell host microbe.* **8**, 77-85, (2010).
4. Paul, D., Hoppe, S., Saher, G., Krijnse-Locker, J., & Bartenschlager, R., Morphological and biochemical characterization of the membranous hepatitis C virus replication compartment. *J. Virol.* **87**, 10612-10627, (2013).
5. Busch, H. *et al.* Isolation of Nucleoli., *Exp Cell Res.*, **24**, SUPPL9: 150-163, (1963).
6. Lam, Y.W., Lyon, C.E., & Lamond, A.I. Large-scale isolation of Cajal bodies from HeLa cells. *Mol. Biol. Cell.* **13**, 2461-2473, (2002).
7. Lam, Y.W., Trinkle-Mulcahy, L., & Lamond, A.I. The nucleolus, *J Cell Sci.* **118**, 1335-1337, (2005).
8. Groitl, P., & Dobner, T. Construction of adenovirus type 5 early region 1 and 4 virus mutants, *Methods Mol Med.*, **130**, 29-39 (2007).
9. Reich, N.C., Sarnow, P., Duprey, E., & Levine, A.J. Monoclonal antibodies which recognize native and denatured forms of the adenovirus DNA-binding protein. *Virology.* **128**, 480-484 (1983).
10. Leppard, K.N. Selective effects on adenovirus late gene expression of deleting the E1b 55K protein. *J Gen Virol.* **74** (Pt 4), 575-582, (1993).
11. Gonzalez, R., Huang, W., Finnen, R., Bragg, C., & Flint, S.J. Adenovirus E1B 55-kilodalton protein is required for both regulation of mRNA export and efficient entry into the late phase of infection in normal human fibroblasts. *J. Virol.* **80**, 964-974, (2006).
12. Castillo-Villanueva, E. *et al.* The Mre11 Cellular Protein Is Modified by Conjugation of Both SUMO-1 and SUMO-2/3 during Adenovirus Infection. *ISRN Virology.* **2014**, 14, (2014).
13. Morris, S.J., Scott, G.E., & Leppard, K.N. Adenovirus late-phase infection is controlled by a novel L4 promoter. *J. Virol.* **84**, 7096-7104, (2010).
14. Wright, J., & Leppard, K.N. The human adenovirus 5 L4 promoter is activated by cellular stress response protein p53. *J. Virol.* **87**, 11617-11625, (2013).

Parallelizing the Bayesian Analysis of Blinking and Bleaching for Super-Resolution Microscopy

Haydee O. Hernández[1,2], Paloma Hidalgo[2,3], Christopher D. Wood[1,2], Ramón González[3], and Adán Guerrero[1,2(✉)]

[1] Laboratorio Nacional de Microscopía Avanzada, Universidad Nacional Autónoma de México, 62210 Cuernavaca, Morelos, Mexico
[2] Instituto de Biotecnología, Universidad Nacional Autónoma de México, 62210 Cuernavaca, Morelos, Mexico
{hoha,hopr,chris,adanog}@ibt.unam.mx
[3] Centro de Investigación en Dinámica Celular. Instituto de Investigación en Ciencias Básicas y Aplicadas, Universidad Autónoma del Estado de Morelos, 62209 Cuernavaca, Morelos, Mexico
rgonzalez@uaem.mx

Abstract. Super-resolution microscopy techniques overcome the diffraction limit of optical microscopy. The bayesian analysis of blinking and bleaching (3B analysis) is a super-resolution microscopy method that resolves biological structures with a lateral spatial resolution in the range of 50 nm. This method requires an extensive processing time to generate each super-resolution image. We present the parallelization of the 3B analysis for a personal computer and for a cluster which reduces the time for 3B analysis, and provide Parallel 3B an ImageJ plugin that extends the current implementation of the algorithm to parallel computing.

Keywords: Super-resolution microscopy · 3B · Cluster · Parallel processing · Image processing

1 Introduction

In optical microscopes the diffraction barrier, also called Abbe's limit, restricts the spatial discrimination of neighboring objects that are closer than approximately half the wavelength of the light used to image the specimen [1]. To overcome Abbe's limit, super-resolution (SR) techniques exploit the fluorescence properties of molecules and proteins (fluorophores) by promoting the switching between dark and emitting states [2].

Localization SR techniques are based on the single-molecule principle. This principle depends on the localization of single emitters from a temporal sequence of images collected with a highly sensitive electron-multiplying CCD (EMCCD) camera coupled to an optical microscope [2, 3]. Localization SR techniques resolve structures separated by as little as 20 nm, however they can only be applied if the density of molecules in the sample is below approximately 10 mol/μm^2 [4]. An alternative approach is to apply the 3B technique which analyzes the entire time series globally [5]. The algorithm generates a probability map of fluorophore localization by deriving a weighted average over all possible models; the set of models includes varying numbers of emitters, emitter

localizations and temporal dynamics of the states of the fluorophores [5]. The information stored in the image sequence is iteratively compared with the models using Bayesian inference [5].

The 3B software is currently supplied as a standalone program that must be compiled and installed before use, thus limiting its usage to those reasonably familiar with programming [5]. The imaging community has greatly benefited from the existence of standard open source software packages; ImageJ in particular has become a standard tool in laboratories that work with microscopy images [6]. The authors of 3B also provide an ImageJ plugin for the 3B software, which includes both a 3B analysis suite, and software for performing the final SR reconstruction [7].

The current implementation of this method has the disadvantage that the analysis is laborious (hours to days), compared with other localization methods as PALM [8], STORM [9] or SOFI [10], which create super-resolution images in a few minutes as adequate sampling from the set of all possible models generated by 3B is a demanding computational task [5].

In 2013, the 3B analysis was parallelized with the use of Amazon EC2 cloud computing servers [11]. This implementation splits the analysis of the image sequence into spatial mosaics covering a minor part of the entire imaging field, usually of 1 μm^2. However, using the Amazon EC2 cloud would be prohibitively expensive for laboratories with scarce resources and/or large numbers of samples to analyze.

Parallelization requires the reduction of the area to be analyzed in the sequence of images. A mosaic of subregions covering the dataset is generated such that the individual mosaic sections are amenable to analysis in parallel on multiple processors.

Frequently, microscopy images include regions that do not provide information, only representing the background. We can improve the processing by detecting and removing these "empty" regions from the analysis pipeline, thus ensuring that only fluorophore-containing sections are sent for processing and analysis.

With this idea in mind and the supplementary codes provided in [11], we implement the parallelization of 3B on both a cluster and a personal computer. Furthermore, we present an analysis of the relationship between the size of the mosaic and both processing time and image quality.

Considering the parallelization and the plugin made for 3B, both were combined both into an ImageJ plugin (Parallel 3B) to parallelize 3B analysis on a personal computer. A graphic user interface is provided to improve user-friendliness.

2   Methods

2.1   Preparation of Biological Samples. Microtubules

Human foreskin fibroblasts (HFF) cells were grown on coverslips to approximately 90% confluence. Cells were processed for immunofluorescence following the description in [12]. Briefly, cells were fixed using 3.7% formaldehyde, permeabilized with PBS/Triton X-100 (137 mM NaCl, 2.7 mM Kcl, 10 mM Na_2HPO_4 and 1.8 mM KH_2PO_4/0.5% Triton X-100), and incubated with the primary mouse monoclonal antibody against alpha-tubulin (1:500) (eBioscience). After application of the primary antibody, cells were

incubated with the secondary antibody mouse anti-IgG Alexa Fluor 488 (Invitrogen). The coverslips were mounted on glass slides in 1.5% glucose oxidase + 100 mM β-mercaptoethanol to induce the blinking of the fluorophores [13, 14]. All samples were examined using an Olympus IX-81 inverted microscope.

2.2   Set up of the Optical Microscope

All super-resolution imaging measurements were performed on an Olympus IX-81 inverted microscope configured for total internal reflection fluorescence (TIRF) excitation (Olympus, cell^TIRF™ Illuminator). The critical angle was set up such that the evanescence field had a penetration depth of ~200 nm (Xcellence software v1.2, Olympus soft imaging solution GMBH). The samples were continuously illuminated using excitation sources depending on the fluorophore in use. Alexa Fluor 488 dyes were excited with a 488 nm diode-pumped solid-state laser. Beam selection and modulation of laser intensities were controlled via xcellence software v.1.2. A full multiband laser cube set was used to discriminate the selected light sources (LF 405/488/561/635 A-OMF, Bright Line; Semrock). Fluorescence was collected using an Olympus UApo N 100x/1.49 numerical aperture, oil-immersion objective lens, with an extra 1.6x intermediate magnification lens. All movies were recorded onto a 65×65 pixel region of an electron-multiplying charge couple device (EMCCD) camera (iXon 897, Model No: DU-897E-CS0-#BV; Andor) at 100 nm per pixel, and within a 50 ms interval (300 images).

2.3   Bayesian Analysis of the Blinking and Bleaching

Sub-diffraction images were derived from the Bayesian analysis of the stochastic Blinking and Bleaching of the Alexa Fluor 488 dye [5]. For each super-resolution reconstruction, 300 images were acquired at 20 frames per second with an exposure time of 50 ms at full laser power, spreading the bleaching of the sample over the length of the entire acquisition time. The maximum laser power coming out of the optical fiber measured at the back focal plane of the objective lens, for the 488 nm laser line, was 23.1 mW. The image sequences were analyzed with the 3B algorithm considering a pixel size of 100 nm and a full width half maximum of the point spread function of 270 nm (for Alexa Fluor 488), measured experimentally with 0.17 μm fluorescent beads (PS-Speck™ Microscope Point Source Kit, Molecular Probes, Inc.). All other parameters were set up using default values. The 3B analysis was run over 200 iterations, as recommended by the authors in [5], and the final super-resolution reconstruction was created at a pixel size of 10 nm with the ImageJ plugin for 3B analysis [7]. The resolution increase observed in our imaging set up by 3B analysis was up to 5 times below the Abbe's limit (~50 nm).

2.4   Parallelization of 3B

Due to the excessive computational time for 3B analysis and the cost of parallelizing in Amazon EC2, we implemented the parallelization on a personal computer and a cluster.

The authors of 3B suggest that 200 iterations are sufficient to ensure the convergence of the ensemble model that provides the best probability map estimation of fluorophore localization, hence the code was modified to finalize the analysis at this iteration point [5].

Parallelization on a Personal Computer. We parallelize the analysis of the sequence of images taken over time using subregions, as devised for use on the Amazon EC2 cloud computing environment. Each subregion was analyzed with the 3B algorithm on a personal computer (PC) with an IntelTM-Corei7-2700 CPU@3.4 GHz processor. For comparative purposes, a sequence of images of podosomes was taken from the original 3B article and used as sample data [5, 7]. This image sequence (300 images) was cropped to end up with a dataset of 52×52 pxs.

For the parallelization test we decided to apply the 3B analysis over the 52×52 pxs podosome dataset with four protocols with the following subregion sizes: 10×10 pxs, 15×15 pxs, 20×20 pxs, and 25×25 pxs. The overlap between the subregions for all the protocols was 5 pxs. (Fig. 1).
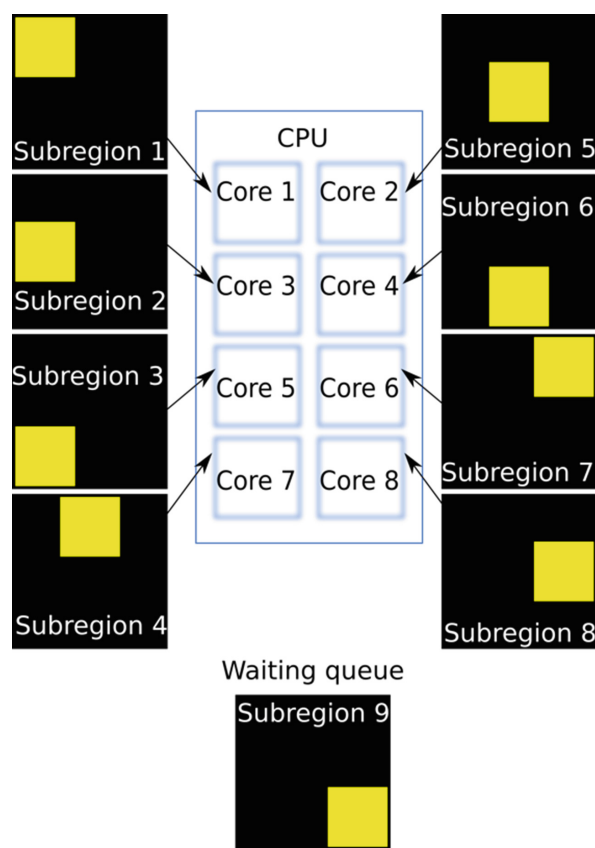
Fig. 1. Parallelization scheme of the protocol with 20×20 pxs subregions with 5 pxs overlapping on a PC with an IntelTM-Corei7-2700 CPU@3.4 GHz processor for a sequence of images of 52×52 pxs. Each subregion was sent to a core with sequence of images to be analyzed with the 3B software. Notice the waiting queue of subregions to be analyzed when all the cores are busy.

All the subregions were defined prior to the 3B analysis. A script was executed to send each subregion to be analyzed by the 3B algorithm to a different core on the PC

(Fig. 1). When all the cores were busy, the next subregion remained in the queue until a core was released, which repeated until all subregions of the protocol were analyzed. Finally, we interleaved all of the resultant analyzed subregions to generate the SR image.

Index of Dispersion. Localization SR techniques require optical microscopes with one or several digital cameras acquiring images of the samples; these cameras most commonly have a CCD image sensor (although sCMOS image sensor cameras are sometimes employed). Photon shot noise results from the inherent statistical variation of the number of incident photons on the CCD [15]. Photoelectrons generated within the semiconductor device constitute the signal, the magnitude of which is perturbed by fluctuations that follow the Poisson statistical distribution of the number of photons incident on the CCD at a given location. The Poisson distribution implies that the variance (σ^2) and the mean (μ) are equal. The shot noise is limited by $\sqrt{N}$, where N is the number of detected photons [15].

Parallelization reduces the computational time of 3B analysis. However if the subregions to be analyzed do not contain relevant information, i.e. the subregion just contains shot noise, calculations are wasted in analyzing spurious information. In order to discriminate the analysis of regions containing just shot noise, we made use of the index of dispersion. This index gives the relation between the variance and the mean, and hence identifies which regions contain only photon shot noise.

Specifically, if the index of dispersion is less or equal to one, it implies that the subregion does not contain relevant information and hence, it can be discarded. Otherwise, it is assumed that emitting fluorophores are present in the subregion (Fig. 2.d).
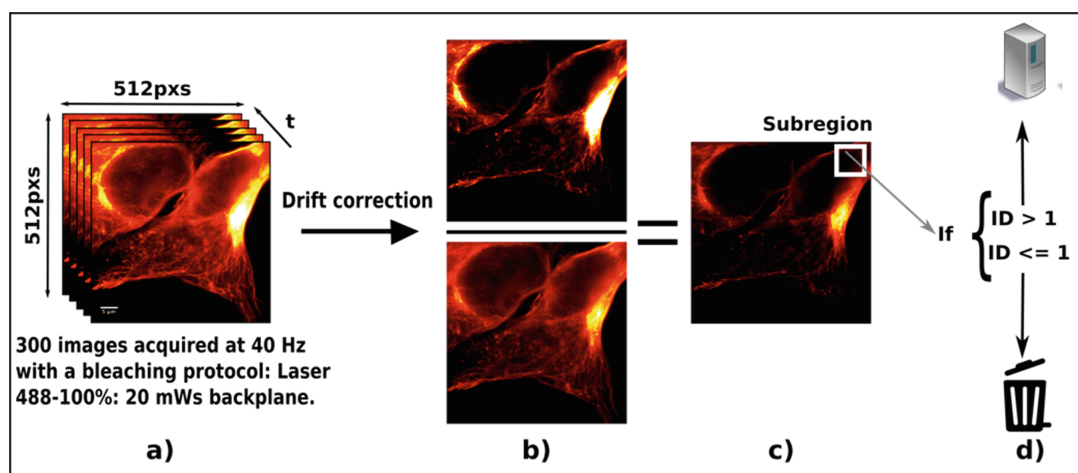
Fig. 2. Parallelization scheme of the 3B analysis on a cluster. (a) Sequence of images of the microtubules limited by diffraction. The scale bar represents 5 μm. (b) Index of dispersion of the entire image sequence, defined as the variance of the sequence divided by the mean (image below). (c) The resulting image of the index of dispersion. The white square is a subregion of 20×20 pxs. (d) Selection of the regions with relevant information. If the subregion generated in (c) has a pixel with a dispersion value greater than one, the subregion is sent to the cluster, otherwise, it is rejected.

This ensures a reduction in the subregions to be analyzed and reduces the computing time to produce the SR image.

Parallelization on a Cluster. In this implementation, we divided the analysis of the data in subregions of 20×20 pxs with an overlap of 5 pxs between the subregions. We used a sequence of images of microtubules (300 images of 512×512 pxs) as samples.

First, we corrected the drift between the images in the sequence because this can affect the analysis [16]. Then, we generated the subregions using the index of dispersion to reduce the number of subregions to be analyzed; thereby reducing the computing time of 3B analysis and the transfer time of the data to the cluster.

Our results are found using the cluster of the Biotechnology Institute of the National Autonomous University of Mexico (UNAM) (cluster.ibt.unam.mx/wordpress).

All parallelization scripts and the Parallel3D plugin for ImageJ are available on the internet at (https://bitbucket.org/hoha441/parallel-3b/src), the Parallel3B plugin for ImageJ is also provided.

3   Results

3.1   Parallelization on a PC

The 3B analysis of the podosomes allowed comparison of our results with those obtained in the article entitled "Accelerating 3B single-molecule super-resolution microscopy with cloud computing" [11]. Podosomes are cylindrical actin based cytoskeletal structures found on the outer surface of the plasma membrane of animal cells that participate in cell adhesion, migration and degradation of the extracellular matrix [17, 18]. We present below the SR images of the podosomes and the computational time for each protocol.

The parallelization of the 3B analysis of the 300 images of the podosomes (52×52 pxs) with the different protocols (10×10 pxs, 15×15 pxs, 20×20 pxs, and 25×25 pxs) generated 81, 16, 9, and 4 subregions, respectively.

The first graph (Fig. 3.a) shows the cumulative distribution function for each of the protocols used in the analysis of the podosome data, which shows the computational time for every subregion of the protocol. The extremes of the distribution are the minimum and the maximum time for each protocol. The computational time for the complete image is not displayed because it took more than 24 h. This indicates that the protocol for the smallest subregion (10×10 pxs) gave the best time for parallelization for a large number of cores, i.e. when we have access at least to the same number of cores at 3.4 GHz as the number of subregions generated.

The following chart (Fig. 3.b) displays the same information as above but in a box plot, which shows the distribution of computational time the parallelization for each of the protocols for analysis of the podosomes data. The computational time of the analysis for the complete image is approximately 125 h, and compared to the other protocols it is clear that parallelization significantly reduces it.
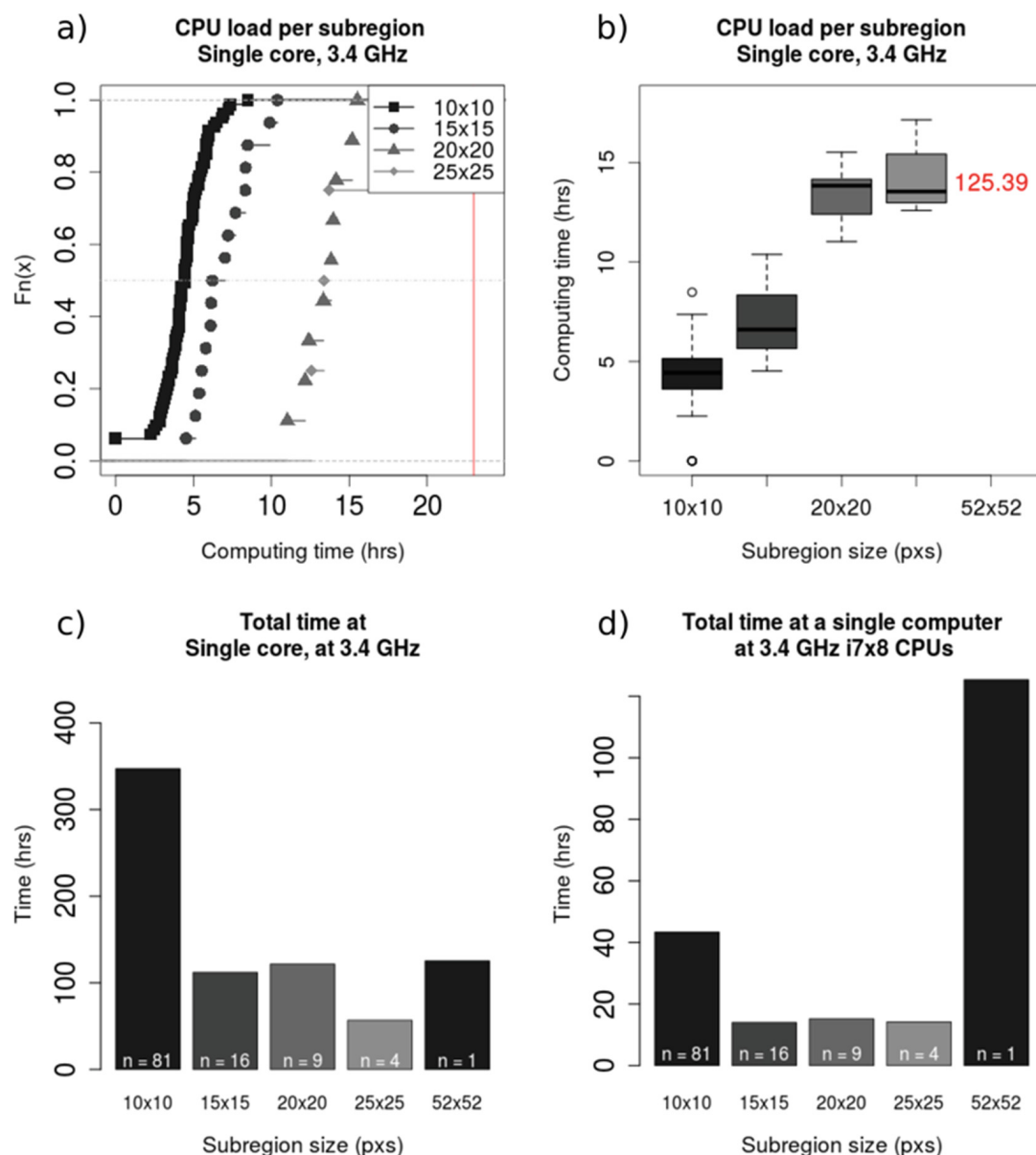
Fig. 3. Total computational times for the analysis of the sequence of images of podosomes with 3B. (a) Cumulative distribution function of the computational time for each parallelization protocol. The vertical line denotes 24 h (b) Distribution of the computational time for each protocol. The optimal computational time was found using the protocol with the smallest subregions. (c) Computational time in a single core, i.e. if the analysis was performed sequential. The best computational time was found using the protocol with subregions of 25×25 pxs. (d) Computational time for the data analysis parallelization with 3B on a PC with eight cores. The protocol for subregions of 15×15 pxs was optimal for a CPU with eight cores.

The third graph (Fig. 3.c) shows the total computational time for the complete analysis of the sequence of images of the podosomes with 3B, if the analysis were sequential, i.e. with only one processor at 3.4 GHz for all the subregions of the different protocols.

This shows given the number of subregions generated and the total computational time of each of these, the optimal protocol is 25 × 25 pxs.

Finally the last chart (Fig. 3.d.) shows the total time for computing all the subregions of the different protocols on a PC with an IntelTM-Corei7-2700 CPU@3.4 GHz processor with eight cores. In this case, the best time for the complete reconstruction was found using the protocols of 15 × 15 pxs and 25 × 25 pxs.

Although the improvement in overall duration of the analysis is considerable, image quality is affected as a consequence of segregating the analysis of the original image in a mosaic of subregions. This artifact manifests as a lack of continuity in the structures of the sample; it appears as a mesh structure, due to the incorrect estimation of the background of the region analyzed [5].

Figure 4 shows the SR images of the podosomes resulting from different parallelization protocols. The SR images of the protocols of 10 × 10 pxs (Fig. 4.b) and 15 × 15 pxs (Fig. 4. c), do not have enough information to correctly process the noise data, and therefore show mesh structures. In contrast, the SR images of the protocols at larger mosaic subregions sizes show continuity in the biological structures and have an
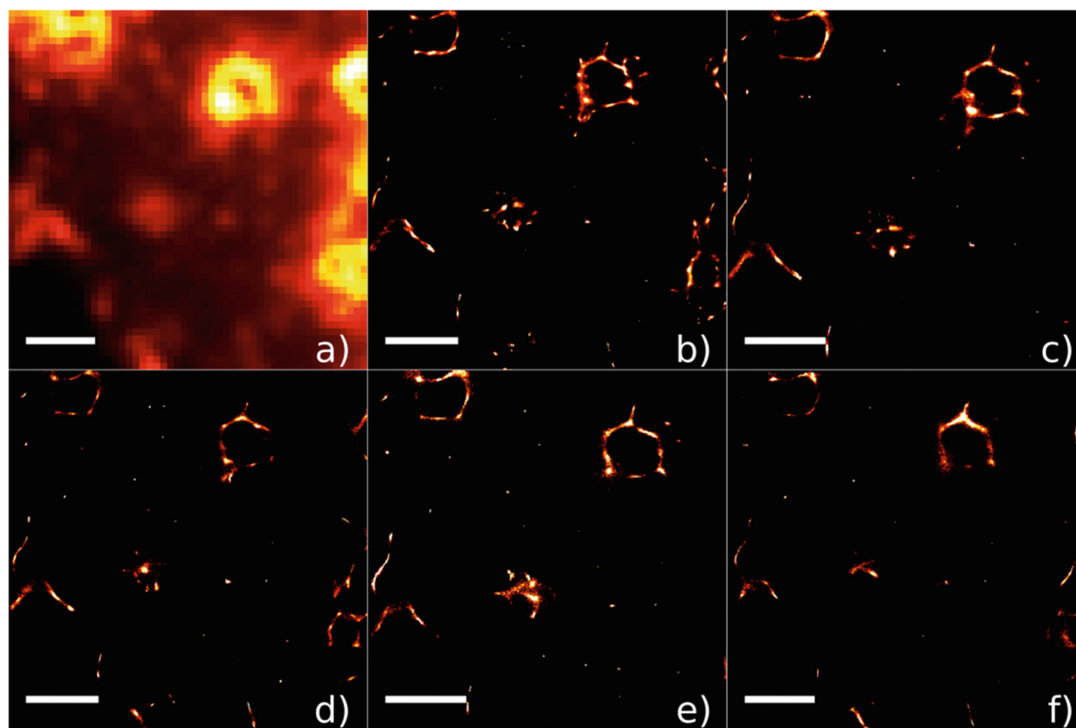
Fig. 4. Podosomes images. The scale bar for all images is 1 μm. (a) Average projection of the 300 diffraction-limited images of the podosomes. (b) Super-resolution image generated with the parallelization protocol for subregions of 10 × 10 pxs with an overlap of 5 pxs. (c) Super-resolution image generated using the parallelization protocol with subregions of 15 × 15 pxs and an overlap of 5 pxs. (d) Super-resolution image generated with the parallelization protocol with subregions of 20 × 20 pxs and an overlap of 5 pxs. (e) Super-resolution image generated using the parallelization protocol with subregions of 25 × 25 pxs and an overlap of 5 pxs. (f) Super-resolution image generated with 3B analysis of the complete image (52 × 52 pxs).

improved spatial resolution compared to the reference to the original sequence of images obtained under diffraction–limited conditions (Fig. 4.a).

3.2 Parallelization on a Cluster

Our test on a computer cluster is performed using a biological sample stained against microtubules. These are well known cytoskeletal structures, widely used to test the proficiency of SR algorithms [19]. The width of a single microtubule is approximately 25 nm.
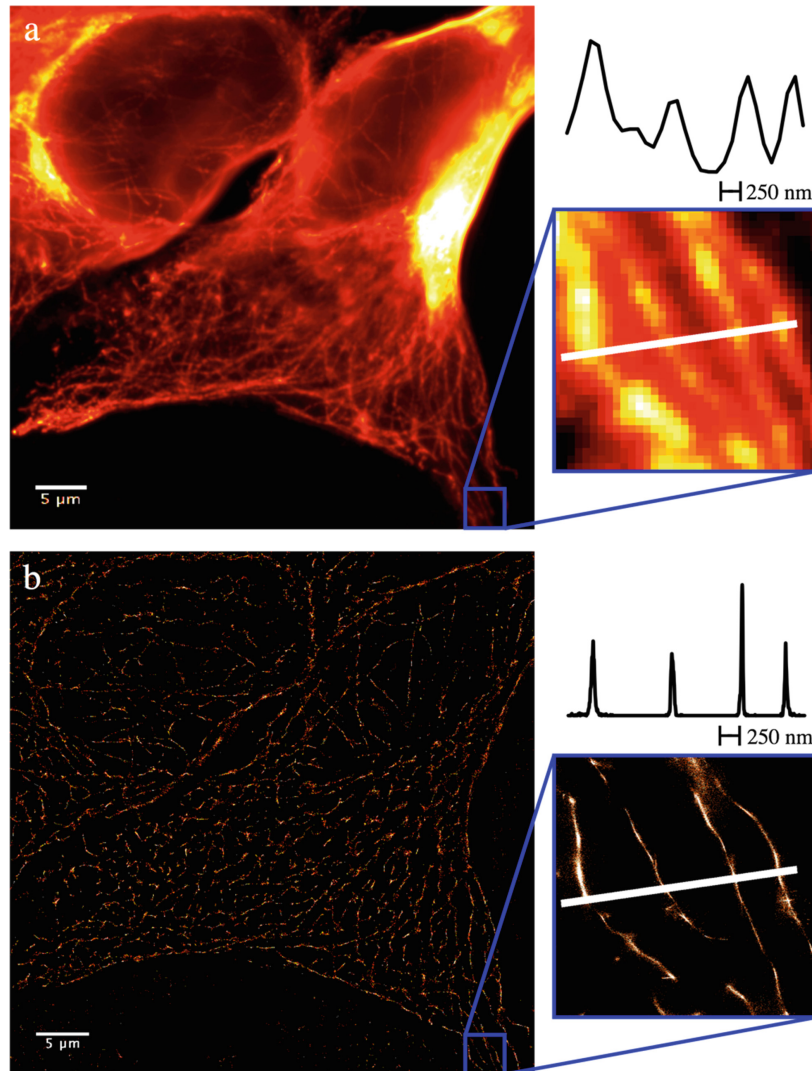
Fig. 5. Microtubules images. (a) Average projection of the 300 images in the sequence limited by diffraction of the microtubules. (b) Super-resolution image generated with the parallelization protocol for a cluster using subregions of 20×20 pxs with an overlap of 5 pxs and discarding the subregions without relevant information.

The first step was to correct the sample drift between the 300 images sequence of 512×512 pxs of the microtubules. After that, we generate subregions of 20×20 pxs

with an overlap of 5 pxs between them, followed by application of the index of dispersion filter to discard fluorophore-free subregions. The remaining regions were then sent to the cluster for 3B analysis.

With this protocol, 1023 subregions were generated instead of the expected 1089; reducing the computation expense for data manipulation and analysis. The image (Fig. 5.a) is the average projection of the sequence of images of the microtubules limited by diffraction. The image below (Fig. 5.b) is the resulting SR image of the parallelization of the analysis of the sequence of the microtubules.

4   Conclusions

The parallelization of data analysis for the 3B SR technique on a 8-core PC processor showed that the optimal size for the subregions is 25×25 pxs, as it generates fewer subregions for analysis and the SR image contains fewer notorious artifacts. These artifacts in the SR images are most problematic for subregions smaller than 20×20 pxs.

The results presented in [11] reduced the computation time to a similar degree to that demonstrated here. However the SR image of the podosomes shown there, present similar in Hu Y et al. (2013) show similar mesh-type artifact to those obtained by us with the protocols using subregions of 10×10 pxs and 15×15 pxs. [11]. We conclude that important care must be taken when parallelizing 3B analysis to avoid the generation of image artifacts, and that the presence of such errors will depend on the size and continuity of the structures to be resolved.

As a result of this study we developed "Parallel 3B", an ImageJ plugin to run 3B in parallel given a size of subregions and overlaps for a sequence of images. We expect that this tool will contribute to the wide adoption of 3B analysis on parallel computing platforms.

References

1. Abbe, E.: Beiträge zur theorie des mikroskops und der mikroskopischen wahrnehmung. Arch. Mikroskop. Anat. **9**, 413 (1873)
2. Small, A., Stahlheber, S.: Fluorophore localization algorithms for super-resolution microscopy. Nat. Methods **11**(3), 267–279 (2014)
3. Deschout, H., Cella Zanacchi, F., Mlodzianoski, M., Diaspro, A., Bewersdorf, J., Hess, S.T., Braeckmans, K.: Precisely and accurately localizing single emitters in fluorescence microscopy. Nat. Methods **11**(3), 253–266 (2014)
4. Holden, S.J., Uphoff, S., Kapanidis, A.N.: DAOSTORM: an algorithm for high- density super-resolution microscopy. Nat. Methods **8**(4), 279–280 (2011)

5. Cox, S., Rosten, E., Monypenny, J., Jovanovic-Talisman, T., Burnette, D.T., Lippincott-Schwartz, J., Jones, G.E., Heintzmann, R.: Bayesian localization microscopy reveals nanoscale podosome dynamics. Nat. Methods **9**(2), 195–200 (2012)
6. Schneider, C.A., Rasband, W.S., Eliceiri, K.W.: NIH Image to ImageJ: 25 years of image analysis. Nat. Methods **9**(7), 671–675 (2012)
7. Rosten, E., Jones, G.E., Cox, S.: ImageJ plug-in for Bayesian analysis of blinking and bleaching. Nat. Methods **10**(2), 97–98 (2013)
8. Betzig, E., Patterson, G.H., Sougrat, R., Lindwasser, O.W., Olenych, S., Bonifacino, J.S., Davidson, M.W., Lippincott-Schwartz, J., Hess, H.F.: Imaging intracellular fluorescent proteins at nanometer resolution. Science **313**(5793), 1642–1645 (2006)
9. Rust, M.J., Bates, M., Zhuang, X.: Sub-diffraction-limit imaging by stochastic optical reconstruction microscopy (STORM). Nat. Methods **3**(10), 793–795 (2006)
10. Dertinger, T., Colyer, R., Iyer, G., Weiss, S., Enderlein, J.: Fast, background-free, 3D super-resolution optical fluctuation imaging (SOFI). Proc. Natl. Acad. Sci. U.S.A **106**(52), 22287–22292 (2009)
11. Hu, Y.S., Nan, X., Sengupta, P., Lippincott-Schwartz, J., Cang, H.: Accelerating 3B single-molecule super-resolution microscopy with cloud computing. Nat. Methods **10**(2), 96–97 (2013)
12. Gonzalez, R., Huang, W., Finnen, R., Bragg, C., Flint, S.J.: Adenovirus E1B 55-kilodalton protein is required for both regulation of mRNA export and efficient entry into the late phase of infection in normal human fibroblasts. J. Virol. **80**(2), 964–974 (2006)
13. Dempsey, G.T., Vaughan, J.C., Chen, K.H., Bates, M., Zhuang, X.: Evaluation of fluorophores for optimal performance in localization-based super-resolution imaging. Nat. Methods **8**(12), 1027–1036 (2011)
14. Heilemann, M., van de Linde, S., Mukherjee, A., Sauer, M.: Super-resolution imaging with small organic fluorophores. Angew. Chem. **48**(37), 6903–6908 (2009)
15. Cheezum, M.K., Walker, W.F., Guilford, W.H.: Quantitative comparison of algorithms for tracking single fluorescent particles. Biophys. J. **81**(4), 2378–2388 (2001)
16. Wang, Y., Schnitzbauer, J., Hu, Z., Li, X., Cheng, Y., Huang, Z.L., Huang, B.: Localization events-based sample drift correction for localization microscopy with redundant cross-correlation algorithm. Opt. Express **22**(13), 15982–15991 (2014)
17. Linder, S., Aepfelbacher, M.: Podosomes: adhesion hot-spots of invasive cells. Trends Cell Biol. **13**(7), 376–385 (2003)
18. Linder, S., Kopp, P.: Podosomes at a glance. J. Cell Sci. **118**(Pt 10), 2079–2082 (2005)
19. Endesfelder, U., Heilemann, M.: Art and artifacts in single-molecule localization microscopy: beyond attractive images. Nat. Methods **11**(3), 235–238 (2014)

CrossMark
← click for updates

Morphological, Biochemical, and Functional Study of Viral Replication Compartments Isolated from Adenovirus-Infected Cells

Paloma Hidalgo,[a,b] Lourdes Anzures,[a,b] Armando Hernández-Mendoza,[a] Adán Guerrero,[c] Christopher D. Wood,[c] Margarita Valdés,[a*] Thomas Dobner,[d] Ramón A. Gonzalez[a]

Centro de Investigación en Dinámica Celular, Instituto de Investigación en Ciencias Básicas y Aplicadas, Universidad Autónoma del Estado de Morelos (UAEM), Cuernavaca, Morelos, México[a]; Instituto de Biotecnología, Universidad Nacional Autónoma de México (UNAM), Cuernavaca, Morelos, México[b]; Laboratorio Nacional de Microscopía Avanzada, Instituto de Biotecnología, Universidad Nacional Autónoma de México (UNAM), Cuernavaca, Morelos, México[c]; Heinrich Pette Institute, Leibniz Institute for Experimental Virology, Hamburg, Germany[d]

ABSTRACT

Adenovirus (Ad) replication compartments (RC) are nuclear microenvironments where the viral genome is replicated and a coordinated program of late gene expression is established. These virus-induced nuclear sites seem to behave as central hubs for the regulation of virus-host cell interactions, since proteins that promote efficient viral replication as well as factors that participate in the antiviral response are coopted and concentrated there. To gain further insight into the activities of viral RC, here we report, for the first time, the morphology, composition, and activities of RC isolated from Ad-infected cells. Morphological analyses of isolated RC particles by superresolution microscopy showed that they were indistinguishable from RC within infected cells and that they displayed a dynamic compartmentalization. Furthermore, the RC-containing fractions (RCf) proved to be functional, as they directed *de novo* synthesis of viral DNA and RNA as well as RNA splicing, activities that are associated with RC *in vivo*. A detailed analysis of the production of viral late mRNA from RCf at different times postinfection revealed that viral mRNA splicing occurs in RC and that the synthesis, posttranscriptional processing, and release from RC to the nucleoplasm of individual viral late transcripts are spatiotemporally separate events. The results presented here demonstrate that RCf are a powerful system for detailed study into RC structure, composition, and activities and, as a result, the determination of the molecular mechanisms that induce the formation of these viral sites of adenoviruses and other nuclear-replicating viruses.

IMPORTANCE

RC may represent molecular hubs where many aspects of virus-host cell interaction are controlled. Here, we show by superresolution microscopy that RCf have morphologies similar to those of RC within Ad-infected cells and that they appear to be compartmentalized, as nucleolin and DBP display different localization in the periphery of these viral sites. RCf proved to be functional, as they direct *de novo* synthesis of viral DNA and mRNA, allowing the detailed study of the regulation of viral genome replication and expression. Furthermore, we show that the synthesis and splicing of individual viral late mRNA occurs in RC and that they are subject to different temporal patterns of regulation, from their synthesis to their splicing and release from RC to the nucleoplasm. Hence, RCf represent a novel system to study molecular mechanisms that are orchestrated in viral RC to take control of the infected cell and promote an efficient viral replication cycle.

Viruses have evolved mechanisms that reorganize and reprogram the infected cell to promote efficient viral replication. However, the molecular mechanisms that harness cellular components in order to establish a productive viral replication cycle are not fully understood. A strategy that seems to be common for all viruses involves the formation of specialized cellular microenvironments where cellular and viral macromolecules are recruited. These have been termed virus factories, viroplasms, or replication centers or compartments (RC). Replication compartments are the sites where viral genome replication and expression occur, and in some cases these virus-induced structures are associated or juxtaposed with sites of virion assembly. Through this strategy, viruses not only promote the progression of a productive replication cycle but also concomitantly coopt cellular factors and counteract a variety of antiviral responses (1–3).

The majority of studies designed to explore the activities associated with viral RC have been made with cytoplasmic viruses, most of them positive-strand RNA viruses or the nucleocytoplasmic large DNA viruses (2–6). Most of these viral RC are associated with cell membranes, and their cytoplasmic localization has, to a

great extent, facilitated their study (7–9), making their detailed morphological and biochemical characterization, as well as their functional analysis, possible (10–15).

In the case of DNA viruses that replicate in the nucleus, the formation of RC does not seem to require membranous structures. Rather, nuclear RC are formed in association with or adjacent to defined nuclear domains, such as the promyelocytic leu-

kemia protein (PML) NB (nuclear domains implicated in DNA replication and transcription regulation, epigenetic silencing, DNA repair, cell senescence, apoptosis, and regulation of the interferon-induced antiviral response; reviewed in reference 16), the nucleolus, or other nuclear domains (17, 18). While less information is available for the RC of DNA viruses that replicate in the nucleus than for cytoplasmic RNA viruses, it is known that these nuclear compartments are vital for virus replication and that they contain DNA and RNA polymerases, transcriptional and post-transcriptional processing factors, and RNA export factors. The assembly of nuclear replication compartments is accompanied by the extensive reorganization of nuclear components that are major constituents of nuclear domains, such as PML NB, interchromatin granules (IG), paraspeckles, Cajal bodies (CB), and nucleoli (reviewed in reference 3). In addition, as for cytoplasmic viruses, nuclear RC also impact cellular antiviral mechanisms (19–26). Hence, replication compartments may represent a control hub of virus-cell interactions that promotes efficient viral replication and simultaneously protects viral macromolecules from cellular antiviral activities. Nevertheless, because of the complexity of the nuclear milieu, RC assembled in the infected cell nucleus have not been isolated; thus, they have been studied only within the complexity of the infected cell nucleus.

Like other DNA viruses that replicate in the nucleus, upon infection of the cell, adenovirus (Ad) DNA is delivered into the cell nucleus, where it localizes to PML NB by an uncharacterized mechanism (27). Components of the PML NB, together with those of nucleoli, Cajal bodies, IG, and other nuclear domains that regulate RNA biogenesis, are recruited to RC, where the adenoviral genome is replicated and expressed (27–32). Components of the DNA repair machinery, signal transduction factors, tumor suppressor proteins, and innate immune response proteins also are recruited to these sites (22–24, 33–36).

Adenovirus RC have been studied only by fluorescence and electron microscopy in infected cells (37–46). These studies have provided valuable information about their morphological organization, such as the localization of viral and cellular factors that participate in viral DNA synthesis and gene expression, suggesting a spatial separation of replication and transcription regions (39) (see Fig. 9). However, direct evidence of the composition and of the molecular activities associated with adenoviral RC still is lacking.

Adenoviral RC and nucleoli seem to have similar functional organization. Neither of these subnuclear structures is membrane enclosed, they both consist of proteins and nucleic acids, and their size ranges between about 0.5 and 5 μm in diameter. Furthermore, both structures appear to have subcompartments or regions that are morphologically and functionally distinguishable (38, 39, 47, 48). The ultrastructural analysis of nucleoli has revealed three subcompartments that include the fibrillar centers (FC) surrounded by the dense fibrillar components (DFC), both embedded in the granular component (GC). The transcription of rRNA genes has been suggested to take place at the interface of FC and DFC, while ribosome assembly takes place in the granular component (48, 49). Besides these main regions, an additional subcompartment, referred to as the intranucleolar body (INB), has been reported in which proteins involved in DNA repair, RNA metabolism, nuclear export, and protein turnover, as well as the posttranslational modifiers SUMO1 and SUMO2/3, are localized (50). Fluorescence and electron microscopy of adenovirus RC suggest that they also

are functionally compartmentalized. Double-stranded DNA (dsDNA) that is not actively replicated or transcribed is localized in the center of RC; separately, single-stranded DNA (ssDNA) is associated with the viral ssDNA binding protein (DBP), in the peripheral replicative zone (PRZ), where spatially separated sites of active replication and transcription are organized. Active transcription leads to the accumulation of clusters of IG surrounding RC (39, 41, 47, 51). Interestingly, SUMO1 and SUMO2/3 paralogues associate with RC, displaying distinct localization where SUMO2/3 exhibits a pattern similar to that of DBP, while SUMO1 localizes to the periphery of DBP foci (26), a pattern that is comparable with their distribution in PML NB (52).

Adenoviruses are ubiquitous infectious agents and one of the main models of tumor virology, as well as one of the most promising alternatives for the development of vectors used in gene and anticancer therapies. Nevertheless, the molecular mechanisms by which adenoviral proteins reorganize and reprogram the infected cell nucleus are not completely understood. Since viral replication compartments seem to represent a regulating center of virus-cell interactions, a detailed study of these viral structures should allow the elucidation of molecular mechanisms that govern the regulation of not only viral genome replication and expression but also cellular activities by viral infection. Therefore, in order to study the molecular mechanisms that promote the formation of replication compartments as a general viral strategy, in the present work we have exploited a recently established cell-free system consisting of enriched RC fractions (RCf) (53) to analyze the morphology, composition, and functions of RC isolated from Ad-infected cells. The analysis of RC particles by superresolution microscopy demonstrated that they possess morphological characteristics indistinguishable from those of RC within the infected cell nucleus. Moreover, this nanoscopic analysis demonstrated, for the first time, the compartmentalized organization of adenoviral RC. Significantly, these RC fractions proved to be functional, as they supported *in vitro* synthesis of viral DNA and RNA, as well as splicing of pre-mRNA, indicating that RC fractions contain sufficient components to direct these processes and that they recapitulate the activities that are associated with RC in the infected cell nucleus. The experiments presented here have revealed that the transcription and splicing of viral late mRNA occur in RC and that the regulation of viral late mRNA biogenesis is more complex than previously thought, as these experiments show for the first time that individual viral late mRNA species display different temporal patterns of synthesis, splicing, and partitioning between both the nucleus and the cytoplasm, as well as between RC and the nucleoplasm.

MATERIALS AND METHODS

Cells and viruses. Primary human foreskin fibroblasts (HFF) were maintained in monolayer cultures in Dulbecco's modified Eagle's medium supplemented with 10% (vol/vol) fetal calf serum (Gibco-Invitrogen Corp.) for no more than 14 passages. HFF were infected with Ad5 at 30 PFU/cell as described previously (54). The Ad5 dl309 and H5pg4100 viruses (55, 56) were propagated in monolayers of HEK-293 cells. Viruses titers were determined as fluorescein-forming units (FFU) on HEK-293 cells as described previously (56).

Ab. The primary antibodies (Ab) used for Western blotting and immunofluorescence assays were Ab specific for Ad5 DBP, including mouse monoclonal Ab B6-8 (57), rabbit polyclonal Ab (a kind gift of T. Dobner), and anti-nucleolin mouse monoclonal Ab ZN004 (Invitrogen). The secondary antibodies used were anti-mouse horseradish peroxidase (HRP)-

conjugated antibody (Jackson ImmunoResearch), anti-mouse Alexa Fluor 568, and anti-rabbit Alexa Fluor 488 (both from Invitrogen).

Preparation of subcellular and subnuclear fractions from Ad5-infected HFF cells. To isolate cytoplasmic and nuclear fractions, Ad5-infected HFF cells were fractionated essentially according to a procedure designed to isolate nucleoli described previously (58) and recently adapted (59), with the following modifications (53). All procedures were carried out on ice, except as indicated. HFF cells were grown in monolayer cultures to 90% confluence. Ad5-infected or mock-infected cells were harvested at the indicated times postinfection and were washed with ice-cold phosphate-buffered saline (PBS; 137 mM NaCl, 2.7 mM KCl, 10 mM Na$_2$HPO$_4$, and 1.8 mM KH$_2$PO$_4$). To disrupt the cellular membrane, 1×10^7 cells were resuspended in ice-cold hypotonic buffer (10 mM HEPES, pH 7.9, 10 mM KCl, 1.5 mM MgCl$_2$, 0.5 mM dithiothreitol [DTT], 20 μg/ml phenylmethylsulfonyl fluoride [PMSF], 10 μg/ml aprotinin, 10 μg/ml pepstatin A, and 10 μg/ml leupeptin). After extensive swelling, cell membranes were lysed by 80 strokes with a Dounce homogenizer and constantly monitored by phase-contrast microscopy to ensure complete cell membrane lysis while avoiding damage to nuclei. The cell homogenate was centrifuged at $300 \times g$ at 4°C for 5 min, and the supernatant containing the cytoplasmic fraction (CYT) was stored at −20°C. To remove cellular debris from nuclei, the pellet was resuspended in solution 1 (S1) (0.25 M sucrose, 10 mM MgCl$_2$, 20 μg/ml PMSF, 10 μg/ml aprotinin, 10 μg/ml pepstatin A, and 10 μg/ml leupeptin), layered over an equal volume of solution 2 (S2) (0.35 M sucrose, 0.5 mM MgCl$_2$, 20 μg/ml PMSF, 10 μg/ml aprotinin, 10 μg/ml pepstatin A, and 10 μg/ml leupeptin), and centrifuged at $1,400 \times g$ at 4°C for 5 min. The supernatant contained cellular debris, and the pellet containing isolated nuclei (NUC) was resuspended in S2 and stored at −20°C. To isolate subnuclear fractions enriched with adenovirus RC (RCf), nuclei were sonicated with a Branson 1510 ultrasonic bath, using two 5-min pulses, until all nuclei were lysed as observed by phase-contrast microscopy. The sonicated nuclei then were layered over an equal volume of solution 3 (S3) (0.88 M sucrose and 0.5 mM MgCl$_2$) and centrifuged at $3,000 \times g$ at 4°C for 10 min. The supernatant containing the nucleoplasmic fraction (Npl) and the pellet containing the RCf or nucleolar fraction (Nlo; in mock-infected cells) were stored at −70°C. This procedure has been performed several times and has proven to be highly reproducible. Data from two independent experiments are shown.

Western blot analyses. To analyze the steady-state concentrations of nucleolin and DBP associated with subcellular fractions, Nlo, RCf, Npl, and CYT, as well as total cell lysates (TL) and total nuclear lysates (NL), were obtained from mock-infected or Ad-infected HFF cells at 16, 24, and 36 h postinfection (hpi). For immunoblotting, gels were transferred onto polyvinylidene difluoride (PVDF) membranes (Millipore) and incubated as described previously (60). Briefly, membranes were blocked for 2 h at room temperature with 3% nonfat milk and incubated overnight at 4°C with primary antibodies (B6-8, 1:500; anti-nucleolin, 1:500). After successive washes with PBS–0.1% Tween 20 (PBS-T), the membranes were incubated with secondary antibody coupled to HRP for 2 h at room temperature. Membranes were developed by enhanced chemiluminescence as recommended by the manufacturer (Pierce, Thermo Fisher Scientific), and bands were visualized on X-ray film (Kodak).

Phase-contrast microscopy, immunofluorescence microscopy, and superresolution analysis. Phase-contrast microscopy with a 40× or 60× objective, as indicated, was used to monitor preparations of subnuclear fractions. For immunofluorescence, HFF cells grown on coverslips to approximately 90% confluence were mock infected or infected with Ad5. Cells were processed for immunofluorescence as described previously (54). After the application of specific primary antibodies, cells were incubated with secondary antibodies. The coverslips were mounted on glass slides in PBS–10% glycerol, and samples were examined using a Zeiss Axiovert 200M inverted microscope with a 63×/1.4-numerical-aperture oil-immersion objective lens with an Axiocam MRM and Axiovision 3.1 software (Carl Zeiss, Inc.). Additionally, the cells were examined using an

Olympus IX-81 inverted microscope, with a 100×/1.49-numerical-aperture oil-immersion objective lens with an extra 1.6× intermediate magnification lens and an electron-multiplying charge-coupled-device (EMCCD) camera (iXon 897; model no. DU-897E-CS0-#BV; Andor).

For superresolution microscopy, cells were mounted on coverslips and treated as described above. RC and nucleolar fractions were spotted onto silane (Sigma)-coated slides as described before (53) and incubated with primary antibodies against DBP (1:50,000) and nucleolin (1:1,500) for 2 h at room temperature. After successive washes with PBS-T, secondary antibodies coupled to Alexa Fluor 568 or Alexa Fluor 488 (1:1,500 each) were added. Samples were washed with PBS-T, mounted in PBS–10% glycerol, and stored at −20°C. All superresolution imaging measurements were performed on an Olympus IX-81 inverted microscope configured for total internal reflection fluorescence (TIRF) excitation (cellTIRF Illuminator; Olympus). The critical angle was set up such that the evanescence field had a penetration depth of ~200 nm (Xcellence software v1.2; Olympus Soft Imaging Solution GMBH). The samples were continuously illuminated using excitation sources depending on the fluorophore used. Blue (Alexa 488)- and yellow (Alexa 568)-absorbing dyes were excited with either a 488-nm or a 561-nm diode-pumped solid-state laser. Beam selection and modulation of laser intensities were controlled via Xcellence software v.1.2. A full multiband laser cube set was used to discriminate the selected light sources (LF 405/488/561/635 A-OMF, Bright Line; Semrock). Fluorescence was collected using an Olympus UApo N 100×/1.49-numerical-aperture oil-immersion objective lens with an extra 1.6× intermediate magnification lens. All movies were recorded onto a 65- by 65-pixel region of an EMCCD camera at 100 nm per pixel. Subdiffraction images were derived from the Bayesian analysis of the stochastic blinking and bleaching (termed 3B analysis) of Alexa Fluor dyes (61). For each superresolution reconstruction, 300 images were acquired at 37 Hz with an exposure time of 23 ms at full laser power. The maximum laser power coming out of the optical fiber for the 488-nm and the 561-nm laser lines, measured at the back of the focal plane of the objective lens, were 23.1 mW and 19.1 mW, respectively. Each of the image sequences was fed into the 3B microscopy analysis plugin of Image J (62), considering a pixel size of 100 nm and a full-width half maximum of the point spread function of 270 nm (for Alexa Fluor 488) and 290 nm (for Alexa Flour 568), both measured experimentally with 0.17-μm fluorescent beads (PS-Speck microscope point source kit; Molecular Probes, Inc.). All other parameters were set up as the default values. The 3B analysis was run over 200 iterations as recommended (61, 62), and the final superresolution reconstructions were created at a pixel size of 10 nm. The spatial resolution observed in our imaging setup by 3B analysis was approximately 50 nm.

DNA purification. Subnuclear fractions from two independent experiments were treated with 1 mg/ml of proteinase K and 1:200 of Tween 20 (both from Promega). This preparation was incubated for 1 h at 55°C. Proteinase K inactivation was performed for 10 min at 95°C. The reactions were centrifuged for 2 min at 14,000 rpm at room temperature, and the supernatant was collected. The DNA was precipitated with a 1/10 volume of 3 M sodium acetate and one volume of isopropanol overnight at 4°C. The samples were centrifuged at 14,000 rpm for 10 min at room temperature. The pellet was washed with 70% ethanol and centrifuged for 5 min at 14,000 rpm at 4°C. The DNA was resuspended in 10 mM Tris-HCl, pH 7.4, quantified using a NanoDrop instrument, and stored at 4°C.

RNA purification. RNA was purified from NUC, CYT, Nlo, RCf, and Npl from two independent experiments using TRIzol according to the manufacturer's instructions (Invitrogen). The RNA pellet was resuspended in DEPC (diethylpyrocarbonate)-treated water and quantified using a NanoDrop instrument. Purified RNA was checked for the absence of DNA contamination by reverse transcriptase-negative (RT$^-$) reactions and stored at −70°C.

Primer design. The CLC Sequence Viewer (CLC Bio), Primer Plex (Premier Biosoft), and Primer-BLAST (NCBI) programs were used to design primers specific for the viral and cellular nucleic acid sequences of

interest. The primers used to detect viral pre-mRNA (ML) and viral DNA allowed the amplification of a region spanning the second intron within the TPL, from nucleotide 7273 to 7353; the primers used to detect the L5 pre-mRNA spanned a unique region within the L5 primary transcript, upstream of the coding sequence (CDS) of pIV/fiber and within the CDS, from nucleotide 29123 to 29239; primers used to detect the spliced L5 mRNA spanned the splice junction between the third exon of the TPL and the pIV exon (nucleotides 9722 to 31048 and 31212); primers for nucleolar DNA and RNA hybridized within the 18S rRNA sequence from nucleotide 1085 to 1224 (GenBank accession number X03205.1); to detect nonnucleolar DNA or RNA, the primers used allowed the amplification of a region within the U1 snRNA sequence from nucleotide 7 to 122 (NCBI reference sequence NR_004430.2). The primers used to detect spliced viral ML mRNA spanned the splice junction within the second and third exons of the TPL, from nucleotide 7172 to 9733; for spliced cellular RNA, the primers spanned the splice junction between exons 4 and 5 in the actin mRNA, from nucleotide 875 to 1013 (NCBI reference sequence NM_001101.3). All primers allowed the amplification of a unique product of the expected size. The sequences of the primer sets used were the following: viral DNA and RNA (ML; sequence within the second intron of the TPL) forward (Fw), GAGCGAGGTGTGGGTGAGC; reverse (Rv), GGATGCGACGACACTGACTTCA; L5 pre-mRNA Fw, GTCCATCCGCACCCACTATCTTC; Rv, AAGGCACAGTTGGAGGACCG; spliced L5-mRNA Fw, GTCACAGTCGCAAGATGAAGCG; Rv, GGTAACTAGAGGTTCGGATAGGCG; nucleolar DNA and RNA (18S) Fw, CGATGCCGACCGGCGATG; Rv, CTCCTGGTGGTGCCCTTC; nonnucleolar DNA (U1) Fw, ACCTGGCAGGGGAGATACCAT; Rv, GCAGTCGAGTTCCCACATTTGG; spliced viral ML mRNA (splice junction within the second and third exons of the TPL) Fw, GCCTCCGAACGGTACTCCGCC; Rv, CGCCACGGTGCTCAGCCTACC; spliced cellular mRNA (actin mRNA) Fw, CTTCCTTCCTGGGCATGGAGTCC; Rv, GCAATGCCAGGGTACATGGTGG.

cDNA synthesis. To analyze RNA, 100 ng of RNA obtained from each subnuclear fraction from two independent experiments was reverse transcribed using Revert-Aid reverse transcriptase according to the manufacturer's instructions (Thermo Scientific) in a 20-μl reaction volume.

PCR. Amplification of viral DNA or cDNA from subnuclear and subcellular fractions obtained from two independent experiments was carried out by PCR using *Taq* DNA polymerase as recommended by the manufacturer (Thermo Scientific) in a 25-μl reaction volume. For RT-PCR assays, RT$^-$ reactions were prepared to confirm the absence of DNA contamination. After PCR amplification, 10 μl of the reaction was loaded in 2% agarose gels, subjected to electrophoresis, and visualized using ethidium bromide staining.

Densitometry analysis. The DNA and RNA gel electrophoresis images, as well as WB films, were analyzed by densitometry using ImageJ (63). Graph Prism was used to plot the data and for statistical analysis by two-way analysis of variance (ANOVA) and Student's *t* test.

DNA replication assay in isolated RC. RCf-associated DNA polymerase activity was assayed in duplicate samples from two independent experiments, incubating RCf for 30 min at 30°C in a solution containing 200 mM ammonium sulfate, 40 mM Tris-HCl, pH 7.9, 5 mM MgCl$_2$, 3 mM DTT, 50 μM each deoxyribonucleoside triphosphate (dNTP), and 1 mM ATP (modified from reference 64). After this time, DNA was purified as described in the DNA purification section, and DNA synthesis was determined by amplifying a region of the adenoviral genome within the TPL sequence by PCR; for cellular DNA, 18S rRNA and U1 snRNA primers were used. The products were amplified for 25 cycles to avoid signal saturation. The amplified PCR products were separated in agarose gels, and bands were quantified by densitometry. Actinomycin D (ActD; 100 ng/ml) was used to inhibit DNA replication. Replication assays were carried out using duplicate samples obtained from two independent experiments, and data were analyzed by two-way ANOVA and *t* test.

Transcription assay in isolated RC. RC transcriptional activity was assayed in duplicate from two independent experiments, incubating RCf

for 10 min at 37°C in a solution containing 200 mM ammonium sulfate, 80 mM Tris-HCl, pH 7.9, 2 mM MnCl$_2$, 0.05 mM DTT, and 1 mM each ribonucleoside triphosphate (NTP) (modified from reference 65). After this time, RNA was isolated using TRIzol reagent as described above and checked for the absence of DNA contamination, and RNA synthesis was determined by RT-PCR using viral primers within the TPL sequence and cellular primers for actin mRNA and 18S rRNA. The products were amplified for 20 cycles to avoid signal saturation. Actinomycin D (25 μg/ml) was used to inhibit transcription. Transcription assays were carried out using duplicate samples from two independent experiments and analyzed by two-way ANOVA and *t* test.

Splicing assay in isolated RC. Splicing activity associated with RCf was assayed in duplicate from two independent experiments, incubating the fractions for 90 min at 30°C in a reaction mixture containing 1 mM ATP, 20 mM creatine phosphate, 3.2 mM MgCl$_2$, 0.25 U/μl of RiboLock (ThermoScientific), 1 mM DTT, 72.5 mM KCl, and 12 mM HEPES-KOH, pH 7.9 (modified from reference 66). After this time, RNA was isolated and checked for the absence of DNA contamination, and pre-mRNA splicing was determined by RT-PCR using primers that hybridized on splice junctions within the TPL (for viral mRNA) and within the actin mRNA (for cellular mRNA). The products were amplified for 25 cycles to avoid signal saturation. Erythromycin (500 μM) was used to inhibit splicing as previously reported (67). Splicing assays were carried out using duplicate samples from two independent experiments and analyzed by two-way ANOVA and *t* test.

Quantitative RT-PCR. Viral ML mRNA and L5 mRNA were quantified in NUC, CYT, Npl, and RCf using the SYBR green PCR master mix kit according to the manufacturer's instructions (Applied Biosystems). The primers used allowed the amplification of ML and L5 pre-mRNA and spliced species; U1 snRNA was used as an endogenous control. All primers were validated, proving to have an amplification efficiency close to 100%, as calculated by the linear regression obtained from standard curve assays. The primers allowed the amplification of a unique product of the expected size, as determined by melting curve analyses. The StepOne system (Applied Biosystems) was used for thermocycling; RT$^-$ and NTC controls were prepared for each experiment. The samples were analyzed by the $\Delta\Delta C_T$ comparative method using triplicate samples from two independent experiments. Statistical analyses were performed by two-way ANOVA and *t* test.

RNA extraction, cDNA library preparation, and sequencing. Total RNA from RCf isolated at 36 hpi from Ad5-infected HFF cells was extracted as described above. The quality of the total RNA was checked with a Bioanalyzer using an RNA Nano chip from Agilent Technologies. The sequencing libraries were generated with the ScriptSeq v2 transcriptome sequencing (RNA-Seq) kit from Epicenter. The quality check of libraries (size and quality) was visualized on a Bioanalyzer high-sensitivity DNA chip (high-sensitivity DNA kit from Agilent Technologies). The cDNA libraries were sequenced on the Illumina HiSeq 2500 system.

Computational analysis of splicing sites. In order to map the splice sites for Ad5, the H5pg4100 genome (wild-type virus that lacks a portion of E3, including the z leader [56]) was aligned to the Ad2 genome annotated sequences (NCBI reference sequence AC_000007.1). FASTQ files were aligned to the human genome, and these sequences were removed from the FASTQ file for this analysis. Using strand-specific FASTQ files, the reads were aligned using Bowtie2 aligner (68) to exon-exon junctions between leaders 2-i, i-3, and 2-3, as well as the exon-exon junctions for fiber mRNA (x, y, and fiber). The quantification of reads aligned to the exon-exon junction was done using the tool Multicov within the Bedtools package, considering at least 10 nucleotides of overlap in the exon-exon junctions.

RESULTS

Morphological and biochemical analysis of RCf. The adenoviral replication cycle comprises a complex interplay between viral and cellular factors that regulate and establish optimal conditions for
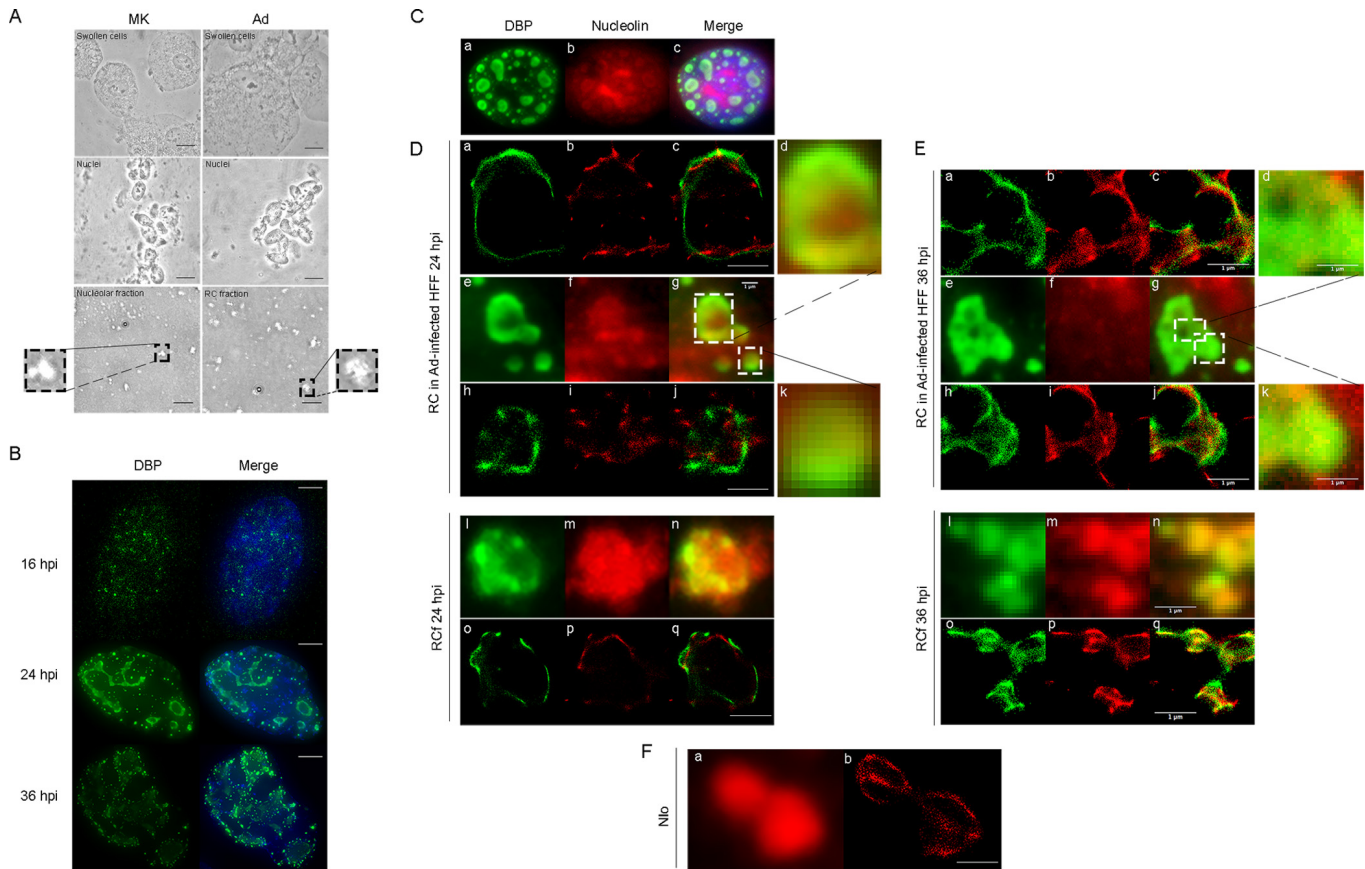
FIG 1 Morphology of isolated RC particles and nucleoli. (A) Procedure to isolate subnuclear fractions. The bright-field micrographs taken with a 40× objective show swollen mock-infected or Ad-infected cells in hypotonic buffer and nuclei in the upper and middle images, respectively (scale bar, 50 μm). Micrographs of RCf and nucleolar fractions were taken with a 63× objective (scale bar, 2 μm), and insets show a 5× zoom of RC or nucleoli of the expected size. (B) Micrographs of Ad-infected HFF, fixed at 16, 24, or 36 hpi (scale bar, 10 μm). DBP is shown in green and DNA in blue (4′,6-diamidino-2-phenylindole [DAPI]). (C) Immunofluorescence analysis of DBP (green) and nucleolin (red) in Ad-infected HFF at 24 hpi. (D and E) Superresolution analysis of RC fractions. TIRF images and 3B reconstructions of Ad-infected HFF, fixed 24 (D) or 36 (E) hpi and immunolabeled for DBP (green) and nucleolin (red). The TIRF images (d to g, k, and l to n) represent averages from 300 micrographs. Scale bar, 1 μm. Superresolution images were obtained for RC in infected cells (a to c and h to j) and for RCf (o to q). (F) Superresolution analysis of nucleolar fractions (Nlo). (a) The TIRF image represents the average from 300 micrographs. (b) The superresolution image of isolated nucleoli is shown. Scale bar, 1 μm.

viral genome replication. The accumulation of newly replicated viral DNA molecules promotes late gene expression and consequently viral progeny production. Viral DNA replication and late gene expression take place in replication compartments (RC); however, a major obstacle in the study of the adenovirus replication cycle has been our limited understanding of the molecular composition of RC and the viral and cellular activities that are influenced or controlled by these compartments. A variety of subnuclear bodies and large macromolecular complexes, such as Cajal bodies (69), nucleoli (58), and spliceosomes (70), have been isolated from the nucleus on the basis of features such as size, molecular mass, and density. Isolated subnuclear fractions have allowed a detailed characterization of the molecular composition and properties of their cognate nuclear domain.

As described in the introduction, viral and cellular proteins that modulate viral DNA replication, transcription, and posttranscriptional processing, as well as components of the cellular antiviral response, are associated with RC. Nevertheless, little is known about their localization within these viral microenvironments. In order to analyze in more detail the morphology and biochemical composition of RC, a fractionation protocol we re-

cently developed to isolate adenovirus RC (Fig. 1A) (53) was used to determine the localization of DBP and nucleolin within isolated RC particles by TIRF microscopy and the Bayesian analysis of blinking and bleaching (3B analysis) to obtain superresolution images (Fig. 1D to F). This approach allowed, for the first time, a nanoscale analysis of isolated RC particles that can help us study their organization at a resolution of approximately 50 nm. In parallel, the intracellular distribution of DBP and nucleolin also was analyzed both by conventional immunofluorescence (IF) microscopy (Fig. 1C) and using a 100×/1.49-numerical-aperture oil-immersion objective lens with an extra 1.6× intermediate magnification lens (Fig. 1B), as described in Materials and Methods.

Using conventional IF microscopy, DBP was seen to accumulate mostly in large foci and ring-like structures in the nuclei of Ad-infected cells, as expected (Fig. 1C, a and c). Nucleolin was detected as a faint, diffuse signal that was mostly nuclear, with some cytoplasmic staining near the periphery of the nucleus (Fig. 1C, b and c). The weak signal was overlaid with a small number of higher-intensity large inclusion-like structures that were devoid of DBP (likely corresponding to nucleoli), as well as numerous structures that matched the periphery of all DBP-containing foci and
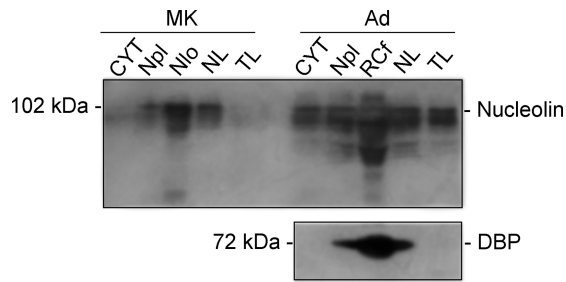
FIG 2 Nucleolin and DBP are enriched in RCf. Western blot (WB) of nucleolin and DBP in subnuclear fractions. Nucleolar (Nlo), replication compartment (RCf), nucleoplasm (Npl), and cytoplasmic (CYT) fractions, as well as total cell lysates (TL) and total nuclear lysates (NL), were obtained from mock-infected or Ad-infected HFF at 36 hpi. The molecular masses are shown for each protein.

rings (Fig. 1C, a to c). When the distribution of DBP was analyzed in Ad-infected cells at different times postinfection by TIRF microscopy (Fig. 1B), the expected pattern of distribution was observed, as DBP accumulated in numerous small foci by 16 hpi and, at later time points, was distributed in ring-like and open structures that appeared to coalesce, forming larger, more morphologically complex structures; however, in contrast to conventional IF microscopy, each of the larger structures was overlaid with numerous small DBP foci, especially by the later time point analyzed (36 hpi) (Fig. 1B). Interestingly, in contrast to the images that have been produced previously by confocal microscopy analysis of individual rings formed by DBP in Ad-infected cells, using TIRF at 24 hpi (Fig. 1D, e to g and insets d and k) or 36 hpi (Fig. 1E, e to g and insets d and k) and processing by the 3B algorithm (Fig. 1D and E, a to c and h to j) showed that DBP occupied the periphery of these rings only partially. Moreover, while nucleolin was associated with these structures, essentially no colocalization with DBP was observed at 24 hpi (Fig. 1D), as each protein localized with a different and separate pattern along defined regions of the rings' periphery, with nucleolin localizing mostly inside the periphery marked by DBP. In contrast to the 24-hpi time point, at 36 hpi (Fig. 1E), colocalization of DBP and nucleolin was observed mainly at the periphery of the ring-like structures. Isolated RC particles like those shown in the insets of Fig. 1A were analyzed by superresolution microscopy from both Ad-infected cells (24 and 36 hpi) and mock-infected cells (Fig. 1D and E, l to q, and F). The distribution of DBP or nucleolin in these particles was essentially the same as that observed in RC within Ad-infected cells (Fig. 1D and E, a to k). Interestingly, the particles obtained in the RCf displayed abundant levels of both DBP and nucleolin, confirming that Ad infection induces the recruitment of nucleolin to RC. RCf isolated at 36 hpi formed clusters (Fig. 1E, o to q), displaying a similar morphology to that observed for RC within Ad-infected cells, where higher colocalization of DBP and nucleolin at the periphery of RC could be observed.

We have recently found that bona fide RC components, such as the viral DNA, the DBP protein, and various representative sequences of viral late mRNA from the major late transcription unit (MLTU) (TPL, L2, L4 and L5 mRNA), are associated with RCf (53). To confirm the association of nucleolin with RCf, the presence of this protein was analyzed by Western blotting. Representative results for the analysis of nucleolin in various subcellular fractions are shown in Fig. 2. The fractions from mock-infected

cells showed that while nucleolin was not detectable in the cytoplasmic fraction (CYT) or total cell lysate (TL), the levels of this protein were approximately 5-fold higher in the nucleolar fraction (Nlo) than in the nucleoplasmic (Npl) and total nuclear fractions (NL). An analysis of nucleolin from the same number of Ad-infected cells showed that the protein was redistributed from the nucleolus to all subcellular fractions, in agreement with IF and superresolution microscopy (Fig. 1) and with previously reported experiments where the adenoviral pV protein induced the relocalization of nucleolin to the cytoplasm in transfection assays (71). Apart from the redistribution of nucleolin, the protein levels were higher than those in mock-infected cells, and the anti-nucleolin antibody detected both faster- and slower-migrating bands that were more prominent in the fraction corresponding to RC (Fig. 2). The nature of the additional bands observed in the nucleolar or RC fractions for nucleolin is unknown, but they could originate from posttranslational modifications or proteolytic cleavage. Nucleolin is known to be phosphorylated and to possess autocatalytic activity, resulting in cleavage fragments with apparent molecular masses of about 100, 70, 60, and 50 kDa (72). Such fragments closely match the bands observed in RCf fractions from Ad-infected cells (Fig. 2). These results confirm that nucleolin was relocalized to RC and suggest that its proteolytic products also are relocalized to these sites (Fig. 1C and D and Fig. 2).

Taken together, these results indicate that isolated RC have morphology similar to that of RC within Ad-infected cells at different stages of the late phase of infection, and that nucleolin is relocalized to the periphery of DBP in the RC, demonstrating that at this level of resolution compartmentalization of RC can be observed, as DBP and nucleolin displayed distinguishable distributions at different times postinfection. These results indicate that RCf can be used to precisely define the spatiotemporal association of DBP, and presumably other viral and cellular molecules, to RC at different stages of the viral replication cycle.

Adenovirus RCf are functional. RC are sites of viral DNA synthesis and late gene expression; thus, in addition to viral DNA, viral mRNA, and DBP (53), RCf could be expected to contain other viral and cellular components that participate in these molecular processes, such as the viral E2B DNA polymerase (Ad pol), the cellular RNA polymerase II (RNA pol II), and spliceosome components. Therefore, we decided to determine if the RCf were functional. To this end the subnuclear fractions were used for *in vitro* synthesis of DNA and mRNA and to evaluate mRNA splicing activity, as described in Materials and Methods.

Viral DNA synthesis in RCf. To determine whether viral DNA replication was associated with RCf, viral DNA synthesis was evaluated in fractions obtained at 16 (not shown), 24, and 36 hpi. The RCf were incubated in a reaction mixture in the presence of ATP and dNTP, DNA then was extracted and purified, and viral DNA was amplified by PCR and analyzed in agarose gels by densitometry as described in Materials and Methods. ActD was used in these assays to inhibit DNA synthesis as a control. One such gel from these experiments is shown as an example, and the data from two independent experiments are included in Fig. 3. No viral DNA synthesis was detected in samples from mock-infected cells or in the absence of ATP or dNTP. Clearly detectable levels of *de novo*-synthesized DNA were obtained at both times postinfection, as the level of DNA increased from input levels by 1.6-fold at 24 hpi and 3.3-fold at 36 hpi. ActD treatment significantly inhibited viral DNA replication, resulting in levels that were comparable to those
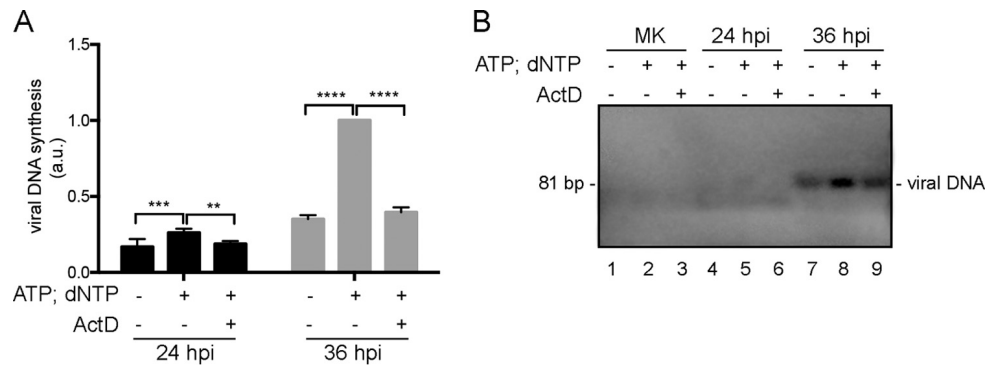
FIG 3 Viral DNA replication assay in RC subnuclear fractions. RCf obtained from Ad WT-infected or mock-infected HFF, harvested at 24 or 36 hpi, were incubated with ATP and dNTP. DNA was isolated, and *de novo* synthesized DNA was amplified by PCR. (A) Densitometry measurements of viral DNA. a.u., arbitrary units. (B) Representative gel with the viral DNA synthesized *de novo*. ActD, actinomycin D (100 ng/ml). The PCR products were measured by densitometry. Data from duplicates of two independent experiments are shown. **, $P < 0.01$; ***, $P < 0.001$; ****, $P < 0.0001$.

of the input DNA at both times postinfection ([Fig. 3A](#) and [B](#)). Both nucleolar DNA (ribosomal DNA) and nonnucleolar DNA (U1 gene) also were measured in these experiments when no amplification from these cellular DNA was observed (data not shown). These results clearly indicate that RCf contain active Ad pol that can direct *de novo* synthesis of viral DNA and that *in vitro* viral DNA synthesis is higher in RC isolated at 36 than at 24 hpi.

RNA synthesis in RCf. RNA pol II synthesis of viral late mRNA was measured to evaluate transcriptional activity associated with

RCf ([Fig. 4A](#) and [B](#)). The samples were incubated in the presence of NTP to determine the *de novo* synthesis of RNA, and as before, ActD served as a control to inhibit *de novo* transcription. No synthesis of viral mRNA was detected in mock-infected cells. As shown in [Fig. 4](#), the levels of viral ML mRNA increased above the level of the input by approximately 2-fold at 24 hpi and 5-fold at 36 hpi. The synthesis was dependent on the presence of NTP and was inhibited to input levels by ActD treatment. The same analysis was made to evaluate cellular mRNA synthesis when no *in vitro*

FIG 4 Transcription assay in RC subnuclear fractions. RCf obtained from Ad WT-infected or mock-infected HFF, harvested at 24 or 36 hpi, were incubated with NTP. RNA was isolated, and *de novo*-synthesized pre-mRNA was amplified by RT-PCR. (A and C) Viral late pre-mRNA (A) and cellular pre-mRNA (C). The mock-infected subnuclear fractions (MK) correspond to nucleoli. (B and D) Representative gels with the viral (B) and cellular (D) mRNA synthesized *de novo*. ActD was used at 25 μg/ml. The RT-PCR products were measured by densitometry. Data from duplicates of two independent experiments are shown. **, $P < 0.01$; ***, $P < 0.001$; ****, $P < 0.0001$.
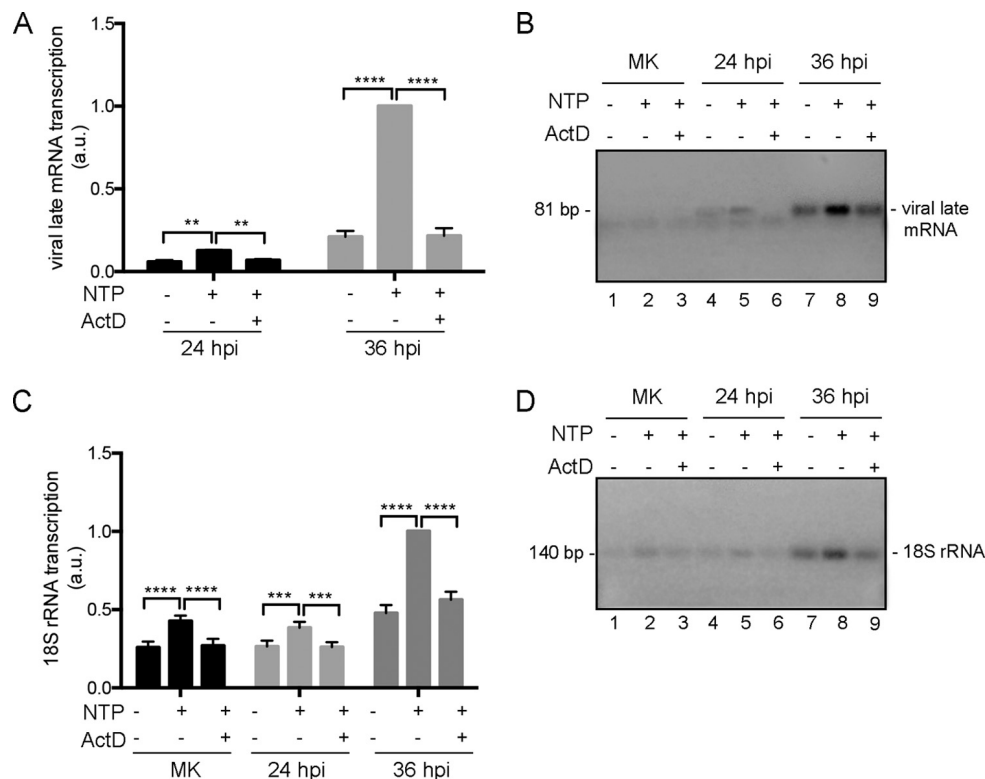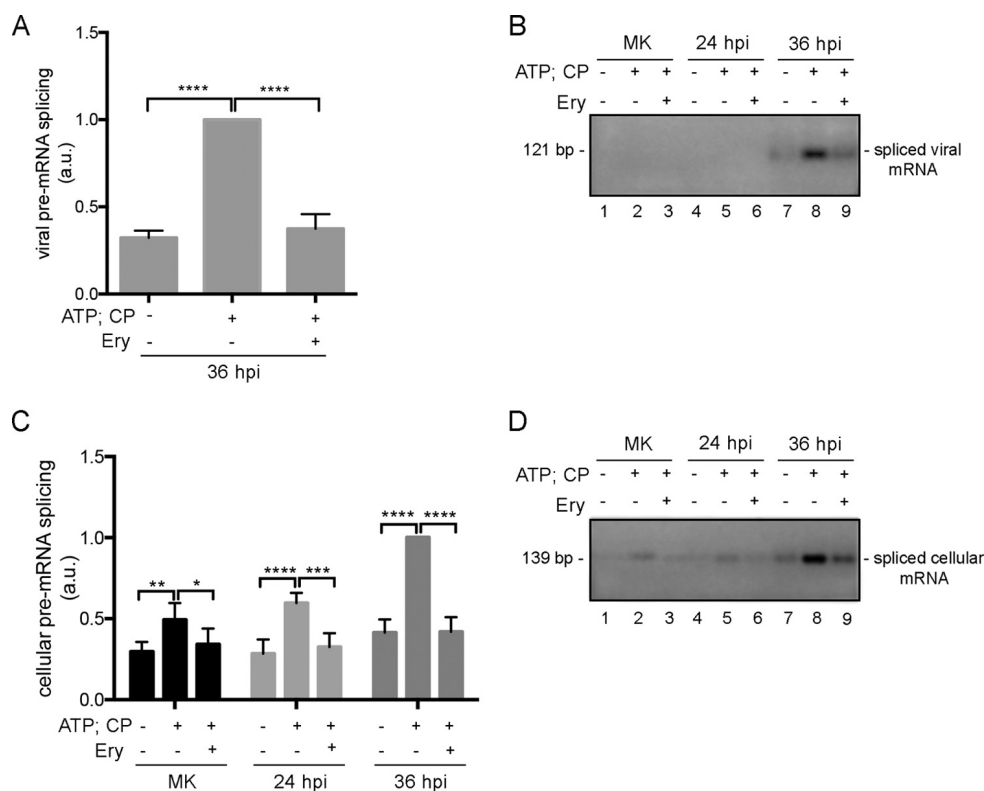
FIG 5 Splicing assay in RC subnuclear fractions. RCf obtained from Ad WT-infected or mock-infected HFF, harvested at 24 or 36 hpi, were incubated with ATP and CP. RNA was isolated, and spliced mRNA was amplified by RT-PCR. (A and C) Spliced viral late mRNA (A) and cellular mRNA (C). The mock-infected subnuclear fractions (MK) correspond to nucleoli. (B and D) Representative gels with the viral (B) and cellular (D) mature mRNA spliced *in vitro* in RCf. Ery, erythromycin (500 μM); CP, creatine phosphate. The RT-PCR products were measured by densitometry. Data from duplicates of two independent experiments are shown. *, $P < 0.05$; **, $P < 0.01$; ***, $P < 0.001$; ****, $P < 0.0001$.

transcription was observed (data not shown), indicating RNA pol II activity in RCf-directed transcription of viral but not cellular genes.

Since nucleoli are sites where rRNA are produced and previous work has established that isolated nucleoli maintain transcriptional activity (73), we decided to determine whether RCf retained RNA pol I activity. Therefore, rRNA synthesis was measured as described above (Fig. 4C and D). *De novo* rRNA synthesis was observed both in mock-infected (MK) and Ad-infected cells and was dependent on the presence of NTP. As with the RNA pol II viral products, rRNA transcription was inhibited by ActD to input levels in mock-infected and RCf fractions. Surprisingly, rRNA synthesis showed an almost 3-fold increase at 36 hpi compared to the level for MK.

Together, these results indicate RCf have both RNA pol I- and pol II-associated activity, and that such activity is higher at 36 than at 24 hpi.

mRNA splicing in RCf. Previous reports have shown that splicing factors and snRNP are localized adjacent to DBP foci (39, 74). ASF/SF2 as well as snRNP colocalize with viral transcription sites (42, 75–77). Since RCf were transcriptionally functional, the molecules necessary to process viral pre-mRNA could be expected to be associated with this fraction. Therefore, viral late mRNA splicing was evaluated in the subnuclear fractions. The RCf were incubated in a reaction mixture in the presence of ATP and creatine phosphate. RNA then was extracted and purified, and spliced viral mRNA was analyzed by RT-PCR. As a control, treatment of

the samples with erythromycin was used to inhibit the formation of the spliceosome C complex as previously reported (67).

Viral pre-mRNA splicing was dependent on the presence of ATP and creatine phosphate, and no products were obtained in samples from mock-infected cells. Mature viral mRNA was detected at levels that were approximately 3-fold higher than input levels at 36 hpi but not at 24 hpi (Fig. 5A and B). Treatment with erythromycin significantly inhibited the posttranscriptional processing of viral transcripts. Additionally, cellular pre-mRNA splicing was evaluated (Fig. 5C and D). In the nucleolar fraction and RCf, cellular actin pre-mRNA splicing was observed and was dependent on ATP and creatine phosphate. In all samples, treatment with erythromycin significantly inhibited pre-mRNA processing. Furthermore, RCf from Ad-infected cells showed a progressive increase at the different times postinfection in the levels of spliced actin mRNA species. It is known that IG are closely associated with DBP foci (32, 77); therefore, it is possible that IG coisolate with RC, which may account for the *de novo* processing of cellular species of pre-mRNA in RCf.

Together, these results demonstrate that RCf are functional and should allow detailed analysis of molecular activities associated with these structures.

Quantification of viral late mRNA synthesis and splicing associated with RCf. Adenovirus late gene expression proceeds through a coordinated and complex transcription program that requires the initiation of viral DNA synthesis for the activation of the major late (MLP) and L4 (L4P) promoters. The complexity of
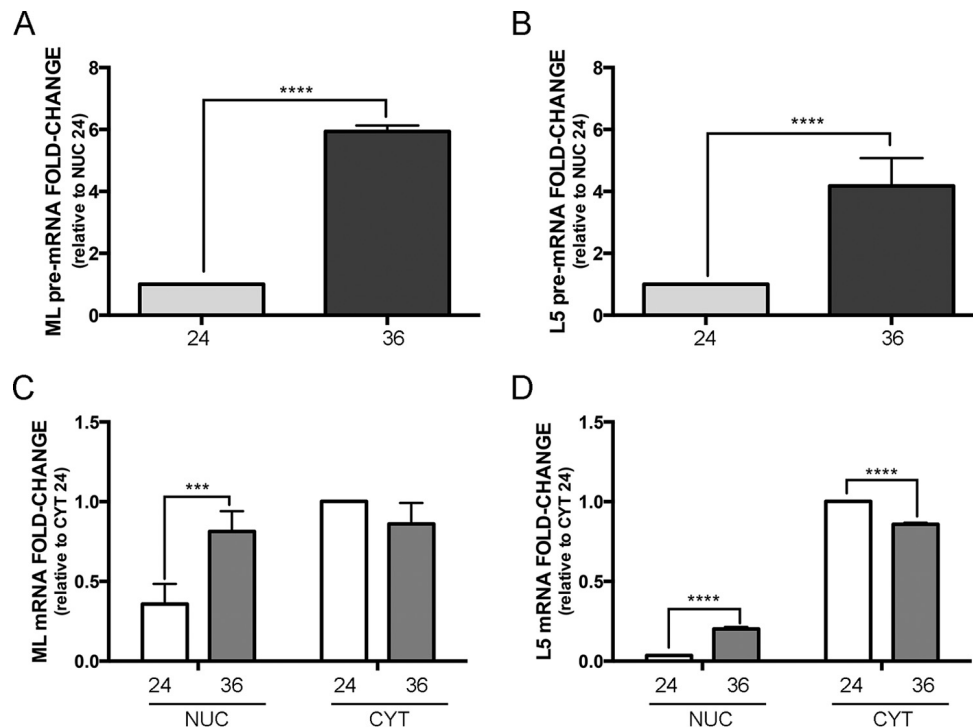
FIG 6 Quantitative analysis of nuclear and cytoplasmic viral late mRNA. Cytoplasmic and nuclear fractions were obtained from Ad WT-infected HFF and harvested at 24 or 36 hpi. Total RNA was isolated from each fraction and analyzed by real-time RT-PCR, as described in Materials and Methods. (A and B) Fold change in synthesis of viral late pre-mRNA (ML pre-mRNA) (A) and L5 pre-mRNA (B) in nuclear (NUC) fractions. (C and D) Fold change of mature ML mRNA (C) and L5 mRNA (D) in cytoplasmic (CYT) and NUC fractions. No amplification of pre-mRNA was detected in cytoplasmic fractions, which indicated there was no nuclear contamination of these fractions. Standard deviations and mean fold change values were plotted for triplicates from two independent experiments. ***, $P < 0.001$; ****, $P < 0.0001$.

the viral late gene expression program is further compounded with posttranscriptional processing of all mRNA species produced by the L1 to L5 viral late mRNA families. Although during the initial stages of the late phase both newly synthesized and spliced ML transcripts are associated with the peripheral replicative zones (PRZ) of RC (74, 78), as the late phase progresses cellular snRNP and spliced ML sequences accumulate in large clusters within surrounding IG (41, 77, 78). Since transcription does not take place in these IG structures (38, 77), it has been suggested that posttranscriptional processing of viral late mRNA continues in these sites (41, 74, 78). Nevertheless, it is not yet clear at which stage of posttranscriptional processing these transcripts may dissociate from RC to be transported to IG and later exported to the cytoplasm, nor is it known whether each viral late mRNA species can be processed in the same compartments or with similar kinetics. Moreover, these studies all have relied on immunofluorescence or electron microscopy, and it is not known whether, at the later stages of viral replication, IG remain a separate nuclear structure or if their components become embedded in viral RC. Since a sequence within the unspliced ML TPL has been detected both in RCf and in Npl (53) and de novo splicing of an ML sequence could be detected in RCf (Fig. 5), we decided to measure the partitioning of viral late pre-mRNA and spliced mRNA between the RC and Npl fractions at different times postinfection by quantitative RT-PCR. Therefore, RNA was isolated from RCf and Npl at 24 and 36 hpi as before, and primers designed to amplify sequences from the ML TPL and L5 spliced or unspliced mRNA were employed as described in Materials and Methods. For these experiments, we

initially measured the synthesis of viral late mRNA using total RNA obtained from the nucleus of Ad-infected cells at 24 and 36 hpi, and steady-state levels of all viral ML or L5 pre-mRNA were determined. The results from representative experiments are shown in Fig. 6, where a similar increase in ML or L5 pre-mRNA was observed from 24 to 36 hpi (Fig. 6A and B). Such increments are in agreement with previous reports that have measured transcription rates for late mRNA (79, 80). To determine the relative accumulation of spliced mRNA in the nucleus and cytoplasm, steady-state levels of spliced ML and L5 mRNA then were quantified (Fig. 6C and D). The increase in nuclear mRNA from 24 to 36 hpi was higher for L5 than for ML, for which a 6-fold increase was observed. Furthermore, the cytoplasmic accumulation of L5 mRNA was more efficient than that of ML, since at 36 hpi a greater number of spliced L5 transcripts was quantified in the cytoplasm than in the nucleus, while the number of ML transcripts was the same in both subcellular fractions. Since nucleocytoplasmic partitioning of mRNA traditionally has been used to measure the export of viral late mRNA (54, 60, 81, 82), these data suggest that the export rate for L5 mRNA is higher than that for all other ML mRNA. An alternative explanation, not necessarily exclusive, is that by the later time point nuclear or cytoplasmic mRNA turnover varies for each mRNA species.

To evaluate whether the observed differences in transcription and splicing or in the temporal pattern of cytoplasmic accumulation of ML and L5 mRNA were consequences of nuclear events during their biogenesis, we decided to measure the partitioning of spliced and unspliced ML and L5 mRNA between RC and Npl
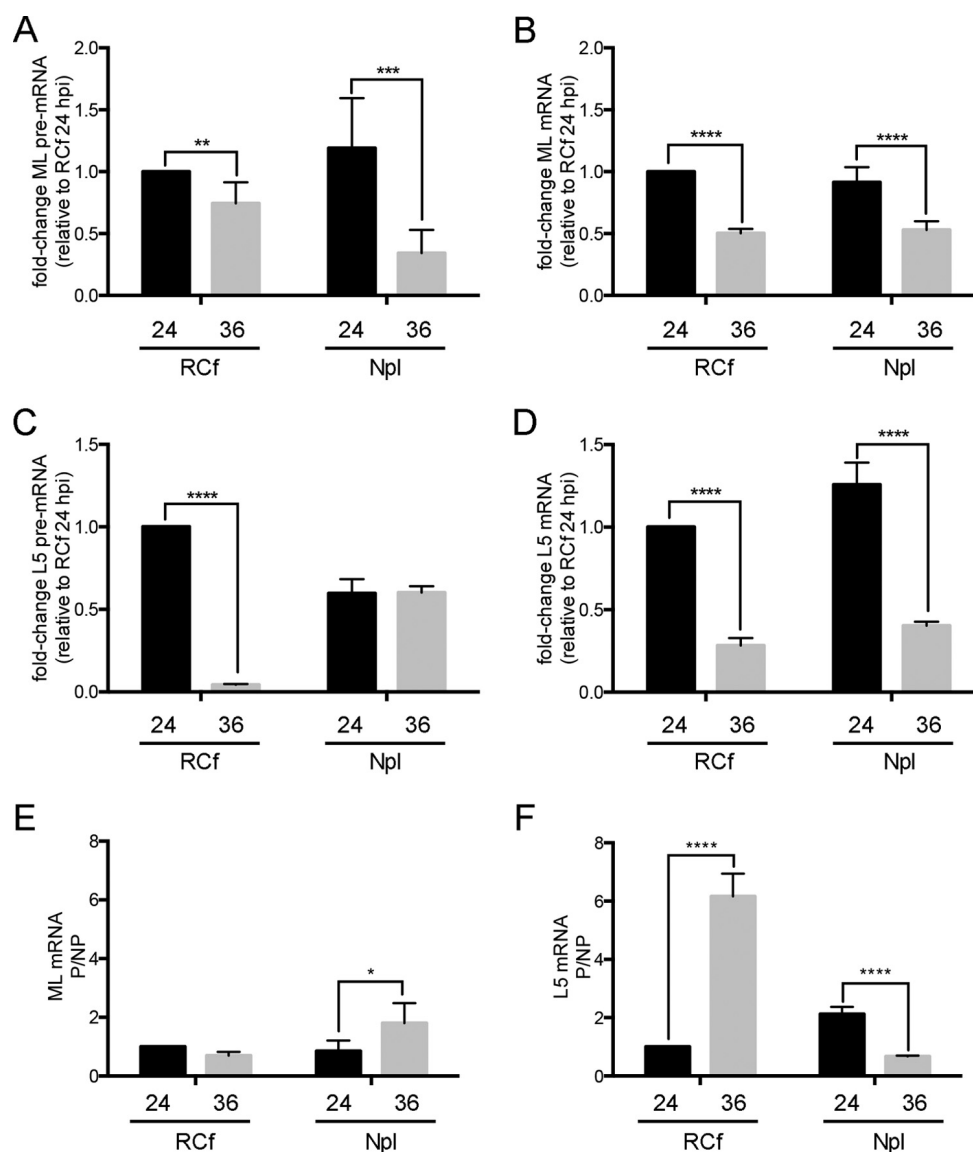
FIG 7 Quantitative analysis of splicing and association of viral late mRNA with RC fractions at different times postinfection. RCf and Npl fractions were obtained from Ad WT-infected HFF and harvested at 24 or 36 hpi. Total RNA was isolated from each fraction and quantified by real-time RT-PCR as described in Materials and Methods. (A to D) The graphs show the fold change for viral late ML pre-mRNA (A) and ML mRNA (B) and for L5 pre-mRNA (C) and L5 mRNA (D). (E and F) The ratios of processed to nonprocessed mRNA (P/NP) for ML (E) and L5 (F) are shown. Standard deviations and mean fold change values were plotted for triplicates from two independent experiments. *, $P < 0.05$; **, $P < 0.01$; ***, $P < 0.001$; ****, $P < 0.0001$.

fractions, as described in Materials and Methods. Representative results where the fold change was measured in these experiments are shown in Fig. 7. At both 24 and 36 hpi, all ML transcripts, unspliced (Fig. 7A) and spliced (Fig. 7B), displayed very similar distributions between RCf and Npl. In contrast, the unspliced L5 mRNA showed a 25-fold decrease in the RCf from 24 to 36 hpi (Fig. 7C), while the ratio of processed to nonprocessed L5 mRNA increased to a greater extent than that for ML mRNA in RCf. Since mRNA splicing activity was detected in RCf at 36 hpi (Fig. 5A), the decrease in the quantity of spliced L5 mRNA in the nucleus (Fig. 7D) and its simultaneous accumulation in the cytoplasm at the same time point (Fig. 6D) indicate that L5 mRNA splicing occurs in the RC and that at the later time postinfection, L5 mRNA splicing and export to the cytoplasm are more efficient than those of the rest of the ML transcripts.

To make a direct quantitative analysis of the unspliced and spliced forms of ML and L5 mRNA associated with RC and to further evaluate if the splicing of all alternative forms of L5 mRNA occurs in RC, we performed an RNA-Seq analysis of the mRNA associated with RCf at 36 hpi and quantified the sequences aligned to the junctions between different exons for these late transcripts (Fig. 8). Posttranscriptional processing of fiber mRNA requires splicing of an intron of close to 18 kb in length, a process that ignores at least 13 potential splice sites upstream of L5 (83, 84). Moreover, the fiber exon can be spliced to different upstream ancillary leader exons, including the TPL and the i leader, in combination with three other potential leaders inside the E3 region (leaders x, y, and z), as shown in Fig. 8B (83–85). Since splice sites for the Ad genome have been reported for serotype 2 (85) but the annotation was not complete for serotype 5, we first made an *in*
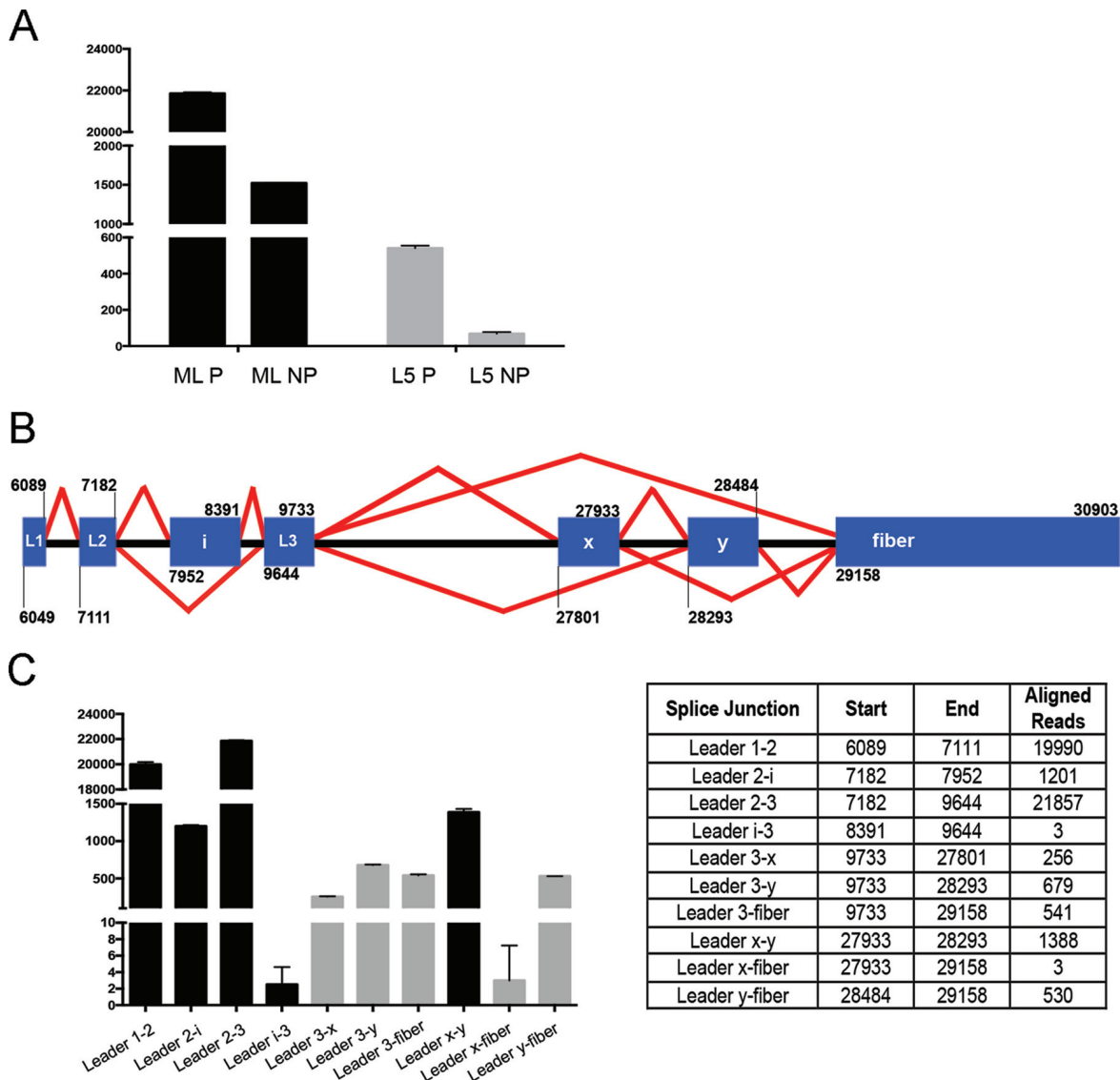
FIG 8 RNA sequence analysis of fiber mRNA splice sites in RCf. (A) The graph shows the sequence reads aligned to the leader 2-3 junction (ML P, black bars), the intron between leaders 2 and 3 (ML NP, black bars), leader 3-fiber junction (L5 P, gray bars), and intron region immediately upstream of fiber (L5 NP, gray bars). P, processed mRNA; NP, nonprocessed mRNA. (B) Splice diagram of fiber mRNA splice sites in the H5pg4100 genome. The numbers indicate the 5′ and 3′ ends of each exon. (C) The graph shows the sequence reads aligned to different potential splice sites for ML (black bars) and fiber (gray bars) mRNA. The number of sequence reads covering these splice sites as well as the nucleotides covering the splice junctions shown in the graph are listed in the table.

silico search to map all possible L5 splice sites in the Ad5 wild-type genome sequence (H5pg4100) (Fig. 8). In this viral genome a region in the E3 transcription unit that includes the 5′ splice site of the z leader has been deleted, while x and y leaders remain intact. To match the regions analyzed by quantitative RT-PCR with the RNA-Seq analysis, we quantified the reads aligned to the leader 2-3 junction (ML P), the intron between leaders 2 and 3 (ML NP), the leader 3-fiber junction (L5 P), and the intron right before the fiber exon (L5 NP) to determine the number of spliced and unspliced mRNA from the total set of viral late mRNA (ML) and the TPL-L5 mRNA (Fig. 8A). As shown in the graph, a greater quantity of spliced than unspliced mRNA was found for both ML and L5 at 36 hpi. As expected, the number of reads aligned for ML mRNA species were greater than those for L5 mRNA. Since the primers used in the quantitative RT-PCR assays only account for

TPL-fiber mRNA, we decided to quantify the RNA-Seq reads for different possible combinations of fiber splice junctions (Fig. 8C). The biological significance of i leader exon inclusion or exclusion has not been elucidated, but it has been shown to depend on the viral E4Orf3 and E4Orf6 proteins, respectively, and that splicing of ML mRNA at late times usually leads to its exclusion (86). Therefore, the low number of reads covering the leader i-3 splice junction could be expected (Fig. 8C). Alternatively, while the processing of all exon junctions leading to the production of L5-fiber mRNA occur in association with RC, the i-3 splice junction may not. The x and y leaders can be spliced to E3 and L5 mRNA, so the reads aligned to the splice junction between leaders x and y could correspond to either of these two viral mRNA species. Interestingly, the overall coverage pattern for reads aligned to L5 splice junctions in RCf closely matched those from total cell lysates re-

cently reported for Ad2 (85), including the high number of reads covering the splice junctions between leaders 3 and y, indicating that the fiber mRNA that contain these exons are the most abundant both in RCf and total cell lysates at 36 hpi. To our knowledge, a spatiotemporal change in the rate of synthesis or posttranscriptional processing of individual viral late transcripts has not been reported. The present results indicate that the quantitative analysis of the differential biogenesis of individual viral late mRNA species at different times of viral replication should be performed to obtain a detailed analysis of these events, and that RCf are amenable to perform such studies. Taken together, the results from quantitative RT-PCR assays and RNA-Seq indicate for the first time that alternative splicing of L5 mRNA is associated with RC and that these mRNA are spliced and accumulate in the cytoplasm more efficiently than the rest of the ML mRNA at late times postinfection.

DISCUSSION

Adenoviruses and other DNA viruses that replicate in the nucleus induce extensive reorganization of nuclear components, some of which are recruited to sites where viral RC are assembled (reviewed in reference 3). These virus-induced microenvironments represent a common viral strategy that promotes a productive replication cycle and simultaneously counteracts the antiviral cellular response. However, most aspects of the structure and function of RC remain to be explored; some of these include the relationship between their molecular components and the activities they regulate, as well as the dynamics of their assembly and the molecules involved in their structural integrity. In this study, we report for the first time the use of a recently established procedure that allows the isolation of adenovirus RC particles in subnuclear fractions obtained from infected cells to perform morphological and functional studies of RC (53). Such fractions recapitulate the spatial organization of RC within infected cells as visualized by superresolution microscopy, where DBP and nucleolin localize in the periphery of RC both in the infected cell nucleus and isolated RC particles. Significantly, these fractions proved to be functional, indicating that this novel approach should help to determine the macromolecular composition of RC and unravel fundamental aspects of the viral replication cycle and virus-cell interactions.

Isolated adenoviral RC are morphologically similar and recapitulate activities associated with RC in the infected cell. The distribution of DBP associated with RC within the infected cell nucleus by conventional or confocal microscopy, like that shown in Fig. 1C, has shown that the protein forms closed circular structures that seem to coalesce, giving rise to larger, morphologically complex open structures (reviewed in reference 3). The detailed analysis of Ad-infected cells presented here using higher magnification has shown for the first time that DBP accumulates in numerous small foci that are distributed in the periphery of the RC rings, forming structures with a beads-on-a-string appearance (Fig. 1B). This complex assembly of RC is stable enough to be isolated, since the morphology of isolated particles was indistinguishable from that of RC inside the infected cell nuclei. Morphological analyses of RC within infected cells, as well as isolated RCf and Nlo fractions by TIRF and superresolution microscopy, produced images in which both DBP and nucleolin could be seen to occupy defined areas of the particles' periphery. When TIRF images were reconstructed using the 3B algorithm, obtaining images close to 50-nm resolution, both proteins appeared as dots that

accumulated in some areas of the periphery of the isolated particles, indicating that, like nucleoli, RC are compartmentalized and that DBP and presumably other proteins (see the discussion on nucleolin below) occupy defined subcompartments localized mainly in the periphery of RC and only in certain areas that may correspond to PRZ. These findings indicate that the isolated particles can reveal detailed ultrastructural features of RC, and studies are under way to determine the localization of viral and cellular proteins that are known to be associated with RC using higher-resolution methods, such as transmission electron microscopy (TEM) and interferometry (87).

The presence of bona fide RC markers in RCf (53) suggested these subnuclear fractions also should contain the enzymatic activities associated with these viral sites in the infected cell. This hypothesis was confirmed, as RCf directed *de novo* synthesis of viral DNA and viral late RNA, as well as splicing of viral late mRNA (Fig. 3, 4A, and 5A). As the infection proceeds into the late phase, IG surround the PRZ, and components of Cajal bodies that participate in viral mRNA posttranscriptional processing are recruited to these sites (30, 78). Splicing factors, such as SC-35 and snRNP, also are relocalized to IG, forming clusters at the periphery of DBP where viral late mRNA enriched in exon sequences accumulate (39, 43, 74, 77, 78, 88, 89). Since in our experiments RCf could direct the splicing of both viral late and cellular mRNA, it is possible that clusters of IG are tightly associated with RC so that they could be coisolated in RCf. An alternative explanation for both the RCf-associated RNA pol I activity and for the splicing of cellular mRNA is that by late times postinfection (36 hpi), the coalescing RC form a meshwork to which actively transcribed mRNA associate and therefore can be sedimented with the RC particles.

The nuclear matrix is commonly defined as the subnuclear fraction that results from sequential salt extractions, using increasing concentrations of detergent and nuclease treatment (90, 91). DNA replication, transcription, RNA processing, and transport are nuclear activities that, although transient, can be associated with the nuclear matrix (reviewed in references 90 and 92). Since the solutions used to isolate RCf exclude salt extraction and detergents, consist solely of sucrose and magnesium, and are disrupted by mild sonication (see Materials and Methods), it is possible that the RC subnuclear fraction contains associated nuclear matrix molecules, explaining the presence of cellular mRNA in the RCf. These observations are in agreement with previous findings by Leppard and Shenk, where both ML and cellular mRNA were shown to transit through a series of biochemically defined nuclear fractions, as they are synthesized in a nuclear matrix fraction and subsequently accumulate in a nuclear soluble fraction prior to entry into the cytoplasm (79, 93). When protease inhibitors are included in procedures used to isolate nuclear matrix that omit RNase treatment, the isolated nuclear matrix contains RNA as the second most abundant component (reviewed in reference 90). Other macromolecules from the nuclear matrix include structural proteins such as the lamins, residual nucleoli, residual elements of the nuclear envelope, and nuclear domains such as PML NB and Cajal bodies (90–92). The proteomic analysis of RCf has revealed the presence of nuclear matrix proteins associated with RC, such as nuclear lamins B1, B2, and A/C (unpublished data). Other molecules that could facilitate the formation of a meshwork in which RC activities and protein/nucleic acid interactions would be fulfilled include PML and the viral early protein E4Orf3. Previous

reports have shown that PML IV can assemble in cage-like structures (94, 95). In the case of E4Orf3, this early protein can oligomerize in linear and branched chains that further form a polymer network that has been described to partition the nuclear volume (96). It will be interesting to determine whether these and other viral and cellular proteins participate in the formation and maintenance of the structural integrity and functions of RC.

Nucleolin is relocalized to RC in adenovirus-infected cells. During adenovirus infection, nuclear domains are extensively reorganized. One prominent example is the reorganization of nucleoli, with major effects on the biogenesis of rRNA and relocalization of nucleolar proteins. For example, the principal nucleolar component, nucleolin, is relocalized from the nucleus to the cytoplasm in the presence of the viral late protein pV (71); the phosphoproteins B23.1 and B23.2 interact with viral E2 proteins and basic core proteins pV and pVII, promoting efficient DNA replication (45, 97, 98); and accumulation of rRNA in the cytoplasm is impaired during adenovirus infection (99, 100). Analyses of the effect of ActD versus viral infection on the proteomic composition of nucleoli have shown no correlation, since inhibiting replication and transcription with ActD treatment induced changes in more than 30% of the nucleolar proteins, while Ad infection showed an effect in only 7% of these proteins (46, 101). These results suggest that the effect of Ad infection on the nucleolar proteome is specific to the infection and not due to a more general effect of nonspecific cellular stress.

Here, we have demonstrated for the first time that nucleolin is relocalized to specific compartments of adenoviral RC. Significantly, nucleolin localized to the periphery of these viral sites in a dynamic spatiotemporal reorganization. The localization of nucleolin initially differed from that of DBP (Fig. 1C, D, and E), but as the late phase progressed (by 36 hpi), both proteins colocalized in a few defined dots around RC. The periphery of RC is the zone where viral DNA replication and gene expression take place (39, 41, 43, 75, 77, 78, 102, 103); hence, the localization of nucleolin at the periphery of RC particles, which likely corresponds to the PRZ, suggests this nucleolar protein could participate in adenoviral genome replication or expression. In cytomegalovirus-infected cells, nucleolin interacts with viral DNA replication factors UL44 and UL84 at the periphery of viral replication compartments, maintaining the architecture of these viral sites and promoting efficient viral DNA synthesis, expression of viral late genes, and virus production (104–106). Other proteins from RNA or DNA viruses have been shown to target nucleolar proteins to subserve viral transcription, translation, and regulation of the cell cycle to promote viral replication (28, 101, 104, 107). In the case of adenovirus, the role of nucleoli during the replication cycle is incompletely understood, and it should be interesting to investigate whether the relocalization of nucleolin to specific subcompartments of the adenoviral RC is required to modulate specific activities associated with viral DNA replication and gene expression or, as it does in the nucleolus, to provide structural integrity to RC. Our experiments have revealed an additional unprecedented finding, as slower- and faster-migrating bands that closely match proteolytic and phosphorylated products of nucleolin were generated in Ad-infected cells (Fig. 2A). Nucleolin is a phosphoprotein with self-cleavage properties, and its fragmentation usually has been observed during extraction procedures, indicating that its association with nuclear molecules, such as DNA, RNA, or the nuclear matrix, promotes the protein's sta-

bility (108). Additionally, the self-cleavage activity of nucleolin correlates with its phosphorylation and with cell cycle regulation (108, 109). In our experiments the faster- and slower-migrating bands detected with the anti-nucleolin antibody were more abundant in RCf than Npl or other subcellular fractions (Fig. 2A, RCf), suggesting Ad infection mimics the conditions in the cell that induce modification and processing of nucleolin. Furthermore, nucleolin also was detected in its intact form, as the expected 102-kDa band was more abundant than the modified products, indicating that the various forms of nucleolin become associated with RCf during infection. It is unlikely that the fractionation procedure accounts for the generation of the proteolytic (or posttranslationally modified) products, since both RCf and nucleoli were isolated using the same procedure, and these bands were almost undetectable in the nucleolar fraction from mock-infected cells (Fig. 2A, MK Nlo). In addition, the procedure to obtain other subcellular fractions, such as CYT, NL, or TL, did not result in the generation of faster- and slower-migrating bands for nucleolin. These data suggest that Ad infection induces the proteolysis of nucleolin and that the proteolytic products are enriched in RCf. Since the isolated particles resemble the morphology of RC in Ad-infected cells (Fig. 1D and E), this strategy should allow the determination of the impact of the posttranslational modifications and relocalization of nucleolin in Ad-infected cells.

As described in the introduction, several other factors that participate in the cellular response to infection are relocalized to adenoviral RC. Some of them include components of the DNA damage response, such as Mre11, ATM, or ATR (24, 26); the tumor suppressor, p53 (23, 110); and STAT1, a key activator of the innate immune response (22) (Fig. 9). Hence, it will be interesting to study the role these cellular proteins play in the activities of RC once they are coopted to these virus-induced sites.

Differential synthesis and splicing of viral late mRNA species associated with RC. The complexity of the adenoviral replication cycle involves a gene expression program with multiple levels of regulation, from sequential regulation of transcription to the selective export and translation of viral late mRNA, that result in the progressive increase of viral late gene products (reviewed in reference 111). Such increases in the expression of viral late genes depends on the accumulation of replicated viral genomes and the presence of a number of cellular and viral proteins. Many features of the biogenesis of major late (ML) mRNA have been studied in detail (111). Using a fractionation scheme that relied on the stepwise extraction of RNA with different salt concentrations, ionic and nonionic detergents, and DNase I, Leppard and Shenk determined that viral late mRNA were synthesized in a nuclear matrix-associated fraction and then were transported to a nuclear soluble fraction before reaching the nuclear membrane and finally a cytoplasmic fraction (79). Interestingly, our experiments have shown a similar pattern of mRNA partitioning between subnuclear compartments and the cytoplasm. However, simultaneous analysis at different times postinfection of the rate of synthesis of ML pre-mRNA, the ratio of spliced to unspliced RNA, partitioning of different ML RNA between the nucleus and cytoplasm, and partitioning between RCf and Npl have not been reported. Therefore, the analysis performed here at different times postinfection, of spliced and unspliced species of all ML and that of L5 mRNA, revealed that although, as expected, all nuclear pre-mRNA increased as the late phase of infection progressed (Fig. 6A and B), the efficiency of the cytoplasmic accumulation of the L5 mRNA
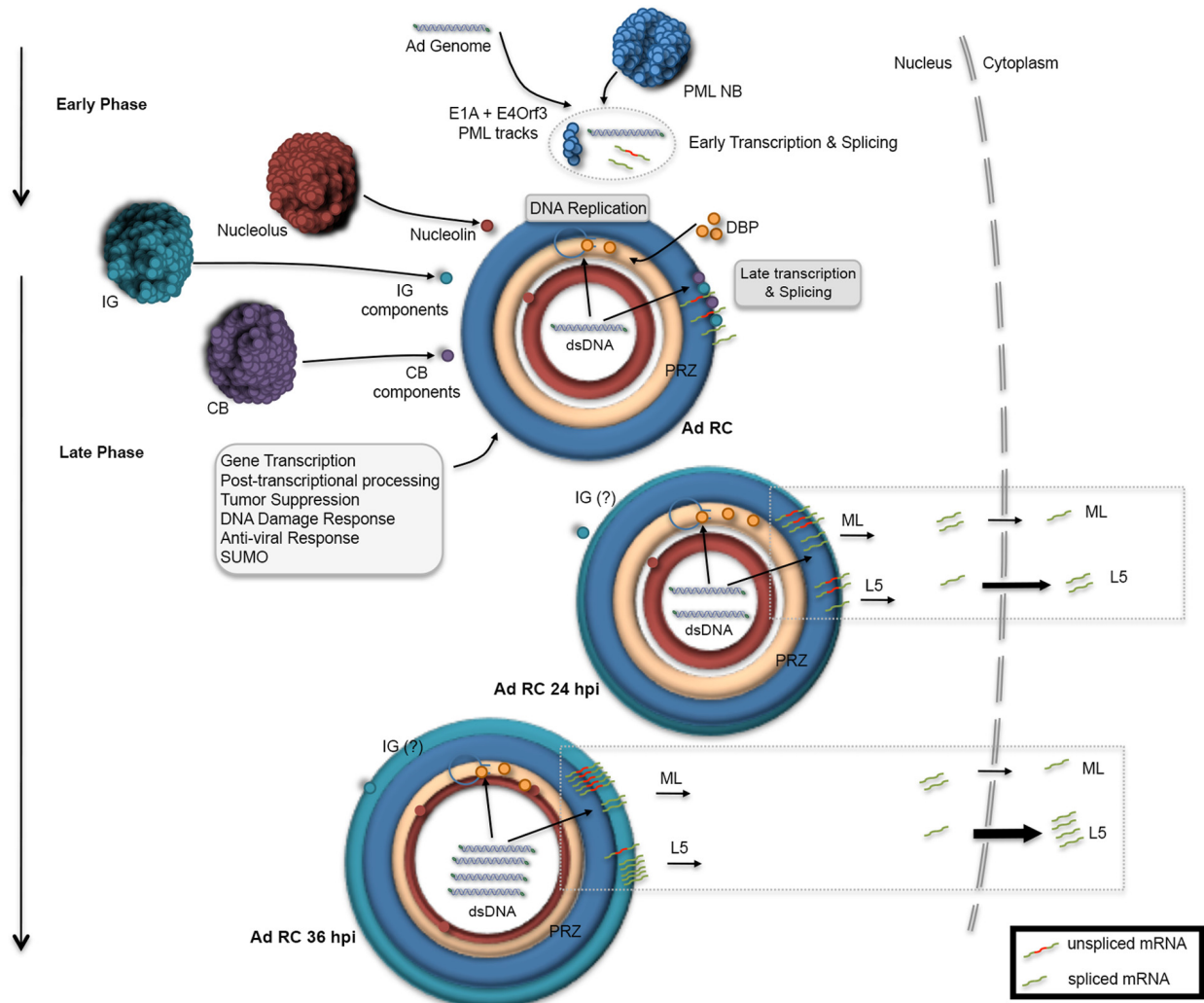
FIG 9 Scheme of adenovirus replication compartments (RC), indicating assembly and compartmentalization during the early and late phases of infection. PML nuclear bodies (PML NB), Cajal bodies (CB), and interchromatin granules (IG), which play important roles during RC formation and activities, are shown in blue, purple, and turquoise, respectively. The nucleolus is shown in red. Upon entry into the infected cell nucleus, the viral DNA is localized adjacent to PML NB. During the early phase, the viral proteins E1A and E4Orf3 induce the reorganization of PML NB into track-like structures. Viral proteins, nucleolin, and other nuclear components are relocalized adjacent to PML tracks, inducing the formation of viral RC. RC are compartmentalized, with DBP at the peripheral replicative zones (PRZ) where viral DNA replication and transcription take place. Nucleolin initially is localized to a compartment different from that of DBP, but as the late phase progresses, DBP and nucleolin colocalize. IG components are reorganized adjacent to DBP, allowing the association of splicing activity with RC. As the replication cycle progresses to the late phase, IG components form clusters at the periphery of DBP, viral late transcription increases, and L5 mRNA are more efficiently spliced and accumulated in the cytoplasm than all other ML mRNA.

was significantly higher than that of the rest of all ML RNA combined (Fig. 6C and D and 9). Interestingly, the partitioning of the spliced versus unspliced L5 mRNA between RCf and Npl also was different from that for ML. The pattern of accumulation of L5 RNA indicated that it is efficiently and completely spliced in association with RC, and that its transit from RCf to cytoplasm also is more efficient than that of the rest of the ML mRNA (Fig. 6 and 7). The L5 pre-mRNA and mRNA displayed temporal patterns of splicing and release from RCf to Npl different from those of all other ML mRNA, and these findings suggest that each viral late RNA family is subject to different regulatory events during their biogenesis associated with RC (Fig. 9). Alternatively, it also is possible that the production of the L5 mRNA has unique features among the viral late mRNA, and that the splicing of the ancillary x and y exons may be biologically significant, as it has been sug-

gested to determine the virus host range (112). Although it has been known for some time that as the late phase of viral replication progresses the splicing of longer introns of the MLTU increases, the large difference in the efficiency of splicing and export of L5 mRNA compared with that of the rest of the ML mRNA observed in these experiments had not been reported. The RNA-Seq analysis of viral late mRNA in RCf indicates that the production of the different species of fiber mRNA is established at adenovirus RC. These findings are in agreement with previous reports that have shown both introns and exons from the MLTU are present in PRZ and in IG, suggesting that splicing occurs in both compartments (31, 32, 37, 38, 41, 42, 74, 77, 78, 88, 102, 113). However, the data presented here suggest either that IG are coisolated in the RCf or that all IG components required for complete splicing of viral late mRNA are coopted to adenovirus RC (Fig. 9).

Quantitative analyses of the proteomic composition and further transcriptomic analyses of RCf are under way and will help to identify viral and cellular proteins and nucleic acids that associate with or are processed in these structures, and they should provide detailed insights into the viral replication cycle and virus-cell interactions.
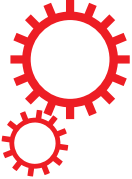
REFERENCES

1. **Netherton C, Moffat K, Brooks E, Wileman T.** 2007. A guide to viral inclusions, membrane rearrangements, factories, and viroplasm produced during virus replication. Adv Virus Res **70:**101–182. http://dx.doi.org/10.1016/S0065-3527(07)70004-0.
2. **Netherton CL, Wileman T.** 2011. Virus factories, double membrane vesicles and viroplasm generated in animal cells. Curr Opin Virol **1:**381–387. http://dx.doi.org/10.1016/j.coviro.2011.09.008.
3. **Schmid M, Speiseder T, Dobner T, Gonzalez RA.** 2014. DNA virus replication compartments. J Virol **88:**1404–1420. http://dx.doi.org/10.1128/JVI.02046-13.
4. **den Boon JA, Diaz A, Ahlquist P.** 2010. Cytoplasmic viral replication complexes. Cell Host Microbe **8:**77–85. http://dx.doi.org/10.1016/j.chom.2010.06.010.
5. **Novoa RR, Calderita G, Arranz R, Fontana J, Granzow H, Risco C.** 2005. Virus factories: associations of cell organelles for viral replication and morphogenesis. Biol Cell **97:**147–172. http://dx.doi.org/10.1042/BC20040058.
6. **Paul D, Bartenschlager R.** 2013. Architecture and biogenesis of plus-strand RNA virus replication factories. World J Virol **2:**32–48. http://dx.doi.org/10.5501/wjv.v2.i2.32.
7. **Uchil PD, Satchidanandam V.** 2003. Architecture of the flaviviral replication complex. Protease, nuclease, and detergents reveal encasement within double-layered membrane compartments. J Biol Chem **278:**24388–24398.
8. **Mazzolini L, Bonneville JM, Volovitch M, Magazin M, Yot P.** 1985. Strand-specific viral DNA synthesis in purified viroplasms isolated from turnip leaves infected with cauliflower mosaic virus. Virology **145:**293–303. http://dx.doi.org/10.1016/0042-6822(85)90162-X.
9. **Paul D, Hoppe S, Saher G, Krijnse-Locker J, Bartenschlager R.** 2013. Morphological and biochemical characterization of the membranous hepatitis C virus replication compartment. J Virol **87:**10612–10627. http://dx.doi.org/10.1128/JVI.01370-13.
10. **Kopek BG, Perkins G, Miller DJ, Ellisman MH, Ahlquist P.** 2007. Three-dimensional analysis of a viral RNA replication complex reveals a virus-induced mini-organelle. PLoS Biol **5:**e220. http://dx.doi.org/10.1371/journal.pbio.0050220.
11. **Green KY, Mory A, Fogg MH, Weisberg A, Belliot G, Wagner M, Mitra T, Ehrenfeld E, Cameron CE, Sosnovtsev SV.** 2002. Isolation of enzymatically active replication complexes from feline calicivirus-infected cells. J Virol **76:**8582–8595. http://dx.doi.org/10.1128/JVI.76.17.8582-8595.2002.
12. **Quinkert D, Bartenschlager R, Lohmann V.** 2005. Quantitative analysis of the hepatitis C virus replication complex. J Virol **79:**13594–13605. http://dx.doi.org/10.1128/JVI.79.21.13594-13605.2005.
13. **van Hemert MJ, de Wilde AH, Gorbalenya AE, Snijder EJ.** 2008. The in vitro RNA synthesizing activity of the isolated arterivirus replication/transcription complex is dependent on a host factor. J Biol Chem **283:**16525–16536. http://dx.doi.org/10.1074/jbc.M708136200.
14. **Roder A, Koschel K.** 1975. Virus-specific proteins associated with the replication complex of poliovirus RNA. J Gen Virol **28:**85–98. http://dx.doi.org/10.1099/0022-1317-28-1-85.
15. **van Hemert MJ, van den Worm SH, Knoops K, Mommaas AM, Gorbalenya AE, Snijder EJ.** 2008. SARS-coronavirus replication/transcription complexes are membrane-protected and need a host factor for activity in vitro. PLoS Pathog **4:**e1000054. http://dx.doi.org/10.1371/journal.ppat.1000054.
16. **Lallemand-Breitenbach V, de The H.** 2010. PML nuclear bodies. Cold Spring Harb Perspect Biol **2:**a000661.
17. **Wang L, Ren XM, Xing JJ, Zheng AC.** 2010. The nucleolus and viral infection. Virol Sin **25:**151–157. http://dx.doi.org/10.1007/s12250-010-3093-5.
18. **Spector DL, Lamond AI.** 2011. Nuclear speckles. Cold Spring Harb Perspect Biol **33:**a000646.
19. **Everett RD.** 2001. DNA viruses and viral proteins that interact with PML nuclear bodies. Oncogene **20:**7266–7273. http://dx.doi.org/10.1038/sj.onc.1204759.
20. **Everett RD.** 2006. Interactions between DNA viruses, ND10 and the DNA damage response. Cell Microbiol **8:**365–374. http://dx.doi.org/10.1111/j.1462-5822.2005.00677.x.
21. **Geoffroy MC, Chelbi-Alix MK.** 2011. Role of promyelocytic leukemia protein in host antiviral defense. J Interferon Cytokine Res **31:**145–158. http://dx.doi.org/10.1089/jir.2010.0111.
22. **Sohn SY, Hearing P.** 2011. Adenovirus sequesters phosphorylated STAT1 at viral replication centers and inhibits STAT dephosphorylation. J Virol **85:**7555–7562. http://dx.doi.org/10.1128/JVI.00513-11.
23. **Cardoso FM, Kato SE, Huang W, Flint SJ, Gonzalez RA.** 2008. An early function of the adenoviral E1B 55 kDa protein is required for the nuclear relocalization of the cellular p53 protein in adenovirus-infected normal human cells. Virology **378:**339–346. http://dx.doi.org/10.1016/j.virol.2008.06.016.
24. **Carson CT, Orazio NI, Lee DV, Suh J, Bekker-Jensen S, Araujo FD, Lakdawala SS, Lilley CE, Bartek J, Lukas J, Weitzman MD.** 2009. Mislocalization of the MRN complex prevents ATR signaling during adenovirus infection. EMBO J **28:**652–662. http://dx.doi.org/10.1038/emboj.2009.15.
25. **Kite GL, Chambers R, Jr.** 1912. Vital staining of chromosomes and the function and structure of the nucleus. Science **36:**639–641. http://dx.doi.org/10.1126/science.36.932.639.
26. **Castillo-Villanueva E, Ballesteros G, Schmid M, Hidalgo P, Schreiner S, Dobner T, Gonzalez RA.** 2014. The Mre11 cellular protein is modified by conjugation of both SUMO-1 and SUMO-2/3 during adenovirus infection. ISRN Virol **2014:**14.
27. **Ishov AM, Maul GG.** 1996. The periphery of nuclear domain 10 (ND10) as site of DNA virus deposition. J Cell Biol **134:**815–826. http://dx.doi.org/10.1083/jcb.134.4.815.
28. **Hiscox JA.** 2002. The nucleolus–a gateway to viral infection? Arch Virol **147:**1077–1089. http://dx.doi.org/10.1007/s00705-001-0792-0.
29. **Rodrigues SH, Silva NP, Delicio LR, Granato C, Andrade LE.** 1996. The behavior of the coiled body in cells infected with adenovirus in vitro. Mol Biol Rep **23:**183–189. http://dx.doi.org/10.1007/BF00351167.
30. **James NJ, Howell GJ, Walker JH, Blair GE.** 2010. The role of Cajal bodies in the expression of late phase adenovirus proteins. Virology **399:**299–311. http://dx.doi.org/10.1016/j.virol.2010.01.013.
31. **Besse S, Puvion-Dutilleul F.** 1995. Anchorage of adenoviral RNAs to clusters of interchromatin granules. Gene Expr **5:**79–92.
32. **Bridge E, Xia DX, Carmo-Fonseca M, Cardinali B, Lamond AI, Pet-**

tersson U. 1995. Dynamic organization of splicing factors in adenovirus-infected cells. J Virol **69:**281–290.

33. **Blackford AN, Bruton RK, Dirlik O, Stewart GS, Taylor AM, Dobner T, Grand RJ, Turnell AS.** 2008. A role for E1B-AP5 in ATR signaling pathways during adenovirus infection. J Virol **82:**7640–7652. http://dx .doi.org/10.1128/JVI.00170-08.

34. **Evans JD, Hearing P.** 2005. Relocalization of the Mre11-Rad50-Nbs1 complex by the adenovirus E4 ORF3 protein is required for viral replication. J Virol **79:**6207–6215. http://dx.doi.org/10.1128/JVI.79.10.6207 -6215.2005.

35. **Rosa-Calatrava M, Puvion-Dutilleul F, Lutz P, Dreyer D, de The H, Chatton B, Kedinger C.** 2003. Adenovirus protein IX sequesters host-cell promyelocytic leukaemia protein and contributes to efficient viral proliferation. EMBO Rep **4:**969–975. http://dx.doi.org/10 .1038/sj.embor.embor943.

36. **Maul GG, Jensen DE, Ishov AM, Herlyn M, Rauscher FJ, III.** 1998. Nuclear redistribution of BRCA1 during viral infection. Cell Growth Differ **9:**743–755.

37. **Puvion-Dutilleul F, Roussev R, Puvion E.** 1992. Distribution of viral RNA molecules during the adenovirus type 5 infectious cycle in HeLa cells. J Struct Biol **108:**209–220. http://dx.doi.org/10.1016/1047 -8477(92)90021-2.

38. **Puvion-Dutilleul F, Pichard E.** 1992. Segregation of viral double-stranded and single-stranded DNA molecules in nuclei of adenovirus infected cells as revealed by electron microscope in situ hybridization. Biol Cell **76:**139–150. http://dx.doi.org/10.1016/0248-4900(92)90206-G.

39. **Pombo A, Ferreira J, Bridge E, Carmo-Fonseca M.** 1994. Adenovirus replication and transcription sites are spatially separated in the nucleus of infected cells. EMBO J **13:**5075–5085.

40. **Besse S, Puvion-Dutilleul F.** 1994. Compartmentalization of cellular and viral DNAs in adenovirus type 5 infection as revealed by ultrastructural in situ hybridization. Chromosome Res **2:**123–135. http://dx.doi .org/10.1007/BF01553491.

41. **Puvion-Dutilleul F, Bachellerie JP, Visa N, Puvion E.** 1994. Rearrangements of intranuclear structures involved in RNA processing in response to adenovirus infection. J Cell Sci **107**(Part 6)**:**1457–1468.

42. **Aspegren A, Bridge E.** 2002. Release of snRNP and RNA from transcription sites in adenovirus-infected cells. Exp Cell Res **276:**273–283. http: //dx.doi.org/10.1006/excr.2002.5530.

43. **Rebelo L, Almeida F, Ramos C, Bohmann K, Lamond AI, Carmo-Fonseca M.** 1996. The dynamics of coiled bodies in the nucleus of adenovirus-infected cells. Mol Biol Cell **7:**1137–1151. http://dx.doi.org/10 .1091/mbc.7.7.1137.

44. **Lawrence FJ, McStay B, Matthews DA.** 2006. Nucleolar protein upstream binding factor is sequestered into adenovirus DNA replication centres during infection without affecting RNA polymerase I location or ablating rRNA synthesis. J Cell Sci **119:**2621–2631. http://dx.doi.org/10 .1242/jcs.02982.

45. **Hindley CE, Davidson AD, Matthews DA.** 2007. Relationship between adenovirus DNA replication proteins and nucleolar proteins B23.1 and B23.2. J Gen Virol **88:**3244–3248. http://dx.doi.org/10 .1099/vir.0.83196-0.

46. **Lam YW, Evans VC, Heesom KJ, Lamond AI, Matthews DA.** 2010. Proteomics analysis of the nucleolus in adenovirus-infected cells. Mol Cell Proteomics **9:**117–130. http://dx.doi.org/10.1074/mcp.M900338 -MCP200.

47. **Puvion-Dutilleul F, Puvion E.** 1990. Replicating single-stranded adenovirus type 5 DNA molecules accumulate within well-delimited intranuclear areas of lytically infected HeLa cells. Eur J Cell Biol **52:** 379–388.

48. **Lam YW, Trinkle-Mulcahy L, Lamond AI.** 2005. The nucleolus. J Cell Sci **118:**1335–1337. http://dx.doi.org/10.1242/jcs.01736.

49. **Schwarzacher HG, Mosgoeller W.** 2000. Ribosome biogenesis in man: current views on nucleolar structures and function. Cytogenet Cell Genet **91:**243–252. http://dx.doi.org/10.1159/000056853.

50. **Hutten S, Prescott A, James J, Riesenberg S, Boulon S, Lam YW, Lamond AI.** 2011. An intranucleolar body associated with rDNA. Chromosoma **120:**481–499. http://dx.doi.org/10.1007/s00412-011-0327-8.

51. **Murti KG, Davis DS, Kitchingman GR.** 1990. Localization of adenovirus-encoded DNA replication proteins in the nucleus by immunogold electron microscopy. J Gen Virol **71**(Part 12)**:**2847–2857. http://dx.doi .org/10.1099/0022-1317-71-12-2847.

52. **Lang M, Jegou T, Chung I, Richter K, Munch S, Udvarhelyi A, Cremer**

C, Hemmerich P, Engelhardt J, Hell SW, Rippe K. 2010. Three-dimensional organization of promyelocytic leukemia nuclear bodies. J Cell Sci **123:**392–400. http://dx.doi.org/10.1242/jcs.053496.

53. **Hidalgo P, Gonzalez RA.** 12 November 2015. Isolation of viral replication compartment-enriched subnuclear fractions from adenovirus-infected normal human cells. J Vis Exp http://dx.doi.org/10.3791/53296.

54. **Gonzalez R, Huang W, Finnen R, Bragg C, Flint SJ.** 2006. Adenovirus E1B 55-kilodalton protein is required for both regulation of mRNA export and efficient entry into the late phase of infection in normal human fibroblasts. J Virol **80:**964–974. http://dx.doi.org/10.1128/JVI.80.2.964 -974.2006.

55. **Jones N, Shenk T.** 1979. Isolation of adenovirus type 5 host range deletion mutants defective for transformation of rat embryo cells. Cell **17:**683–689. http://dx.doi.org/10.1016/0092-8674(79)90275-7.

56. **Groitl P, Dobner T.** 2007. Construction of adenovirus type 5 early region 1 and 4 virus mutants. Methods Mol Med **130:**29–39.

57. **Reich NC, Sarnow P, Duprey E, Levine AJ.** 1983. Monoclonal antibodies which recognize native and denatured forms of the adenovirus DNA-binding protein. Virology **128:**480–484. http://dx.doi.org/10.1016/0042 -6822(83)90274-X.

58. **Busch H, Muramatsu M, Adams H, Steele WJ, Liau MC, Smetana K.** 1963. Isolation of nucleoli. Exp Cell Res **24**(Suppl 9)**:**150–163.

59. **Andersen JS, Lyon CE, Fox AH, Leung AK, Lam YW, Steen H, Mann M, Lamond AI.** 2002. Directed proteomic analysis of the human nucleolus. Curr Biol **12:**1–11.

60. **Gonzalez RA, Flint SJ.** 2002. Effects of mutations in the adenoviral E1B 55-kilodalton protein coding sequence on viral late mRNA metabolism. J Virol **76:**4507–4519. http://dx.doi.org/10.1128/JVI.76.9.4507-4519.2002.

61. **Cox S, Rosten E, Monypenny J, Jovanovic-Talisman T, Burnette DT, Lippincott-Schwartz J, Jones GE, Heintzmann R.** 2012. Bayesian localization microscopy reveals nanoscale podosome dynamics. Nat Methods **9:**195–200.

62. **Rosten E, Jones GE, Cox S.** 2013. ImageJ plug-in for Bayesian analysis of blinking and bleaching. Nat Methods **10:**97–98. http://dx.doi.org/10 .1038/nmeth.2342.

63. **Schneider CA, Rasband WS, Eliceiri KW.** 2012. NIH Image to ImageJ: 25 years of image analysis. Nat Methods **9:**671–675. http://dx.doi.org/10 .1038/nmeth.2089.

64. **Brison O, Kedinger C, Wilhelm J.** 1977. Enzymatic properties of viral replication complexes isolated from adenovirus type 2-infected HeLa cell nuclei. J Virol **24:**423–435.

65. **Wilhelm J, Brison O, Kedinger C, Chambon P.** 1976. Characterization of adenovirus type 2 transcriptional complexes isolated from infected HeLa cell nuclei. J Virol **19:**61–81.

66. **Hicks MJ, Lam BJ, Hertel KJ.** 2005. Analyzing mechanisms of alternative pre-mRNA splicing using in vitro splicing assays. Methods **37:**306–313. http://dx.doi.org/10.1016/j.ymeth.2005.07.012.

67. **Hertweck M, Hiller R, Mueller MW.** 2002. Inhibition of nuclear pre-mRNA splicing by antibiotics in vitro. Eur J Biochem **269:**175–183. http: //dx.doi.org/10.1046/j.0014-2956.2001.02636.x.

68. **Langmead B, Salzberg SL.** 2012. Fast gapped-read alignment with Bowtie 2. Nat Methods **9:**357–359. http://dx.doi.org/10.1038/nmeth.1923.

69. **Lam YW, Lyon CE, Lamond AI.** 2002. Large-scale isolation of Cajal bodies from HeLa cells. Mol Biol Cell **13:**2461–2473. http://dx.doi.org/10 .1091/mbc.02-03-0034.

70. **Lindsey LA, Garcia-Blanco MA.** 1999. Prespliceosome and spliceosome isolation and analysis. Methods Mol Biol **118:**351–364.

71. **Matthews DA.** 2001. Adenovirus protein V induces redistribution of nucleolin and B23 from nucleolus to cytoplasm. J Virol **75:**1031–1038. http://dx.doi.org/10.1128/JVI.75.2.1031-1038.2001.

72. **Fang SH, Yeh NH.** 1993. The self-cleaving activity of nucleolin determines its molecular dynamics in relation to cell proliferation. Exp Cell Res **208:**48–53. http://dx.doi.org/10.1006/excr.1993.1221.

73. **Cheutin T, O'Donohue MF, Beorchia A, Vandelaer M, Kaplan H, Defever B, Ploton D, Thiry M.** 2002. Three-dimensional organization of active rRNA genes within the nucleolus. J Cell Sci **115:**3297–3307.

74. **Aspegren A, Rabino C, Bridge E.** 1998. Organization of splicing factors in adenovirus-infected cells reflects changes in gene expression during the early to late phase transition. Exp Cell Res **245:**203–213. http://dx.doi .org/10.1006/excr.1998.4264.

75. **Lindberg A, Gama-Carvalho M, Carmo-Fonseca M, Kreivi JP.** 2004. A single RNA recognition motif in splicing factor ASF/SF2 directs it to

nuclear sites of adenovirus transcription. J Gen Virol **85:**603–608. http://dx.doi.org/10.1099/vir.0.19722-0.

76. **Gama-Carvalho M, Condado I, Carmo-Fonseca M.** 2003. Regulation of adenovirus alternative RNA splicing correlates with a reorganization of splicing factors in the nucleus. Exp Cell Res **289:**77–85. http://dx.doi.org/10.1016/S0014-4827(03)00251-9.

77. **Bridge E, Carmo-Fonseca M, Lamond A, Pettersson U.** 1993. Nuclear organization of splicing small nuclear ribonucleoproteins in adenovirus-infected cells. J Virol **67:**5792–5802.

78. **Bridge E, Pettersson U.** 1996. Nuclear organization of adenovirus RNA biogenesis. Exp Cell Res **229:**233–239. http://dx.doi.org/10.1006/excr.1996.0365.

79. **Leppard KN, Shenk T.** 1989. The adenovirus E1B 55 kd protein influences mRNA transport via an intranuclear effect on RNA metabolism. EMBO J **8:**2329–2336.

80. **Pilder S, Moore M, Logan J, Shenk T.** 1986. The adenovirus E1B-55K transforming polypeptide modulates transport or cytoplasmic stabilization of viral and host cell mRNAs. Mol Cell Biol **6:**470–476. http://dx.doi.org/10.1128/MCB.6.2.470.

81. **O'Shea CC, Johnson L, Bagus B, Choi S, Nicholas C, Shen A, Boyle L, Pandey K, Soria C, Kunich J, Shen Y, Habets G, Ginzinger D, Mc-Cormick F.** 2004. Late viral RNA export, rather than p53 inactivation, determines ONYX-015 tumor selectivity. Cancer Cell **6:**611–623. http://dx.doi.org/10.1016/j.ccr.2004.11.012.

82. **Flint SJ, Huang W, Goodhouse J, Kyin S.** 2005. A peptide inhibitor of exportin1 blocks shuttling of the adenoviral E1B 55 kDa protein but not export of viral late mRNAs. Virology **337:**7–17. http://dx.doi.org/10.1016/j.virol.2005.04.007.

83. **Uhlen M, Svensson C, Josephson S, Alestrom P, Chattapadhyaya JB, Pettersson U, Philipson L.** 1982. Leader arrangement in the adenovirus fiber mRNA. EMBO J **1:**249–254.

84. **Leppard KN.** 1998. Regulated RNA processing and RNA transport during adenovirus infection. Semin Virol **8:**301–307. http://dx.doi.org/10.1006/smvy.1997.0132.

85. **Zhao H, Chen M, Pettersson U.** 2014. A new look at adenovirus splicing. Virology **456–457:**329–341.

86. **Nordqvist K, Ohman K, Akusjarvi G.** 1994. Human adenovirus encodes two proteins which have opposite effects on accumulation of alternatively spliced mRNAs. Mol Cell Biol **14:**437–445. http://dx.doi.org/10.1128/MCB.14.1.437.

87. **Handwerger KE, Cordero JA, Gall JG.** 2005. Cajal bodies, nucleoli, and speckles in the Xenopus oocyte nucleus have a low-density, sponge-like structure. Mol Biol Cell **16:**202–211.

88. **Bridge E, Riedel KU, Johansson BM, Pettersson U.** 1996. Spliced exons of adenovirus late RNAs colocalize with snRNP in a specific nuclear domain. J Cell Biol **135:**303–314. http://dx.doi.org/10.1083/jcb.135.2.303.

89. **Jimenez-Garcia LF, Spector DL.** 1993. In vivo evidence that transcription and splicing are coordinated by a recruiting mechanism. Cell **73:**47–59. http://dx.doi.org/10.1016/0092-8674(93)90159-N.

90. **Verheijen R, van Venrooij W, Ramaekers F.** 1988. The nuclear matrix: structure and composition. J Cell Sci **90**(Part 1):11–36.

91. **Keaton MA, Taylor CM, Layer RM, Dutta A.** 2011. Nuclear scaffold attachment sites within ENCODE regions associate with actively transcribed genes. PLoS One **6:**e17912. http://dx.doi.org/10.1371/journal.pone.0017912.

92. **Wunderlich F, Herlan G.** 1977. Reversibly contractile nuclear matrix. Its isolation, structure, and composition. J Cell Biol **73:**271–278.

93. **Denome RM, Werner EA, Patterson RJ.** 1989. RNA metabolism in nuclei: adenovirus and heat shock alter intranuclear RNA compartmentalization. Nucleic Acids Res **17:**2081–2098. http://dx.doi.org/10.1093/nar/17.5.2081.

94. **Reichelt M, Joubert L, Perrino J, Koh AL, Phanwar I, Arvin AM.** 2012. 3D reconstruction of VZV infected cell nuclei and PML nuclear cages by serial section array scanning electron microscopy and electron tomography. PLoS Pathog **8:**e1002740. http://dx.doi.org/10.1371/journal.ppat.1002740.

95. **Reichelt M, Wang L, Sommer M, Perrino J, Nour AM, Sen N, Baiker A, Zerboni L, Arvin AM.** 2011. Entrapment of viral capsids in nuclear PML cages is an intrinsic antiviral host defense against varicella-zoster virus. PLoS Pathog **7:**e1001266. http://dx.doi.org/10.1371/journal.ppat.1001266.

96. **Ou HD, Kwiatkowski W, Deerinck TJ, Noske A, Blain KY, Land HS, Soria C, Powers CJ, May AP, Shu X, Tsien RY, Fitzpatrick JA, Long JA, Ellisman MH, Choe S, O'Shea CC.** 2012. A structural basis for the assembly and functions of a viral polymer that inactivates multiple tumor suppressors. Cell **151:**304–319. http://dx.doi.org/10.1016/j.cell.2012.08.035.

97. **Samad MA, Komatsu T, Okuwaki M, Nagata K.** 2012. B23/nucleophosmin is involved in regulation of adenovirus chromatin structure at late infection stages, but not in virus replication and transcription. J Gen Virol **93:**1328–1338. http://dx.doi.org/10.1099/vir.0.036665-0.

98. **Samad MA, Okuwaki M, Haruki H, Nagata K.** 2007. Physical and functional interaction between a nucleolar protein nucleophosmin/B23 and adenovirus basic core proteins. FEBS Lett **581:**3283–3288. http://dx.doi.org/10.1016/j.febslet.2007.06.024.

99. **Castiglia CL, Flint SJ.** 1983. Effects of adenovirus infection on rRNA synthesis and maturation in HeLa cells. Mol Cell Biol **3:**662–671. http://dx.doi.org/10.1128/MCB.3.4.662.

100. **Ledinko N.** 1972. Nucleolar ribosomal precursor RNA and protein metabolism in human embryo kidney cultures infected with adenovirus 12. Virology **49:**79–89. http://dx.doi.org/10.1016/S0042-6822(72)80008-4.

101. **Hiscox JA, Whitehouse A, Matthews DA.** 2010. Nucleolar proteomics and viral infection. Proteomics **10:**4077–4086. http://dx.doi.org/10.1002/pmic.201000251.

102. **Puvion-Dutilleul F, Puvion E.** 1991. Sites of transcription of adenovirus type 5 genomes in relation to early viral DNA replication in infected HeLa cells. A high resolution in situ hybridization and autoradiographical study. Biol Cell **71:**135–147.

103. **Puvion-Dutilleul F.** 1993. Protocol of electron microscope in situ nucleic acid hybridization for the exclusive detection of double-stranded DNA sequences in cells containing large amounts of homologous single-stranded DNA and RNA sequences: application to adenovirus type 5 infected HeLa cells. Microsc Res Tech **25:**2–11. http://dx.doi.org/10.1002/jemt.1070250103.

104. **Strang BL, Boulant S, Kirchhausen T, Coen DM.** 2012. Host cell nucleolin is required to maintain the architecture of human cytomegalovirus replication compartments. mBio **3:**e00301–11.

105. **Bender BJ, Coen DM, Strang BL.** 2014. Dynamic and nucleolin-dependent localization of human cytomegalovirus UL84 to the periphery of viral replication compartments and nucleoli. J Virol **88:**11738–11747. http://dx.doi.org/10.1128/JVI.01889-14.

106. **Strang BL, Boulant S, Coen DM.** 2010. Nucleolin associates with the human cytomegalovirus DNA polymerase accessory subunit UL44 and is necessary for efficient viral replication. J Virol **84:**1771–1784. http://dx.doi.org/10.1128/JVI.01510-09.

107. **Malik-Soni N, Frappier L.** 2014. Nucleophosmin contributes to the transcriptional activation function of the Epstein-Barr virus EBNA1 protein. J Virol **88:**2323–2326. http://dx.doi.org/10.1128/JVI.02521-13.

108. **Chen CM, Chiang SY, Yeh NH.** 1991. Increased stability of nucleolin in proliferating cells by inhibition of its self-cleaving activity. J Biol Chem **266:**7754–7758.

109. **Warrener P, Petryshyn R.** 1991. Phosphorylation and proteolytic degradation of nucleolin from 3T3-F442A cells. Biochem Biophys Res Commun **180:**716–723. http://dx.doi.org/10.1016/S0006-291X(05)81124-6.

110. **Pennella MA, Liu Y, Woo JL, Kim CA, Berk AJ.** 2010. Adenovirus E1B 55-kilodalton protein is a p53-SUMO1 E3 ligase that represses p53 and stimulates its nuclear export through interactions with promyelocytic leukemia nuclear bodies. J Virol **84:**12210–12225. http://dx.doi.org/10.1128/JVI.01442-10.

111. **Imperiale MJ, Akusjärvi G, Leppard KN.** 1995. Post-transcriptional control of adenovirus gene expression. Curr Top Microbiol Immunol **199**(Part 2):139–171.

112. **Anderson KP, Klessig DF.** 1984. Altered mRNA splicing in monkey cells abortively infected with human adenovirus may be responsible for inefficient synthesis of the virion fiber polypeptide. Proc Natl Acad Sci U S A **81:**4023–4027. http://dx.doi.org/10.1073/pnas.81.13.4023.

113. **Berget SM, Moore C, Sharp PA.** 1977. Spliced segments at the 5′ terminus of adenovirus 2 late mRNA. Proc Natl Acad Sci U S A **74:**3171–3175. http://dx.doi.org/10.1073/pnas.74.8.3171.

SCIENTIFIC REPORTS

OPEN

Automatic detection and measurement of viral replication compartments by ellipse adjustment

Yasel Garcés[1], Adán Guerrero[3,4], Paloma Hidalgo[2,3], Raul Eduardo López[2,3], Christopher D. Wood[3,4], Ramón A. Gonzalez[2] & Juan Manuel Rendón-Mancha[1]

Viruses employ a variety of strategies to hijack cellular activities through the orchestrated recruitment of macromolecules to specific virus-induced cellular micro-environments. Adenoviruses (Ad) and other DNA viruses induce extensive reorganization of the cell nucleus and formation of nuclear Replication Compartments (RCs), where the viral genome is replicated and expressed. In this work an automatic algorithm designed for detection and segmentation of RCs using ellipses is presented. Unlike algorithms available in the literature, this approach is deterministic, automatic, and can adjust multiple RCs using ellipses. The proposed algorithm is non iterative, computationally efficient and is invariant to affine transformations. The method was validated over both synthetic images and more than 400 real images of Ad-infected cells at various timepoints of the viral replication cycle obtaining relevant information about the biogenesis of adenoviral RCs. As proof of concept the algorithm was then used to quantitatively compare RCs in cells infected with the adenovirus wild type or an adenovirus mutant that is null for expression of a viral protein that is known to affect activities associated with RCs that result in deficient viral progeny production.

Virus replication can induce extensive rearrangement of cellular components that results in de novo formation of specialized intracellular compartments where the viral genome is replicated. Depending on the virus family such compartments, which have been termed viroplasms, virus factories, replication centers or compartments (RCs), may associate with cellular membranes, the cytoskeleton, or nuclear domains[1,2]. In every case RCs assemble complex macromolecular platforms, where viral and cellular proteins responsible for viral genome replication are concentrated, thus increasing viral replication efficiency. Interestingly, the same compartments recruit, regulate and co-opt cellular factors that participate in a variety of host defense mechanisms. Therefore, RCs seem to act as molecular hubs where many aspects of virus-host cell interaction are controlled and there is considerable interest in understanding the impact of their formation on virus replication as well as on the cellular activities that are altered as a consequence of their assembly.

Like other DNA viruses that replicate in the cell nucleus, adenoviruses induce formation of RCs (AdRC) that assemble in association or adjacent to specific nuclear domains (ND). However, most aspects of the structure and function of AdRC remain to be explored; some of these include the relationship between their molecular components and the activities they regulate, as well as the molecules involved in their structural integrity and the dynamics of their assembly.

A strategy that has been commonly used to study RCs has relied on the phenotypic analysis of recombinant viruses that harbor substitutions or deletions in the genes that are known or suspected to affect RCs formation or activities. Such studies have typically used fluorescence microscopy to screen for alterations in the morphology

[1]Centro de Investigación en Ciencias, Instituto de Investigación en Ciencias Básicas y Aplicadas, Universidad Autónoma del Estado de Morelos (UAEM), Cuernavaca, Morelos, México. [2]Centro de Investigación en Dinámica Celular, Instituto de Investigación en Ciencias Básicas y Aplicadas, Universidad Autónoma del Estado de Morelos (UAEM), Cuernavaca, Morelos, México. [3]Instituto de Biotecnología, Universidad Nacional Autónoma de México (UNAM), Cuernavaca, Morelos, México. [4]Laboratorio Nacional de Microscopía Avanzada, Instituto de Biotecnología, Universidad Nacional Autónoma de México (UNAM), Cuernavaca, Morelos, México. Correspondence and requests for materials should be addressed to J.M.R.-M. (email: rendon@uaem.mx)
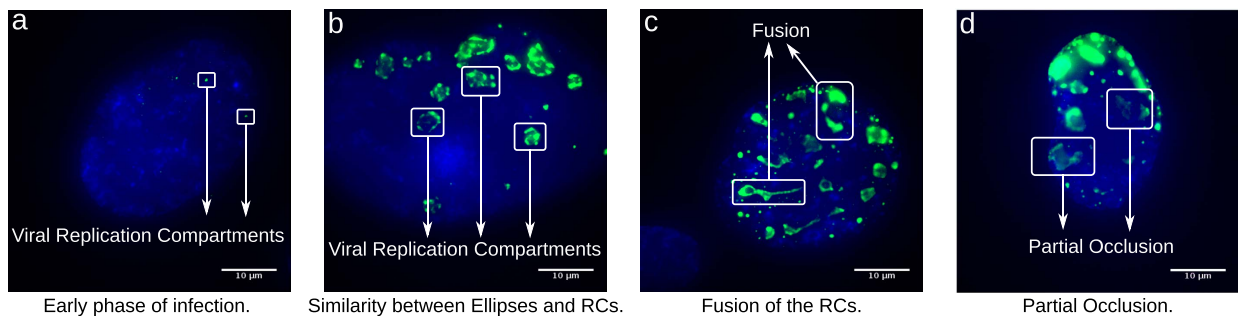
Figure 1. **Examples of Ad-infected cells, at various times post-infection.** The green color marks the viral replication compartments revealed by DBP staining, and DNA is marked with DAPI staining in blue. (**a**) AdRC appear as foci during the early phase of the replication cycle. (**b**) During the late phase AdRC form doughnut, crescent or spherical structures. (**c**) Very late in the replication cycle some RCs coalesce resulting in amorphous structures. (**d**) In the viral replication cycle, some RCs can present partial occlusion in some areas. For these four images the contrast of the images was increased to improve the visualization.

or dynamics of formation of RCs at different times of the viral replication cycle[3]. Because the viral DNA binding protein (DBP) associates with ssDNA, it is a useful marker to study RCs by fluorescence microscopy. Analysis by fluorescence microscopy of AdRC formation through the viral replication cycle has shown that the DBP protein initially accumulates in small foci that seem to increase in size and number resulting in doughnut-shaped, crescent or spherical structures. Very late during the replication cycle, the latter structures appear to coalesce resulting in complex amorphous structures that may occupy most of the cell-nucleus. Although informative, these studies have major drawbacks and provide limited information because they are qualitative and depend on subjective visual analysis for classification of the RCs at different stages of assembly. Previous data on the visual analysis of RCs suggest that these structures can be approximated as ellipse-shaped structures, a potentially oversimplified approach considering the complexity and variability of their number, shape and size during the viral replication cycle (see Fig. 1). Nevertheless, the use of ellipses allows for considerable data reduction and simplification, and consequently provides a fast and simple image analysis pipeline to be employed.

Some of the best known image processing approaches for detection and adjustment of ellipses are the Hough Transform[4–6], Random Sample Consensus (RANSAC)[7–10] and least squares[11–14]. Grouping approaches (Hough Transform and RANSAC) are robust against noise and detect multiple ellipses, but are relatively slow, require a lot of memory and suffer from low accuracy. On the other hand, least squares approaches are comparatively fast and accurate, yet can only adjust one ellipse at a time and are sensitive to noise. In 1996 Fitzgibbon[15] proposed a new algorithm for adjustment of ellipses in scattered data. The main idea is to force the least squares problem in a way that the solution is always an ellipse, taking into account the constraint $4ac - b^2 = 1$. The optimization problem is solved using Lagrange multipliers and generalized eigenvectors. Two years after the initial proposal of Fitzgibbon's algorithm, Halir and Flusser presented a numerically stable version, incorporating a block decomposition strategy[16]. This is the most commonly used alternative for the implementation of the "Direct Least Square Fitting Ellipse" or DLSFE algorithm. This method is known to be a robust deterministic algorithm, invariant under affine transformations, computationally efficient and a non-iterative approach whose result is always an ellipse. A simple Matlab implementation is available in the paper of Halir and Flusser[16]. The DLSFE can only adjust one ellipse to a data set (it is not possible to adjust multiple ellipses) and it is very sensitive to outliers. For these reasons, the direct application of this algorithm in problems of image segmentation is not generally considered viable. To our knowledge RCs measurements have never been performed using ellipse adjustment, nor are there any reports where RCs have been analyzed making quantitative measurements.

In this work a very simple and efficient approach to detect RCs by adjusting ellipses is proposed. This new algorithm is automatic, deterministic, non iterative, can simultaneously detect multiple viral RCs and has a linear computational complexity. The algorithm was validated using a synthetic ground truth image base, and was then applied to real images obtained by fluorescence microscopy of Ad-infected cells processed at various time-points post-infection. As a proof of concept, it was then used to adjust and measure various parameters of AdRC in cells infected with the wild type virus (Ad wt) or with a virus mutant that does not express an adenoviral oncogene, which encodes the multifunctional protein E1B-55K, that is known to associate with RCs and affect various activities that result in inhibition of cellular defense mechanisms and production of viral progeny. Using a set of useful parameters: the number of RCs per cell nucleus; the area of RCs within nuclei; the intensity of the signal associated with RCs; and the ellipse eccentricity, as a measure that facilitates distinction between different RCs morphologies, the method allowed the automatic determination of a previously unrecognised effect of this mutation on the dynamics of formation of AdRC.

Results

Segmentation of the viral replication compartments. To study the dynamics of the formation of AdRC, we developed a new algorithm that provides an efficient approach to automatically detect and measure RCs by adjusting ellipses. Fluorescence microscopy images generated as described in the methods section were used. The fluorescent staining of DBP was used as a bona fide marker to detect RCs, which were approximated through ellipses at various times of the viral replication cycle. As shown in Fig. 1, very late in the replication cycle,

RCs may coalesce forming complex amorphous structures. The following steps summarize the work-flow of the algorithm (described in detail in the methods section):

1. Filter RCs zones: This step consists in thresholding the image in order to segment the zones of interest (remove noise and atypical values). Our proposal performs an automatic selection of threshold value for each image $\mathbf{I}$ ($n \times m$) considering the mean value ($M_\mathbf{I}$) and the standard deviation ($S_\mathbf{I}$) per column of the image. The threshold value is defined by:

$$T_{lower} = \min\left(\overbrace{\frac{\sum_{j=1}^{m}\mathbf{I}(1, j)}{m}}^{M_1}, \ldots, \overbrace{\frac{\sum_{j=1}^{m}\mathbf{I}(n, j)}{m}}^{M_n} \right)$$
$$+ 2 \ \max\left(\sqrt{\frac{\sum_{j=1}^{m}(\mathbf{I}(1, j) - M_1)^2}{m}}, \ldots, \sqrt{\frac{\sum_{j=1}^{m}(\mathbf{I}(n, j) - M_n)^2}{m}} \right) \tag{1}$$

$$\underbrace{\mathbf{I}_{new}(i, j) = \begin{cases} 0, & I(i, j) \leq T_{lower} \\ I(i, j), & \text{in other cases} \end{cases}}_{New \ Image}. \tag{2}$$

2. Compute the connected components: The connected components labelling is used to detect connected regions in the image (there exists a digital continuous path between all pairs of points in the same component). This heuristic consists of visiting each pixel of the image and creating exterior boundaries using pixel neighbours according to a specific type of connectivity. These arcs belong to the viral replication centers because the algorithm only uses the information of the color that marks the RCs. The results of this step are N connected components A_i, $i = 1, 2, \ldots, N$, where each A_i is part of one RCs.

3. Adjust the exterior boundaries using ellipses: For each connected component A_i apply the DLSFE algorithm. For more details see the methods section.

Step 1 of the algorithm filters out noise and atypical values, step 2 divides the images in N connected components on the location of the RCs, and finally, the DLSFE adjusts each RC with an ellipse. These three steps constitute the adaptation of the DLSFE for detection and adjustment of multiple ellipses in images of any size or resolution. In the Fig. 2(1) we show graphically the steps of the proposed algorithm.

The results shown in panels 2b and 2c of Fig. 2 are consequences of eliminating some steps of the proposed algorithm. Both images show poor adjustment to RCs, because there is no delimitation of each RC. This is a consequence of the global adjustment by one ellipse. The results of our algorithm are shown in Fig. 2 panel 2d, where a good fit of the RCs is observed, suggesting this algorithm provides a tool that can be used to make automatic and quantitative measurements of RCs.

The algorithm presented in this work is automatic, deterministic, non-parametric, non iterative, and these results demonstrate that it can detect and adjust multiple ellipses of any size, eccentricity, position or rotation angle. Furthermore, this new method has a linear computational complexity and is invariant under affine transformations.

Validation of the algorithm. The algorithm validation was performed using synthetic ground truth images generated taking into account diffraction, white noise, dark-current noise and signal amplification[17]. These images contain ellipses of different sizes, eccentricities, positions and rotation angles, for which real parameters of their implicit equations are known. This facilitates analysis of the algorithm's response against several plausible events, hence permitting comparison of the obtained results with "ground-truth" ellipses considering different signal/noise ratios (SNR).

The results are shown in Fig. 3, where panels 3(a) to 3(c) show some examples of these images considering three levels of noise and panels 3(d) to 3(f), the results obtained from these images. In each case we obtained an adequate adjustment regardless of the level of noise, size, position or eccentricity of RCs, demonstrating that this approach can be used to adjust multiple viral RCs through ellipses with a small error.

Microscopy images of viral RCs may present partial overlapping in some zones, which might lead to erroneous results for most segmentation algorithms (Fig. 1(d))[18]. This problem is significant when the aim is to obtain precise and quantitative measurements of the properties of RCs. Therefore, we tested the algorithm against images presenting partially overlapping RCs. For this, the algorithm was applied to twenty-five synthetic images presenting different levels of partial occlusion, and different levels of lack of information. Fig. 4(a–c) show three of these images considering different angles of partial occlusion.

Figure 4(d–f) show the algorithm outcome obtained for the synthetic images of 4(a), 4(b), and 4(c) respectively. In the test images all viral RCs were detected successfully. Regarding an approximate qualitative assessment of the accuracy of the adjustment, each partial occlusion angle determines the degree of information eliminated in the simulated viral RCs. In Fig. 4(d,e) an accurate adjustment of RCs is observed, even in zones where information is poor and can be confused with the image background (see the red arrows). In the case of $\theta = \pi$, Fig. 4(f) shows results of decreased accuracy despite the detection of all RCs. In this example, where only 50% of the data for each image generated is preserved and can be considered as an extreme and unusual case (note that it is difficult to detect the position and form of some RCs by visual inspection), the algorithm can still adjust RCs, although with lower accuracy. The proposed method for detection and approximation of the RCs was evaluated
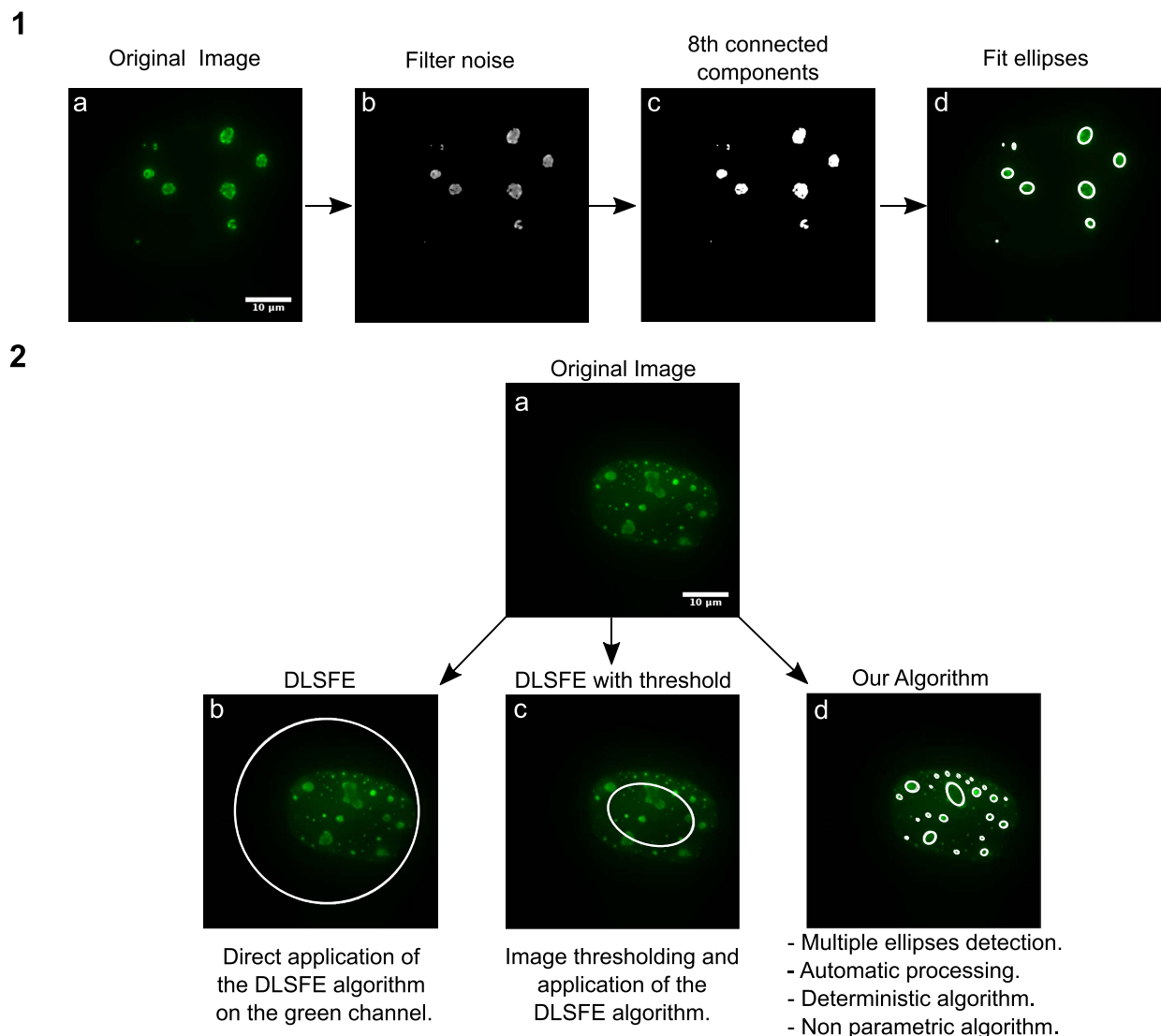
Figure 2. Visual comparison of our algorithm with other applications of the DLSFE algorithm. Panels 1a–d: Shows the steps of the proposed algorithm in a real image. Panel 2a: Original image. Panel 2b: DLSFE algorithm using all the pixels with non-zero value in green channel. Panel 2c: DLSFE algorithm application to the filtered image considering the threshold defined by Eq. (1). Panel 2d: Result using our algorithm.

quantitatively using synthetic images. Images were generated drawing ellipses from analytical formulas. The parameters (*a*, *b*, *cx*, *cy*) of analytical formulas are the ground truth used for evaluation. The rotation angle was not taken into account in this manuscript. However in Supplementary Information the performance of the proposed algorithm is scrutinized against the impact of noise over the identification of rotation angles.

In order to evaluate the thresholding process (Step 1) of the algorithm, we compared our proposed algorithm with four well known thresholding alternatives: Intermodes, MaxEntropy, Otsu and Yen. Intermodes smoothes the histogram in an iterative way until only two peaks remain[19]. MaxEntropy choses the threshold which maximizes entropies of distributions above and below the threshold[20]. Otsu's method selects the thresholding that maximizes interclass variance and minimizes intraclass variance[21]. Yen's method uses a maximum correlation criterion to select threshold[22]. The experiment was conducted taking into account that each image (one for each level of SNR) contains a set of synthetic RCs with different sizes, positions and eccentricities. For the validation we used the index of Jaccard, the Precision and the Recall in order to evaluate the performance of the methods in different scenarios like noise and partial occlusion. More details about these indexes and their application in our specific problem are explained in the methods section.

Figure 5 shows the obtained results for the Precision, Recall and Jaccard Index for 6 different Signal/Noise ratios ($SNR = \{2.3, 2.5, 2.8, 3.2, 4, 7.6\}$). With methods like Otsu, MaxEntropy and Yen we obtain bad results for all Signal/Noise ratios, even with high quality in the images (high Signal/Noise level). On the other hand, the best results can be observed when we use our method or the Intermodes alternative, in this case the Precision, Recall and Jaccard index are all superior with our proposal for any SNR. For these experiments we generated synthetic images with low Signal/Noise ratios ($SNR = \{2.3, 2.5, 2.8\}$), even though real microscopy images do not have such
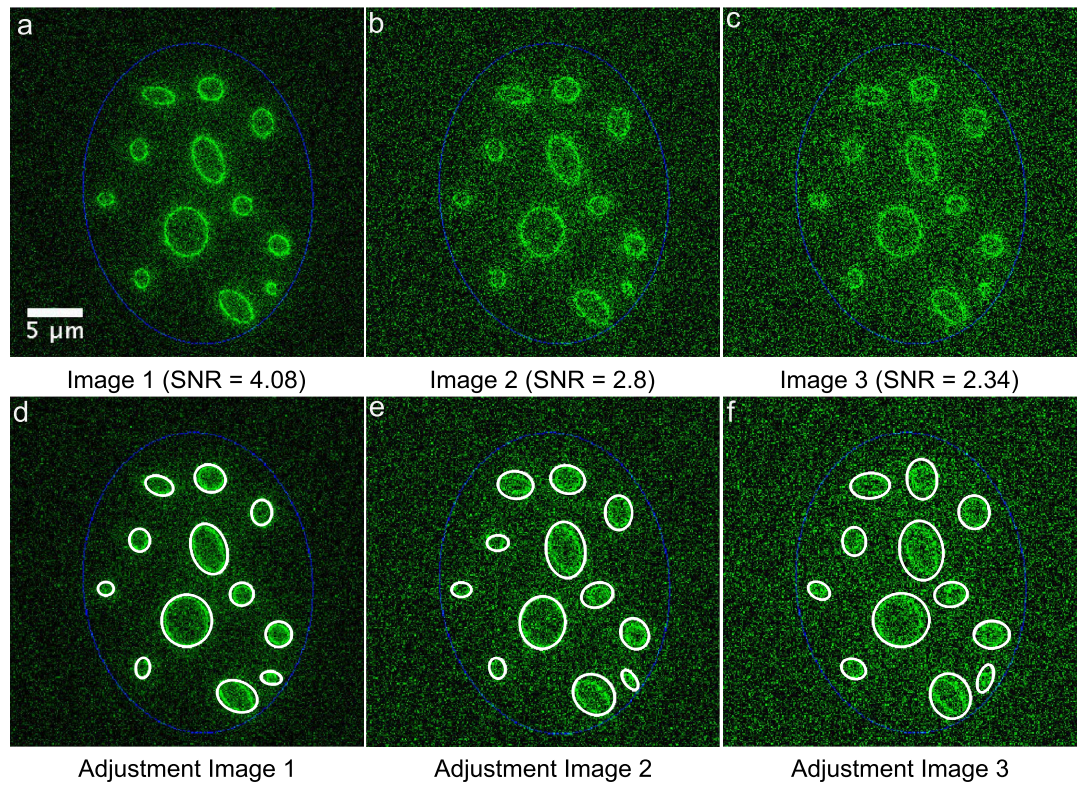
Image 1 (SNR = 4.08) Image 2 (SNR = 2.8) Image 3 (SNR = 2.34)

Adjustment Image 1 Adjustment Image 2 Adjustment Image 3

Figure 3. Adjustment of artificial images with different levels of Signal/Noise. The panels 3(a), 3(b), 3(c) show the synthetic images generated artificially. In the second row panels 3(d) to 3(f) show the results of our algorithm for these images. The blue ellipses simulate the nucleus of the cell.
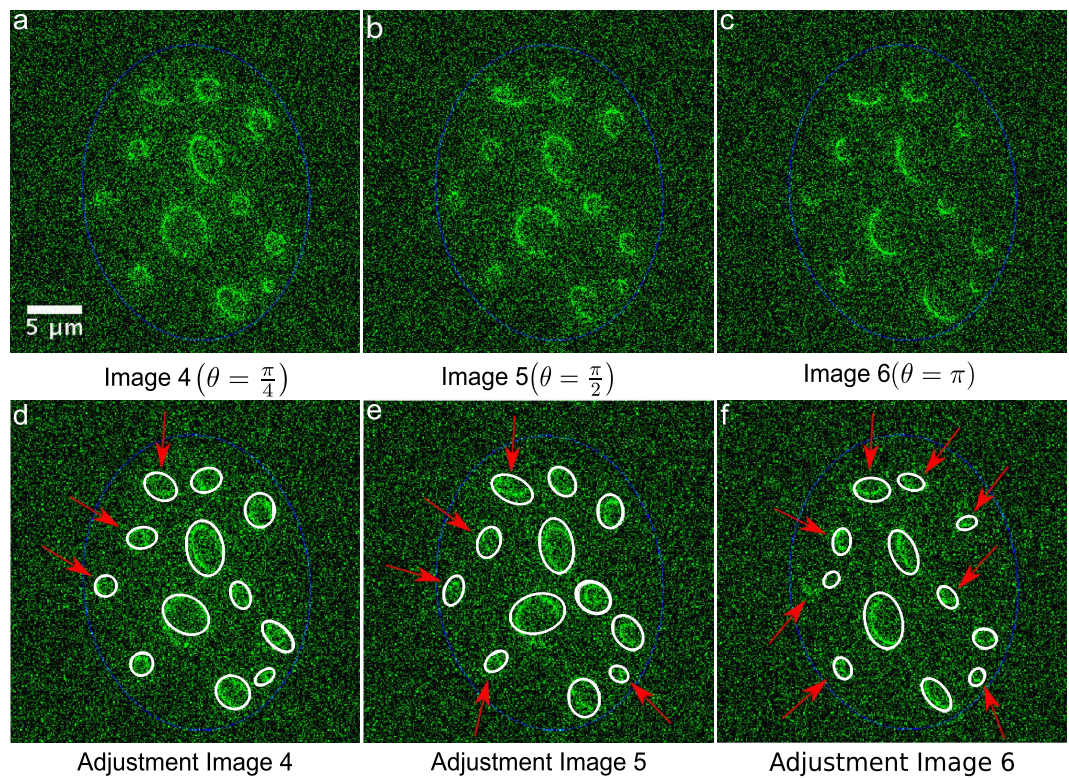

Image 4 $\left(\theta = \frac{\pi}{4}\right)$ Image 5$\left(\theta = \frac{\pi}{2}\right)$ Image 6$(\theta = \pi)$

Adjustment Image 4 Adjustment Image 5 Adjustment Image 6

Figure 4. Adjustment of artificial images with partial occlusion ($SNR = 2.34$). The panels 4(a), 4(b), 4(c) show the synthetic images generated artificially with partial occlusion. In the second row, panels d to f, show the results of the algorithm for these images.
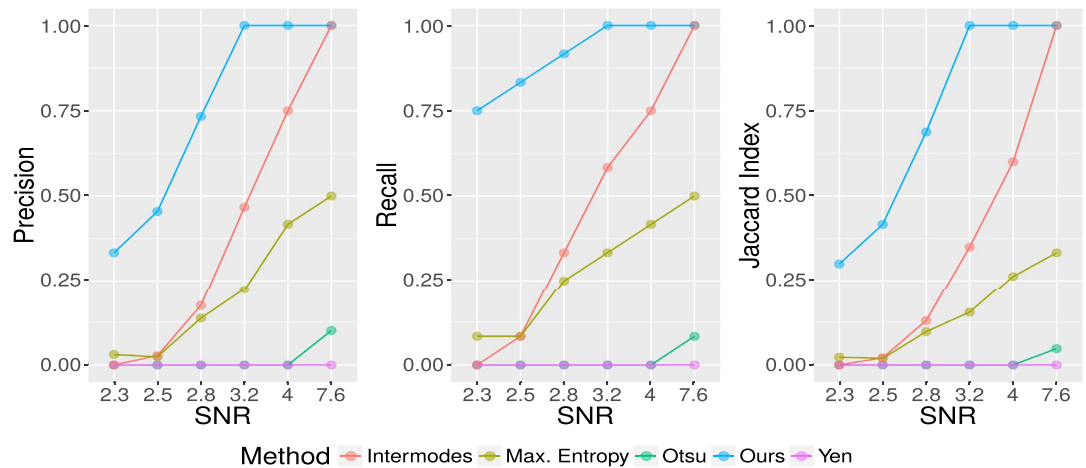
Figure 5. Precision, Recall and Jaccard indices for the detection and approximation of the viral RCs considering different levels of signal/noise in the synthetic images. Five different thresholding methods were tested (Intermodes, Maximum Entropy, Otsu, Yen and our method), each panel illustrates the results for these alternatives.
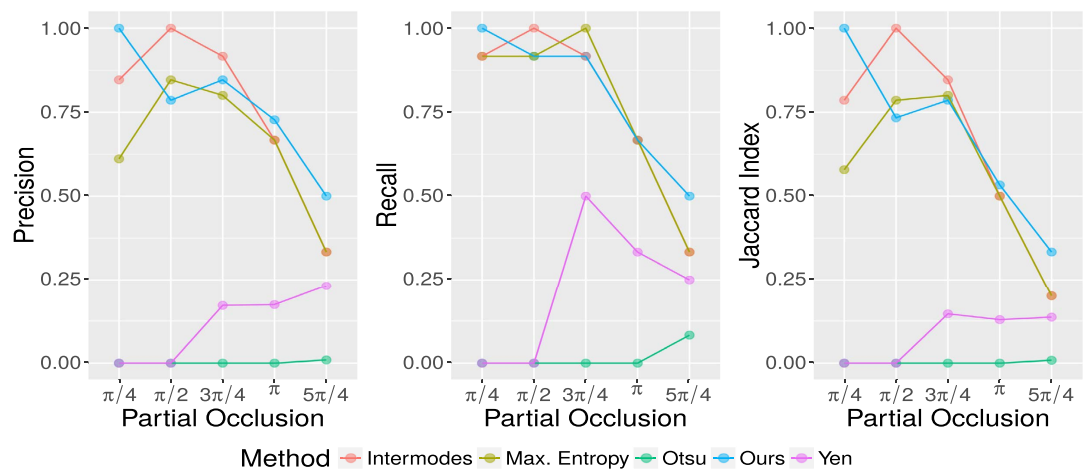

Figure 6. Precision, Recall and Jaccard indices for the detection and approximation of the viral RCs considering different levels of partial occlusion in the synthetic images. Five different thresholding methods were tested (Intermodes, Maximum Entropy, Otsu, Yen and our method).

poor quality. With these SNR values the algorithm could succesfully some RCs (Precision, Recall, and Jaccard indices >0.25 in all cases). For images with SNR that are closer to expected values ($SNR = \{3.2, 4\}$), our method can correctly detect all RCS (Precision, Recall, and Jaccard indices equal to 1).

Figure 6 shows the performance of our method compared with four alternative thresholding techniques in synthetic images with partial occlusion. For this experiment we consider a fixed SNR equal to 3.2 and five angles for partial occlusion $\theta = \{\pi/4, \pi/2, 3\pi/4, \pi, 5\pi/4\}$. The SNR value of 3.2 was chosen as representative of the SNR "normally" found in epifluorescence images. The worst results are obtained with the threshold of Otsu and Yen. In these cases the Precision and Jaccard indices are always less than 0.25, while the Recall have a maximum value of 0.5 with a partial occlusion $\theta = 3\pi/4$. The performance of the proposed algorithm by means of considering Intermodes thresholding is superior to the other tested thresholding algorithms for $\pi/2$ and $3\pi/4$ degrees of partial occlusion. In these particular cases, the heights of the two peaks of the histogram computed from their corresponding synthetic images were comparably similar, therefore Intermodes outperforms other thresholding methods. However, such particular cases are far from being representative. In general, the results shown in Fig. 5 indicate that Intermodes thresholding does not guarantee the identification of the best threshold level for all images. Whatever the case, the data presented in Fig. 6 represent a particular adaptation of the proposed algorithm, which itself is completely compatible with any desired thresholding method. More thresholding algorithms might provide an advantage for other given particular cases, e.g. local thresholding will perform much better that global thresholding in images taken with heterogeneous illumination. When partial occlusion angles are within
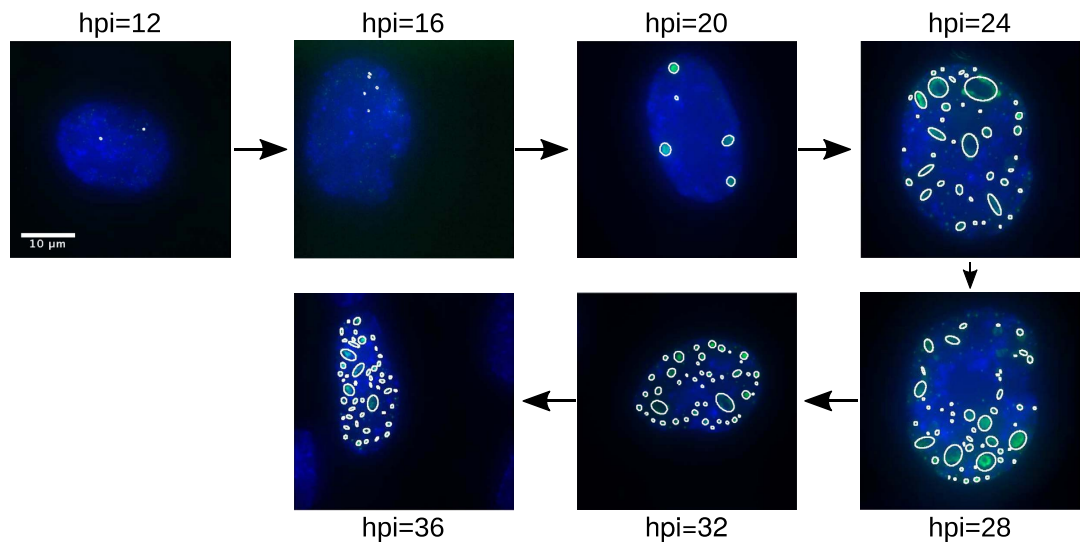
Figure 7. Detection and adjustment of the RCs in real images. A set of images each representative of a different time point of the viral replication cycle, and the results obtained using the algorithm are shown.

interval $[0, \pi)$ the Precision, Recall and Jaccard indices are relatively high, i.e. the proposed algorithm is reliable when more than half of the data of interest are present.

Analysis of viral replication compartments in Ad-infected cells. The algorithm was then used to analyze RCs in Ad-infected cells. Images of Ad-infected cells obtained at various times post-infection by fluorescence microscopy were grouped in eight different sets (12; 16; 20; 24; 28; 32; and 36 hpi). For each time-point, 60 images of infected cells were recorded, hence the results of this section represent the analysis of 420 images of the adenovirus infection process (a typical personal computer requires about 0.01 seconds to process a single image).

Figure 7 depicts representative results obtained for each time-point. At the earlier time-points ($hpi = \{12, 16\}$), before the onset of viral DNA replication, RCs are just becoming apparent, and those which were detected by the algorithm were small dot-like foci. At 20 hpi, although still scarce and isolated, RCs were larger and better defined. Qualitatively, in the time period between 20 and 32 hpi a significant rise in the number of RCs, as well as of their size and the fluorescence intensity, was observed. The results obtained at 36 hpi, showed an appreciable rise in the number of RCs in comparison with the previous time-points. At the latter time-points the larger RCs seem to coalesce, occupying a large proportion of the cell nucleus and forming complex amorphous structures, for which the adjustment of ellipses is no longer accurate (see Discussion section).

One of the main advantages of approximation through ellipses is the possibility to obtain quantitative data, e.g. position, area, perimeter, form and average fluorescence intensity of the RCs. These indicators allow for a statistic study of the behaviour of RCs at different time-points, providing relevant information about the viral replication cycle.

Therefore, we conducted statistical analysis of the data obtained by the algorithm from processing images of cells infected either with the wt virus (Ad5 H5pg4100) or with a mutant virus (Ad5 H5pm4149), as described in the methods section. This virus mutant (E1B-) does not direct the synthesis of the early protein, E1B-55K, and has been shown to display defects in viral late gene expression, as well as in inhibition of cellular anti-viral defenses, resulting in decreased production of viral progeny. The results obtained are shown in Fig. 8, where violin plots of the number of RCs per cell nucleus; the area of RCs; their fluorescence intensity; and eccentricity of RCs were plotted against various time-points post-infection. For clarity, the analysis was divided into three different time intervals ($hpi = \{12–16\}$; $hpi = \{20–28\}$; $hpi = \{32–36\}$). The analysis of the data showed that except for few time-points and parameters (the area at 12 hpi; the intensity at 32 and 36 hpi; and the eccentricity at 28 hpi) there exists in all variables a statistically significant difference between the wild type and mutant virus according to the test of Kruskal-Wallis[23].

At the time interval between 12 and 16 hpi, the violin plots (see Fig. 8) show that for the Ad5 wt virus there was a clear increase in the number of RCs, and a slight increase in their area and intensity. Interestingly, for the E1B- virus, while a slight rise in the number of RCs was observed, their area, intensity and eccentricity decreased in this time interval. Significantly, these data indicate that during the early times post-infection the algorithm is able to distinguish small changes in the number, size and shape of RCs. During the next time interval (20 to 28 hpi), viral genome replication initiates and the expression of viral late genes is known to increase several fold. In the Ad5 wt-infected cells, the number of RCs displayed further increase from the 16 hpi time point, and they reached their maximum area and intensity between 24 and 28 hpi. In contrast, cells infected with the E1B-virus displayed a complex behaviour, as the RCs increased in number between 16 and 20, but dropped slightly at 24 hpi. Interestingly, the area of RCs increased only transiently (at 24 hpi) before 32 hpi. The interval between 32 and 36 hpi corresponds to a phase during viral replication where viral late proteins and genomes are produced in large quantities and assembly of viral progeny reaches its highest level. The number of RCs detected in the Ad5 wt infected cells showed a steady rise during this interval; however, in contrast to the wt virus, where RCs
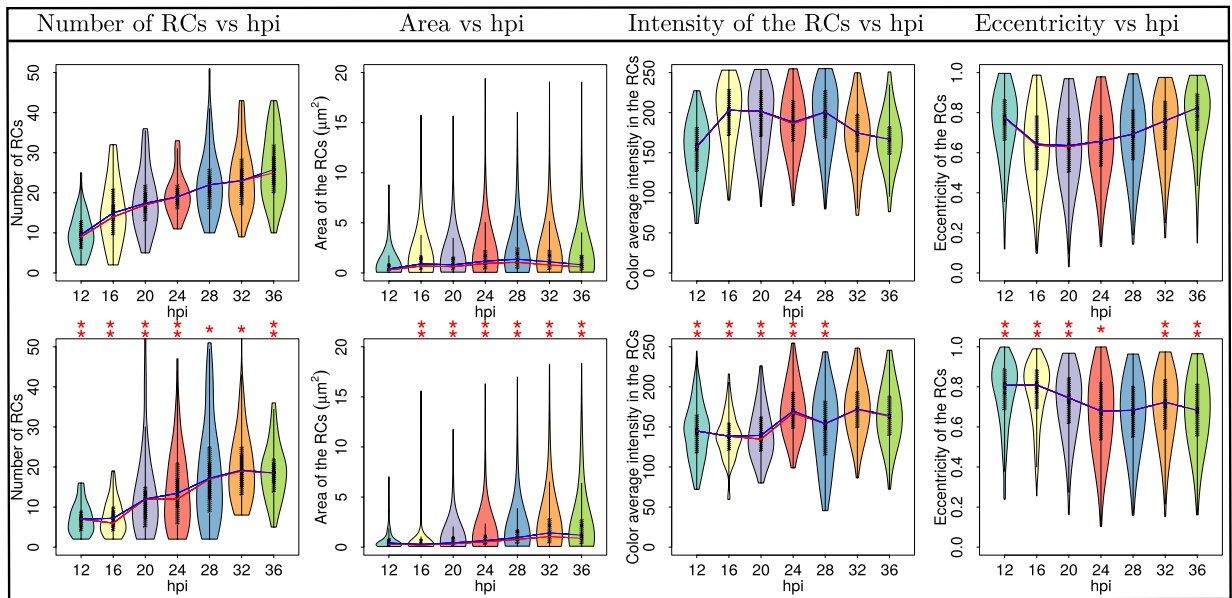
Figure 8. Descriptive statistical analysis of the number, area, mean intensity and eccentricity of the RCs.
First row: Ad5 wt virus violin graphs (H5pg4100); second row: Ad5 mutant virus (H5pm4149). The number of cells analysed for each experimental condition was $n \geq 60$. The blue line represents the mean and the red line the median. The red asterisks represent the statistical significance difference between the wild type and mutant virus using the test of Kruskal-Wallis[23]: *ρ-value ≤ 0.05; **ρ-value ≤ 0.01.
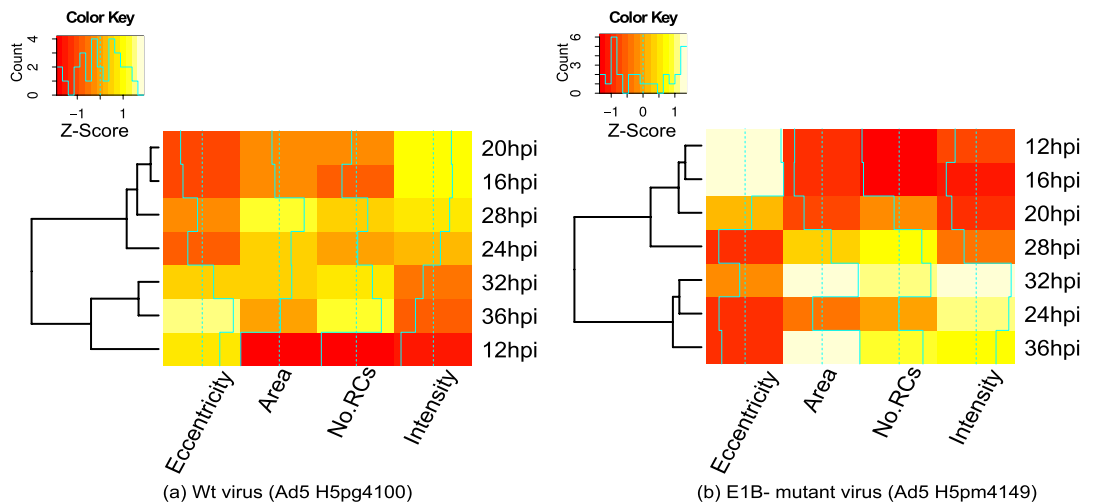

Figure 9. Hierarchically clustered heatmap for eccentricity, area, number of RCs and intensity, considering all times post-infection.

reach a size that is nearly constant between the 20 hpi and 32 hpi time-point, the mutant virus showed again a complex behaviour in which RCs reached a maximum value that decreased not only in size but also in number after 32 hpi. An altered behaviour was also matched by the fluctuations in intensity and eccentricity of the RCs for the E1B- virus. For the Ad5 wt the maximum level of intensity after the initial rise at 16 hpi was reached at 28 hpi; in contrast a nearly opposite behaviour was observed for the E1B- virus as the initial rise that was observed only after 20 hpi was followed by a clear drop at 28 hpi. Interestingly, while the lowest values of eccentricity are reached in the 16–20 hpi interval in Ad5 wt, for the E1B- virus the lowest values are only reached at 24 hpi.

The hierarchical clustering maps presented in Fig. 9 for the Ad5 wt and E1B- mutant virus show some of the characteristics of RCs described above. The dendrograms indicate conglomerates according to qualitative and quantitative results: For the Ad5 wt virus the first group level contains classes {16, 20}, {32, 36}. The second group level contains {12, 32, 36}, {16, 20, 28}, while the third level contains {16, 20, 24, 28}. The latter group was an expected result because the items of each class are different to each other by 4 hours, and therefore, the results are more similar for any two time-points that are chronologically close to each other; however, it is interesting to note that such hierarchical clustering would be anticipated for the progressive formation of RCs as the viral replication

cycle advances. In contrast, the results for the E1B- mutant virus display different sets of conglomerates, where the 12, 16 and 28 hpi time-points remain ungrouped in the first two or three levels, respectively, and seem to display an arrest, as there is no clear progression from the 12 hpi to the 20 hpi in the area, intensity or number of RCs, and a similar defect is apparent between the 24 and 28 hpi time points. These results indicate a defective progression from these two time-points, which correspond to the initial formation of RCs (12 hpi) and to the transition to the late phase of the viral replication cycle (20 to 24 hpi). The dendrograms also show that for both Ad5 wt and the E1B- mutant virus conglomerates tend to group around the 24, 28 and 32 time-points, suggesting these two time points may be of particular relevance for RCs during latter periods post-infection.

Significant differences between Ad5 wt and E1B- through the viral replication cycle were clearly detected by the algorithm, as in contrast to Ad5 wt, where the transition to the late phase of infection clearly showed an increase in the area and intensity of the RCs, as well as a shift of decreased eccentricity, the E1B- mutant displayed a seemingly biphasic behaviour for the number, intensity and eccentricity of RCs.

Discussion

The formation of RCs and the association of viral and cellular molecules to these structures have been studied using a variety of experimental strategies that have relied mostly on fluorescence or electron microscopy[24-33]. Because the viral DBP associates with ssDNA and participates directly in viral DNA replication, many studies have used this protein as a bona fide marker of RCs. The data produced by such studies indicate that RCs assemble in association with the viral DNA, where transcription and post-transcriptional processing of viral genes progressively results in the recruitment to these sites of viral and cellular proteins that direct the various steps of regulated gene expression[27]. As the late phase of viral replication progresses RCs display changes in their size, number and shape. And although it is clear that the dynamics of their formation parallel not only progression of the viral replication cycle, but also the inhibition of cellular defenses, quantitative studies of the dynamic behaviour of RCs have not been conducted. The adjustment of the viral RCs using ellipses presented in this work allowed us to obtain for the first time relevant quantitative data, such as the area, perimeter and form of RCs within the nuclei of infected cells, enabling statistical analysis of these parameters at various time-points of the adenoviral replication cycle.

During the earliest times post-infection, the initial localization of DBP was detected in a few small nuclear foci (at 12 hpi), followed by a progressive increase in their number and size. At time-points post-infection that are known to correspond to the initiation of viral DNA synthesis and the resulting transition to the late phase of the viral replication cycle (between 20 and 24 hpi), larger spherical or doughnut-shaped structures were prominent. Both of these structures increased in number at the later time-point (32–36 hpi). At very late time (36 hpi) some RCs coalesce, resulting in decreased precision of the algorithm. Therefore, except for the latest time-points, when the likelihood of RCs fusion becomes higher, and the adjustment using ellipses can be used for an initial approximation with other strategies, like Level Set, or other dynamic instead of global thresholding methods, the detection of RCs throughout viral replication by the algorithm is in agreement with the qualitative description that has been reported previously by various studies[24,27,34,35].

In addition to the qualitative description of RCs formation the algorithm allowed us to obtain quantitative measurements that had hitherto not been performed. The statistical analysis of RCs from Ad5 wt compared with the E1B- mutant showed that the absence of the E1B protein is clearly associated with a previously unidentified lower efficiency of RCs formation and altered morphological features of RCs at different time-points of viral replication (Fig. 8). The E1B protein is known to participate in both the selective and efficient expression of viral late genes[36-40] and in the inhibition of cellular factors that participate in the anti-viral cellular response[41]. The association of E1B with these structures correlates also with efficient viral DNA synthesis[37,42-46]. The accumulated evidence indicates that E1B is a multifunctional protein that participates in various processes of viral replication, and that its timely synthesis and localization are necessary for the protein to function as a transcriptional repressor of interferon-inducible genes[47,48], and presumably formation of RCs. The latter, however, has not been demonstrated and the data obtained here allowed us to quantitatively determine for the first time that the E1B impacts each of the parameters used to measure RCs formation. In the absence of E1B, formation of RCs between 12 and 16 hpi displayed similar characteristics as Ad wt, however a clear decrease in their number, area, intensity and eccentricity (Fig. 8), as well as a marked difference in the hierarchical clustering of the 12 hpi time-point (Fig. 9) suggest this early protein may be required for the initial steps of RCs formation. Moreover, the large differences in the range and distribution of the average fluorescence intensity, which indicate variations in the level of DBP that is associated to different RCs, suggest that in the absence of E1B fewer of the DBP-containing small foci that form early or increase in size and give rise to the larger doughnut-shaped structures. These results were not anticipated and suggest that E1B may impact the association of DBP to RCs; experiments are currently in progress to assess this possibility.

The defects displayed by the E1B- mutant virus were not limited to the early time-points. In the absence of this protein the violin plots (Fig. 8) displayed a sine behaviour with the time post-infection, where similar times were observed for the maximum number and intensity of RCs (32 hpi), which paralleled the times for the maximum value for eccentricity (especially at 28 hpi). Interestingly, while hierarchically clustering the variables used to analyze RCs formation dynamics in Ad5 wt-infected cells showed that, as expected, any two time-points that are chronologically closer are more similar to each other (between 16 and 28 hpi), and describe a continuous progression of increasing size, number and intensity of RCs as viral replication progresses (Fig. 9), the area and intensity of RCs reach a maximum value at a time that corresponds to the peak of viral DNA synthesis (28 hpi). In stark contrast, the E1B- mutant displayed alterations in the hierarchical clustering of variables. Notably, the 20 to 24 hpi time-points, which correspond to the initiation of viral DNA synthesis, were no longer grouped together, suggesting that the absence of E1B results in a defect in the adequate formation of RCs that correlates and may be directly linked to the initiation of viral DNA replication.

In summary, in this work the development of a simple and efficient approach to detect and quantitatively measure viral RCs is presented. The proposed algorithm is automatic, non iterative and can detect multiple ellipses of any size and eccentricity. It is deterministic, has a linear algorithmic complexity, and is robust against noisy datasets, even with partial occlusion. This algorithm does not depend on the size or resolution of the images and is invariant to affine transformations. Quantitative statistic analyses of RCs could detect some defects in the formation and maturation of RCs in cells infected with the E1B- mutant virus, indicating that the algorithm represents a simple and powerful tool with predictive capabilities that can be used for the detailed study of RCs formed in cells infected with adenovirus as well as other viruses that induce formation of RCs.

Methods

Cells and viruses.   Primary human foreskin fibroblasts (HFFs) were maintained in monolayer cultures in Dulbecco's modified Eagle's medium supplemented with 10% (vol/vol) fetal calf serum (Gibco-Invitrogen Corp.) for no more than 14 passages. HFFs were infected with Ad5, wt or with an E1B- mutant at 30 PFU/cell, as described previously[39]. The Ad5 H5pg4100 and Ad5 H5pm4149 viruses[49,50] were propagated in monolayers of HEK-293 cells. Viruses were titered as fluorescent forming units (FFU) on HEK-293 cells as described previously[49].

Antibodies.   The primary antibodies used for immunofluorescence assays were rabbit polyclonal Ab specific for Ad5 DBP (a kind gift from Thomas Dobner, Heinrich-Pette Leibniz Institute, Hamburg, Germany). The secondary antibodies used were, either anti rabbit Alexa Fluor 350 or anti rabbit Alexa fluor 488 (Invitrogen). DAPI was used to stain DNA.

Fluorescence microscopy.   For immunofluorescence, HFF cells grown on coverslips to approximately 90% confluence were mock-infected or infected with Ad5 wt or E1B- mutant. Cells were processed for immunofluorescence as described previously[39]. After application of specific primary antibodies, cells were incubated with secondary antibodies. The cover-slips were mounted on glass slides in PBS/10% glycerol and samples were examined using a Zeiss Axiovert 200 M inverted microscope with a $63x/1.4$- numerical-aperture oil-immersion objective lens with an Axiocam MRM and Axiovision 3.1 software (Carl Zeiss, Inc.). For each condition 60 $2D$ images were collected. The final images were created with ImageJ $v1.48o$ and were later analyzed in Matlab $R2011b$.

Implementation and details about the proposed algorithm.   The objective of the thresholding algorithm is to separate the background from the foreground. Because fluorescence images can have different levels of intensity in the background and it is possible that some columns will not have any information for the RCs, we compute the minimum of the mean intensity of all columns to estimate the average intensity of the background. The standard deviation for the columns was taken into account to estimate the maximum variation of the intensity.

The third step of our algorithm uses the DLSFE approach to adjust the RCs using ellipses, details of this method are presented below:

Direct Least Square Fitting Ellipses (DLSFE).   The equation of a conic is given by[11]:

$$F(\Phi, X) = ax^2 + bxy + cy^2 + dx + ey + f = 0,$$

where $\Phi = [a, b, c, d, e, f]^t$ (parameters) and $X = [x^2, xy, y^2, x, y, 1]^t$ (data points in $\mathbb{R}^2$). Given n points X_i, $i = \overline{1, n}$ the adjustment to the general form of a conic can be seen like the next minimization problem:

$$\min_{\Phi} \sum_{i=1}^{n} F(\Phi, X)^2. \tag{3}$$

The restriction $b^2 - 4ac < 0$ guarantees that the conic $F(\Phi, X)$ is an ellipse, and since $F(\Phi, X)$ and $\alpha F(\Phi, X)$ is the same conic for all scalar $\alpha \neq 0$, it is possible to rescale the parameters and consider the next restriction:

$$b^2 - 4ac = -1 \Leftrightarrow 4ac - b^2 = 1.$$

The problem (3) can be expressed as:

$$\left\{ \begin{array}{c} \min_{\Phi} \sum_{i=1}^{n} F(\Phi, X)^2 \\ \text{subject to:} \ \ 4ac - b^2 = 1 \end{array} \right. . \tag{4}$$

The matrix form of the equation (4) is given by:

$$\min_{\Phi} \|D\Phi\|^2 \text{ subject to: } \Phi^t C \Phi = 1, \tag{5}$$

where

$$D = \begin{pmatrix} x_1^2 & x_1 y_1 & y_1^2 & x_1 & y_1 & 1 \\ \vdots & \vdots & \vdots & \vdots & \vdots & \vdots \\ x_i^2 & x_i y_i & y_i^2 & x_i & y_i & 1 \\ \vdots & \vdots & \vdots & \vdots & \vdots & \vdots \\ x_n^2 & x_n y_n & y_n^2 & x_n & y_n & 1 \end{pmatrix} \underbrace{}_{\text{design matrix of } n \times 6} \text{and} \, C = \begin{pmatrix} 0 & 0 & 2 & 0 & 0 & 0 \\ 0 & -1 & 0 & 0 & 0 & 0 \\ 2 & 0 & 0 & 0 & 0 & 0 \\ 0 & 0 & 0 & 0 & 0 & 0 \\ 0 & 0 & 0 & 0 & 0 & 0 \\ 0 & 0 & 0 & 0 & 0 & 0 \end{pmatrix} \underbrace{}_{\text{constraint matrix of } 6 \times 6}.$$

The following system is obtained using Lagrange multipliers and differentiating in problem (5):

$$\begin{cases} 2D^t D\Phi - 2\lambda C\Phi = 0 \\ \qquad\qquad \Phi^t C\Phi = 1 \end{cases} \tag{6}$$

which can be expressed as the equivalent system,

$$S\Phi = \lambda C\Phi \tag{7}$$

$$\Phi^t C\Phi = 1, \tag{8}$$

where S is the dispersion matrix:

$$S = D^t D = \begin{pmatrix} S_{x^4} & S_{x^3 y} & S_{x^2 y^2} & S_{x^3} & S_{x^2 y} & S_{x^2} \\ S_{x^3 y} & S_{x^2 y^2} & S_{xy^3} & S_{x^2 y} & S_{xy^2} & S_{xy} \\ S_{x^2 y^2} & S_{xy^3} & S_{y^4} & S_{xy^2} & S_{y^3} & S_{y^2} \\ S_{x^3} & S_{x^2 y} & S_{xy^2} & S_{x^2} & S_{xy} & S_x \\ S_{x^2 y} & S_{xy^2} & S_{y^3} & S_{xy} & S_{y^2} & S_y \\ S_{x^2} & S_{xy} & S_{y^2} & S_x & S_y & S_1 \end{pmatrix} \text{and} \, S_{x^a y^b} = \sum_{i=1}^{n} x_i^a y_i^b.$$

The representation (7) is solved using generalized eigenvectors. In this case the solution is composed of 6 real eigenvalues because the matrices C and D are symmetrical. If (λ_i, u_i) (u_i is an eigenvector associated to an eigenvalue λ_i) solve (7), then for all μ, the pair $(\lambda_i, \mu u_i)$ is the solution to (7). Taking into account the equation (8):

$$\mu_i^2 u_i^t C u_i = 1 \Rightarrow \mu_i = \sqrt{\frac{1}{u_i^t C u_i}}.$$

The solutions of the system (6) are of the form $\hat{\Phi}_i = \mu_i u_i$. Since there are six solutions, the problem (5) is solved considering the solution associated to the less positive eigenvalue λ_i.

All methods have been coded and run in Matlab R2011b (7.13.0.564), under Linux-Ubuntu 14.04, with a processor Intel(R) Core(TM) i5-2450M CPU @ 2.50 GHz and 16 GB of RAM.

Generation of synthetic images. The steps to generate the synthetic images are the following[17]:

1. Create an image A containing ellipses of different sizes, eccentricities and positions according to desired characteristics.
2. Convolute A using the point spread function (PSF). For this step we use the plug-in "Diffraction PSF-3D" of ImageJ with the following parameters: Index of refraction of the media $n = 1.33$, Numerical Aperture $NA = n \sin(\theta) = 1.3$, Wavelength $\gamma = 510\,nm$, Image Pixel Spacing $px = 100\,nm$, Width (pixels) $= 512$, Height (pixels) $= 512$. Rayleigh resolution $r = 0.61\lambda/NA = 240\,nm$. For more details of this plug-in see[51].
3. Add Gaussian noise in order to consider auto-fluorescence and Poisson noise for the purpose of considering electronic noise. Finally, amplification in an EM-CCD detector has been included[17]. The description of the method to compute the SNR has been included as Supplementary Information.

Generation of partial occlusion in synthetic images. Each synthetic image has n viral RCs simulated through ellipses, whose implicit equation parameters are known. In order to simulate the partial occlusion of the RCs the representation in polar coordinates of the ellipse is considered:

$$r(\theta) = \frac{1}{\sqrt{\frac{\cos^2\theta}{a^2} + \frac{\sin^2\theta}{b^2}}}.$$

Varying θ in a specific interval, points are generated only in the arc determined by this interval, which can be considered as a simulated effect of partial occlusion. Figure 10 shows an example of the ellipse arc generated for $\theta \in \left[\frac{\pi}{4}, 2\pi\right]$, the information enclosed into the angular interval $\left(0, \frac{\pi}{4}\right)$ is eliminated as a consequence of the partial occlusion.
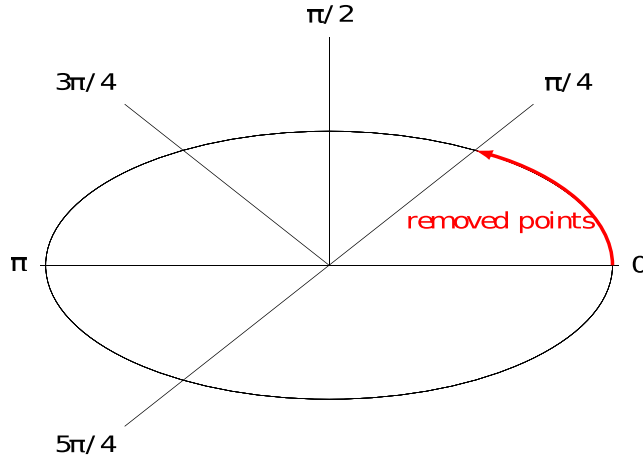
Figure 10. Partial occlusion simulation.

The percentage of points conserved with respect to the total, based on the partial occlusion angle is given by:

$$P_\% = 100\left(1 - \frac{\theta}{2\pi}\right).$$

In the case of Fig. 10, 87.5% of total data is conserved.

Validation of the algorithm. The validation of the algorithm was conducted using measures like the Jaccard index, the Recall and the Precision. Hereinafter each ellipse is represented as a vector of four components $E = (a, b, cx, cy)$, where the elements of this vector are the coefficients of the implicit form of the ellipse, that is:

$$\underbrace{E = (a,\, b,\, cx,\, cy)}_{\text{ellipse in vector form}} \Leftrightarrow \underbrace{\frac{(x - cx)^2}{a^2} + \frac{(y - cy)^2}{b^2} = 1}_{\text{implicit form of the ellipse}}.$$

Let $\hat{E} = \{\hat{E}_i = (\hat{a}_i, \hat{b}_i, \hat{cx}_i, \hat{cy}_i),\, i = \overline{1, n}\}$ the set of n ellipses that simulate the RCs in the image I, and $E^r = \{E^r_j = (a^r_j, b^r_j, cx^r_j, cy^r_j),\, j = \overline{1, k}\}$ the set of k ellipses obtained as a result of the segmentation of the image I. The sets $\hat{E}$ and E^r can be compared following the next rules of classification:

1. True Positive (TP): $E^r_j \in E^r$ is a true positive (good adjust) if:

$$\{\exists\, \hat{E}_i \in \hat{E}\colon |\hat{E}_i - E^r_j| = |(\hat{a}_i, \hat{b}_i, \hat{cx}_i, \hat{cy}_i) - (a^r_j, b^r_j, cx^r_j, cy^r_j)| \leq (0.5, 0.5, 0.5, 0.5)\mu m\}.$$

   That is, that the absolute error in each coefficient is less than $0.5\,\mu m$.

2. False Positive (FP): $E^r_j \in E^r$ is a false positive (bad adjust) if:

$$\{\nexists \hat{E}_i \in \hat{E}\colon |\hat{E}_i - E^r_j| = |(\hat{a}_i, \hat{b}_i, \hat{cx}_i, \hat{cy}_i) - (a^r_j, b^r_j, cx^r_j, cy^r_j)| \leq (0.5, 0.5, 0.5, 0.5)\mu m\}.$$

3. False Negative (FN): $\hat{E}_i \in \hat{E}$ is a false negative if:

$$\{\nexists E^r_j \in E^r\colon |\hat{E}_i - E^r_j| = |(\hat{a}_i, \hat{b}_i, \hat{cx}_i, \hat{cy}_i) - (a^r_j, b^r_j, cx^r_j, cy^r_j)| \leq (0.5, 0.5, 0.5, 0.5)\mu m\}.$$

A true positive is a detected ellipse that is similar enough to one of the synthetic ellipses. A false positive is a detected ellipse that is not similar enough to any of the synthetic ellipses and a false negative is a synthetic ellipse that was not detected.

The Jaccard index[52] is defined as:

$$J(\hat{E}, E^r) = \frac{\hat{E} \cap E^r}{\hat{E} \cup E^r}, \text{ in our specific problem and considering}$$

the three rules above we obtain that

$$= \frac{\sum TP}{\sum TP + \sum FP + \sum FN},$$

where $\sum TP$, $\sum FP$ and $\sum FN$ indicate the total number of true positive, false positive and false negative respectively.

The Recall[53] in the context of our application can be referred as the true positive rate or sensitivity, and it is defined as:

$$Recall = \frac{\sum TP}{\sum TP + \sum FN}.$$

On the other hand, the Precision[53] is also referred to as positive predictive value, and it is defined as:

$$Precision = \frac{\sum TP}{\sum TP + \sum FP}.$$

The $0.5\,\mu m$ threshold was chosen based on the resolution limit of optical microscopes, which in agreement with Rayleigh's criteria, is $r = (0.61\,\lambda)/NA$, with λ being the emission wavelength of the fluorophore and NA the numerical aperture of the objective. For fluorophores that emit in the visible spectrum the optical resolution of a common epifluorescence microscope is approximately $0.25 - 0.3\,\mu m$ (along the xy imaging plane). For a single emitter, r approximates the radius of the zero order Airy ring. For the sake of simplicity, we define a $0.5\,\mu m$ threshold as an approximation to the diameter of the zero order Airy ring, because in diffraction limited images it does not make sense to segment replication compartments smaller than $2r$. Moreover, transmission electron microscopy (TEM) has shown that replication centers measure between 0.5 and $2\,\mu m$ in diameter[54].

Statistical analyses. All statistical tests were performed using R version 3.2.4 (2016-03-16) software.

References

1. Boon, J., Diaz, A. & Ahlquist., P. Cytoplasmic viral replication complexes. *Cell Host Microbe* **8,** 77–85 (2010).
2. Schmid, M., Speiseder, T., Dobner, T. & Gonzalez., R. DNA virus replication compartments. *Journal of Virology* **88,** 1404–1420 (2014).
3. Wimmer, P. *et al.* Cross-talk between phosphorylation and SUMOylation regulates transforming activities of an adenoviral oncoprotein. *Oncogene* **32,** 1626–1637 (2013).
4. Hough V, P. C. Method and means for recognizing complex patterns (1962).
5. Wang, C., Kaba, D. & Li., Y. Level set segmentation of optic discs from retinal images. *Journal of Medical and Bioengineering* **4** (2015).
6. Mukhopadhyay, P. & Chaudhuri, B. A survey of hough transform. *Pattern Recognition, Elsevier* **48,** 993–1010 (2015).
7. Fischler, M. & Bolles., R. Random sample consensus: a paradigm for model fitting with applications to image analysis and automated cartography. *Communications of the ACM* **24** (1981).
8. Hongxia, G., Jianhe, X., Yueming, H. & Ze., Y. Hough-RANSAC: A fast and robust method for rejecting mismatches. *Communications in Computer and Information Science* **483,** 363–370 (2014).
9. Hassner, T., Assif, L. & Wolf., L. When standard RANSAC is not enough: cross-media visual matching with hypothesis relevancy. *Machine Vision and Applications* **25,** 971–983 (2014).
10. Litman, R., Korman, S., Bronstein, A. & Avidan., S. Inverting RANSAC: Global model detection via inlier rate estimation. *Proceedings of the IEEE Conference on Computer Vision and Pattern Recognition* 5243–5251 (2015).
11. Fitzgibbon, A., Pilu, M. & Fisher., B. Direct least squares fitting of ellipses. *IEEE Transactions on Pattern Analysis and Machine Intelligence* **21** (1999).
12. Kuo, N. *et al.* Automatic segmentation of radiographic fiducial and seeds from X-ray images in prostate brachytherapy. *Medical Engineering & Physics* **34,** 64–77 (2012).
13. Nectow, A., Kilmer, M. & Kaplan., D. Quantifying cellular alignment on anisotropic biomaterial platforms. *Journal of Biomedical Materials Research* **102,** 420–428 (2014).
14. Prasada, D., Leungb, K. & Queka., C. Ellifit: An unconstrained, non-iterative, least squares based geometric ellipse fitting method. *Pattern Recognition* **46,** 1449–1465 (2013).
15. Fitzgibbon, A., Pilu, M. & Fisher., B. Direct least squares fitting of ellipses. In *International Conference on Pattern Recognition* (1996).
16. Halir, R. & Flusser., J. Numerically stable direct least-squares fitting of ellipses. In *Sixth International Conference of Computer Graphics and Visualization* (1998).
17. Sinko, J., Szabó, G. & Erdélyi., M. Ray tracing analysis of inclined illumination techniques. *Optics Express* **22,** 18940–18948 (2014).
18. Arteta, C., Lempitsky, V., Noble, J. & Zisserman., A. Detecting overlapping instances in microscopy images using extremal region trees. *Medical Image Analysis* **27,** 3–16 (2015).
19. Prewitt, J. & Mendelsohn., M. The analysis of cell images. *Annals of the New York Academy of Sciences* **128,** 1035–1053 (1965).
20. Kapur, N., Sahoo, P. & CWong., A. A new method for gray-level picture thresholding using the entropy of the histogram. *Computer vision, graphics, and image processing.* **29,** 273–285 (1985).
21. Otsu., N. A threshold selection method from gray-level histograms. *IEEE Transactions on Systems, Man, and Cybernetics.* **9,** 62–66 (1979).
22. Yen, J., Chang, F. & Chang., S. A new criterion for automatic multilevel thresholding. *IEEE Transactions on Image Processing* **4,** 370–378 (1995).
23. Kruskal, H. & Wallis., W. Use of ranks in one-criterion variance analysis. *Journal of the American Statistical Association* **47,** 583–621 (1952).
24. Puvion-Dutilleul, F. & Pichard., E. Segregation of viral double-stranded and single-stranded DNA molecules in nuclei of adenovirus infected cells as revealed by electron microscope *in situ* hybridization. *Biology of the Cell* **46,** 139–150 (1992).
25. Puvion-Dutilleul, F., Roussev, R. & Puvion., E. Distribution of viral RNA molecules during the adenovirus type 5 infectious cycle in HeLa cells. *Journal of Structural Biology* **108,** 209–220 (1992).
26. Besse, S. & Puvion-Dutilleul., F. Anchorage of adenoviral RNAs to clusters of interchromatin granules. *Gene Expression* **5,** 79–92 (1995).
27. Pombo, A., Ferreira, J., Bridge, E. & Carmo-Fonseca., M. Adenovirus replication and transcription sites are spatially separated in the nucleus of infected cells. *The EMBO Journal* **13,** 5075–5085 (1994).
28. Puvion-Dutilleul, F., Bachellerie, J., Visa, N. & Puvion., E. Rearrangements of intranuclear structures involved in RNA processing in response to adenovirus infection. *Journal of cell science* **107,** 1457–1468 (1994).
29. Rebelo, L. *et al.* The dynamics of coiled bodies in the nucleus of adenovirus-infected cells. *Molecular Biology of the Cell* **7,** 1137–1151 (1996).
30. Aspegren, A. & Bridge., E. Release of snRNP and RNA from transcription sites in Adenovirus-Infected cells. *Experimental Cell Research* **276,** 273–283 (2002).

31. Lawrence, F., McStay, B. & Matthews., D. Nucleolar protein upstream binding factor is sequestered into adenovirus DNA replication centres during infection without affecting RNA polymerase I location or ablating rRNA synthesis. *Journal of Cell Science* **119,** 2621–2631 (2006).
32. Hindley, C., Andrew, D. & Matthews., D. Relationship between adenovirus DNA replication proteins and nucleolar proteins B23.1 and B23.2. *Journal of General Virology* **88,** 3244–3248 (2007).
33. Lam, Y., Evans, V., Heesom, K., Lamond, A. & Matthews., D. Proteomics analysis of the nucleolus in adenovirus-infected. *Cells. Molecular & Cellular Proteomics* **9,** 117–130 (2010).
34. Puvion-Dutilleul, F. & Puvion., E. Replicating single-stranded adenovirus type 5 DNA molecules accumulate within well-delimited intranuclear areas of lytically infected HeLa cells. *European Journal of Cell Biology* **52,** 379–388 (1990).
35. Lam, Y., Trinkle-Mulcahy, L. & Lamond, A. The nucleolus. *Journal of Cell Science* **118,** 1335–1337 (2005).
36. Babiss, L., Ginsberg, H. & Darnell., J. Adenovirus E1B proteins are required for accumulation of late viral mRNA and for effects on cellular mRNA translation and transport. *Molecular and Cellular Biology* **5,** 2552–2558 (1985).
37. Pilder, S., Moore, M., Logan, J. & Shenk., T. The adenovirus E1B-55K transforming polypeptide modulates transport or cytoplasmic stabilization of viral and host cell mRNAs. *Molecular and Cellular Biology* **6,** 470–476 (1986).
38. Leppard., K. Selective effects on adenovirus late gene expression of deleting the e1b 55k protein. *Journal of General Virology* (1993).
39. Gonzalez, R., Huang, W., Finnen, R., Bragg, C. & Flint., S. Adenovirus E1B 55-kilodalton protein is required for both regulation of mRNA export and efficient entry into the late phase of infection in normal human fibroblasts. *Journal of virology* **80,** 964–974 (2006).
40. Woo, L. & Berk., J. Adenovirus ubiquitin-protein ligase stimulates viral late mRNA nuclear export. *Journal of Virology* **81,** 575–587 (2007).
41. Querido, E. *et al.* Degradation of p53 by adenovirus e4orf6 and e1b55k proteins occurs via a novel mechanism involving a cullin-containing complex. *Genes & Development* **15,** 3104–3117 (2001).
42. Leppard, K. & Shenk., T. The adenovirus E1B 55 kd protein influences mRNA transport via an intranuclear effect on RNA metabolism. *EMBO Journal* **8,** 2329–2336 (1989).
43. Bridge, E. & Ketner., G. Interaction of adenoviral E4 and E1b products in late gene expression. *Virology* **174,** 345–353 (1990).
44. Gonzalez, R. & Flint., S. Effects of mutations in the adenoviral E1B 55-kilodalton protein coding sequence on viral late mRNA metabolism. *Journal of Virology* **76,** 4507–4519 (2002).
45. Cardoso, F., Kato, S., Huang, W., Flint, S. & Gonzalez., R. An early function of the adenoviral E1B 55 kDa protein is required for the nuclear relocalization of the cellular p53 protein in adenovirus-infected normal human cells. *Journal of Virology* **378,** 339–346 (2008).
46. Chahal, J. & Flint., S. Timely synthesis of the adenovirus type 5 E1B 55-kilodalton protein is required for efficient genome replication in normal human cells. *Journal of Virology* **86,** 3064–3072 (2012).
47. Chahal, J., Qi, J. & Flint., S. The human adenovirus type 5 E1B 55 kDa protein obstructs inhibition of viral replication by type I interferon in normal human cells. *PLOS Pathogens* **8** (2012).
48. Chahal, J., Gallagher, C., DeHart, C. & Flint., S. The repression domain of the E1B 55-kilodalton protein participates in countering interferon-induced inhibition of adenovirus replication. *Journal of Virology* **87** (2013).
49. Groitl, P. & Dobner., T. Construction of adenovirus type 5 early region 1 and 4 virus mutants. *Methods in molecular medicine* **130,** 29–39 (2007).
50. Jones, N. & Shenk., T. Isolation of adenovirus type 5 host range deletion mutants defective for transformation of rat embryo cells. *Cell* **17,** 683–689 (1979).
51. Dougherty, B. Diffraction PSF 3D (2005). http://www.optinav.com/Diffraction-PSF-3D.htm.
52. Pang-Ning, T., Steinbach, M. & Kumar, V. *Introduction to Data Mining* (2005).
53. https://en.wikipedia.org/wiki/Precision_and_recall (2016).
54. K. Murti, a., Davis, D. & Kitchingman, G. Localization of adenovirus-encoded dna replication proteins in the nucleus by immunogold electron microscopy. *Journal of General Virology* **71,** 2847–2857 (1990).

Acknowledgements

Author Contributions

Y.G., J.M.R.-M., R.A.G. and A.G. conceived the project, participated in the design and drafting of the manuscript. P.H., R.E.L. and A.G. performed the experiments. Y.G. developed the algorithms for the quantitative, automated analysis of the viral replication compartments. J.M.R.-M. and A.G. supervised the elaboration of the algorithms. Y.G. and A.G. created the synthetic data. C.D.W. contributed to writing the paper. All authors approved the final manuscript.

Additional Information

Supplementary information accompanies this paper at http://www.nature.com/srep

Competing financial interests: The authors declare no competing financial interests.

How to cite this article: Garcés, Y. *et al.* Automatic detection and measurement of viral replication compartments by ellipse adjustment. *Sci. Rep.* **6,** 36505; doi: 10.1038/srep36505 (2016).

Publisher's note: Springer Nature remains neutral with regard to jurisdictional claims in published maps and institutional affiliations.